1-1-2004

Influence of subgrade improvement and non-uniformity on pavement performance

Tyson David Rupnow
Iowa State University

Influence of subgrade improvement and non-uniformity on pavement performance

by

Tyson David Rupnow

A thesis submitted to the graduate faculty

in partial fulfillment of the requirements for the degree of

MASTER OF SCIENCE

Major: Civil Engineering (Geotechnical Engineering)

Program of Study Committee
David J. White (Major Professor)
Halil Ceylan
Thomas J. Rudolphi

Iowa State University

Ames, Iowa

2004

Graduate College
Iowa State University

This to certify that the master's thesis of

Tyson David Rupnow

has met the thesis requirements of Iowa State University

Signatures have been redacted for privacy

TABLE OF CONTENTS

LIST OF FIGURES

LIST OF TABLES

LIST OF EQUATIONS

GENERAL INTRODUCTION

PROJECT STATEMENT

This thesis describes results from three project areas. The first project investigates the effectiveness of using self-cementing fly ashes in combination with recycled asphalt pavement (RAP) to stabilize weak parking lot subgrade prior to repaving with asphalt concrete. In-situ and laboratory testing was used to determined the effectiveness of the mixtures.

The second project describes laboratory mix design testing and field construction operations for a road constructed from mixtures of waste products (self-cementing fly ash, cement kiln dust, and limestone screenings). Key parameters studied included strength and durability. Laboratory mixtures were evaluated from unconfined compression, freeze-thaw, and wet-dry tests. Field-testing included DCP, nuclear density gauge, GeoGauge vibration tests, Clegg Impact Hammer, Falling Weight Deflectometer, and field prepared unconfined compression samples. Air and ground temperatures were monitored to determine heat generation during construction and the number of freeze-thaw cycles in winter/spring months.

The third project presents results from field measurements and numerical analysis to determine the influence of subgrade non-uniformity on pavement performance. Several in-situ testing devices were used to generate engineering parameter values. Test results were collected in a grid pattern and used in a linear elastic finite element software program to model pavement behavior under load. Results were compared to perfectly uniform subgrade

support to determine if a significant relationship exists between the pavement performance and the subgrade non-uniformity. Statistical analysis techniques were used to evaluate the results.

THESIS ORGANIZATION

This thesis is organized into three sections. Each section includes its own abstract and literature review, and details in depth, the laboratory and field procedures used in each individual project. Each project also includes a section pertaining to that projects results, discussion, conclusions, and recommendations. A general conclusions and general recommendations is also included.

CHAPTER 1. SUBGRADE STABILIZATION USING RECYCLED ASPHALT PAVEMENT AND SELF-CEMENTING FLY ASH MIXTURES

ABSTRACT

Delays due to road construction cost millions of dollars in lost productivity every year. These costs impact the general public especially local businesses. Unstable subgrade is one major construction setback that increases costs. Unstable subgrade causes a wide variety of problems such as: asphalt pavement rutting, premature pavement failure, and construction difficulties.

To address unstable subgrade problems, civil engineering experts need to develop new materials or construction practices. The purpose and goal of this study was to evaluate the suitability of one particular construction process and specific materials (soil, self-cementing fly ash, and recycled asphalt pavement (RAP)) for asphalt parking lot subgrade stabilization. This project set forth three objectives:

1. Document construction processes for subgrade stabilization;
2. Perform a detailed laboratory analysis of materials used during the construction process to evaluate their suitability;
3. Conduct field analysis to evaluate the suitability of the final product.

Dynamic Cone Penetrometer (DCP) tests were used to evaluate strength gain in the field. Laboratory testing consisted of unconfined compression strength tests and consolidated undrained (CU) triaxial compression tests.

Overview of Results and Conclusions

DCP test results show time dependent strength-gain due to the cementing and pozzolanic action of the fly ash. Falling weight deflectometer (FWD) results show increased pavement durability and performance. CU triaxial load tests show normally consolidated behavior for the soil and soil-RAP mixtures and overconsolidated behavior for self-cementing fly ash-soil-RAP mixtures. Self-cementing fly ash-soil-RAP mixtures demonstrate an undrained shear strength gain of about 2 to 4 times of the soil-RAP mixture.

Conclusions of this study illustrate that the documented construction process and fly ash-soil-RAP mixtures are well suited for subgrade stabilization. Depending upon the back calculation method applied to falling weight deflectometer measurements, the fly ash-soil-RAP mixtures demonstrated increases stiffness leading to 7 to 21 times greater traffic capacity.

INTRODUCTION

Unstable subgrade causes a wide variety of costly problems such as: asphalt pavement rutting, premature pavement failure, and construction difficulties. In road and parking lot construction subgrade becomes unstable for a variety of reasons. Unstable subgrade is most commonly compromised of a large percentage of fines with high moisture content. Delays due to road construction cost millions of dollars in lost productivity every year. When engineers have to address problems relating to unstable subgrade, cost of labor and materials increase. This has a direct economic impact on local businesses and lost productivity.

To increase the stability of the subgrade, engineers have experimented with several solutions that involve adding granular subbase to the subgrade and chemically stabilizing the subgrade with lime, Portland cement, or self-cementing fly ash. Though self-cementing fly ash stabilization works well under certain conditions, there is still debate on the effectiveness of current construction processes, as well as the composition of construction materials to be included.

This chapter documents the construction process and analyzes the materials used in the Jack Trice Football Stadium parking lot reconstruction. The purpose and goal of this study was to evaluate the suitability of the construction process and final product for parking lot stabilization. The three objectives needed to accomplish this goal are as follows:

1. Document construction process for parking lot stabilization;
2. Perform a detailed laboratory analysis of materials used during the construction process to evaluate their suitability;
3. Conduct field analysis to evaluate the suitability of the final product.

Conclusions of this research confirmed that the construction procedures and fly ash-soil-recycled asphalt pavement (RAP) mixtures used were effective in providing suitable final product in parking lot subgrade stabilization. Fly ash-soil-RAP mixtures demonstrated increased undrained shear strength of about 2 to 4 times that of soil-RAP mixtures. Depending upon the back calculation method applied, the fly ash-soil-RAP mixtures demonstrated increases stiffness leading to 7 to 21 times greater traffic capacity. A comparative cost analysis shows that the construction procedure employed costs about the same as conventional parking lot reconstruction techniques. The Dynamic Cone Penetrometer (DCP) has the potential to be used for evaluation of in-situ unconfined

compressive strength through the use of a characteristic mean DCP index versus unconfined compressive strength curve.

This paper is organized in the following manner:

- Literature Review
- Methods
- Materials
- Results
- Discussion
- Conclusions
- Recommendations

LITERATURE REVIEW

To provide context for this project, this section details case studies describing the use of self-cementing fly ash, RAP, or a mixture of self-cementing fly ash and RAP as stabilizers for base or subbase construction. This review briefly describes the chemical properties and binding mechanisms of self-cementing fly ash, procedures for mixing, moisture control, compaction, and curing of stabilized bases, and the properties of RAP aggregate.

Overview

Unstable subgrade can cause a wide variety of problems such as: rutting, premature pavement failure, and construction difficulties. Subgrade becomes unstable when it is no longer able to support construction traffic. Usually unstable subgrade has high water content and large fines content, i.e. a large fraction passing the number 200 sieve, leading to low soil

shear strength. Typical California Bearing Ratio (CBR) values for unstable subgrade are below three.

Several alternatives to improve unstable subgrade are: addition of a drainage layer such as granular backfill underneath the pavement, lime stabilization, self-cementing fly ash stabilization, and Portland cement stabilization. Granular backfill is particularly attractive since the increased CBR value of the granular material provides additional support for the pavement layer while removing excess water from the structure. Lime stabilization is useful as it provides long-term strength gain due to pozzolanic action in clayey soils while acting as a drying agent. Portland cement stabilization increases the strength of unstable subgrade, but due to the large amount of Portland cement required, 10-15% by dry weight, it is usually not cost effective due to the high cost of Portland cement. Self-cementing fly ash is attractive due to the drying capabilities and the initial strength gain due to the hydration process. Long term strength gain from pozzolanic activity also makes self-cementing fly ash stabilization an attractive solution.

Case Studies Involving RAP Stabilization

Cement Stabilization of RAP for Road Base and Subbase Construction

This study was completed in 2001 and involved cement stabilization of RAP for road bases and subbases. The study took place in the Sultanate of Oman where the recycling of pavement materials is not practiced widely. The objective of the study was to investigate the potential use of Type I Portland cement with RAP-virgin aggregate mixtures for road base construction. Test procedures included: physical characterization of the RAP and aggregate mixtures, modified Proctor compaction tests, and unconfined compressive strength tests.

Type I Portland cement was added to the mixtures at the rate of 0, 3, 5, and 7% by dry weight. Pavement design analysis was also conducted by varying the base properties from laboratory data.

This study concluded that all RAP-virgin aggregate blends with no cement yield impractical base thicknesses, and that RAP-virgin aggregate blends with no cement need a thicker surface course as the percent RAP increases in the base in order to protect the weak base course. Other results demonstrate that as more cement is used for each mixture, the base course thickness is decreased. As the percent RAP is increased, the thickness of the base course will increase. Conclusions of this study are as follows: optimum moisture content, maximum dry density and the unconfined compressive strength generally increase as the cement content and virgin aggregate contents increase, 100% RAP aggregate could be used in base construction if stabilized with cement, and RAP aggregate seemed to be a viable alternative to dense graded aggregate in road base and subbase construction (Taha et al. 2002).

Kansas Route 27

Several test sections were constructed and subsequently tested from 1992 to 1996 on Kansas Route 27 (Wu 1999). A total of 11 test sections were constructed. Three sections were stabilized using a cationic, medium setting, polymerized asphalt emulsion; five were constructed using a cationic, medium setting asphalt emulsion; and three were constructed using 13% ASTM Class C fly ash as the binder. All layer thicknesses were 4 inch, with a 1.5 inch hot mix asphalt overlay.

One conclusion from this study was cold in place recycled pavements (CIPR) with class C fly ash as a binder reduces the potential of rutting when compared to the other test sections built with conventional binders. The self-cementing fly ash sections consistently showed the lowest surface deflection values for Falling Weight Deflectometer (FWD) testing. Shear strains in the fly ash treated layer were very uniformly distributed across the pavement layers. Lastly, for pavement damage, rutting controlled this project, not fatigue (Wu 1999).

Recycled Pavement, 93rd Street, Shawnee County, Kansas

Constructed in June of 1987, this 1.5-mile section of rural road carries a high volume of truck traffic (Glogowski et al. 1992). The surface course varied in thickness from 2 to 6 inches with a 1 to 8 inch granular base overlying a clay subgrade. The design process concluded that 18% class C fly ash and 10% moisture content was needed to stabilize the material.

The construction process began with recycling the existing pavement and base to a depth of 6 inches and compacting it. The fly ash was deposited in windrows and spread uniform and mixed with a Bomag MPH 100 Recycler. For this project, water was added through nozzles in the mixing drum. Initial compaction was completed with a vibratory padfoot roller while final compaction was completed with a smooth drum or pneumatic-tired roller. The surface was kept moist for the five-day cure period. A layer of asphalt was then applied followed by a chip seal wearing surface two months later. Observations four years after construction yield no distress or deterioration (Glogowski et al. 1992)

Fly Ash Stabilization of RAP, City of Mequon, Wisconsin

This study discussed two test sections 250 m long built on the eastern end of Highland Avenue (Crovetti 1998). Both sections had a surface thickness of about 140 mm overlying a 170 to 450 mm base course overlying a cohesive subgrade. The project was started and completed in August of 1997.

For construction, both sections were pulverized to a depth of 200 mm. The asphalt emulsion section was repulverized to a depth of 100 mm and emulsified asphalt was added at the rate of 7 L/m^2. The section was then graded, compacted, and an 87.5 mm HMA surface was placed. The fly ash section was constructed by placing the ash at 7% by dry weight on the RAP and mixing to a depth of 125 mm. The layer was graded and water was applied to the surface to achieve 5% moisture content. The stabilized layer was then graded, compacted, and a 100 mm HMA surface was applied. FWD testing shows excellent performance through the first year for the fly ash section due to the increased structural capacity of the pavement (Crovetti 1998).

Fly Ash Stabilization of RAP, Waukesha County, Wisconsin

This project was undertaken on highway JK in Waukesha, Wisconsin, and is a ¾ mile long county road lying in a low area with very silty subgrade soils. Problems with frost heave have been experienced due to availability of water and the silty nature of the underlying soil. Construction began in October 2001 on the new road base. Fly ash stabilization was used because it was cost effective. The existing asphalt pavement was pulverized to a depth of 6 inches, and water was added to the milled material. Then a second pass of the pulvamixer was used to pulverize the material to a depth of 12 inches. The target

water content for the project was 6%, and fly ash was added to the RAP at 8%. The final pass of the mixer was then completed. Initial compaction was completed with a vibratory sheepsfoot with a compaction delay of less than half an hour. Final compaction was then completed using a smooth drum roller. The compacted stabilized section was allowed to cure for 24 hours before 5 inches of E-3 Superpave mix was laid down. No frost heave was observed the following winter (Gantenbein 2002).

Properties of Recycled Asphalt Pavement (RAP)

Recycled asphalt pavement (RAP) is produced through the recycling of existing asphalt pavements. The Asphalt Paving Association of Oregon, (APAO) (2003), estimates that 91 million metric tone of asphalt is removed through the course of resurfacing and widening projects each year in the United States. It is estimated that 73 million metric tone of asphalt removed is recycled as a part of a new road, roadbed, shoulder or embankment (APAO 2003). The use of RAP in roadway construction is economically attractive, especially in areas with an aggregate shortage.

There are three main types of asphalt pavement recycling: surface, central plant, and in place base and subbase recycling (Taha et al. 1999). Studies indicate that using a cold-in-place recycling technique of an existing bituminous pavement could be structurally equivalent to a roadway reconstructed with a new base course (Taha et al. 1999). Other studies show that RAP can be used effectively as a base and subbase material for conventional flexible pavements if stabilized with Portland cement (Taha et al. 2002).

RAP use in Hot Mix Asphalt (HMA) varies from state to state; some states allow full use while others do not allow RAP to be used anywhere within the pavement structure (Nady 1997). In Iowa, specifications for the use of RAP are as follows (Nady 1997):

- RAP must be from a known source;
- RAP may be used in base and binder courses.

Physical Properties of RAP

For classification purposes, RAP generally classifies GW, well-graded gravel (Taha et al. 1999 and Taha et al. 2002). Nady (1997) stated that virgin aggregate properties from local Iowa producers show more variability than the RAP aggregate properties over a four year testing period. Binder content was shown to be about five percent. Nady, (1997), states that the recycling method chosen has a great impact on the gradation characteristics. Portable crushing plants with jaw-type primary and roll-type secondary crusher reduce RAP chunk size by shearing the chunk along the weakest plane in the asphalt films (Nady 1997). Milling machines, on the other hand, produce an aggregate with significantly higher fines content (Nady 1997).

Atterberg limit tests show that the RAP is essentially non-plastic, and other physical tests conclude that the moisture content is relatively low with little water absorption. Taha et al. (1999) showed that the modified Proctor curve for RAP generally falls well below the Proctor curve for virgin aggregate. RAP aggregate tends to break up during the compaction process due to the soft aggregate. Other physical properties of interest are the moisture holding capabilities of RAP, permeability, and California Bearing Ratio (CBR). Tests conclude that RAP is highly permeable (Taha et al. 1999 and Taha et al. 2002). Taha et al.

(1999, 2002) state that the moisture holding capability of RAP is a function of the percent passing the number 200 sieve, and is generally negligible due to the little amount passing the number 200 sieve. CBR data show low CBR values of about 11 for RAP aggregate (Taha et al. 1999).

Self Cementing Fly Ash

The majority of electricity produced in the United Sates is produced from the combustion of coal at coal-fired utilities. As a result over 117 million tons of coal combustion byproducts are produced per year (American Coal Ash Association 2003). The American Coal Ash Association (ACAA) (2003) estimates that fly ash comprise 68 million tons. The 68 million tons is broken down into the following categories and tonnages (ACAA 2003):

- Bottom ash is approximately 18.7 million tons;
- Boiler slag totals approximately 2.5 million tons;
- Other byproducts are approximated at 24.8 million tons.

The ACAA (2003) states that fly ash use continually grows, but less than 32% of coal combustion byproducts are recycled each year leading to a sluice pond or landfill disposal practices. Of the fly ash being recycled, the widest application is as a partial replacement of cement in Portland cement concrete. Another application is soil stabilization. Self-cementing fly ash reacts chemically with soil minerals producing long term pozzolanic strength gain. Initial rapid strength gain is due to hydration of tricalcium aluminates (C_3A).

A discussion on the benefits of using self-cementing fly ash for soil stabilization can be found from the following sources: Thomas 2003; Glogowski et al. 1992; White and

Bergeson 2000; Zia and Fox 2002; Senol et al. 2002, Rupnow 2002; Parsons 2002; Nalbantoglu and Gucbilmez 2002; Misra 1998; Khoury and Zamon 2002; Ferguson 1993; Cokca 2001; ACAA 1999; Klassen and Jones 1985. The benefits are:

1. Environmental incentives, material does not have to be wasted and;
2. Cost savings, lime and cement are generally more expensive than fly ash;
3. Creation of a stable working platform;
4. Elimination of expensive borrows;
5. Expedition of the construction timeline;
6. Reductions in pavement thickness;
7. Drying agent in soft, saturated soils;
8. Reduction of swell potential;
9. Modification of plasticity characteristics;
10. Increased shear strength of poor soils;
11. Increased freeze-thaw durability;
12. Stabilization of erodible soil;
13. Stabilization of backfill to reduce lateral earth pressures.

Chemical Properties and Reaction Mechanisms of Self-Cementing Fly Ash

ASTM C618 [Standard Specification for Coal Fly Ash and Raw or Calcined Natural Pozzolan for Use as a Mineral Admixture in Concrete] defines fly ash as the fine residue produced from the burning of ground or powdered coal. Fly ash is collected from the flu gas of coal-fired boilers by the means of an electrostatic precipitator or bag house. Fly ash color may vary from tan to gray (Misra 2000). Self-cementing fly ash is produced from the

burning of low sulfur, subbituminous and lignite coals. Fly ash particles are typically spherical in nature and contain some crystalline as well as carbonaceous matter (Barnes 1997; Misra 2000). Misra (2000) noted that a large percentage of fly ash is in the form of silica, alumina, ferric oxide, and calcium oxide. Table 1 shows typical class C fly ash composition. ASTM C618 chemical requirements are also shown in Table 1.

Positive Reaction Products

ASTM C618 states, "A pozzolan is a material rich in silica and alumina that has little or non self-cementing properties, but will, in the presence of moisture, chemically react with calcium hydroxide at ordinary temperatures to form compounds possessing cementitious properties."

Barnes (1997), Misra (2000), and Glogowski et al. (1992), state that the pozzolinity of fly ash is mainly dependent upon the fineness of the ash, amounts of silica and alumina, and the presence of moisture and free lime. Winkerton and Pamukcu (1991) also state that density, amount of carbon, temperature, and age also affect the rate of pozzolanic reaction.

Initial cementitious reaction products are attributed to the hydration of tricalcium aluminate. These cementitious reaction products can create problems if a long compaction delay time is used due to the required energy to break the cemented particle apart during the compaction process (ACAA 1999). The strength gain over 28 days can be attributed to pozzolanic reactions between calcium oxide and the aluminous and siliceous materials in the fly ash.

Table 1. Typical Chemical Composition of a Class C Fly Ash and ASTM C 618 Chemical Requirements for a Class C Fly Ash

Oxide	Self Cementing Fly Ash (% of Total Weight)	ASTM C 618
SiO_2	20-40	Summation between 50% and 70%
Al_2O_2	10-30	
FeO3	3-10	
CaO	10-32	
MgO	0.8-8	
Na_2O	0.5-6	
K_2O	0.5-4	
TiO_2	0.5-2	
SO_3	1-8	Maximum of 5%
LOI	0-3	Maximum of 5%

Negative Reaction Products

Negative reaction products occur when crystals composed of sulfate compounds develop after the high sulfate fly ash is added to the material to be stabilized. Ettringite and thaumasite form as the calcium sulfate reaction products are being formed. Ettringite and thaumasite form and continue to form, producing long-term expansion (ACAA 1999). Calcium, sulfates, alumina, and water combine to form ettringite and thaumasite. Ettringite is formed initially and occupies a volume over 200% of the volume of its constituents. Ettringite the further expands through its conversion to thaumasite resulting in another 200% volume increase (ACAA 1999). Thaumasite is formed at a lower temperature than ettringite. The reaction takes place when the temperature drops below 16°C via isomorphous substitution of the alumina for silica in the ettringite (ACAA 1999).

The following guidelines for stabilization with high sulfur ashes have been proposed by the ACAA (1999):

- Fly ashes with sulfur contents ranging from 5% to 10% should be considered expansive until laboratory results show otherwise.
- Fly ashes with sulfur contents greater than 10% should not be used for stabilization purposes.
- Soluble sulfates in the soil as well as the groundwater used for the project must be considered as these can influence the volumetric stability of the stabilized mix.
- Non-saturated conditions tend to slow crystal growth.
- Saturated conditions make ions needed for growth more mobile.
- Increasing clay and colloids content can be related to larger swell increases.

Although the destruction due to sulfates and calcium based stabilizers is astounding, there are several ways to prevent it from occurring (Kota et al. 1996):

- Double application of lime.
- Non-calcium stabilizers.
- Low calcium stabilizers like cement and fly ash.
- Using a top surface constructed with non-sulfate select fill material.
- Barium compound pretreatment.
- Geotextile or Geogrid soil reinforcement.
- Asphalt stabilization of the soils containing sulfates.
- Compacting to lower densities.

Self-Cementing Fly Ash Stabilization Construction Procedures

Mixing of Self-Cementing Fly Ash and Soil

When considering the use of self-cementing fly ash as a soil stabilizer, there are two mixing options: (1) Off-site mixing using a continuous or batch type mixing, and (2) On-site mixing (see discussions provided by Thomas 2003; ACAA 1991; CMI Corp. 1994).

Addition of Water to Ensure Proper Hydration

The addition of water during stabilization operations must be monitored, as it is one of the most important ingredients to a successful project (ACAA 1991). See ACAA 1991; Vandenbossche and Johnson 1994; ACAA 1991 for discussion on different water addition processes and rates.

Compaction of Self-Cementing Fly Ash Stabilized Soil

Compaction of a fly ash stabilized soil can be done with a range of compaction equipment. The type of equipment used is a function of the soil type. For a discussion on roller types and compaction procedures see: ACAA 1991; FHWA 1979; Vandenbossche and Johnson 1994; ACAA 1999.

Curing of Self-Cementing Fly Ash Stabilized Soil

Curing fly ash stabilized sections is defined as sealing the sections before the pavement sections are placed to allow for hydration of the fly ash and gain the specified strength (FHWA 1979; Vandenbossche and Johnson 1994). Factors affecting strength gain are as follows (FHWA 1979; ACAA 1991; ACAA 1999):

- Availability of moisture;
- Temperature during the curing period;
- Length of the curing period.

For a discussion on curing periods and methods of curing see: FHWA 1979; Johnson and Vandenbossche 1994; Armed Forces 1994; Klassen and Jones 1985. For a discussion on stabilization construction temperatures see: ACAA 1999; Vandenbossche and Johnson 1994; ACAA 1991; Glogowski et al. 1992; Thomas 2003.

METHODS

The methods section overviews the testing and observation methods used throughout this study. Methods include: (1) Project background (2) Documentation of construction operations, (3) Laboratory analysis of the construction materials, and (4) Field analysis of the completed product.

Project Background

This section describes the project location, site condition, and materials used throughout the duration of the project.

In May 2002 pavement reconstruction was initiated to replace a large section (25,351 m^2) of deteriorating asphalt pavement at Iowa State University's Jack Trice Football Stadium shown in Figure 1. Previous construction activity in the area revealed wet unstable subgrade conditions, which was believed to have contributed to the existing poor pavement performance.

This prompted a review of the proposed construction plans and procedures. It was determined that complete removal of the existing pavement and stabilization of the subgrade to a depth of about 300 mm would provide the most effective and economical solution. Stabilization was determined to be economical for the contractor because the new paving platform would be able to sustain construction traffic during paving operations. Subgrade stabilization was achieved by incorporating the milled Recycled Asphalt Pavement (RAP) in addition to self-cementing fly ash.

Self-cementing fly ash sources were: Ames Municipal Generating Station, Ottumwa Generating Station, and Prairie Creek Generating Station. Although all three ashes were used on the project, Ames Municipal fly ash was the principal fly ash used throughout the duration of the project.

Figure 1. Jack Trice Stadium Parking Lots

Objective One: Document Construction Operations

Construction designs were completed by Snyder and Associates located in Ankeny, Iowa, and construction operations were carried out by Manatts Construction Inc.

Construction operations were documented to determine the effectiveness of the process used. Construction operations were studied through the use of digital photography, digital video camcorder recordings, and note taking.

Task 1: Mill Asphalt to Required Gradation

The existing asphalt surface was determined to be 100 to 300 mm thick for full depth patches. First the existing asphalt surface was milled in place with a CAT RM 3500 reclaimer to a depth of about 150 mm. This depth was chosen to allow the cutting teeth to cool in the underlying subgrade soil. One pass of the reclaimer was required to bring the RAP to the desired maximum particle size of about 25 mm. Figure 2 shows the asphalt surface being milled.

Task 2: Level RAP to Contain Fly Ash

The recycled asphalt pavement (RAP) was then leveled with a motor grader and windrows were created to contain the class C fly ash.

Task 3: Add Water to Desired Moisture Content

Once the windrows were established, water was added to the subgrade to provide sufficient moisture to hydrate the fly ash. The target moisture content for this project was determined to be 13%. Figure 3 shows the addition of the water to the subgrade.

Figure 2. Milling of Existing Asphalt Surface

Figure 3. Addition of Water to Subgrade

Task 4: Add Class C Fly Ash

Class C fly ash was then placed on the wetted subgrade using bottom dump trucks. Figure 4 shows the addition of fly ash. For this project, the fly ash addition rate was 10% by dry weight of the subgrade soil-RAP mixture. After placement of the fly ash, it was spread to a uniform thickness with the use of the motor grader.

Figure 4. Addition of Class C Fly Ash from Bottom Dump

Task 5: Mix Fly Ash, RAP, and Subgrade Soil

Next the CAT RM 3500 reclaimer was used to thoroughly mix the fly ash, RAP, and subgrade soil to a depth of about 300 mm. Mixing was complete when the material exhibited

a uniform light tan color and was close to the 13% optimum moisture content. Figure 5 illustrates the mixing operation. Target time from mixing to final compaction was 30 minutes. Observed time from initial mixing to final compaction was about two hours.

Figure 5. Mixing of Class C Fly Ash, RAP, and Subgrade Soil

Task 6: Compact Mixture

A vibratory padfoot roller conducted four to six roller passes for initial compaction of the mixture. Once four to six passes had been completed with the vibratory padfoot roller, a steel drum roller conducted two to four roller passes for final compaction. Final compaction produced a smooth surface to inhibit surface water infiltration. Figures 6 and 7 show the vibratory padfoot roller and smooth drum roller operations respectively.

Figure 6. Initial Compaction Using a Vibratory Padfoot Roller

Figure 7. Final Compaction Using a Flat Drum Roller

Task 7: Establish Final Grade for Paving Operations

Next a motor grader was used to establish final grade for paving operations. Final grade consisted of an l% crown in the center of the parking lot. The 1% crown was needed to ensure proper drainage of surface water. Figure 8 shows the final grading operation.

Task 8: Apply Pavement Surface

Lastly, the 150 mm Hot Mix Asphalt (HMA) surface was applied. The binder course was placed to a depth of 100 mm and the surface course completed the remaining 50 mm. Figure 9 shows the placement of the 100 mm asphalt binder course.

Figure 8. Final Grading with Motor Grader

Figure 9. Placement of the Hot Mix Asphalt Surface

Objective Two: Conduct Laboratory Analysis

The materials for this project were analyzed and studied to determine their effectiveness in producing a suitable paving platform. The materials studied included: RAP, fly ash, and the subgrade soil.

Task 1: Analyze soil

To fully analyze the subgrade soil, several standard ASTM test methods were employed.

- ASTM D 422-63 [Standard Test Method for Particle-Size Analysis of Soils]
- ASTM D 2487-90 [Standard Test Method for Classification of Soils for Engineering Purposes]

- ASTM D 4318-84 [Standard Test for Liquid Limit, Plastic Limit, and Plasticity Index of Soils]

First the subgrade soil was sampled using three, five gallon plastic containers with lids to ensure no moisture loss. The samples were transported back to the laboratory and the soil clods were reduced. The material was left to air dry overnight. The material was then prepared for particle-size analysis following ASTM D 422-63. Once the particle-size analysis was completed, the index properties of the soil were determined according to ASTM D 4318. Soil classification was completed using ASTM D 2487.

Task 2: Chemically Analyze and Classify Fly Ash

The chemical analysis included X-ray diffraction analysis (XRD), and x-ray fluorescence analysis (XRF). Fly ash was collected during construction operations in two five gallon containers. XRD provides an indication of the chemical compounds and minerals while XRF provides analytical chemical content expressed as oxides. This information was used to classify the fly ash according to ASTM C-618-01 [Standard Specification for Coal Fly Ash and Raw or Calcined Natural Pozzolan for Use as a Mineral Admixture in Concrete].

Task 3: Analyze Fly Ash-RAP-Soil Mixtures

The fly ash-RAP-soil mixtures were analyzed using the following ASTM standard test methods:

- ASTM C 593 [Standard Specification for Fly Ash and Other Pozzolans for Use with Lime]
- ASTM D 422-63 [Standard Test Method for Particle-Size Analysis of Soils]

- ASTM D 698 [Standard Test Methods for Moisture Density Relations of Soils and Soil-Aggregate Mixtures Using 5.5 lb. (2.49kg) Rammer and 12 in (305 mm) Drop]
- ASTM D 2487-90 [Standard Test Method for Classification of Soils for Engineering Purposes]
- ASTM D 4318-84 [Standard Test for Liquid Limit, Plastic Limit, and Plasticity Index of Soils]
- ASTM D 4767 [Standard Test Method for Consolidated Undrained Triaxial Compression Test for Cohesive Soils]

The fly ash-soil-RAP mixtures were sampled and classified using ASTM D 422, ASTM D 2487, and ASTM D 4318. The mixtures were also tested for unconfined compressive strength (ASTM C 593 and ASTM D 698), and consolidated undrained shear strength (ASTM D 4767). The aforementioned test results are described in later sections.

Task 4: Produce Unconfined Compression Strength Samples

ASTM D 698 was used to produce three field unconfined compression strength samples for testing 28-day compressive strength. The material was collected on site and samples were produced at the time of initial compaction. Three samples were produced to obtain an average strength. ASTM D 698 was also used in producing laboratory samples used in comparisons between field data. ASTM C 593 was used in order to allow 7-day oven curing of samples to shorten the laboratory testing timeframe. Deviation from ASTM C 593 was that only the 7-day oven curing portion of the ASTM standard was used. ASTM D 422,

D 2487, and D 4318 were used to classify the fly ash-soil-RAP mixtures obtained from the field.

A set of three specimens was produced for testing at 24 hours, 7 day, 14 day, and 28 day unconfined compressive strength. Samples were capped with sulfur to ensure even distribution of force during testing.

The RAP and subgrade soil were mixed at a 50% RAP to soil mixture by dry weight. The standard Proctor test (ASTM D 698) was conducted to determine the optimum moisture content and maximum dry density.

Once the optimum moisture content was determined, unconfined compressive strength samples were produced at varying moisture contents to determine the relationship between moisture and strength. Once the unconfined compression strength was determined, the results were compared to the field results.

Task 5: Prepare Consolidated Undrained Triaxial Load Test Samples

ASTM D 4767 was used to determine the consolidated undrained (CU) shear strength of the soil-RAP-fly ash mixtures. The CU test was chosen to replicate saturated and potentially undrained loading conditions. Three samples were produced on grade using a Marshall hammer and a 100 mm X 200 mm PVC mold. The PVC mold was split in three vertical pieces and held together with standard hose clamps. The material was deposited and compacted in three even lifts using standard Proctor energy. Seventeen blows per lift were required to achieve standard Proctor energy. The samples were transported to the laboratory, bagged, labeled, and placed in the humidity room for about one year prior to testing.

Task 6: Produce Scanning Electron Microscopy Images

Scanning electron microscopy (SEM) images were taken after CU testing to gain further knowledge of the soil-self-cementing fly ash-RAP interaction. A sample of the Ames ash-soil-RAP was used for the SEM images since this was the major mix used for the project.

Objective Three: Perform Field Analysis

Objective three was accomplished using two field testing techniques. The first field test used was the Falling Weight Deflectometer (FWD). The FWD test was used because the results allow for back calculation of subgrade moduli values. The FWD tests were also conducted so that the before and after deflection basin results could be plotted and compared. The FWD test was conducted on two lots before and after construction. Lot S3 served as the control section because no construction activity occurred within the lot. Lot S5 served as the test section.

The Dynamic Cone Penetrometer (DCP) test was the second field testing technique applied. The DCP test is an apparatus that measures the stiffness of the soil in terms of mm per blow. The DCP test is a useful test due to the many published correlations to the California Bearing Ratio (CBR). Figure 10 shows a DCP test being conducted. An 18 kg weight is operated on a 900 mm slide hammer driving a 60 degree cone into the soil. The distance driven per blow is then measured. DCP tests were conducted in the field during and after construction at specified time intervals. The time intervals after compaction were as follows: 0 minutes, 1 hour, 24 hours, 3 days, 7 days, and as close to 28 days after compaction as construction operations would allow.

Figure 10. DCP Test Being Conducted

MATERIALS

This section presents an analysis of the materials used during this study: (1) self-cementing fly ash, (2) soil, (3) RAP, (4) Soil Fly Ash-RAP mixtures. Self-cementing fly ash was selected to be a suitable method for stabilizing the subgrade soil at the Iowa State University Jack Trice Stadium Parking Lots.

Self-Cementing Fly Ash Chemical Analysis

The sources of fly ash were as follows: (1) Prairie Creek fly ash from the Cedar Rapids, Iowa Power Plant; (2) fly ash from the Ottumwa Generation Station (OGS) in Chillicothe, Iowa; and (3) fly ash from Ames Municipal Generating Station located in Ames, Iowa.

Table 2 shows the chemical analysis results for the OGS and Ames fly ashes. Figure 11 shows the overlay of the XRD results in graphical form. Note that the OGS fly ash

contains more glass than the Ames Municipal fly ash. Another observation is the levels of tricalcium aluminate, C_3A, in each of the two samples. Note that the Ames fly ash has a greater amount of C_3A. This is useful in showing that the Ames Municipal fly ash is a fast setting fly ash.

Figure 12 shows the set time for the Ames and OGS fly ash. Note the rapid set time associated with the Ames ash being set up after 20 minutes compared to the set time of the OGS fly ash being about 75 minutes. The target compaction delay was set at 30 minutes for this reason.

Table 2. XRF Chemical Analysis Results for Ames and OGS Fly Ash

Sample Name	OGS	AMES
SiO_2	37.10	33.42
Al_2O_3	21.47	17.52
Fe_2O_3	5.71	5.89
SUM	64.28	56.84
SO_3	2.19	3.46
CaO	22.51	26.65
MgO	4.27	5.90
Na_2O	3.27	2.41
K_2O	0.52	0.52
P_2O_5	1.44	1.08
TiO_2	1.53	1.64
SrO	0.42	0.30
BaO	0.75	0.73
Total	101.20	99.54

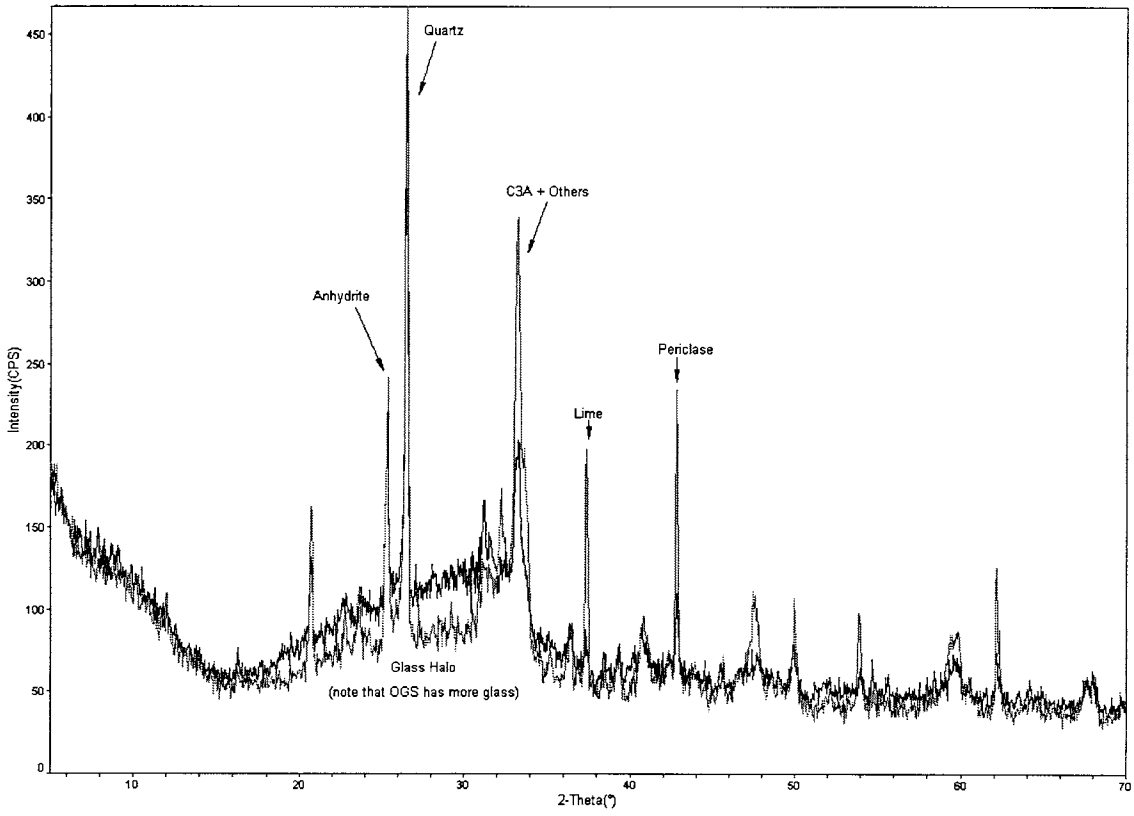

Figure 11. XRD Pattern Overlay for Ames Municipal and OGS Fly Ash

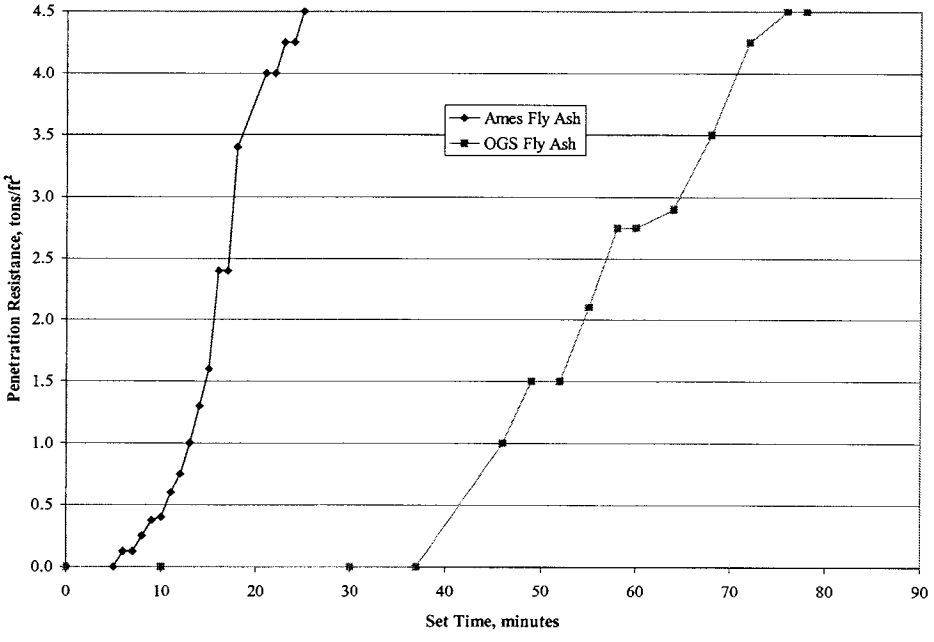

Figure 12. Set Time for Ames and OGS Fly Ash

Soil Grain Size Distribution

In-situ soils in the affected area lie in the floodplain of the South Skunk River and are highly saturated and unstable under construction equipment. The high in-situ moisture content of the soil makes it nearly impossible to move construction machinery around without severe rutting and deformation. The area soils have a gravel, sand, silt, and clay content of about 18.8%, 46.7%, 24.5%, and 10% respectively. Figure 16 shows the subgrade soil gradation curve. Table 3 shows the subgrade soil classification.

RAP

In addition to fly ash, which is a chemical stabilizer, the existing asphalt pavement was milled and mixed into the subgrade to increase the aggregate content of the soil. The existing asphalt pavement was severely deteriorated with large full depth (300 mm thick) patches and extensive areas of fatigue cracking, alligator cracking, and large potholes. Figure 13 shows the existing pavement with fatigue cracking and a large pothole. Figure 14 shows an up-close picture of alligator cracking. Figure 15 depicts large full depth patches and alligator cracking.

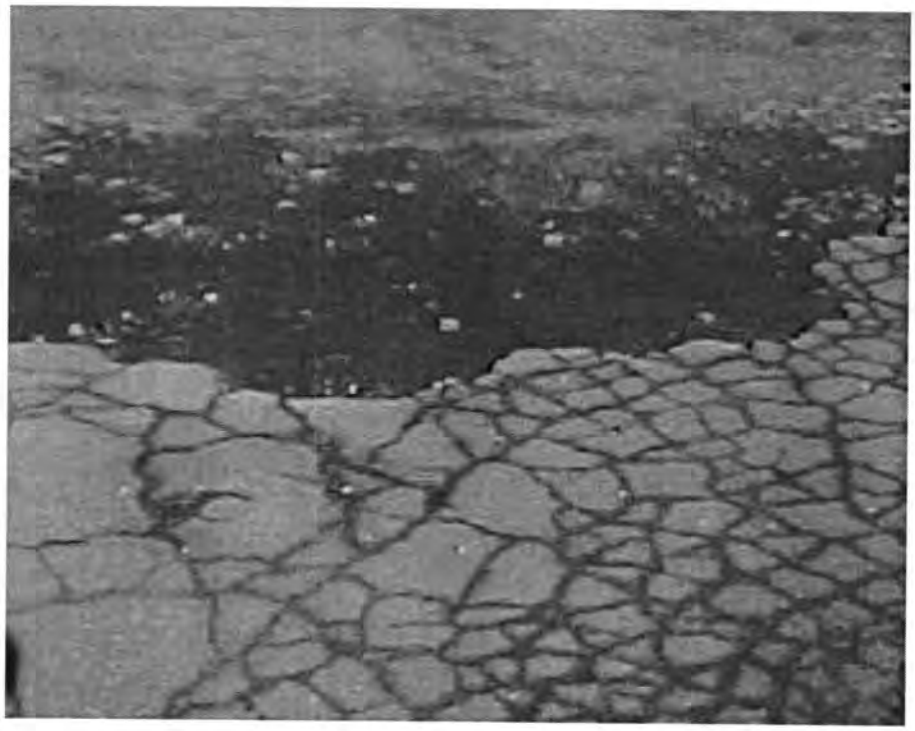

Figure 13. Existing Asphalt Pavement Showing Pothole and Fatigue Cracking

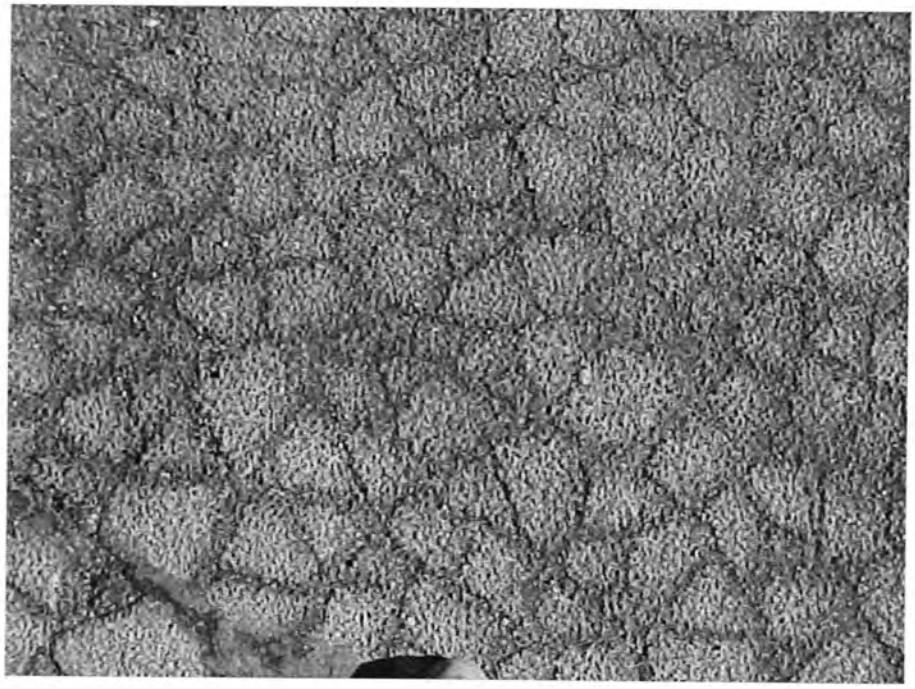

Figure 14. Severe Alligator Cracking

Figure 15. Alligator Cracking with Large Patches

Comparative Grain Size Analysis of Soil, Soil-Rap, and Fly Ash-RAP-Soil Mixtures

Figure 16 shows the grain size distribution curves for the various samples collected. Note the increase in gravel and sand particles due to the addition of RAP. Table 3 shows the classification of each soil tested.

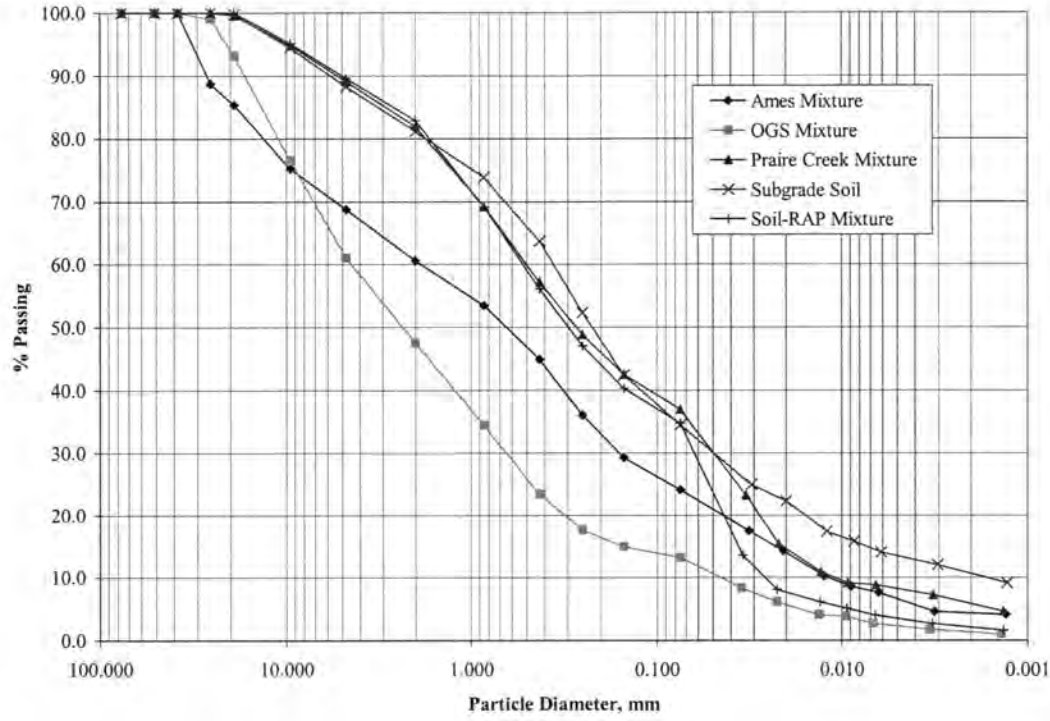

Figure 16. Grain Size Distributions for Soil, Soil-RAP, and Soil-RAP-Fly Ash Mixtures

Table 3. AASHTO and USCS Soil Classification for Soil, Soil-RAP, and Soil-RAP-Fly Ash Mixtures

Sample	AASHTO	USCS	LL	PI	% Gravel	% Sand	% Silt	% Clay
RAP/Soil	A-2-6	SC	24	11	17.1	48.1	32.8	2.0
Prairie Creek Fly Ash/RAP/Soil	A-4	SC	27	7	18.0	45.1	30.9	6.0
OGS Fly Ash/RAP/Soil	A-1-a	SC-SM	19	5	52.5	34.3	12.2	1.0
Ames Municipal Fly Ash/RAP/Soil	A-1-b	SM	29	2	39.4	36.5	19.1	5.0
Subgrade Soil	A-2-6	SC	25	11	18.8	46.7	24.5	10.0

RESULTS

This results section is divided into three components: (1) Construction Operations, (2) Field Results, and (3) Laboratory Results. Each section details specific outcomes pertaining to that section.

Construction Operations

Using the previously detailed construction operation, three results were attained: (1) Improved paving platform, (2) Improved pavement durability and performance, and (3) Cost effectiveness.

Result 1: Improved Paving Platform

The first result was an improved paving platform that adequately supported paving operations. Figure 17 shows excessive rutting due to unstable subgrade under construction traffic loading. Figure 18 shows the same location 27 days later during the application of the binder course in the paving operation. Note the absence of rutting.

Result 2: Improved Pavement Durability and Performance

Analysis of the FWD data shows increased AASHTO structural number and increased equivalent single axle load (ESAL's) to failure. Table 4 shows the relationship between the 8.84 inch pavement section and newly constructed Lot S5's durability and performance. The new AASHTO structural number was about 1.3 times the existing AASHTO structural number, and the ESAL's increased 7 to 21 times depending upon the calculation method.

Figure 17. Severe Rutting Due to Unstable Subgrade

Figure 18. New Paving Platform without Rutting

Table 4. Structural Comparison Between the 8.84 inch and Constructed Pavement Sections (Courtesy of Brian Tomlinson of Snyder and Associates)

	Constructed	8.84 Inch
AASHTO Structural Number	5.04	3.09
ESAL's Using winPASS	51,460,300	7,434,500
ESAL's Using PEDMOD	11,919,000	557,500

Result 3: Comparative Cost Effectiveness

Table 5 displays the comparative cost analysis for the 8.84 inch construction method to the stabilized subgrade technique used. Note that the two pavement replacement techniques are essentially the same in cost.

Table 5. Comparative Cost Analysis for the 8.84 inch and Constructed Pavement Sections (Courtesy of Brian Tomlinson of Snyder and Associates)

	Constructed	8.84 Inch
Cost per Square Yard	$21.62	$21.63

Field Results

This section details results obtained from the DCP testing procedures and FWD tests both before and after pavement rehabilitation. The DCP and FWD tests reveal a stiffer subgrade that is more resistant to deformation under load.

DCP Field Testing Results

DCP field testing results show a remarkable decrease in mean DCP index from 40 to 5 mm per blow. Figure 19 shows the relationship between the mean DCP index and time

after compaction for the Ames fly ash-soil-RAP mixture with 95% confidence intervals. This outcome is to be expected with the cementing and pozzolanic action of the self-cementing fly ash. Figures 20 and 21 show the California Bearing Ratio (CBR) plots for the Ames fly ash-RAP-soil mixture immediately after compaction and 27 days after compaction respectively. Note that the CBR is increased about 15 to20 times. Other DCP and CBR data can be found in the Appendix.

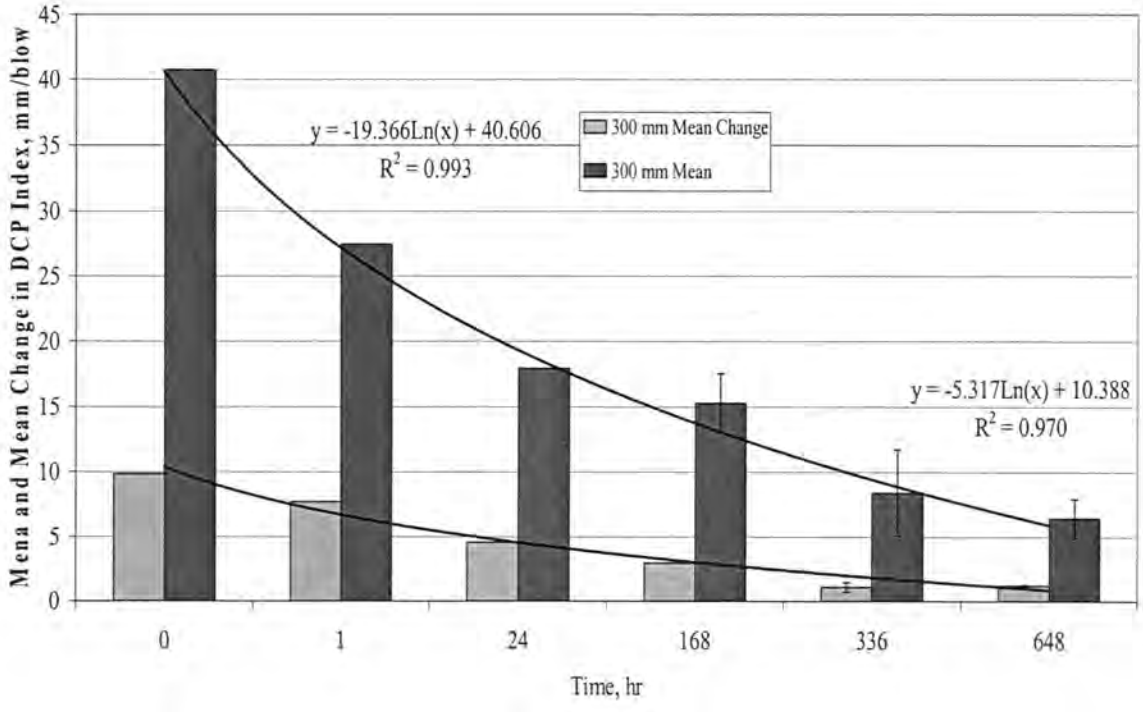

Figure 19. Mean and Mean Change in DCP Index versus Time after Compaction for Ames Municipal Fly Ash-RAP-Soil Mixture

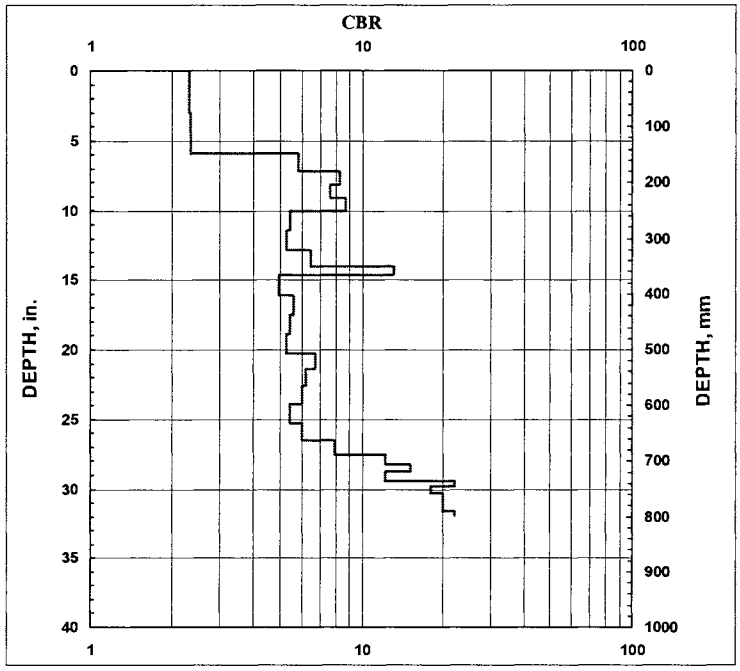

Figure 20. CBR Profile for the Ames-RAP-Soil Mixture Immediately After Compaction

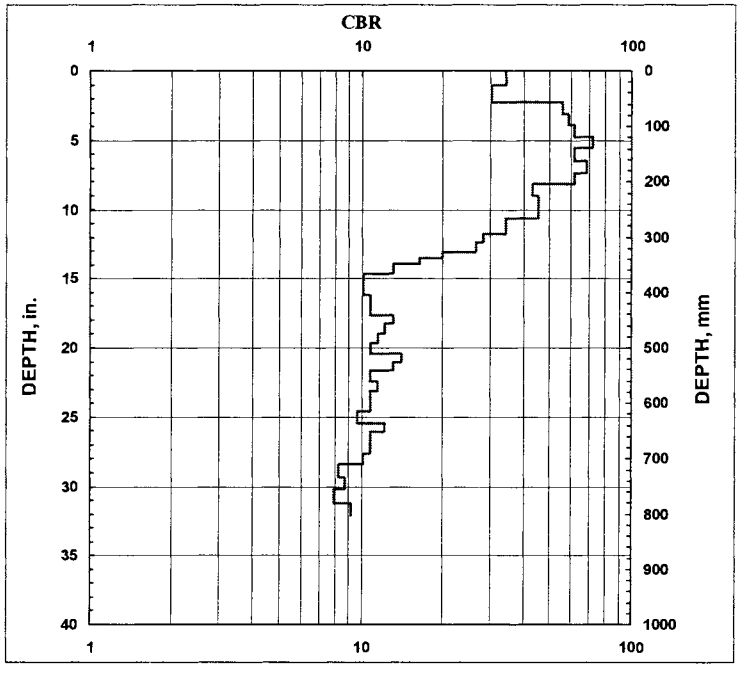

Figure 21. CBR Profile for the Ames-RAP-Soil Mixture 27 Days After Compaction

FWD Results

FWD testing completed both before and after stabilization revealed that the Lot S5 stabilized basin was reduced about 80% or a deflection reduction of about 30 mils. Figure 22 shows the FWD deflection basins for Lots S3 and S5 before stabilization, and Figure 23 shows the average FWD deflection basins for Lots S3 and S5 after completion of stabilization and paving operations. Note that Lot S3 is the control lot as no construction work was completed in that lot.

Figures 24 and 25 show the back calculated modulus results for the pavement sections before and after reconstruction respectively. Note that the modulus of rupture for the stabilized base is about 8.5 times that of the subgrade.

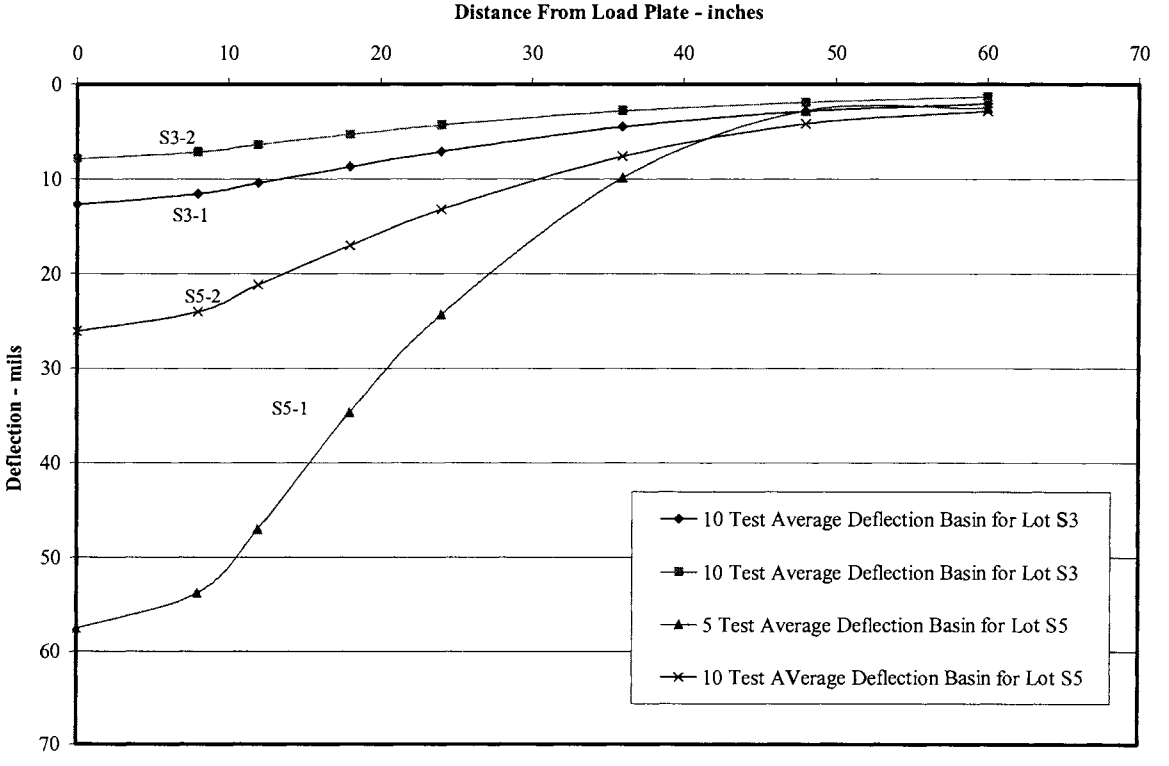

Figure 22. FWD Deflection Basins for Parking Lots S3 and S5 before Reconstruction

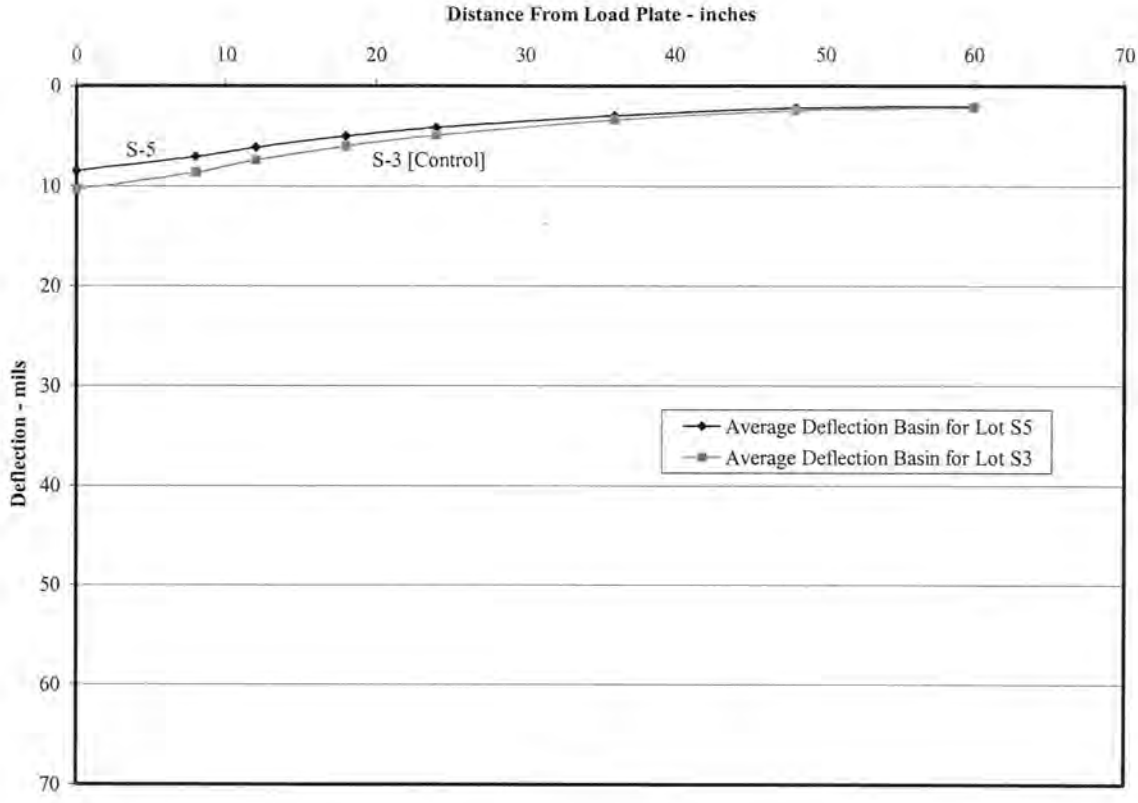

Figure 23. Average (10 Tests) FWD Deflection Basins for Lots S3 and S5 after Reconstruction

6" HMA Mr = 340,000 psi

Subgrade Mr = 170,000 psi

Figure 24. Back Calculated Modulus of Rupture Results for the Pavement Section before Reconstruction

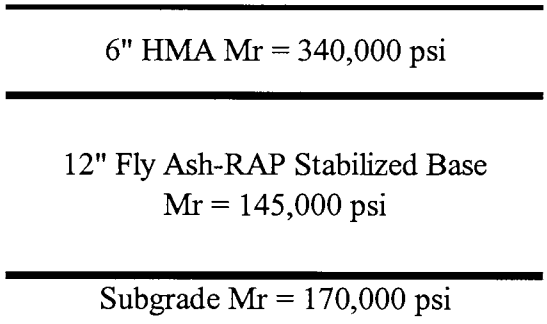

Figure 25. Back Calculated Modulus of Rupture Results for the Pavement Section after Reconstruction

Laboratory Results

This section details results obtained from the laboratory testing procedures including: unconfined compression test, Proctor test, consolidated undrained (CU) triaxial load test, and scanning electron microscopy (SEM) analysis. Unconfined compression test results show increased compressive strength with cure time. Laboratory prepared unconfined compression strength tests results are about the same as field prepared unconfined compression strength results. CU triaxial load test results show a two to four times increase of the CU strength with the addition of self-cementing fly ash. SEM analysis shows even coating of the soil and RAP particles with fly ash and no formation of undesirable byproducts.

Unconfined Compression Tests

Table 6 shows that the average 28-day unconfined compression strengths for the Chillicothe, Prairie Creek, and Ames fly ash mixtures range from 600 to 800 kPa. The resulting difference in unconfined compressive strengths between the various fly ash sources

may be due to varying moisture content at compaction. Strength differences could also arise due to varying amounts of fly ash in each sample.

Figure 26 shows the relationship between strength gain and curing time for the Ames fly ash mixtures with 95% confidence intervals. The tests show that the majority of the strength gain is achieved within the first one to two days after compaction.

Table 6. Average 28-Day Unconfined Compressive Strengths

Fly Ash Treatment	Number of Tests	Average Unconfined Compressive Strength (kPa)	Standard Deviation
Prairie Creek	3	603	111
OGS	2	868	93
Ames	5	595	417

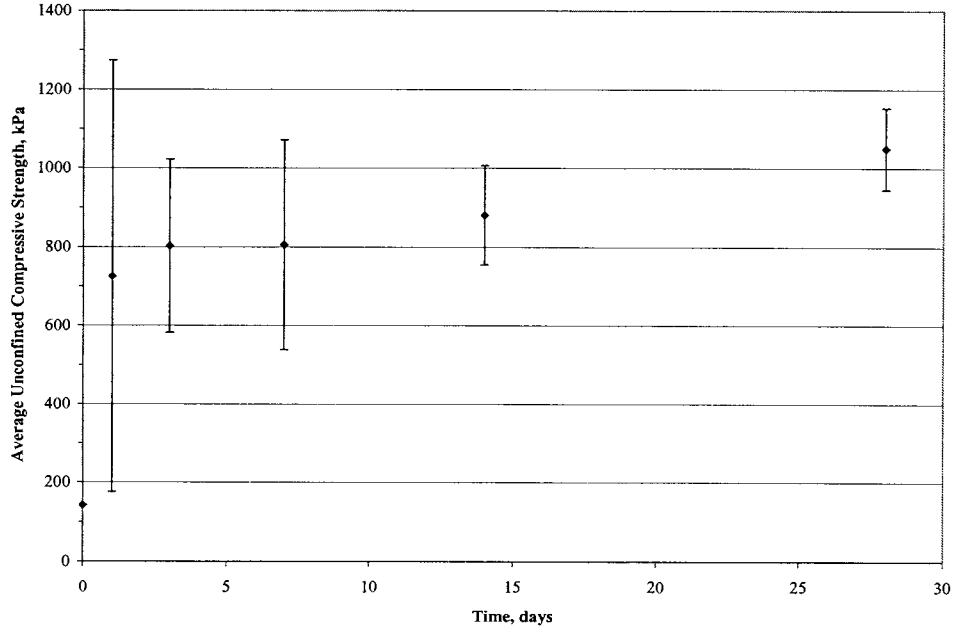

Figure 26. Strength Gain versus Time for the Ames Ash-RAP-Soil Mixture

While studying the effect of time on the DCP index and strength of the stabilized mixture, it was noted that both increased or decreased dramatically. It was hypothesized that there would be a characteristic curve correlating unconfined compressive strength with DCP stiffness. Figure 27 shows this linear relationship for the mean DCP index interval shown. Note that the linear relationship is moderate, and would be an indicator of field strengths.

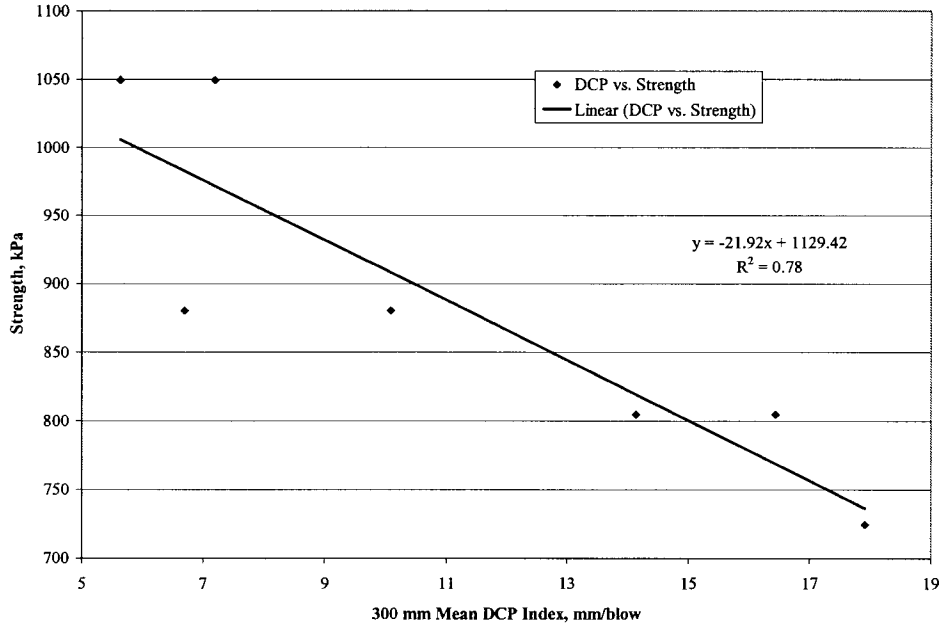

Figure 27. Relationship between Unconfined Compressive Strength and 300 mm Mean DCP Index

Laboratory Proctor and Unconfined Compression Strength Test Results

Figure 28 shows Proctor test results for the 50% RAP, 50% subgrade soil, and 10% Ames fly ash mixture. The figure indicates a maximum dry density of about 1870 kg/m^3 and optimum moisture content of about 11.5%. Figure 29 shows the comparison of unconfined compressive strengths between the various samples versus the percent moisture.

Note that strength of the soaked samples was half the unsoaked samples dry of 8% moisture content. Samples performed comparable to the non-soaked samples wet of 8% moisture content. Also, the non-soaked samples strength curve continues upward dry of optimum moisture content based on strength, which is to be expected.

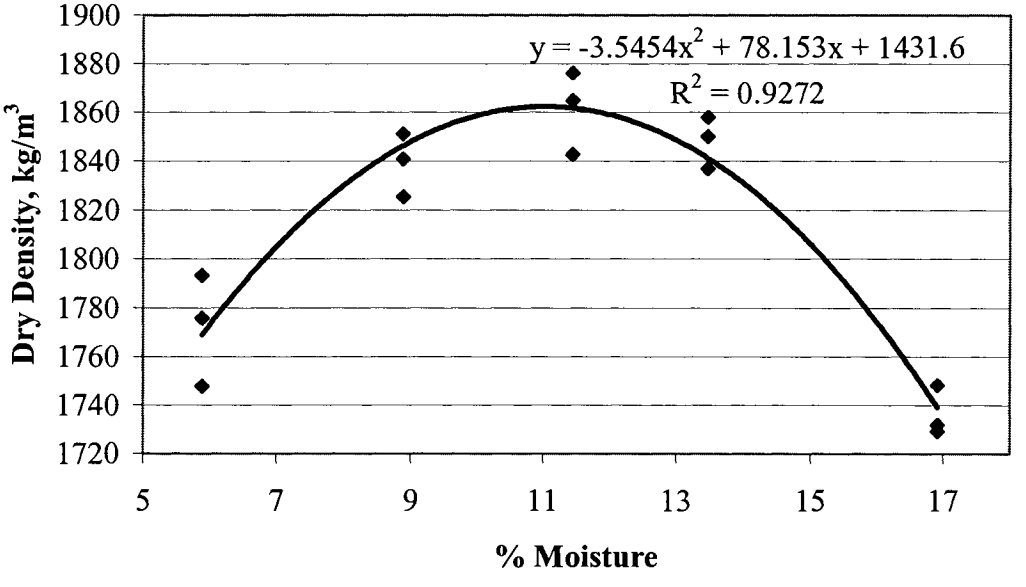

Figure 28. Proctor Curve for 50% RAP, 50% Subgrade Soil, and 10% Ames, Fly Ash Mixture by Dry Weight

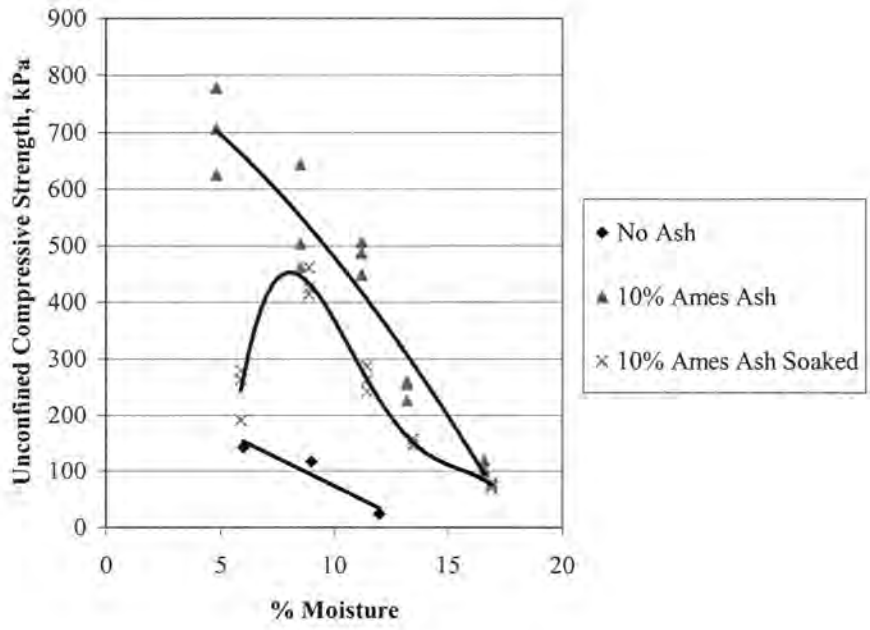

Figure 29. Comparison of Unconfined Compressive Strength versus Percent Moisture

Consolidated Undrained Triaxial Load Test

This section details results obtained from CU tests conducted on the following mixtures: subgrade soil, soil-RAP, OGS fly ash-soil-RAP, Prairie Creek fly ash-soil-RAP, and Ames fly ash-soil-RAP.

Table 7 shows the results for all CU test samples. Negative pore pressures indicate expansion at failure. The soil, soil-RAP, and Ames ash-soil-RAP mixtures exhibit strain-hardening behavior. The OGS-soil-RAP mixture shows a slight strain-softening behavior, and the Prairie Creek ash-soil-RAP mixture shows strain-softening behavior. The strength gain from the addition of fly ash is shown with the increasing major principle stresses.

Table 7. CU Triaxial Load Test Results for All Samples

	Property at Failure						
Mixture	Confining Pressure (kPa)	Axial Strain %	Deviator Stress (kPa)	Pore Pressure (kPa)	Effective Major Principal Stress (kPa)	Effective Minor Principal Stress (kPa)	Effective Principal Stress Ratio
Subgrade Soil	20.7	1.3	18.5	-15.2	54.5	35.6	1.5
	48.3	1.3	18.0	2.1	64.2	46.2	1.4
Subgrade Soil-RAP	20.7	1.3	17.5	-9.7	47.9	30.3	1.6
	34.5	1.3	18.9	-9.7	63.0	44.1	1.4
	48.3	1.3	17.9	5.5	60.7	42.7	1.4
Ames Fly Ash-Soil-RAP	20.7	1.0	42.2	-6.9	70.0	27.6	2.5
	34.5	1.0	67.1	-5.5	107.1	40.0	2.7
	48.3	1.2	71.1	-37.9	157.2	86.2	1.8
Prairie Creek Fly Ash-Soil-RAP	20.7	1.2	73.8	-26.9	121.4	45.6	2.6
	48.3	1.2	92.6	-17.9	158.8	66.2	2.4
OGS Fly Ash-Soil-RAP	20.7	3.8	94.4	-209.6	324.7	230.3	1.4
	48.3	3.8	93.6	-171.7	313.6	219.9	1.4

Subgrade Soil Mixture

Figures 30 to 34 show the CU results for the subgrade soil. Note the negative pore pressures generated during loading. The stress-strain relationship is characteristic of strain-hardening behavior. The negative pore water pressures also show expansion of the sample during testing.

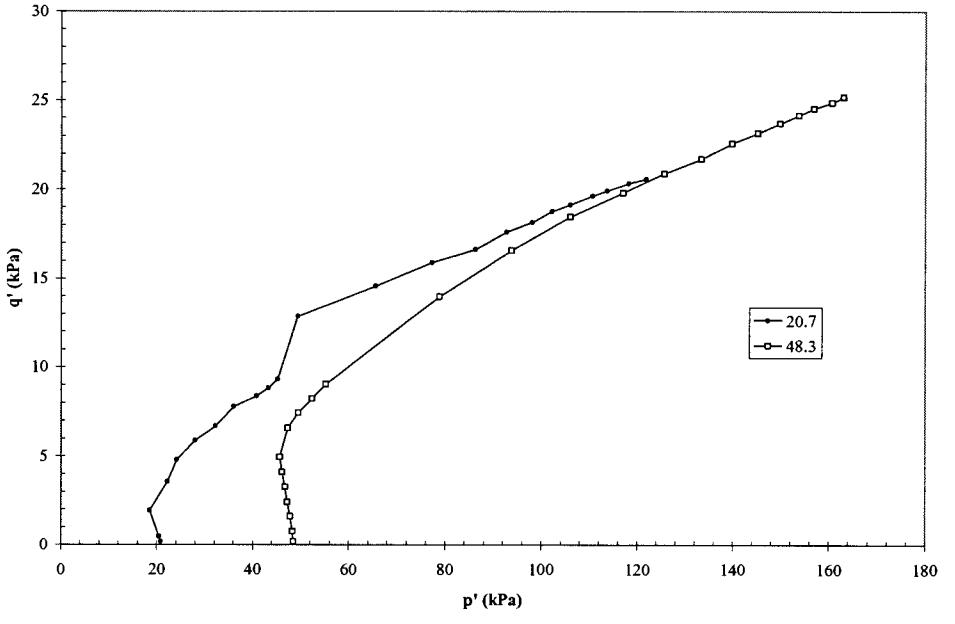

Figure 30. p-q Diagram for Subgrade Soil

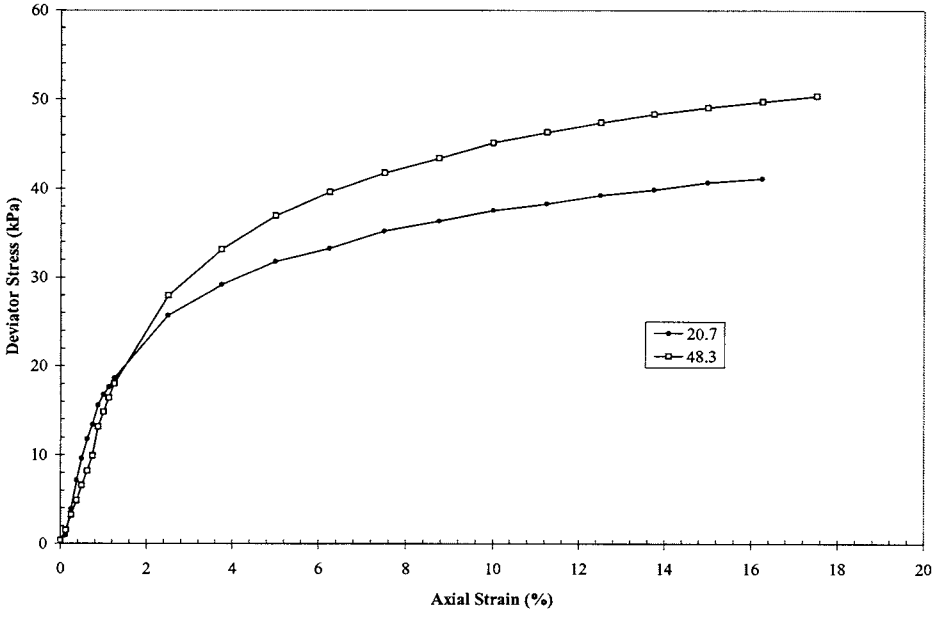

Figure 31. Deviator Stress versus Axial Strain for Subgrade Soil

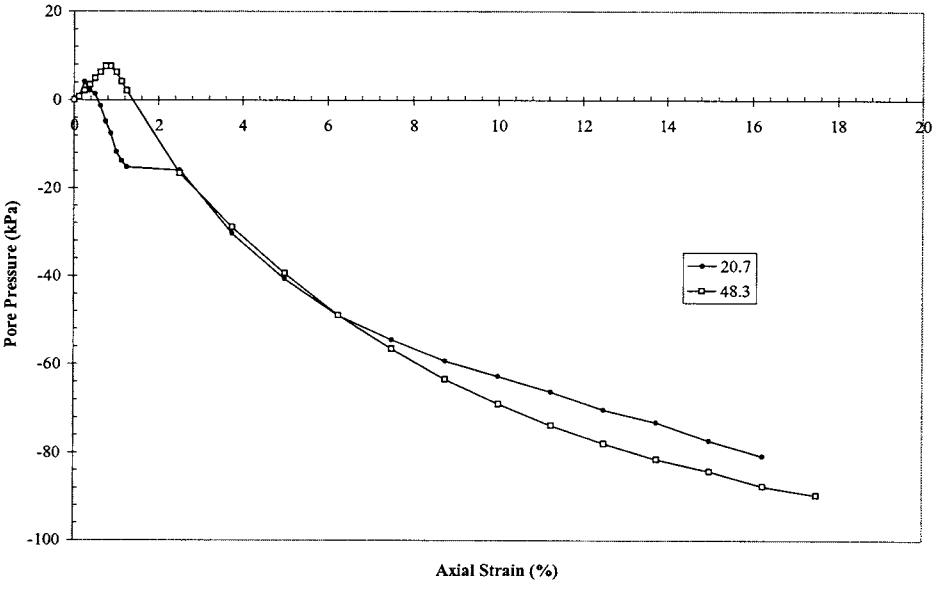

Figure 32. Pore Pressure versus Axial Strain for Subgrade Soil

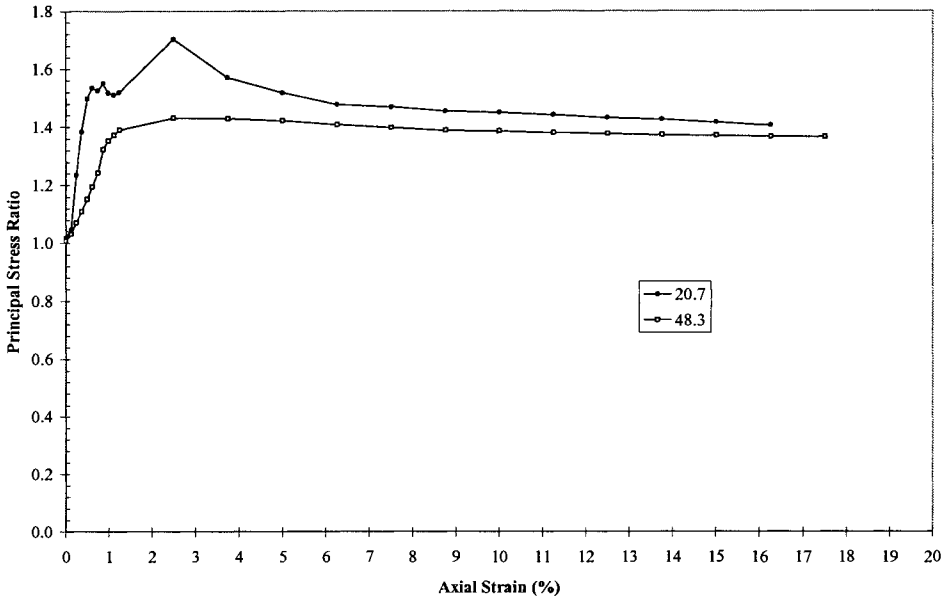

Figure 33. Principal Stress Ratio versus Axial Strain for Subgrade Soil

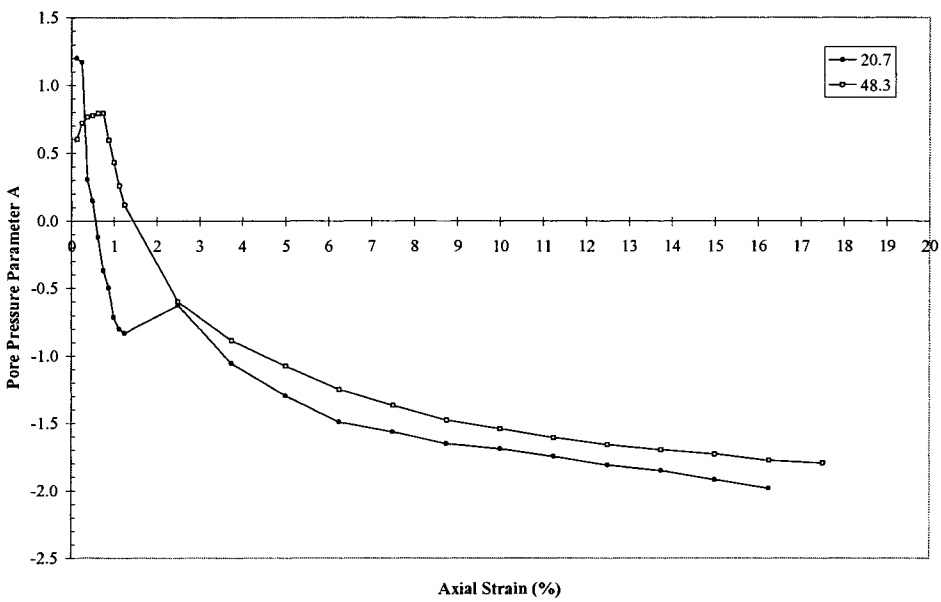

Figure 34. Pore Pressure Parameter A versus Axial Strain for Subgrade Soil

Soil-RAP Mixture

Figures 35 to 39 show the CU results for the soil-RAP mixture. Note that the stress-strain curves exhibit strain-hardening behavior. The deviation stress to failure is about one kPa lower than that of the subgrade soil. The addition of RAP allows failure surfaces to extend out through the sample instead of continuing along the fracture plane. The negative pore water pressure developed during testing indicates expansion during testing.

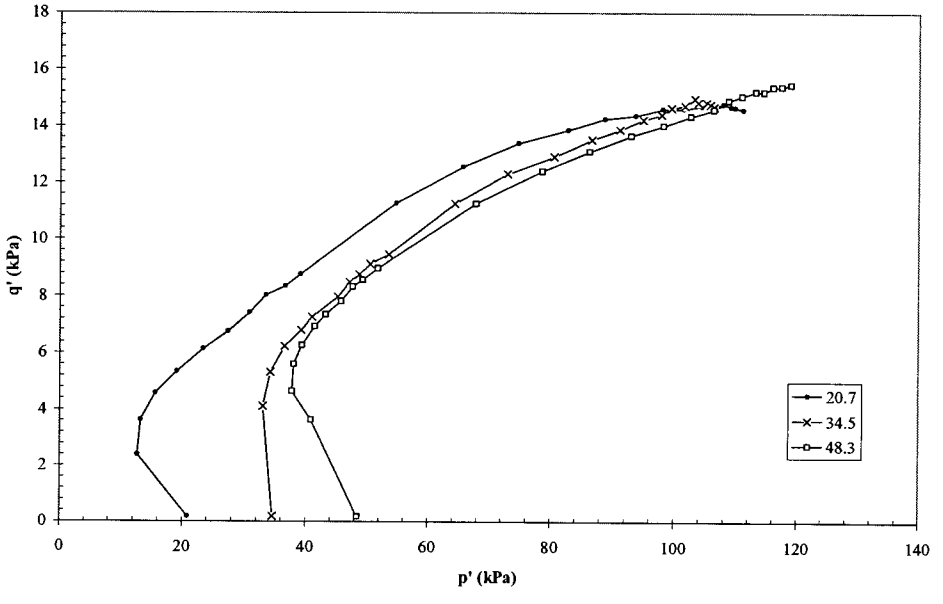

Figure 35. p-q Diagram for the Soil-RAP Mixture

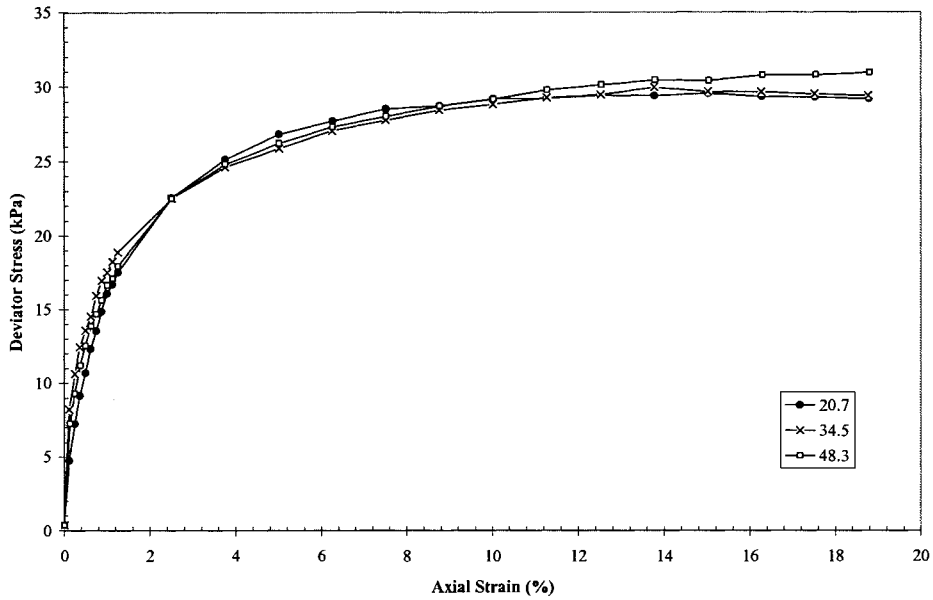

Figure 36. Deviator Stress versus Axial Strain for the Soil-RAP Mixture

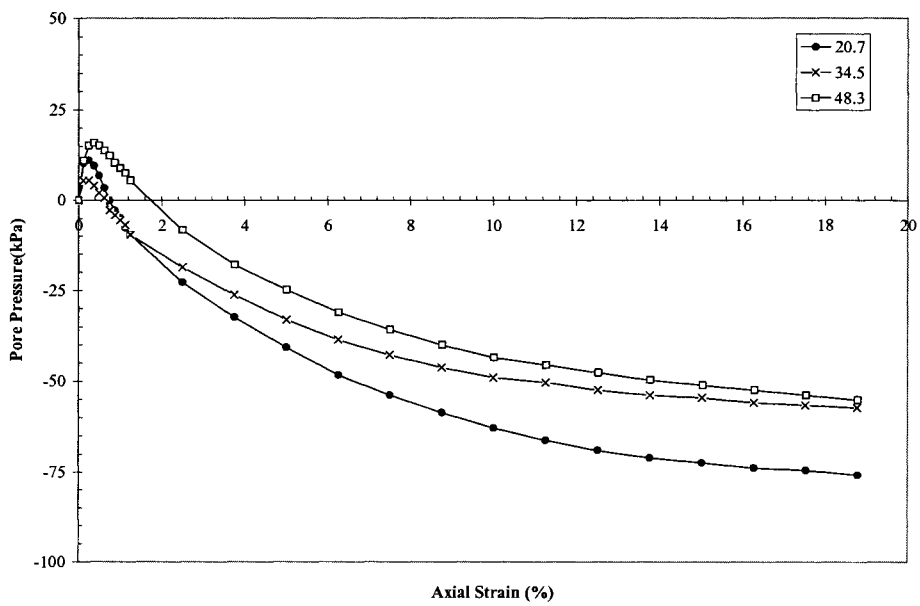

Figure 37. Pore Pressure versus Axial Strain for the Soil-RAP Mixture

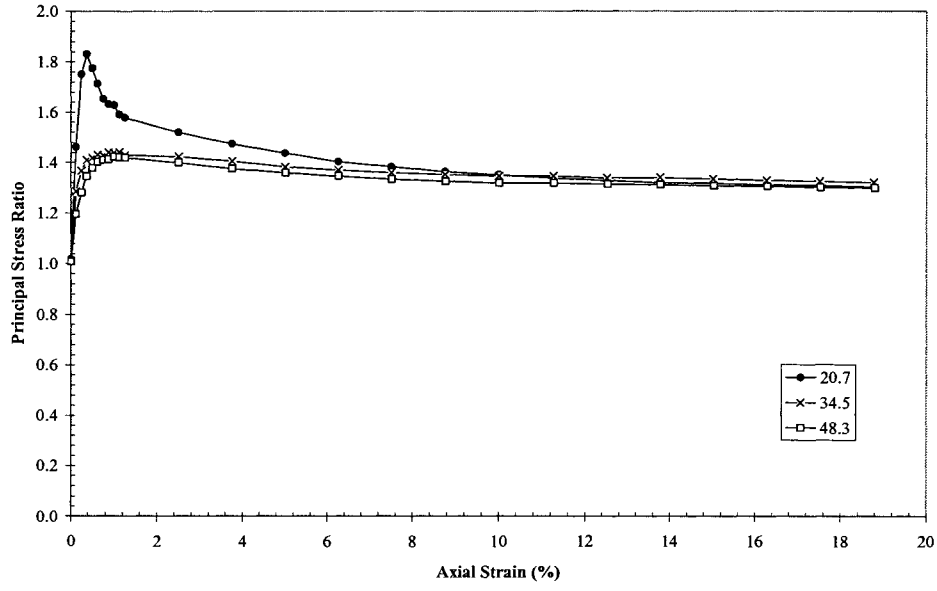

Figure 38. Principal Stress Ratio versus Axial Strain for the Soil-RAP Mixture

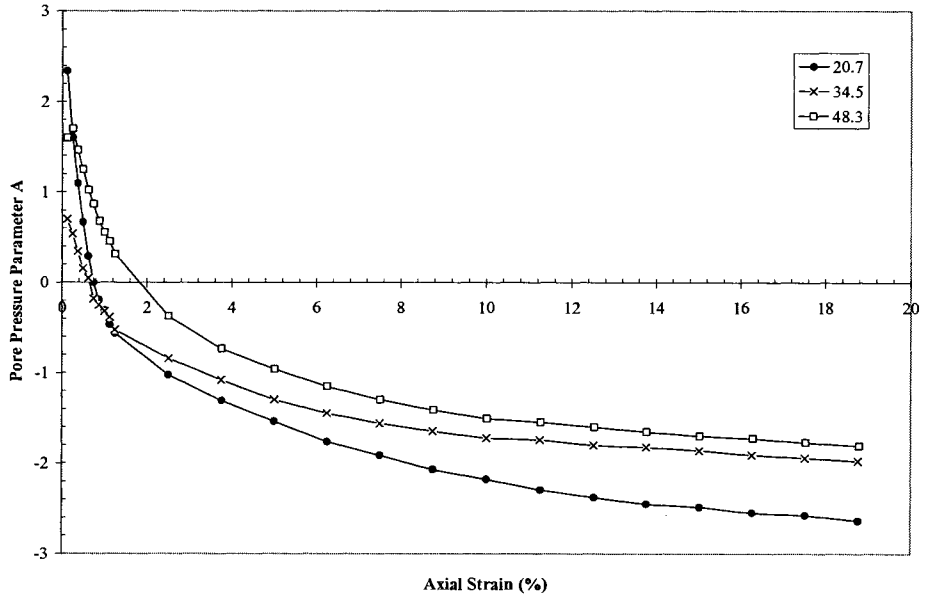

Figure 39. Pore Pressure Parameter A versus Axial Strain for the Soil-RAP Mixture

OGS Fly Ash-Soil-RAP Mixture

The addition of OGS fly ash increases the undrained shear strength about 4 times. The undrained shear strength of the OGS fly ash-soil-RAP mixture is about 5 times greater than that of the soil-RAP mixture, and about 1.5 to 2 times greater than the Ames-soil-RAP mixture. The CU test results for the OGS-soil-RAP mixture are shown in Figures 40 to 44. The stress-strain curve also shows slight strain softening. The OGS-soil-RAP mixture attained the highest undrained shear strength of the three samples with self-cementing fly ash.

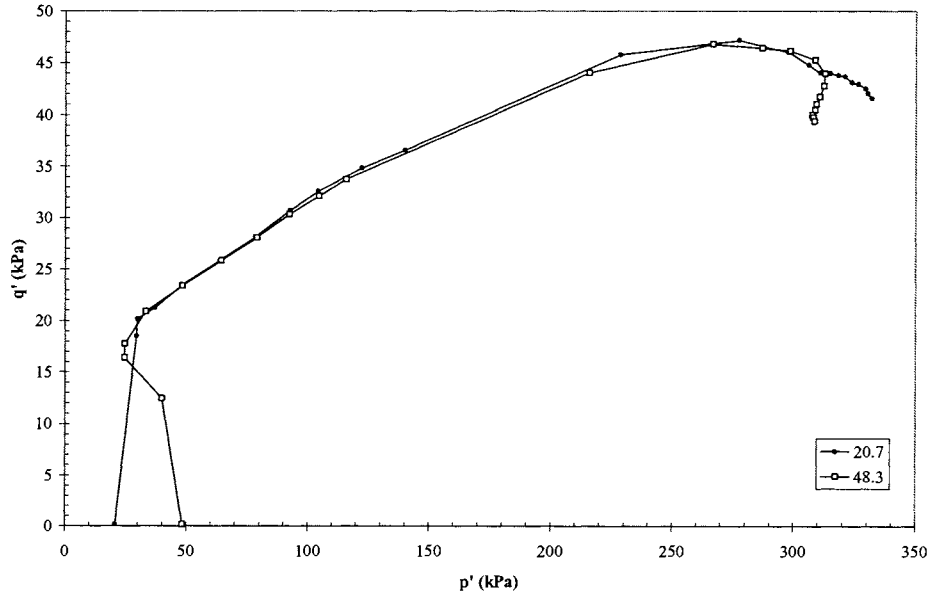

Figure 40. p-q Diagram for the OGS-Soil-RAP Mixture

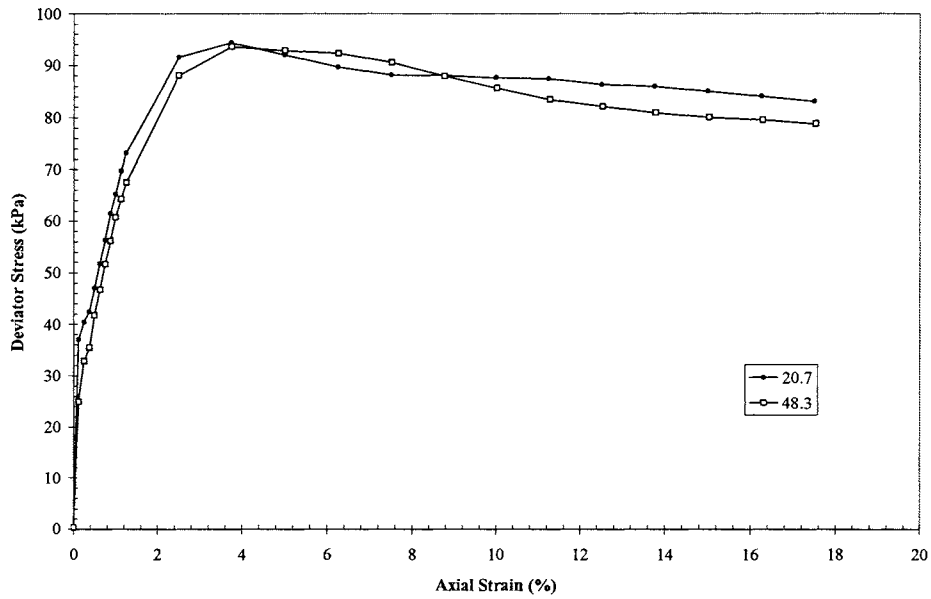

Figure 41. Deviator Stress versus Axial Strain for the OGS-Soil-RAP Mixture

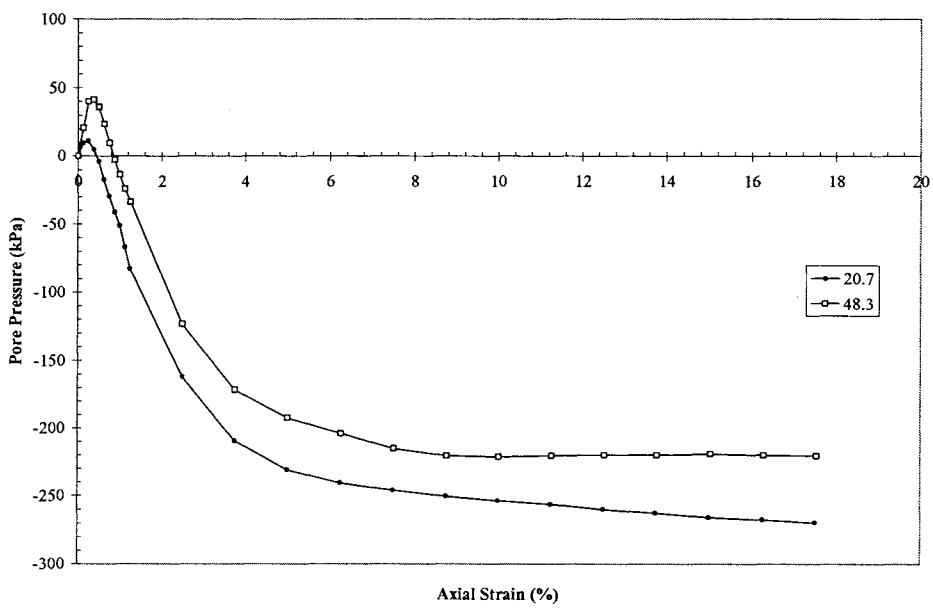

Figure 42. Pore Pressure versus Axial Strain for the OGS-Soil-RAP Mixture

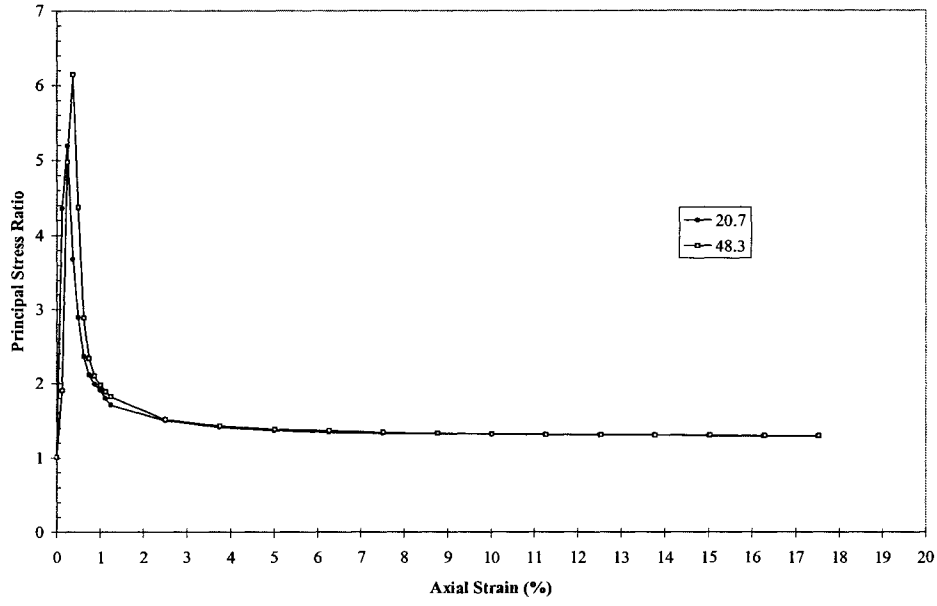

Figure 43. Principal Stress Ratio versus Axial Strain for the OGS-Soil-RAP Mixture

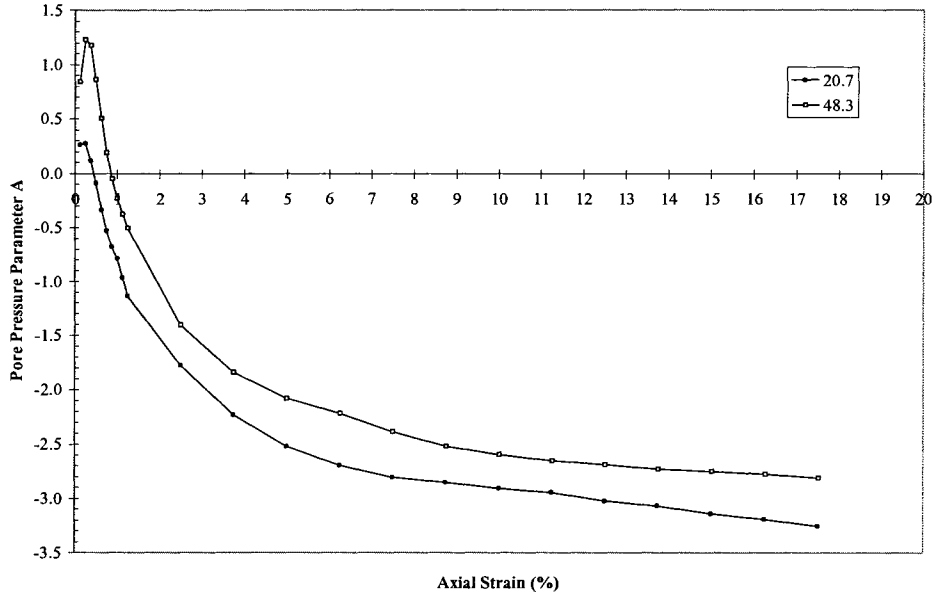

Figure 44. Pore Pressure Parameter A versus Axial Strain for the OGS-Soil-RAP Mixture

Prairie Creek Fly Ash-Soil-RAP

The addition of Prairie Creek fly ash increases the undrained shear strength by about 4 times. The undrained shear strength of the Prairie Creek fly ash-soil-RAP mixture is about 5 times greater than that of the soil-RAP mixture. The CU results for the Prairie Creek fly ash-soil-RAP mixture are described in Figures 45 to 49. The Prairie Creek-soil-RAP samples exhibited strain-softening behavior that expanded upon shearing. This is can be seen with the peak in the stress-strain curve and the high negative pore water pressures developed during loading.

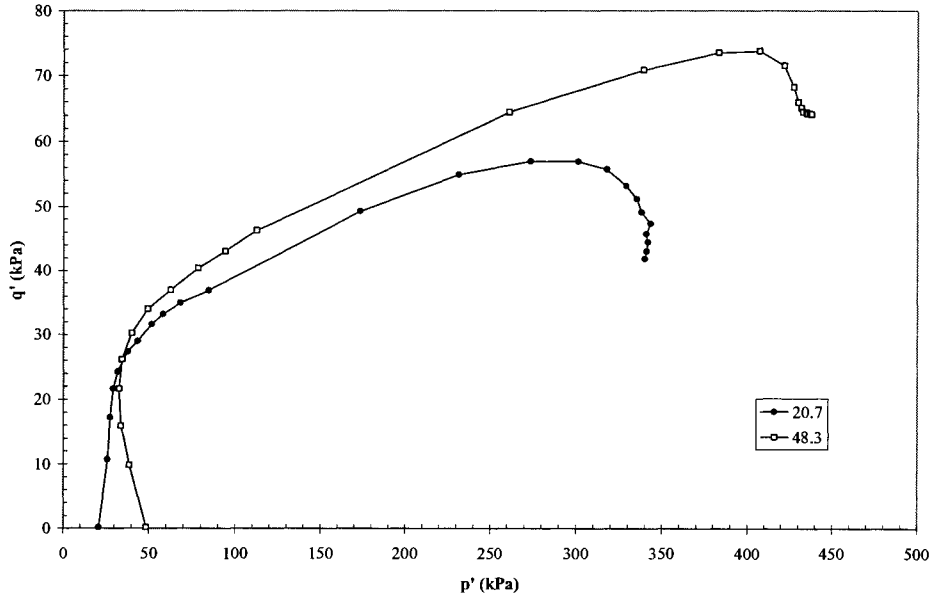

Figure 45. p-q Diagram for the Prairie Creek Fly Ash-Soil-RAP Mixture

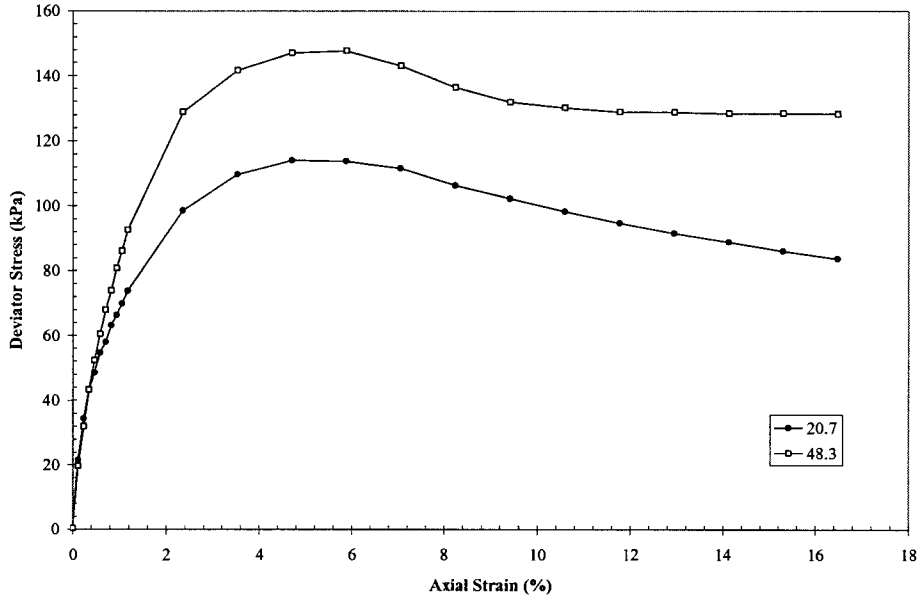

Figure 46. Deviator Stress for the Prairie Creek Fly Ash-Soil-RAP Mixture

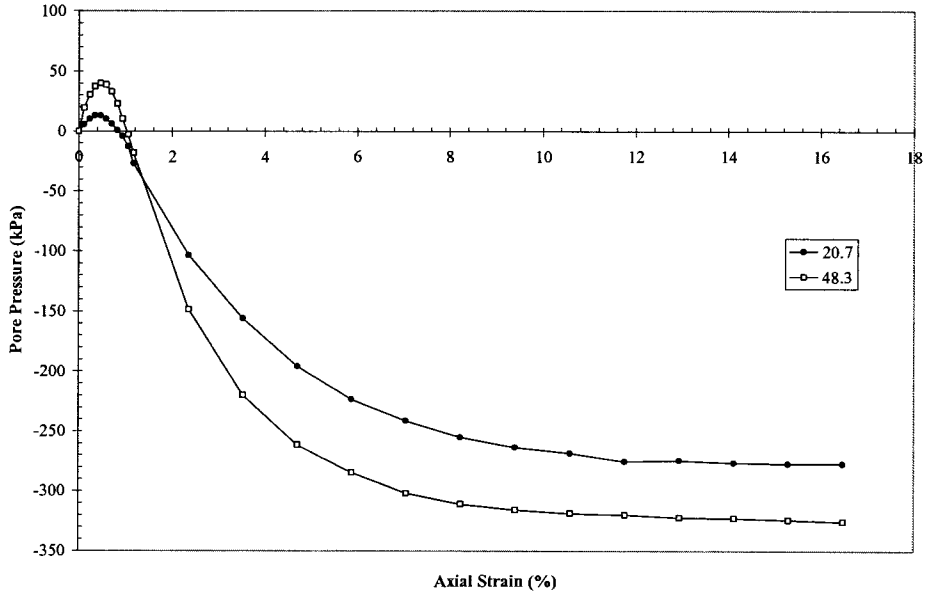

Figure 47. Pore Pressure versus Axial Strain for the Prairie Creek Fly Ash-Soil-RAP Mixture

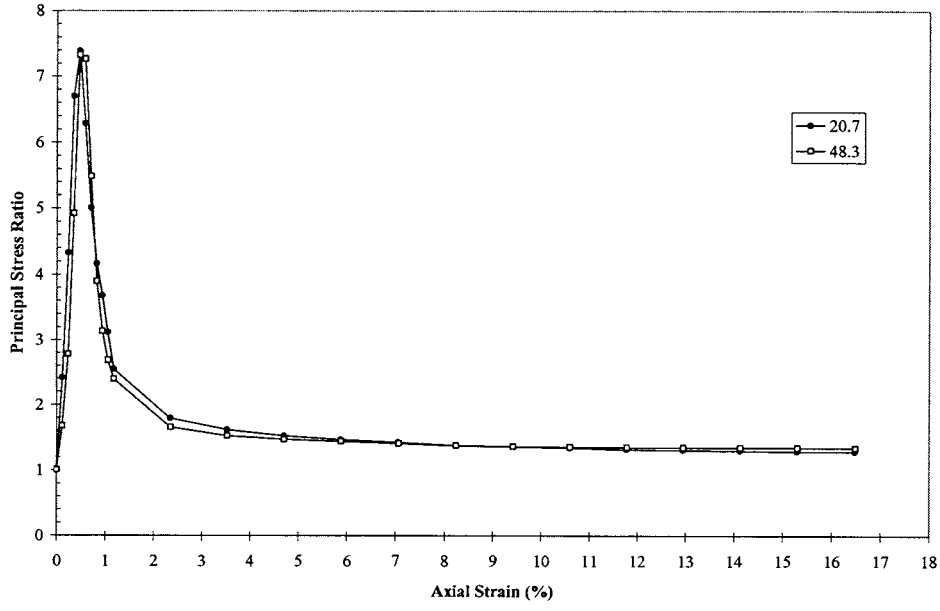

Figure 48. Principal Stress Ratio versus Axial Strain for the Prairie Creek Fly Ash-Soil-RAP Mixture

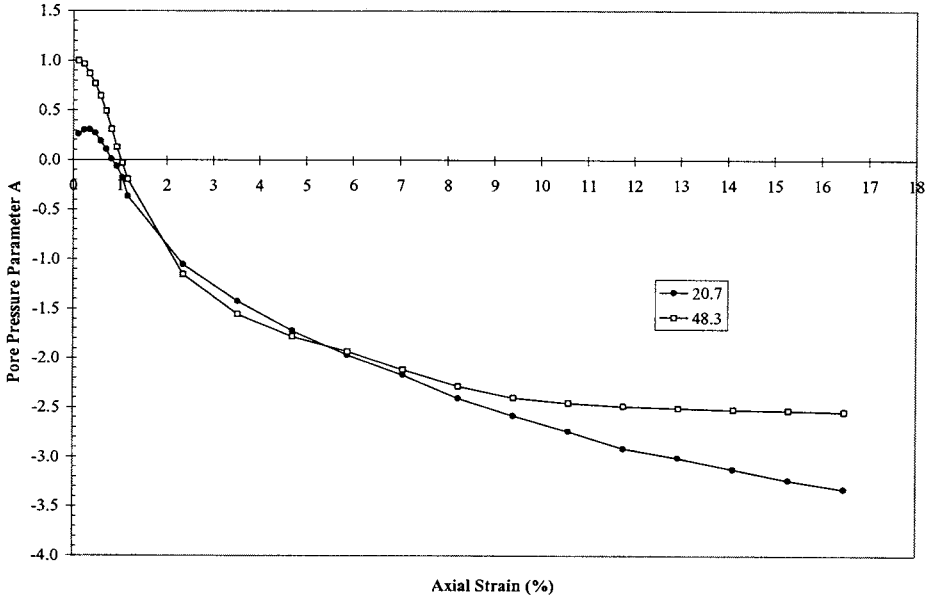

Figure 49. Pore Pressure Parameter A versus Axial Strain for the Prairie Creek Fly Ash-Soil-RAP Mixture

Ames Fly Ash-Soil-RAP Mixture

The addition of Ames fly ash dramatically increases the undrained shear strength by about 3 times. The undrained shear strength of the Ames ash-soil-RAP mixture is about 2 to 4 times greater than that of the soil-RAP mixture. Figures 50 to 54 show the CU test results for the Ames fly ash-soil-RAP Mixture. Note the dramatic increase in shear strength due to the addition of fly ash. The stress-strain curves in Figure 51 show strain-hardening behavior.

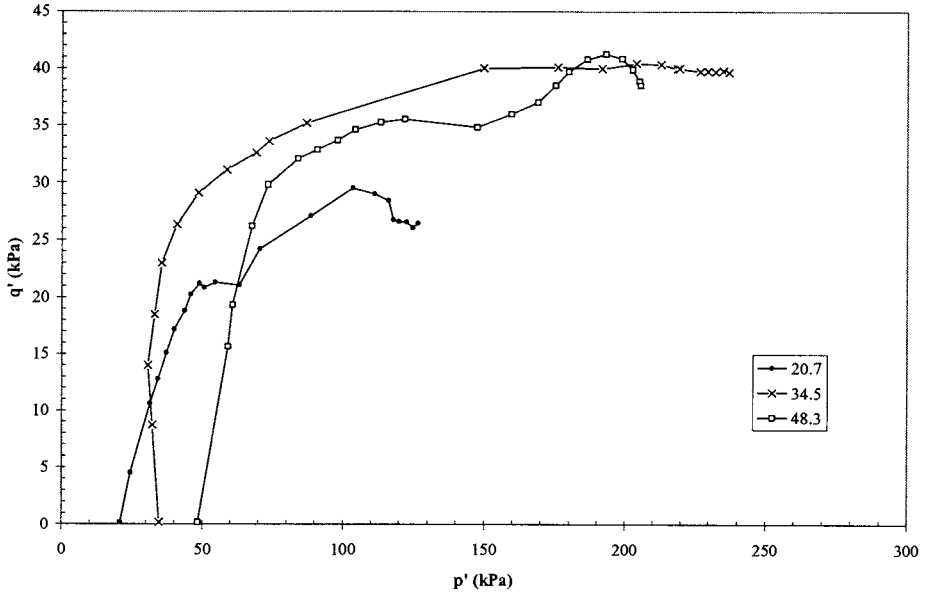

Figure 50. p-q Diagram for the Ames Fly Ash-Soil-RAP Mixture

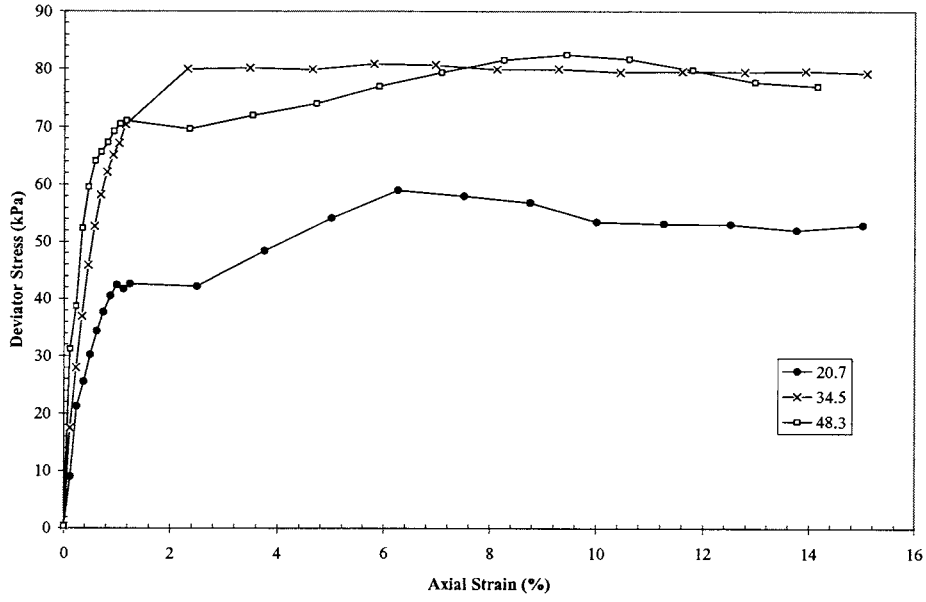

Figure 51. Deviator Stress versus Axial Strain for the Ames Fly Ash-Soil-Rap Mixture

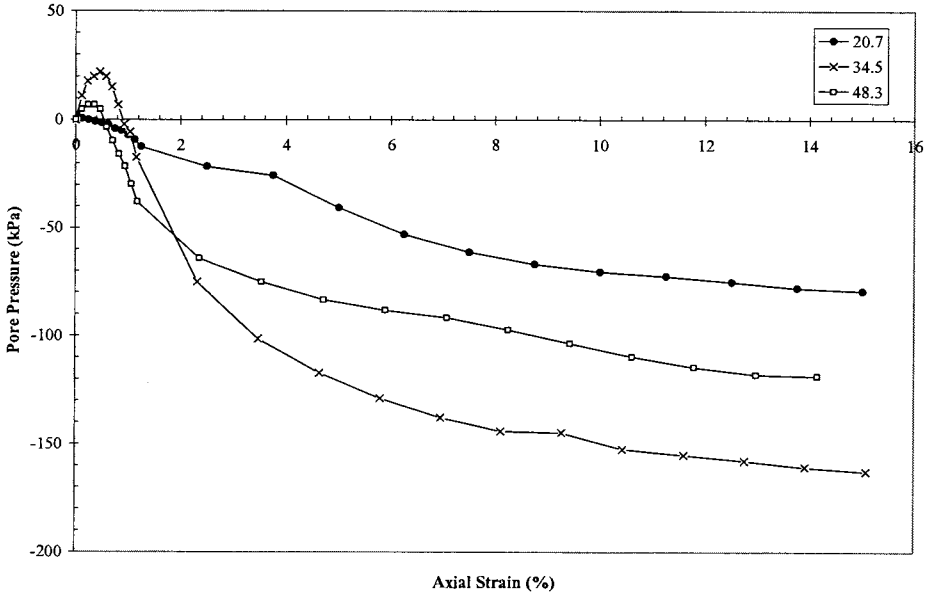

Figure 52. Pore Pressure versus Axial Strain for the Ames Fly Ash-Soil-RAP Mixture

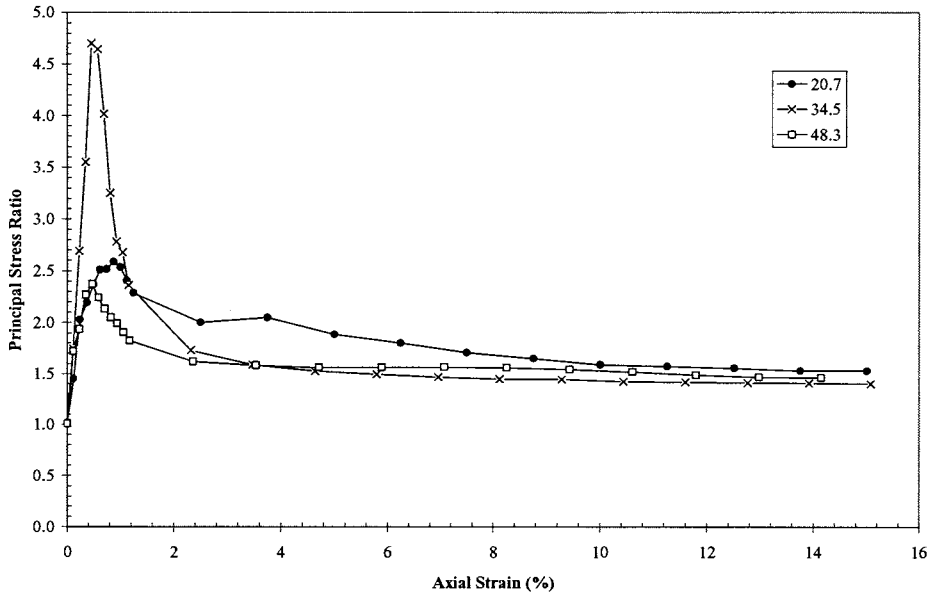

Figure 53. Principal Stress Ratio versus Axial Strain for the Ames Fly Ash-Soil-RAP Mixture

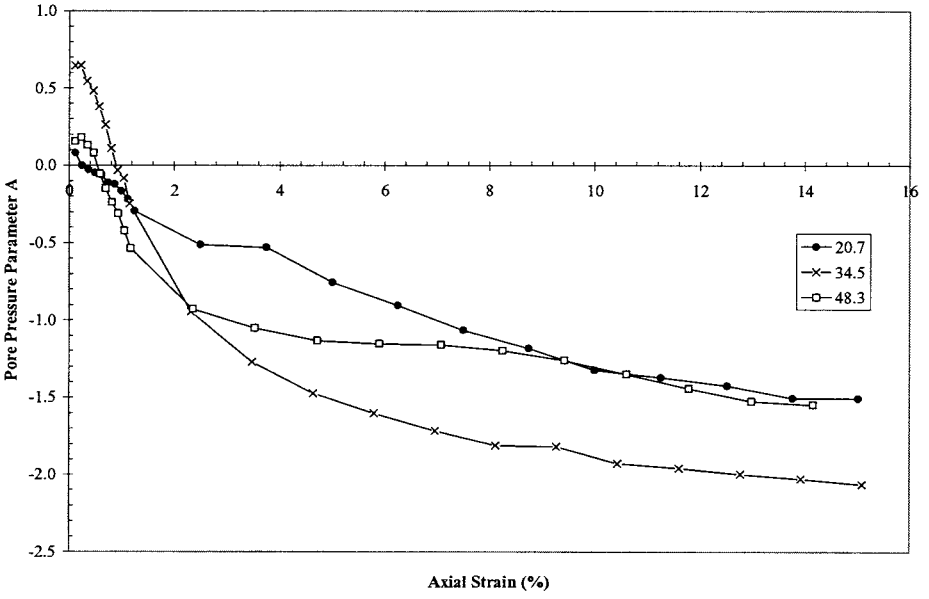

Figure 54. Pore Pressure Parameter A versus Axial Strain for the Ames Fly Ash-Soil-RAP Mixture

Table 8 shows a summary of the effective cohesion and friction angle, as well as the modulus at 50% of failure. Note that there is no apparent friction angle for the subgrade soil-RAP and OGS fly ash-soil-RAP mixtures. Addition of self cementing fly ash increased the friction angle 3 to 5 times compared to the subgrade soil.

Table 8. Effective Cohesion, Effective Friction Angle, and Modulus at 50% of Failure

Mixture	C' kPa	Φ' Degrees	E_{50} kPa
Subgrade Soil	11	2	18
Subgrade Soil-RAP	11	0	23
Ames Fly Ash-Soil-RAP	14	11	86
Prairie Creek Fly Ash-Soil-RAP	25	7	73
OGS Fly Ash-Soil-RAP	47	0	64

Scanning Electron Microscopy

This section details results from SEM analysis of the Ames fly ash-soil-RAP mixture. SEM results show even coating of the RAP and soil particles with fly ash and very little to no formation of expansive minerals. Results also indicate abundance of calcium, silica, and aluminum.

The SEM images are shown in Figures 55 to 57. Figure 55 shows the rough RAP-soil-fly ash surface magnified 150 X illustrating intact pozzolan spheres and coating of the RAP. Figure 56 shows the same image magnified 500 X. Note the long needle-like formations in the top center of the figure. These are potentially sulfur based expansive

minerals. Figure 57 shows the soil-RAP-fly ash magnified 1500 X. Note the intact pozzolan spheres present in the figure.

Figure 58 shows the SEM x-ray analysis, and Figure 59 shows the elemental map for this sample. Note the abundance of calcium, silica, and aluminum. This shows coverage of RAP particles with soil and fly ash because there is no definitive peak for carbon. Figure 58 shows a small peak for sulfur showing that there may be some formation of expansive minerals. Other SEM images can be found in the Appendix.

Figure 55. Ames Fly Ash-Soil-RAP SEM Image Magnified 150X

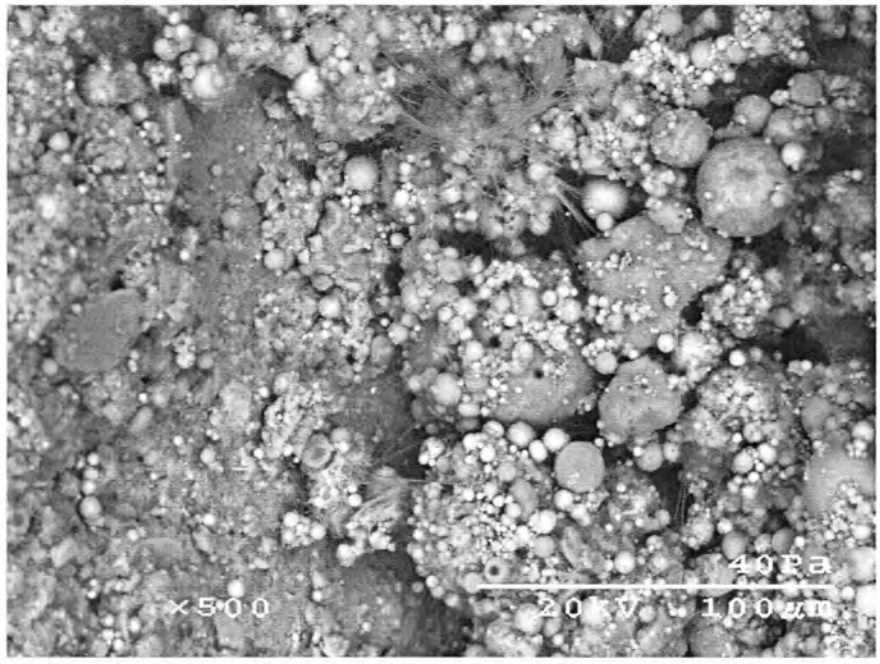

Figure 56. Ames Fly Ash-Soil-RAP SEM Image Magnified 500X

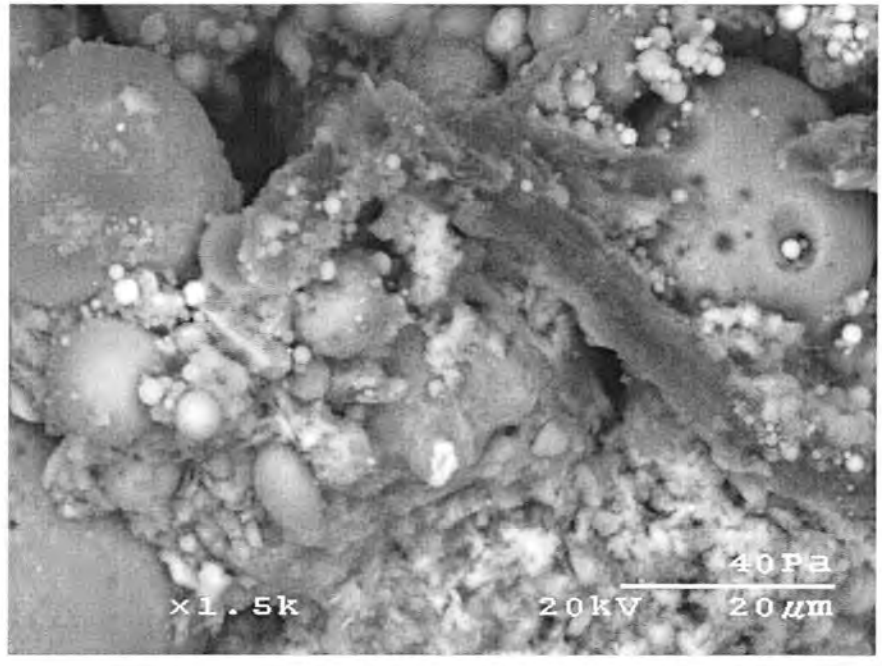

Figure 57. Ames Fly Ash-Soil-RAP SEM Image Magnified 1500X

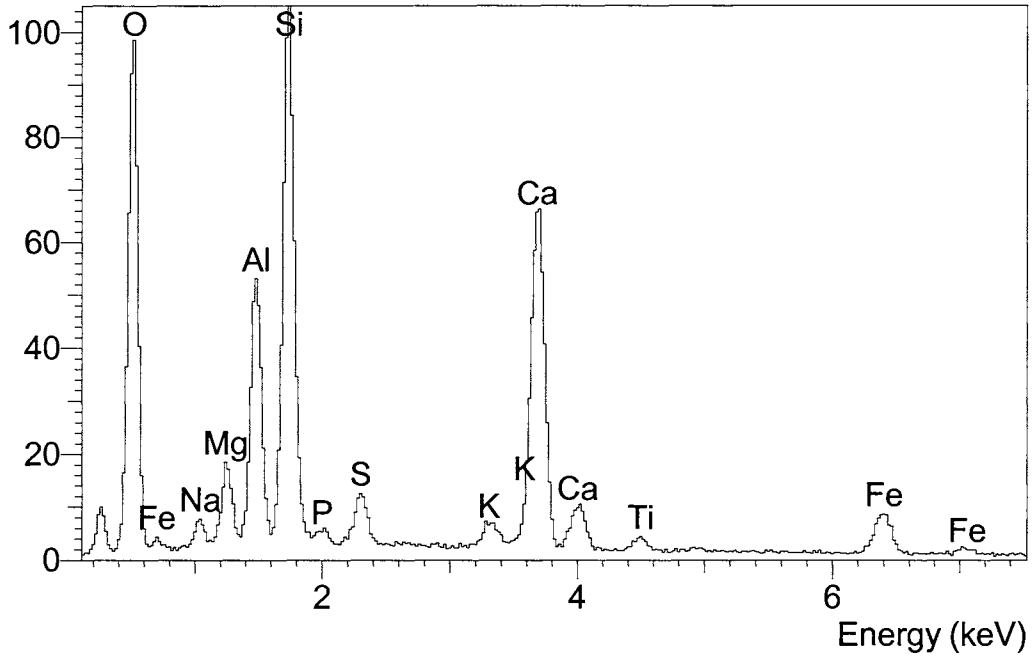

Figure 58. SEM X-Ray Analysis for Ames Ash-Soil-RAP Mixture

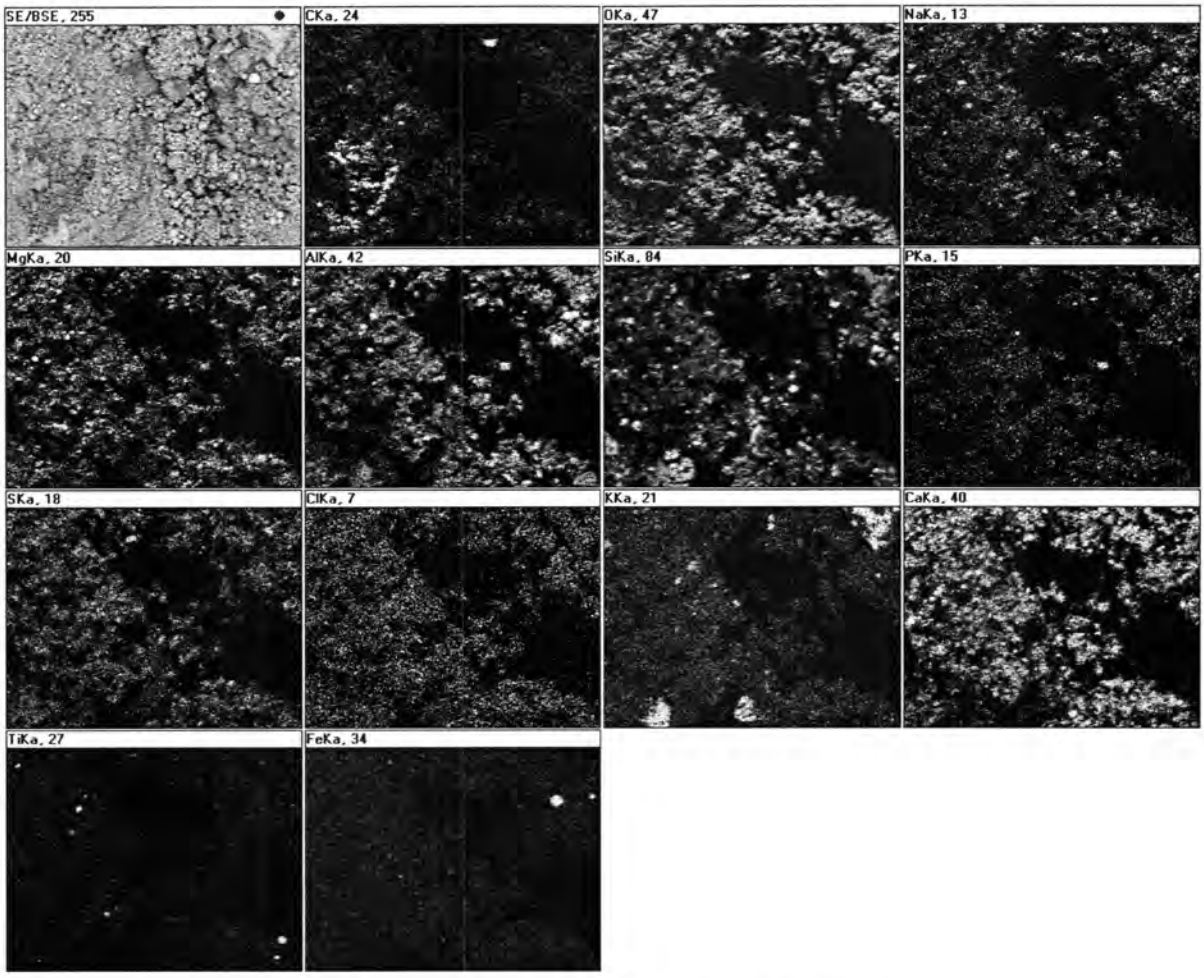

Figure 59. SEM Elemental Map for Ames Fly Ash-Soil-RAP Mixture

DISCUSSION

This section discusses implications and applications detailed in the results section. The discussion section is broken into three categories: (1) Construction operations, (2) Field results, and (3) Laboratory results.

Construction Operations

Construction operations used for this project produced a suitable paving platform. Although an excellent finished product was attained, several improvements could be made to increase the effectiveness of the procedure.

The first improvement would be the construction operations. Many different reclaimers and pavement recyclers are commercially available in the United States. Many of these have the capability to add water to the subgrade through the use of a spray bar located in the mixing drum. Addition of water in this fashion allows the fly ash to be deposited first and then mixing process can be completed.

By moving water addition to the mixing process, water would be added more efficiently and precisely eliminating the potential for unstable subgrade encountered in the completion of this project. This procedure also eliminates guesswork when adding water to the subgrade. Another added benefit is a reduction in compaction delay through the use of this construction sequence.

The second improvement would be in the fly ash deposition process. Fly ash particles are small and act like a liquid when en masse. Deposition from a bottom dump was a dusty process. The dust generated from this process has harmful side effects when contacting human skin causing a drying effect. A modification of a dump truck with an auger box spreader would provide a solution to this problem.

Field Results

Field results show a quality finished product. The increase in stiffness exhibited by the reduction in mean DCP index and FWD data shows an increased resistance to

deformation. This resistance to deformation ultimately leads to a longer lasting and more durable pavement surface. Rutting in asphalt pavement is controlled by compressive forces on the top of the subgrade layer. By introducing a stabilized structural layer, the compressive forces are reduced thus reducing the rutting potential for the pavement surface. Reducing the rutting potential would provide for a safer, smoother ride for vehicles if this process were used for a roadway.

Increasing the overall stiffness of the pavement system will result in a decrease pavement thickness. Increasing the strength of the supporting layers in pavement design allows for reductions in pavement thickness. This reduction in pavement thickness usually pays for the added thickness that would have been required, and, as shown previously, a longer lasting pavement is the outcome.

DCP results show an increased stiffness or strength as curing time is increased. This shows that plotting the stiffness as a function of time provides important information as to when paving operations can start. The DCP can therefore be used as a fast, easy way to determine if construction operations can proceed.

Laboratory Results

Laboratory results show a remarkable improvement for all materials used in this project. The addition of self-cementing fly ash increases the unconfined compressive strength significantly. This increased strength allows construction traffic to easily move about by eliminating an unstable subgrade situation.

The correlation between unconfined compressive strength and the mean DCP index of the stabilized layer leads to an interesting discussion. If a project was set up in several test

sections, one could determine the characteristic DCP strength correlation curve for each section and eliminate field sampling to determine strength. This would save both time and money for the contractor and contracting agency by eliminating a set of samples. The DCP test is a quick easy test that requires no experienced personnel to conduct or interpret the results.

Laboratory analysis verified field results proving sufficient strength for stabilization. CU analysis showed about a 5 time increase in consolidated undrained shear strength over the subgrade soil and the soil-RAP mixtures. This result is an indicator of field behavior because the area soils have high in-situ moisture contents and are saturated for a good portion of the year.

Finally SEM analysis proved that field construction operations were sufficient to produce a uniform product. SEM images showed coating of all particles with self-cementing fly ash thus proving that the mixing process was complete and thorough.

CONCLUSIONS

This section discusses the conclusions for this case study and is organized into the following sections: (1) Materials, (2) Construction operations, (3) Field results, and (4) Laboratory results.

Materials

Chemical analysis showed that the Ames and OGS fly ash are well suited for soil stabilization, and the addition of RAP to the subgrade soil increased the gravel and sand content mechanically stabilizing the soil.

Testing of the materials confirms that addition of self-cementing fly ash to RAP-soil mixtures increases the unconfined compressive strength making the final product suitable for parking lot subgrade stabilization. The final product was able to withstand construction traffic and paving operations.

Construction Operations

The documentation of construction operations provides proof that the construction process is satisfactory in providing a workable paving platform with minimal difficulties during the construction process. This construction procedure was very effective at this site to reduce construction delays due to unstable subgrade.

Field Results

The field results warrant three conclusions. The stiffness gain exhibited by the addition of self-cementing fly ash increases the traffic capacity ensuring long term performance of the pavement. DCP results display a time dependant stiffness gain concluding that the DCP is an effective tool at determining as to when construction operations may proceed. The cost analysis proved that this construction method was cost effective.

Laboratory Results

Laboratory results bring about three conclusions. Unconfined compression strength results show a remarkable strength gain for the materials when self-cementing fly ash is added. This enabled the materials to perform adequately as a stabilized base paving platform. Soaking the sample prior to testing showed that if the stabilized material were

compacted wet of the optimum moisture content for strength, saturation of the material produces little strength loss proving that slightly wet of optimum compaction procedures are the best for low lying areas such as the site conditions encountered. CU results also proved increased durability and suitability of the materials by increasing the CU shear strength about 5 times with the addition of self-cementing fly ash.

RECOMMENDATIONS

The author recommends studying the effects of varying the percent RAP in the mixture. This would allow the experimenter to analyze the effect of RAP on the soil-RAP structure and strength. Another area of future research would be to vary the percent fly ash in the soil-fly ash-RAP mixtures. This would allow a better understanding of the strength gain due to fly ash addition.

Along with studying the fly ash addition rate, the author recommends further investigation into determining if it is feasible to produce characteristic curves for strength and mean DCP index. These curves have the potential to be a maturity curve of sorts for future stabilization projects.

The author recommends further CU testing with production of three samples for each confining pressure to attain an average deviator stress to failure. Finally, the author recommends studying the same construction procedure in Western Iowa Loess to determine if this procedure would be an effective solution to stabilize Loess soils.

CHAPTER 2. A PILOT STUDY TO INVESTIGATE THE USE OF LIMESTONE SCREENINGS IN ROADWAY CONSTRUCTION

ABSTRACT

Disposal of limestone screenings, or limestone fines, creates problems for many quarry operations. Much of the fines is either stockpiled or deposited back into the quarry pit. Limestone screenings are too fine for use in Portland cement concrete and asphalt cement concrete, and do not meet most gradation requirements for use in roadway base and subbase construction.

To use limestone screenings in road construction, the particle size distribution needs to be altered, or the material needs to be stabilized to increase the shear strength and durability. The purpose and goal of this laboratory study and pilot project was to determine if limestone screenings could be stabilized and used as a structural layer in road construction. This project set forth the following objectives:

1. Determine from laboratory experiments if limestone screenings could be stabilized and used as a structural layer in road construction;
2. Document field construction operations;
3. Evaluate the effectiveness of stabilized limestone screenings as a structural layer in road construction through performance monitoring.

Compaction, unconfined compression, freeze-thaw durability, and wet-dry durability tests were performed to determine if limestone screenings could be stabilized and used as a

structural layer in road construction. Falling Weight Deflectometer (FWD), Clegg Impact Hammer, Dynamic Cone Penetrometer (DCP), and GeoGauge tests were used to compare stiffness differences, and temperature data was used to determine the number of freeze-thaw cycles each test section underwent.

Overview of Results and Conclusions

Laboratory compaction and unconfined compression test results confirm that limestone screenings can be stabilized for use as a structural layer. Freeze-thaw and wet-dry durability test results show that cement kiln dust (CKD) is not an acceptable stabilizer due to poor durability performance. Portland cement (PC) stabilized mixtures were determined to be acceptable for two different gradations of limestone screenings. Fly ash (FA) and CKD mixtures were determined to be acceptable for one of the two limestone screenings gradations.

Results from this pilot project demonstrate that self-cementing fly ash combined with CKD can produce a stabilized structural mixture. CKD should be not used as the sole stabilizer.

Construction should proceed using the optimum moisture content based on strength. Test section one (30% CKD) most likely failed due to freeze-thaw action. Visual observations show good performance of test section two (15% FA and 15% CKD) and control sections one (600 mm limestone screenings) and two (300 mm limestone screenings and 300 mm manufactured sand) with no rutting or pothole formation.

INTRODUCTION

Limestone screenings are a byproduct of aggregate production and the industry problem lies in waste management. Significant amounts of limestone screenings are produced each year throughout the United Stated. There exists an opportunity to use this waste product to generate revenue by applying it to roadway construction.

Currently, limestone screenings are not used in road construction or concrete production due to gradation requirements (excess fines content). A solution that this paper investigates is stabilizing the limestone screenings to meet the structural and durability needs for roadway construction.

The overall goal of this project was to investigate the use of limestone screenings as a structural layer in road construction. To meet this goal three objectives were outlined:

1. Determine from laboratory experiments if limestone screenings could be used as a structural layer in road construction;
2. Document field construction operations;
3. Evaluate the effectiveness of stabilized limestone screenings as a structural layer in road construction.

Results from this study demonstrate that properly stabilized limestone screenings can be used as a structural layer in road construction. Monitoring of field conditions shows that limestone screenings stabilized with both cement kiln dust (CKD) and class C fly ash produced an effective structural layer for an access road.

This paper is organized in the following manner:

- Literature Review

- Methods
- Materials
- Results
- Discussion
- Conclusions
- Recommendations

LITERATURE REVIEW

To provide context for this pilot study, this literature review section details case studies describing the use of self-cementing fly ash (FA), limestone screenings (LS), or cement kiln dust (CKD) as stabilizers for base or subbase construction and limestone screenings properties.

Overview

Limestone screenings are very abundant in the United States. It is known that many quarries have large stockpiles of material that are too fine for use in Portland cement concrete and asphalt cement concrete or conventional road construction.

Since a large quantity of material is available, if a solution for incorporating these materials into road construction were found, many disposal problems could be diminished. Stabilization of limestone screenings is particularly attractive because there are many potential stabilizers available for use including: Portland cement, self-cementing fly ash, and CKD. Using CKD or self-cementing fly ash as stabilizers is an attractive solution because both products are byproducts of Portland cement or power production, respectively.

Case Histories and Past Research

This section of the literature review details several past projects utilizing CKD or self-cementing fly ash stabilization. It also details use of limestone screenings in road construction.

Emulsified Limestone Screenings, East Main Street, Robbins, Iowa

Construction of this 1.27 mile section of road started in July of 1988 with subgrade work including replacement of pipes and culverts. Base construction was completed from August 1, 1988 to August 13, 1988. Base materials included waste limestone screenings from the quarry in Robbins, and a CSS-1 emulsion. Limestone screenings (3/8 inch and finer) were fed into a continuous drum mixer and emulsion was sprayed into the drum to coat the screenings. Emulsion rates were 2.5%, 3.5%, and 4.5%. Balling of the emulsion occurred, but it was not considered a problem. After mixing in the drum, the material was trucked to the site and placed with an asphalt paver. The paver was abandoned due to constructability issues, and a Jersey type spreader was used throughout the remainder of the project. Base thickness, originally 6 inches, was reduced to 4 inches.

One to three hours was required for aeration before being compacted with a vibratory padfoot roller. A motor grader was used to smooth the surface before final compaction was completed using a pneumatic tired roller to provide a smooth, tight surface. A double seal coat was applied over the entire project to ensure a watertight wearing surface.

Performance testing was completed for five years after completion. Conclusions obtained from this study are: a low maintenance roadway can be constructed using a seal coat

on top of 6 inches of stabilized limestone screenings with 4.5% asphalt cement (Nelson et al. 1994).

Use of Screenings in Hot Mix Asphalt Mixtures

This study was initiated to study the feasibility of using the growing amount of limestone and granite screenings as the sole aggregate portion of a HMA for thin lift applications. The main objectives of the study were to determine if rut-resistant HMA mixtures could be constructed with limestone screenings (100% passing the 3/8 sieve and about 12% passing the number 200 sieve) and granite screenings (100% passing the 3/8 sieve and about 15% passing the number 200 sieve) as the sole aggregate source and to determine what effect modified asphalt binders and fiber additives may have on rutting performance.

The asphalt binders used in the study were PG 64-22 and PG 76-22. Materials were combined to produce eight test mixtures at three air void contents of 4, 5, and 6%. Each mix was analyzed with the Asphalt Pavement Analyzer after conditioning to evaluate the magnitude of rutting. The average binder content was determined to be 5.0 percent for the limestone screenings and 7.7 percent for the granite screenings. Mixes with fibers tended to increase the optimum binder content about 0.7 percent and lead to a stiffening effect.

Results of the study show that screenings mixtures can be designed to be rut-resistant. The study did not research other areas such as long term durability. Mixtures should be designed at 4% air voids for low volume roadways. Mixtures designed at 4 percent air voids had significantly higher rut depths than mixtures designed at 5 or 6 percent air voids (Cooley et al. 2002).

Improvement of County Road 6040, Apache County, Arizona

In 1981, the Superior Mines Company proposed to give the county a stockpile of rejected limestone screenings fines (majority finer than the ½ inch sieve) provided that they use it to improve County Road 6040. Construction started in summer of 1981 with a one-mile test section near the mine entrance. Thickness of the limestone screenings layer was 4 inches. The material was spread and initially compacted with a motor grader. Water was not added during the compaction process. This section was observed 6 years later and only occasional blading was needed to maintain its good condition.

The remaining 5 miles was treated in 1984 based on the performance of the test section. Maintenance of this section is limited to blading twice a month or light dragging during the dry season. Observations note that the road surface is traffic compacted to a concrete-like surface that provides a smooth ride and is free of dust. Use of limestone screenings provided a dust-free roadway at low construction and maintenance costs. Future plans were to expand the project within the 30 mile economical hauling radius form the source (Broadbent 1988).

Power Plant Access Road, Marshalltown, Iowa

Construction began in June 1994 on a 1700-foot long by 22-foot wide access road to the Sutherland Generating Station located in Marshalltown, Iowa. The road was constructed on a 10-inch thick base of conditioned fly ash (CFA) from the Prairie Creek Generation Station in Cedar Rapids, Iowa. Since the base material had been previously conditioned, the project called for a pozzolanic activator. Cement kiln dust (CKD) and atmospheric fluidized bed combustion (AFBC) residue were both used as activators on the project. The activators

were mixed at 15% by dry weight of CFA. The CKD was used on 1000 feet of the access road. For this portion of the project, the CFA was placed on-site, and then the CKD was spread over it. Next a road reclaimer mixed the CFA, CKD, and water together to a loose depth of 12 inches. This mixing process was repeated until the proper moisture content for compaction was reached, at which time the mixture was compacted using a padfoot roller for initial deep compaction and then a smooth steel drum roller for final compaction. The compacted section was kept in a moist condition until paving. The 700-foot long AFBC section was completed in much the same manner except that the CFA was pre-wetted prior to application of the AFBC, and water was again applied after the first pass of the reclaimer. Compaction of the AFBC was the same as the CKD section and the compacted AFBC section was also kept in a moist condition. A 2-inch chip seal completed the pavement layer. Since November 1994, ISU personnel have extracted cores of the base material annually though July 2002. The AFBC became unrecoverable several years ago and recently the CKD cores have shown horizontal delamination near the top and vertical cracks that extend down through the samples. These cracks are believed to stem from high vehicle loads and freeze/thaw damage. The materials are currently behaving like a Macadam base. The cores recovered in 2002 still had compressive strengths of 970 psi. Overall the pavement is performing well with some areas along the turning radii of the road having to be resurfaced with hot mix asphalt in early 2002 (White 2002).

Ottumwa-Midland Landfill Access Road, Ottumwa, Iowa

The Ottumwa-Midland Landfill is located 5 miles north of Ottumwa, Iowa. Construction of the road base occurred from May 30 to June 1, 1995. The road is 2500 feet

long, and had 1800 feet of CKD stabilized hydrated fly ash (HFA) base and 700 feet of AFBC stabilized HFA base constructed. The CKD and AFBC were mixed at 10% and 15% by dry weight respectively. The stabilized HFA was placed on a 4-inch aggregate subbase. The aggregate subbase was placed on top of a 12-inch (300-mm) fly ash stabilized subgrade.

Construction of the project began in April 1995 with clearing and grubbing, along with cut and fill operations, stabilization of the subgrade, and placement of the aggregate base. The activators and HFA were mixed at the Ottumwa Generating Station. The activators were spread on the compacted HFA and a reclaimer mixed the materials to a depth of 8 inches. Stockpiles were created with a loader. The mixtures were then hauled to the access road construction site and spread on the aggregate subbase. Water was then applied before final mixing was completed. Compaction equipment included: a 50 ton double drum roller for initial compaction, and a smooth drum roller for final compaction. An asphalt prime coat was used to keep the stabilized material moist. After curing for one week, a 1.5-inch asphalt concrete surface was applied. Coring of the base has been completed annually since August 1995 by ISU personnel. A maximum compressive strength of 2235 psi was reached in 1997. Although the strength has decreased since 1997, the 2002 cores still had an average compressive strength of 2055 psi. Longitudinal cracking of the asphalt surface is occurring in both the AFBC and CKD sections. Breakdown of the activated HFA base is causing the material to behave as a Macadam base. Overall the road is still performing well (White 2002).

Lula Road, Ada, Oklahoma

Objectives of the study were to evaluate the effectiveness of CKD in reducing the plasticity of clayey soils. Other objectives included: evaluating the durability of CKD treated soils with freeze/thaw and wet/dry tests, evaluating the effectiveness of CKD to improve the bearing strength and stiffness of low to moderate plastic soils, and evaluate three sources of CKD.

Construction of tests sections occurred between January and March 1998. A test section was first constructed with granular quicklime (4% by dry weight), and the remaining three test sections were constructed with 15% CKD by dry weight. Each CKD test section was about 305 m long. Construction observations noted that the CKD reaction occurred much more quickly than the quicklime reaction, and windy days posed a dust hazard due to material being blown off-site. Unconfined compression strength samples were produced on site in triplicate. Falling weight deflectometer tests were conducted to provide information on structural integrity of the completed sections. FWD data showed the average back calculated Modulus was about the same for the CKD sections and the quicklime section with the exception of one CKD source which was about three times greater (Miller and Zamon 2000).

CKD Stabilized Dune Sand

This study investigated the stabilization of dune sand located in Saudi Arabia with varying contents of CKD. CKD was added at the following percentages: 10, 20, 50, and 75% by dry weight of sand. Samples were prepared using the standard Proctor test, wrapped to

prevent moisture loss, and cured at three temperatures for seven, 28, and 90 days before being tested in unconfined compression.

The results of this study warranted the following conclusions: unconfined compressive strengths increased continually with the CKD content and curing time, a higher curing temperature accelerates the chemical reaction between the CKD and water, and a CKD content of 50% is satisfactory for base courses carrying heavy traffic. The CKD treated dune sand showed an increase in CBR from 29% to 317%, exhibited high compressive strengths, but failed to meet freeze-thaw durability requirements (Baghdadi et al. 1995).

Evaluation of CKD and Lime for Stabilizing Clayey Silt, Iroquois Falls, Ontario

Laboratory testing for this project included unconfined compression strengths (UCS), Atterberg limits, and Proctor tests. Laboratory results show that area soils responded well to treatment with: Portland cement, CKD, and CKD-lime mixtures. Results show that the lime-CKD mixture was most suitable for area soils. Field tests were selected as 6% CKD and a mixture of 6% lime-CKD at a ratio of 1:1.

Full scale field implementation began in the summer of 2001, and performance monitoring continued throughout 2002. Construction operations started with earth embankments being constructed. Each test section was 300 m in length. Treated areas were 4.6 m wide and depth of treatment was 250 mm. Binders were spread on the grade and mixed with one pass of a Bomag MPH100 recycler. The roadbed was then shaped and crowned before initial compaction by a padfoot roller. Final compaction was completed with a smooth drum roller. A 300 mm gravel surface layer was added as a running surface. The CKD only section performed poorly due to high water contents during construction. No

visible rutting was observed 30 days after construction in the lime-CKD test section, but rutting was observed in the control and CKD only section (Legere and Tremblay 2003).

CKD Stabilized RAP Aggregate Systems

This laboratory testing study took place in the Sultan of Oman in 1998 and 1999. CKD was blended with recycled asphalt pavement (RAP) and virgin aggregate in the following amounts: 0%, 3%, 5%, 7%, 10%, 15% and 20% (by dry weight). Conclusions obtained from this study are: maximum dry density and UCS generally increase as virgin aggregate content and CKD content increases, optimum CKD content for stabilization of RAP and virgin aggregate blends is 15%, and CKD stabilized RAP mixtures can be successfully used as base or subbase materials (Taha 2003).

Limestone Screenings

Background and History

Limestone is a naturally occurring mineral consisting primarily of calcium carbonate (Oates 1998). Limestone is found in many forms and is classified by its origin, composition, structure, and geological formation (Oates 1998). Limestone occurs throughout the world, and is used in many industries as a raw material. Oates (1998) estimated that 4,500 million tonnes of limestone are used per year world wide. Most countries use limestone as an aggregate in construction and building. It is also used as the primary raw material for production of cement as a source of calcium oxide. In the United States, limestone sales were about 800 million tonnes in 1994 (Oates 1998). Oates (1998) noted that this was about 72% of all crushed rock sales.

Limestone has been in use since the Stone Age (2 million years ago to about 2500 bc) where the first records show use in building the Egyptian Pyramids (Oates 1998). Romans also used limestone as an aggregate in lime-based concrete (Oates 1998).

Production

Limestone aggregate production is accomplished by the use of crushers. There are two categories of crushers: (1) impact crushers and (2) compression crushers (Oates 1998). Oates (1998) states that impact crushers produce more fines than compression crushers. Typical crushing operations have three crushers in place: primary crushers, secondary crushers, and tertiary crushers (Oates 1998). Primary crushers reduce particle size to coarse aggregate. Secondary crushers reduce coarse aggregate to a marketable size range, and tertiary crushers are used primarily to crush surplus quantities of larger products into smaller size ranges (Oates 1998).

Screens are used to create a desirable gradation for the crushed limestone. Any material that does not meet the desired specification either gets recycled back to the crushers or disposed. Disposal is typically associated with material that has excessive fines (Oates 1998). Most fines are either stockpiled on site or disposed in the quarry bottom. Numerical figures for limestone screenings production are very hard to find since records are not kept stating that the screenings have been produced. Nelson et al. (1994) states that many quarries across Iowa have large stockpiles of limestone screenings. Conversations with quarry officials note that the amount of limestone screenings produced is a function of the product being produced. An aggregate being used for Portland cement concrete will generate a larger fines rejection than an aggregate being produced for a granular roadbase.

Use of Limestone Screenings

An internet search produced an extensive review of limestone screenings use. The most notable use of limestone screenings is for landscaping or low volume traffic areas such as a parking lot or a bike trail. Limestone screenings use in landscaping comes in the form of a base material for either concrete or brick pavers for a driveway, walking path, or patio.

Limestone screenings can also be used in agricultural facilities. Use of limestone screenings in this way is termed agricultural or ag-lime (Oates 1998; Searle 1935). Searle (1935), Oates (1998), and Boynton (1980) noted that limestone screenings can be used as filler in fertilizer with addition rates up to 250 pounds per ton of mixed fertilizer. Finely ground limestone can also be used as a calcium source for farm animals (Oates 1998; Boynton 1980). Oates (1998) and Boynton (1980) note that limestone fines can be used in poultry feed enabling the poultry to better digest the feed with the limestone fines in their gizzards.

Construction uses for limestone screenings are limited. Limestone is crushed finely and used in Portland cement production (Oates 1998; Boynton 1980). Boynton, (1980), states that Portland cement production uses the greatest amount of raw limestone with exception only to use of limestone aggregate. Finely crushed and processed limestone (hydrated lime or quicklime) can be used for lime stabilization of high plasticity clayey soils. Limestone screenings (fines passing the 3/8 sieve) can also be used as filler in asphalt concrete to reduce the voids content (Oates 1998; Boynton 1980). Cooley et al. (2002) showed that limestone screenings (100% passing the 3/8 inch sieve and about 12% passing the number 200 sieve) can be used as the sole aggregate portion of hot mix asphalt (HMA).

Self-Cementing Fly Ash

For a detailed discussion on self-cementing fly ash pertaining to the following: production, positive and negative reaction products, modification of engineering properties, and construction methods; please see the discussion provided in Chapter 1.

Cement Kiln Dust

Cement kiln dust (CKD) is a byproduct of Portland cement production. CKD is defined as a fine material carried by hot gasses in a cement kiln collected by a filter system during Portland cement production (Collins and Emery 1983; Taha 2003). In 1983 it was estimated that 18 to 20 million tons of CKD was produced annually in the United States (Collins and Emery 1983). Collins and Emery (1983) also note that 6 to 10 million tons was recycled, and 8 to 12 million tons was wasted. 100 million tons of cement kiln dust is estimated to be stockpiled (Collins and Emery 1983). CKD disposal is usually accomplished by placement in a landfill either on or off site of the cement production plant.

Although a byproduct, CKD has distinct advantages for several uses. Uses include: solidifying wastes in environmental remediation, stabilization of soft or wet soils, pozzolan initiators, palletized lightweight aggregate, mineral filler in asphalt pavements, and as fill material in earth embankments (Collins and Emery 1983).

CKD Chemical Properties

CKD's chemical and physical properties can vary widely from cement plant to cement plant. Miller and Zaman (2000) state that even though there is a large variation between cement plants, variation of CKD collected from the same kiln producing the same

cement type can be consistent. The amount of variation between cement plants depends on raw materials, type of collection process used, and whether or not the CKD is recycled and reused in the manufacturing process (Miller and Zaman 2000).

CKD has four main components: (1) Calcium oxides, (2) Alkalies, (3) Sulfates, and (4) Loss on ignition (LOI) (Collins and Emery 1983). The amounts and characteristics of each of these components are determined by: raw feed materials; kiln design and operation; fuel type; and design of the dust collection system (Collins and Emery 1983). Collins and Emery (1983) note the free lime is the single most important mineralogical constituent for determining suitability for stabilization. The amount of free lime dictates the hydraulic reactivity of the kiln dust.

The hydraulic reactivity of the cement kiln dust is affected by two factors: whether or not it has been stockpiled, and whether or not water was injected into the heated exhaust stream (Collins and Emery 1983; Miller and Zaman 2000). CKD that has been stockpiled has no free lime available to react. Miller and Zaman, (2000) note that water injected into the heated exhaust stream partially hydrates the CKD and renders it less reactive as a soil stabilizer.

Although Collins and Emery (1983) note that free lime content is the most important mineralogical component in CKD, they are quick to state that the oxides content should not be overlooked due to their cementing properties. Miller and Zamon (2000) show that a significant amount of cement forming oxides, up to two-thirds of that found in Portland cement, may be present in CKD.

Previous literature notes that sulfates present in soil stabilizers can pose significant reductions in long term durability (Thomas 2003; Thomas 2002; ACAA 1999; White and

Bergeson 2000). The reduction in durability is due to compounds developing after the sulfate is added to the material to be stabilized. Ettringite and thaumasite form, and continue to form, producing long-term expansion. Ettringite is formed initially and occupies a volume over 200% of the volume of its constituents, and ettringite further expands through its conversion to thaumasite resulting in another 200% volume increase (ACAA 1999). The reaction takes place when the temperature drops below 16°C via isomorphous substitution of the alumina for silica in the ettringite (ACAA 1999). Collins and Emery (1983) state that CKD's with sulfur contents greater than 10% should be avoided to obtain durable compositions.

Loss on ignition (LOI) is a large factor in the chemical and physical properties of the CKD. Loss on ignition affects the effectiveness of the CKD. The effectiveness for stabilization is affected because a higher LOI generally means that there is more water bound in the structure of the CKD (Miller and Zamon 2000). Collins and Emery (1983) and Miller and Zamon (2000), state that the effectiveness of the CKD is reduced with the increase in LOI due to the reduction in calcium oxide available as free lime for reaction.

Soil Stabilization with CKD

Soil stabilization with CKD is useful because CKD has the ability to increase strength, decrease the plasticity index (PI), and reduce the collapse potential and compressibility of compacted shales (Miller and Zaman, 2000). The ion exchange between soil and calcium additives lowers the PI, makes the material less sensitive to moisture changes, increases the compressive strength, and increases freeze/thaw and wet-dry

durability. Miller and Zamon (2000) noted that the main drawback to soil stabilization with CKD is that the soil becomes brittle.

METHODS

The methods section overviews the testing and observation methods used throughout this pilot study. Methods include: (1) Project Background, (2) Determining if limestone screenings can be used as a structural layer, (3) Documentation of construction procedures, and (4) Field evaluation of the effectiveness of limestone screenings as a structural layer.

From here forth, limestone screenings shall refer to a byproduct of crushed limestone production with a maximum particle size of about 9.56 mm (3/8 in) and a large percentage of fines passing the number 200 sieve of about 25%. Manufactured sand shall refer to crushed limestone sand with a maximum particle size of about 9.56 mm (3/8 in) and a low fines content passing the number 200 sieve of about 10%.

Project Background

Early 2003 Iowa State University was contacted by Martin Marietta Aggregates, Cedar Rapids Quarry and Sand, about the feasibility of stabilizing limestone screenings for use as a pavement layer for an access road into a new sand production facility located about 10 miles east of Cedar Rapids and 1 mile north of U.S. Highway 30 on Old River Road. Figure 60 shows the pilot study location.

A site visit was conducted by Iowa State University personnel in June 2003. Another visit was scheduled to obtain limestone screenings samples for testing. It was also agreed

that cement kiln dust (CKD) and class C fly ash, along with Portland cement, would be investigated as potential stabilizers.

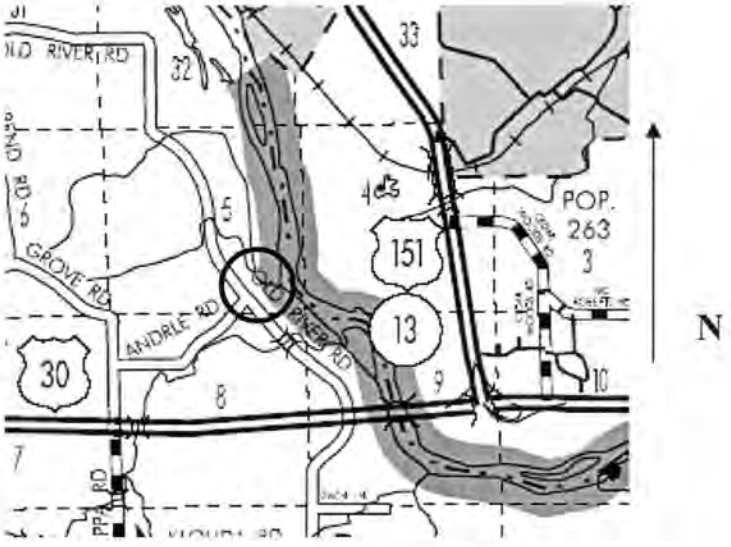

Figure 60. Pilot Study Location

The original source of class C fly ash was to be Prairie Creek fly ash (PCFA) from the Cedar Rapids Generating Station, but due to increased energy demand in late summer, this fly ash source was removed from consideration as the burning of a higher BTU coal lead to the production of a class F fly ash. The other sources of class C fly ash were Ottumwa Generating Station fly ash (OGSFA) from Chillicothe, Iowa, and Riverside fly ash (RFA) from Muscatine, Iowa. The CKD source was the Holcim Portland Cement Production Facility located in Mason City, Iowa.

Objective One: Determine if Limestone Screenings can be used as a Structural Layer in Road Construction

The materials for this project were analyzed to determine if they could be used as a structural layer in road construction. Materials studied include two gradations of limestone screenings with CKD, FA, and PC stabilizers.

Task 1: Analyze Limestone Screenings

To analyze the limestone screenings samples, the following test methods were employed.

- ASTM D 422 [Standard Test Method for Particle-Size Analysis of Soils]
- ASTM D 4318 [Standard Test Method for Liquid Limit, Plastic Limit, and Plasticity Index of Soils]

First the samples were sampled using 15 five gallon plastic containers with lids. The samples were left to air dry overnight and then prepared for particle size analysis according to ASTM D 422. The index properties were determined according to ASTM D 4318.

Task 2: Chemically Analyze CKD, Portland Cement, and Fly Ash

The chemical analysis included X-ray diffraction analysis (XRD), and X-ray fluorescence analysis (XRF). Samples of CKD, Portland cement, and fly ash were collected from the Portland cement production facility and respective generating stations in two five gallon containers. The information obtained from XRD and XRF was used to classify the fly ash according to ASTM C 618-01 [Standard Specification for Coal Fly Ash and Raw or Calcined Natural Pozzolan for Use as a Mineral Admixture in Concrete].

Task 3: Perform Proctor Compaction Test to Determine Moisture-Density Characteristics

Several mix designs were evaluated using two gradations of limestone screenings materials. Both gradations were combined with varying amounts of Type I Portland cement, CKD, and class C fly ash. Combinations of CKD and Class C fly ash were also investigated.

Each stabilizer was evaluated using five addition rates. Table 9 shows the material to be stabilized, mixture number, stabilizer, and stabilizer rate for each mixture. For each mix evaluated, a five point Proctor test (ASTM D 698 [Standard Test Method for Moisture Density Relation of Soils and Soil-Aggregate Mixtures Using 5.5 lb. (249kg) Rammer and 12 in (305 mm) Drop]) was conducted in order to determine the moisture-density relationship.

Compaction delay is known to have an effect on the strength and density of stabilized materials (ACAA, 1999). Field compaction delay time was expected to be about 30 minutes; therefore, laboratory testing proceeded using a compaction delay of 30 minutes.

Table 9. Mixture and Stabilizer Percentages for Mixtures Tested

		% Binder Content By Dry Weight of Limestone Screenings and Manufactured Sand						
			OGS / CKD		Riverside / CKD			
Material	Mixture Number	CKD	OGS Fly Ash	CKD	Riverside Fly Ash	CKD	Portland Cement	Prairie Creek Fly Ash
Limestone Screenings	1	10	5	5	5	5	1	10
	2	20	10	10	10	10	3	20
	3	30	15	15	15	15	5	30
	4	40	20	20	20	20	7	40
	5	50	25	25	25	25	9	50
Manufactured Sand	1	10	5	5	5	5	1	--
	2	20	10	10	10	10	3	--
	3	30	15	15	15	15	5	--
	4	40	20	20	20	20	7	--
	5	50	25	25	25	25	9	--

Task 4: Measure Strength to Determine Moisture-Strength Characteristics

The moisture-strength characteristic of a stabilized mixture is important to understand. A stabilized mixture compacted at the correct moisture content will attain the design strength, where as if it were compacted at a moisture content other than the optimum moisture content based on strength, the maximum strength may not be attained. The optimum moisture content for maximum density and maximum strength are usually not the same. This leads to the need for understanding the moisture-strength characteristics of the mixtures being tested.

To measure the unconfined compression strength, several test methods were used.

- ASTM C 593 [Standard Specification for Fly Ash and Other Pozzolans for Use with Lime]
- ASTM D 698 [Standard Test Methods for Moisture Density Relations of Soil and Soil-Aggregate Mixtures Using 5.5 lb. (2.49kg) Rammer and 12 in (305mm) Drop]

ASTM D 698 was used to produce three samples per moisture content along the five point Proctor compaction curve as stated in Task 4. This allowed for a three point average for unconfined compression strength. Upon production of each sample, they were individually wrapped in plastic wrap, aluminum foil, labeled, and then sealed in Ziploc bags to prevent moisture loss. The samples were then placed in an oven at 38°C to cure for 7-days according to ASTM C 593. Deviation from ASTM C 593 was that only the 7-day oven curing portion of the standard was used.

Upon completion of the curing period, the samples were removed, capped with sulfur capping compound to ensure even distribution of compressive force, soaked for four hours to simulate saturated conditions, and tested for unconfined compressive strength.

Task 5: Perform Freeze-Thaw Durability Tests on the Maximum Strength of Each Stabilized Mixture

To complete freeze-thaw durability tests, ASTM D 560 [Standard Test Methods for Freezing and Thawing Compacted Soil-Cement Mixtures] was used on the maximum average compression strength samples determined in Task 4. The moisture content at which the maximum strength occurred was chosen as the optimum moisture content for testing freeze-thaw durability. Samples were prepared according to ASTM D 698 then cured and tested according to ASTM D 560.

Task 6: Perform Wet-Dry Durability Tests of the Maximum Strength of Each Stabilized Mixture

ASTM D 559 [Standard Test Methods for Wetting and Drying Compacted Soil-Cement Mixtures] was used to test each mixture at the previously determined maximum strength. The optimum moisture content for strength was also chosen as the moisture content for preparation of the wet-dry durability samples. ASTM D 698 was used to prepare samples, and ASTM D 559 was followed in curing and testing the samples.

Objective Two: Document Field Construction

This pilot study project was constructed by C.J. Moyna and Sons. The construction operations were documented to ensure that the process could be duplicated or altered in

future research projects. Construction operations were documented through the use of digital photography and note taking.

Access road construction proceeded in October of 2003 with the construction of two test sections and two control sections. The first test section was constructed of 300 mm CKD stabilized limestone screenings overlying 300 mm of manufactured sand. Figure 61 illustrates the layers and thicknesses for test section one. The second test section was constructed of a combination of CKD and OGS fly ash stabilized limestone screenings overlying manufactured sand. The stabilized layer was about 300 mm thick. The layer thicknesses for the second test section are shown in Figure 62.

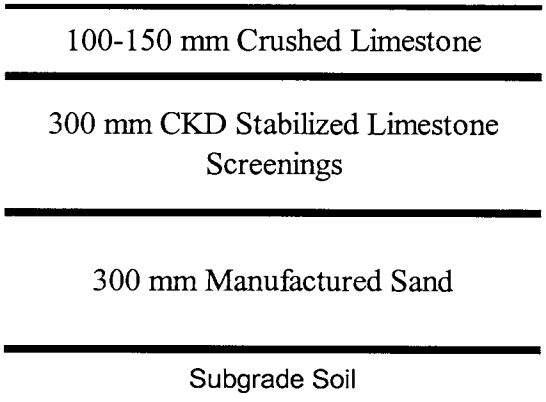

Figure 61. Layer Identification and Thickness for Test Section 1

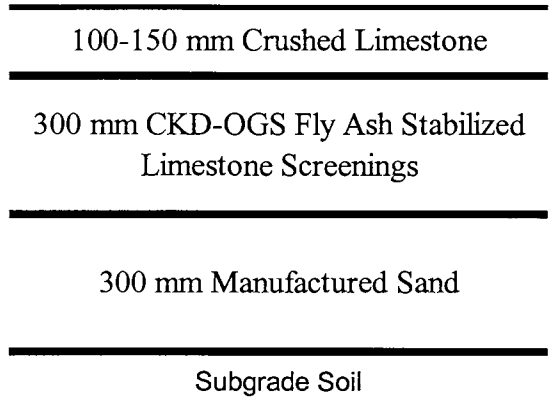

Figure 62. Layer Identification and Thickness for Test Section 2

Two control sections were constructed to provide a baseline of comparison between the two test sections. Control section one was constructed of 600 mm of limestone screenings. Control section two was constructed of 300 mm of limestone screenings overlying 300 mm of manufactured sand. All sections are covered with 100 to 150 mm of crushed limestone as a wearing surface. Control section one and two are illustrated in Figures 63 and 64 respectively.

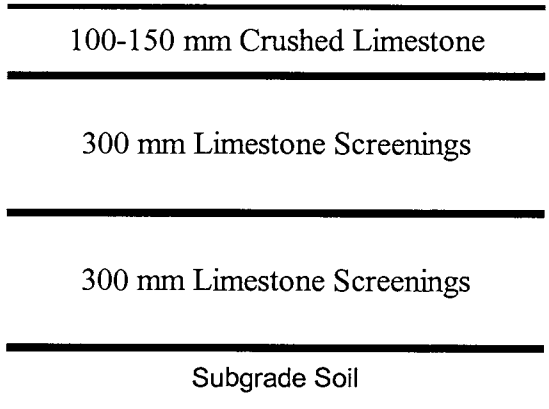

Figure 63. Layer Identification and Thickness for Control Section 1

100-150 mm Crushed Limestone

300 mm Limestone Screenings

300 mm Manufactured Sand

Subgrade Soil

Figure 64. Layer Identification and Thickness for Control Section 2

Task 1: Place Manufactured Sand

First the manufactured sand was placed and compacted to provide a base and drainage layer. Figure 65 shows the placed and compacted manufactured sand before placement of limestone screenings.

Figure 65. Test Sections One and Two before Placement of Limestone Screenings

Task 2: Place Limestone Screenings

Next limestone screenings were placed by dump trucks and leveled smooth with a bulldozer. Windrows were created along the edges to contain the CKD and class C fly ash. Figure 66 shows the placement of the limestone screenings.

Figure 66. Placement of Limestone Screenings

Task 4: Place Fly Ash and CKD

Once the limestone screenings were leveled, the fly ash and CKD were then deposited within each test section per plan and spread with a bulldozer. The fly ash was deposited using bottom dump trucks, and the CKD was deposited using pneumatic tanker trucks. The CKD and class C fly ash were each added at the rate of about 15% by dry weight of the

screenings for test section two. The CKD was added at a rate of about 30% by dry weight of the limestone screenings for test section one. Figures 67 and 68 show the placement and spreading of fly ash, respectively. Figures 69 and 70 show the placement and spreading of CKD, respectively.

Figure 67. Placement of Fly Ash in Test Section Two with a Bottom Dump

Figure 68. Spreading of Fly Ash with a Bulldozer

Figure 69. Placement of CKD in Test Section One and Two

Figure 70. Spreading CKD in Test Section One

Task 5: Mix Fly Ash, CKD, and Limestone Screenings

Next the sections were mixed with a CMI RS 425 road reclaimer using one pass. Water was added through the reclaimer with the use of a spray bar to bring the water content to optimum based on strength. Figure 71 shows the reclaimer used for this project.

Figure 71. CMI RS 425 Road Reclaimer Used for Mixing

Task 6: Compact Mixture

Initial compaction was achieved with a vibratory padfoot roller. Initial compaction was completed within fifteen minutes of mixing. Final compaction was completed using a steel drum roller to seal the stabilized layer. Construction operations for each pass were completed within 30 minutes. Figures 72 and 73 show the vibratory and steel drum rollers used for this project. Figure 74 shows the entire mixing operation in test section two.

Figure 72. Vibratory Padfoot Roller Used for Initial Compaction

Figure 73. Steel Drum Roller Used for Final Compaction

Figure 74. Mixing, Initial, and Final Compaction in Test Section Two

Task 6: Water Stabilized Sections

The stabilized layers were then sprinkled with water from a water truck to unsure proper hydration. Figure 75 shows water being added from the water truck.

Task 7: Apply Wearing Surface

A thin layer of crushed limestone, about 150 mm, was added as a wearing surface to protect the stabilized sections from traffic. Figure 76 shows the completed test sections with a crushed limestone wearing surface.

Figure 75. Watering of Stabilized Sections to Ensure Proper Hydration

Figure 76. Completed Test Sections with Crushed Limestone Wearing Surface

Objective Three: Evaluate the Effectiveness of Stabilized Limestone Screenings as a Structural Layer

Objective three was accomplished using several field testing techniques. The field testing techniques used were: the Falling Weight Deflectometer (FWD), Dynamic Cone Penetrometer (DCP), Clegg Impact Hammer, I-Button temperature readings, and visual observation and documentation.

Task 1: Conduct FWD Tests

The first field test used was the FWD. The FWD test was used because it allowed for a comparisons of deflection basins between the two test and control sections. Figure 77 shows the FWD apparatus.

Figure 77. Falling Weight Deflectometer

Task 2: Conduct DCP Tests

The DCP test was used because it shows a measure of the soil stiffness versus depth. The DCP results allow the user to determine if there is a weak layer within the pavement system. DCP testing was conducted immediately after construction, and then discontinued due to the rapid strength gain of the stabilized sections possibly doing damage to the DCP.

The DCP test was also conducted several times five months after construction in March due to an apparent failure of test section one.

Task 3: Conduct Clegg Impact Hammer Tests

The Clegg Impact Hammer test is another measure of the soil stiffness. The Clegg Impact Hammer measures the soil stiffness by means of dropping a hammer from a fixed distance and measuring the deceleration. The output of the device is the Clegg Impact Value (CIV). The Clegg Impact Hammer test was used because it is an easy fast test to conduct. Figure 78 shows the Clegg Impact Hammer.

CIV were recorded three placed within each test section every 21 days. The Clegg Impact Hammer tests were discontinued when the stabilized sections became frozen as the CIV was beyond the capabilities of the testing apparatus.

Task 4: Record Temperature Data

Temperatures within the stabilized sections were recorded through the use of I-Buttons placed at the bottom of the stabilized layer during construction. The I-Button records and stores the temperature once very 15 minutes. The data is then downloaded onto a PDA for analysis. Two I-Buttons were installed in test section one and four were installed

in test section two. One I-Button was installed in the air to record ambient air temperature. I-Button data allows determination of exactly how many freeze-thaw cycles each section has underwent, as well as a documentation of air temperatures. In addition to recording the number of freeze/thaw cycles, I-button data was also used to gain a better understanding of the hydration temperatures for each of the sections.

Figure 78. Clegg Impact Hammer

MATERIALS

This section presents and analysis of the materials used in this project: (1) Limestone screenings, (2) Manufactured sand (3) Self-cementing fly ash, (4) CKD, and (5) Type I Portland cement.

Limestone Screenings Analysis

The source of limestone screenings used throughout this project was Martian Marietta Aggregates, Cedar Rapids Quarry and Sand, located in Cedar Rapids, Iowa. The limestone screenings are characteristic of a byproduct from crushed limestone aggregate production with a maximum particle size of about 9.56 mm (3/8 in) and high fines content of about 25 percent passing the number 200 sieve. The particle size distribution of the limestone screenings is shown in Figure 79. The USCS classification is SM, silty sand, and the AASHTO classification is A-2-4, silty, clayey gravel and sand.

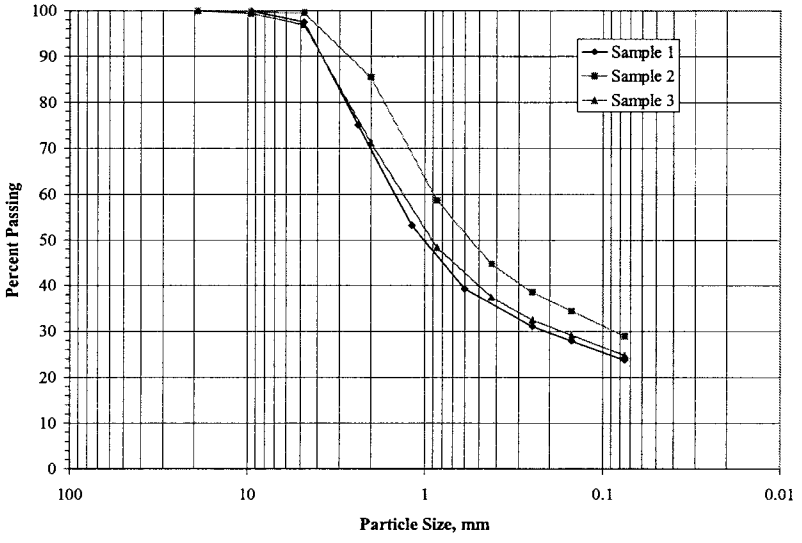

Figure 79. Particle Size Distribution for Limestone Screenings

Manufactured Sand Analysis

The source of manufactured sand was also Martin Marietta Aggregates, Cedar Rapids Quarry and Sand, located in Cedar Rapids, Iowa. The manufactured sand is characteristic of crushed sand composed of limestone with a fines content of about 10%. Figure 80 shows the

particle size distribution for the manufactured sand used throughout the course of this study. The USCS classification is SW-SM, well graded sand with silt, and the AASHTO classification is A-1-a.

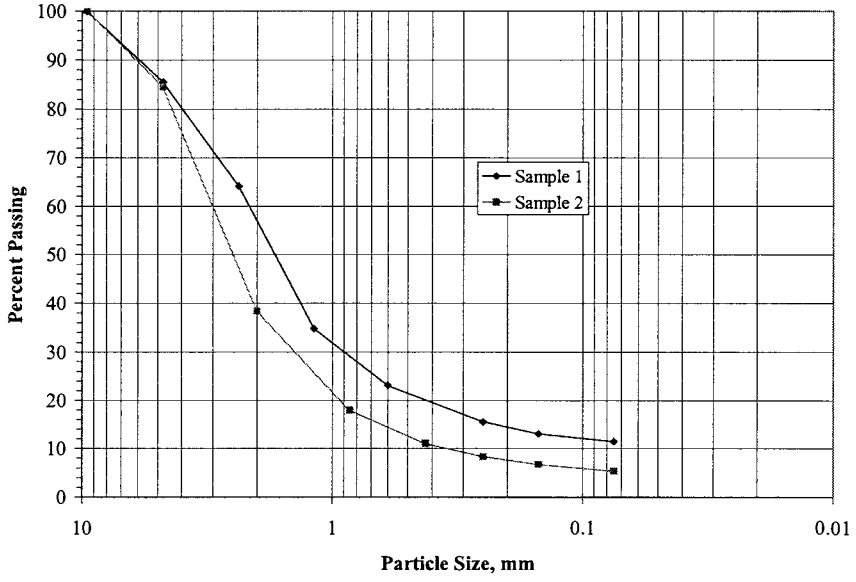

Figure 80. Particle Size Distribution for Manufactured Sand

Self Cementing Fly Ash Chemical Analysis

The sources of the class C fly ash were as follows: (1) Prairie Creek fly ash from the Prairie Creek Generating Station located in Cedar Rapids, IA; (2) Ottumwa Generating Station (OGS) fly ash from Ottumwa Generating Station located in Chillicothe, Iowa; and (3) Riverside fly ash form the Riverside Generating station located in Muscatine, Iowa.

The original source of class C fly ash was intended to be Prairie Creek, but due to increased energy demand, a higher BTU coal had to be burned. Burning the higher BTU coal lead to the production of class F fly ash. For this reason, the OGS and Riverside fly ash was included in the study.

A chemical analysis was conducted on the fly ashes used, and the results can be seen in Table 10. Note that both the OGS and Riverside fly ash meet ASTM C 618 classification for class C fly ash. SEM images were also taken of the OGS fly ash. The result can be seen in Figure 81. Note the round spheres typical of fly ash. Other SEM images of the OGS fly ash can be found in the Appendix.

Table 10. Chemical Analysis Results for Stabilizers Used During this Pilot Study

	Sample				
Mineral (%)	**Type I Portland Cement**	**CKD**	**OGS Fly Ash**	**Riverside Fly Ash**	**Prairie Creek Fly Ash**
Na_2O	0.16	0.45	2.45	1.65	1.32
MgO	2.48	3.41	4.44	4.97	3.61
Al_2O_3	5.28	4.77	19.84	17.63	18.81
SiO_2	19.14	14.48	38.18	36.60	37.94
P_2O_5	0.39	0.07	1.02	0.88	1.23
SO_3	2.67	9.52	1.41	2.55	1.59
K_2O	0.48	6.56	0.52	0.48	0.48
CaO	64.31	53.60	23.51	24.63	19.96
TiO_2	0.22	0.17	1.48	1.45	1.36
Fe_2O_3	2.27	1.62	5.75	7.82	5.29
SrO	0.05	0.04	0.39	0.31	0.34
Mn_2O_3	0.06	0.03	0.04	0.02	0.00
BaO	not meas'd	not meas'd	0.68	0.67	0.60
LOI	1.83	2.24	0.27	0.39	7.47
TOTAL	**99.4**	**97.0**	**100.0**	**100.0**	**100.0**

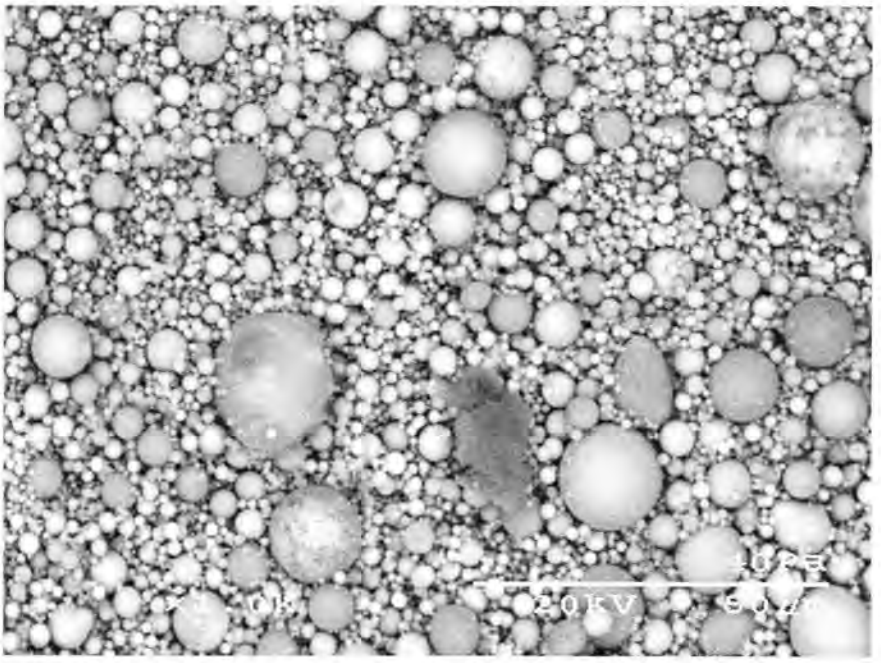

Figure 81. SEM Image of OGS Fly Ash Magnified 1000X

CKD Chemical Analysis

The CKD source was the Holcim Portland cement plant located in Mason City, Iowa. A chemical analysis was conducted to determine the composition of the CKD. Table 10 shows the results for the CKD chemical analysis. Note the high CaO content. This shows that the material will be reactive as a pozzolanic activator. Also note the high SO_3 content. This material may show expansive tendencies in the future.

SEM images were taken of the CKD to compare to the fly ash. The CKD has much more angular particles. The SEM image for the CKD is shown in Figure 82. Other SEM images of the CKD can be found in the Appendix.

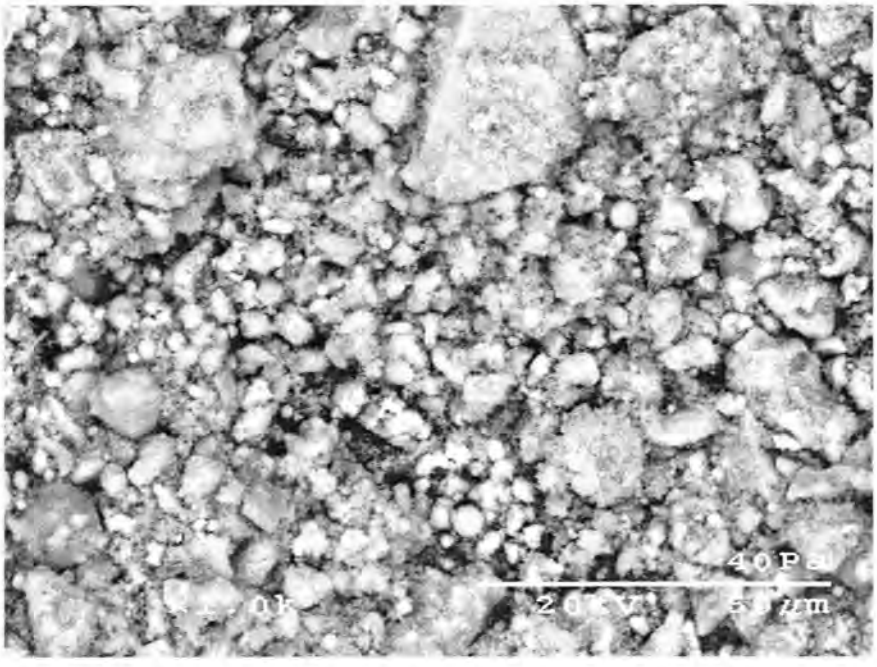

Figure 82. SEM Image of CKD Magnified 1000X

Type I Portland Cement Chemical Analysis

The Holcim Portland cement plant located in Mason City, Iowa was also the source of the type I Portland cement used in this study. A chemical analysis was completed on the type I Portland cement, and the results can be found in Table 10.

RESULTS

This results section is divided into three components: (1) Laboratory evaluation of the proposed stabilized mixtures, (2) Construction operations, and (3) Performance monitoring to evaluate the effectiveness of stabilized limestone screenings as a structural layer in road construction. Each section details specific outcomes pertaining to that section.

Laboratory Evaluation of Proposed Stabilized Mixtures

This section details results obtained from laboratory tests including: (1) Moisture-Density relationship, (2) Moisture-Strength relationship, (3) Wet/Dry durability, and (4) Freeze/Thaw durability.

Moisture-Density Relationship

This section shows the results obtained from the five point Proctor compaction testing conducted on each stabilized mixture proposed. Results are shown for both the limestone screenings and manufactured sand. Results show a decrease in maximum dry density with an increase in stabilizer percentage.

Limestone Screenings

The moisture-density characteristics for limestone screenings mixtures tested are shown in Figures 83 to 132. Note that the maximum densities shown are an average of three samples, and the error bars shown are for a 95% confidence interval. Note that with the increase in stabilizer, there is a general decrease in maximum dry density and an increase in the optimum moisture content required to obtain maximum density.

Note the behavior shown in Figures 87 and 97. The decrease in maximum density with the increase in water content shows the bulking behavior of the material. Granular material exhibits this behavior at low moisture contents.

The optimum moisture content for density and the average maximum density results for each limestone screenings mixture are shown in Table 11. Note that the addition of CKD reduces the maximum densities compared to the other stabilizers.

Manufactured Sand

The moisture-density relationships for manufactured sand mixtures tested are shown in Figures 133 to 172. Note that the maximum densities shown are an average of three samples, and the error bars shown are for a 95% confidence interval. Also note that as the percent stabilizer is increased, there is a decrease in maximum dry density and an increase in moisture required to reach the maximum density.

Note the behavior shown in Figure 147. The sudden decrease in maximum density with the increase in water content shows the bulking behavior of the material. Granular material exhibits this behavior at low moisture contents.

The optimum moisture content for density and the average maximum density results for each manufactured sand mixture are shown in Table 12. Note the decrease in density and increase in moisture content as the binder contents increase for each stabilizer tested.

Table 11. Optimum Moisture Contents, Maximum Densities, and Maximum Unconfined Compressive Strengths for All Limestone Screenings Mixtures

Binder	Mixture Number	Optimum Moisture Content for Strength %	Optimum Moisture Content for Density %	Average Maximum Density kg/m^3	Average Maximum Unconfined Compressive Strength kPa
CKD	1	10.0	12.6	1929	2074
	2	12.7	12.7	1861	3998
	3	13.5	15.4	1770	4780
	4	18.6	21.8	1706	4572
	5	17.3	17.3	1607	7896
Riverside / CKD	1	8.9	11.7	2028	8305
	2	10.7	10.7	2011	11566
	3	12.7	12.7	1937	15676
	4	9.3	9.3	1899	9975
	5	16.1	13.7	1834	14765
OGS / CKD	1	8.9	11.7	2026	7387
	2	10.9	10.9	2014	12874
	3	10.9	10.9	1953	20303
	4	16.9	11.5	1842	17732
	5	14.7	14.7	1769	19425
Portland Cement	1	9.2	12.1	2020	1736
	2	9.0	12.0	2014	4296
	3	8.0	11.1	2034	7726
	4	8.1	11.0	2055	9306
	5	10.9	10.9	2049	8415
Prairie Creek Fly Ash	1	9.0	11.0	2025	1015
	2	11.0	11.0	1970	2197
	3	11.7	13.8	1856	2502
	4	11.2	13.7	1845	2900
	5	13.4	13.4	1772	3015

Table 12. Optimum Moisture Contents, Maximum Densities, and Maximum Unconfined Compressive Strengths for All Manufactured Sand Mixtures

Binder	Mixture Number	Optimum Moisture Content for Strength %	Optimum Moisture Content for Density %	Average Maximum Density kg/m^3	Average Maximum Unconfined compressive Strength kPa
CKD	1	10.7	11.6	1963	1007
	2	10.2	12.8	1958	3461
	3	14.2	14.2	1851	4827
	4	20.9	12.4	1907	5369
	5	19.0	19.0	1632	5245
Riverside / CKD	1	11.0	14.1	2027	4375
	2	8.9	12.2	2030	14957
	3	10.5	10.5	2044	22183
	4	12.6	12.6	1926	19338
	5	13.4	13.4	1841	16931
OGS / CKD	1	10.9	15.6	2268	4870
	2	9.9	9.9	2099	16466
	3	12.2	8.4	2041	16715
	4	12.8	9.5	2003	11451
	5	15.0	12.1	1882	10025
Portland Cement	1	0.6	0.6	1873	0
	2	7.1	9.5	1888	2073
	3	6.5	11.5	1976	6017
	4	8.2	11.8	2027	9769
	5	7.8	7.8	2117	12345

Moisture-Strength Relationship

This section details results obtained from unconfined compression strength testing for both the manufactured sand and limestone screenings stabilized mixtures. Results show a dramatic decrease in unconfined compressive strength once the moisture content increases beyond the optimum moisture content for strength. The second result shows that the addition of stabilizer greatly affects the unconfined compressive strength of the mixture. Unconfined compressive strengths increased with an increase in stabilizer percentage.

Limestone Screenings

The moisture-strength relationships for limestone screenings mixtures tested are shown in Figures 83 to 132. Note the dramatic decrease in strength due to an increase in moisture past the optimum moisture contents based on strength. Note that the maximum strengths shown are a three point average, and the error bars shown are for a 95% confidence interval.

The maximum unconfined compressive strengths and their corresponding moisture contents are shown in Table 11. Note that there is an increase in strength with an increase in stabilizer content. The optimum moisture content for strength generally increases as the binder content increases.

Pictures detailing completed unconfined compression strength testing for all limestone screening mixtures can be found in the Appendix.

Manufactured Sand

The moisture-strength characteristics for manufactured sand mixtures tested are shown in Figures 133 to 172. Note the dramatic drop in strength associated with a slight increase in moisture past the optimum moisture content based on strength. Note that the maximum unconfined compressive strengths shown are three point averages, and the error bars shown are for a 95% confidence interval.

Table 12 shows a tabular form of the results for the maximum unconfined compressive strengths and the optimum moisture contents for strength for all manufactured sand mixtures. Note the increase in unconfined compressive strength as the stabilizer content is increased. Also note that the optimum moisture content based on strength increases as the binder contents are increased.

Pictures showing completed unconfined compression strength testing for all manufactured sand samples can be found in the Appendix.

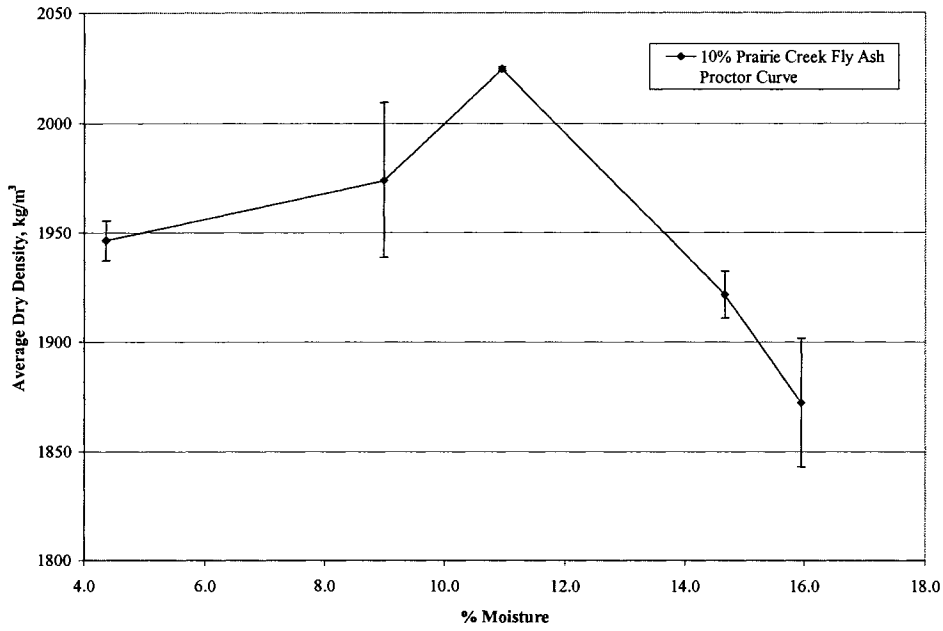

Figure 83. Limestone Screenings and 10% Prairie Creek Fly Ash Proctor Curve

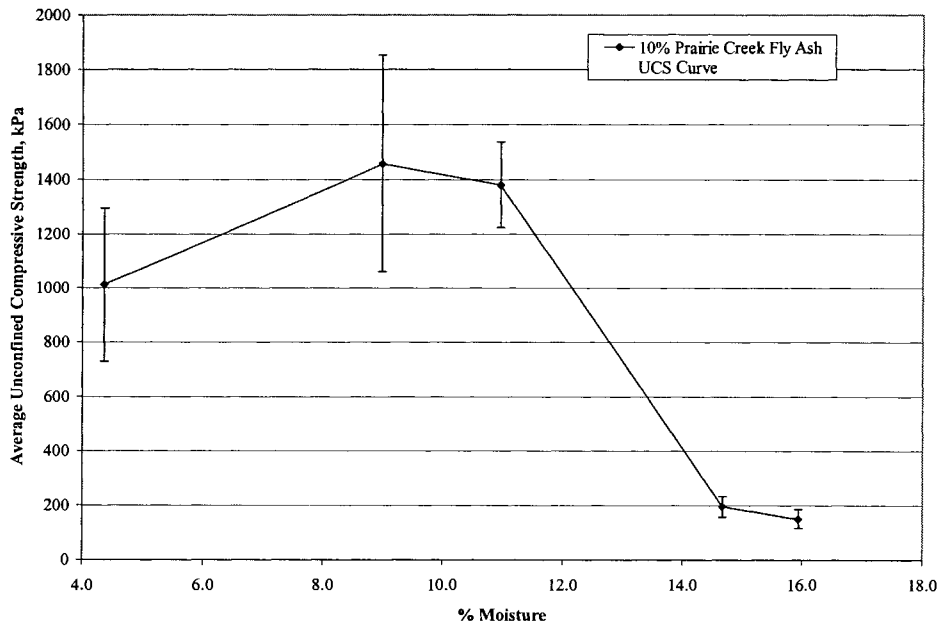

Figure 84. Moisture-Strength Curve for Limestone Screenings and 10% Prairie Creek Fly Ash

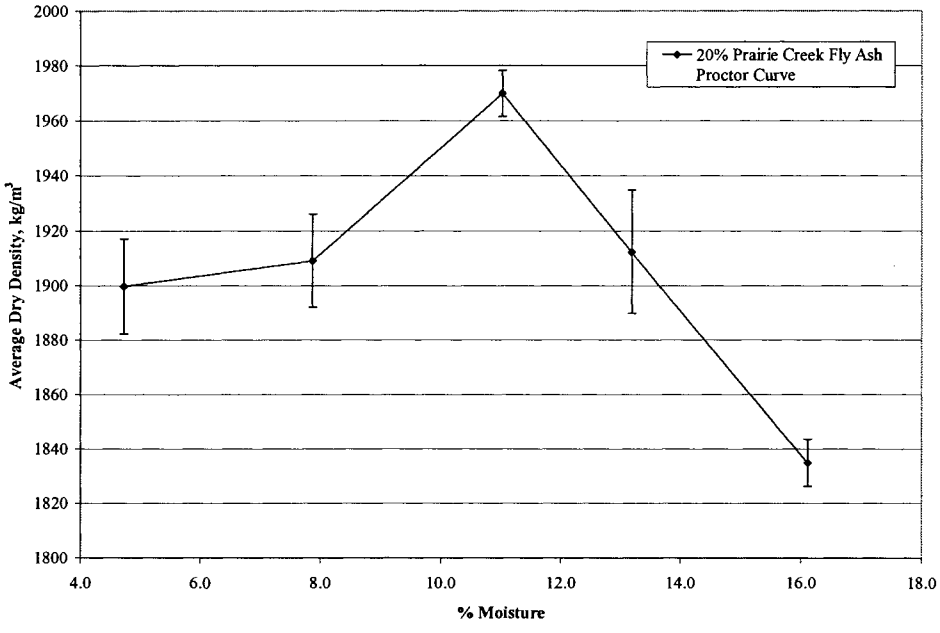

Figure 85. Limestone Screenings and 20% Prairie Creek Fly Ash Proctor Curve

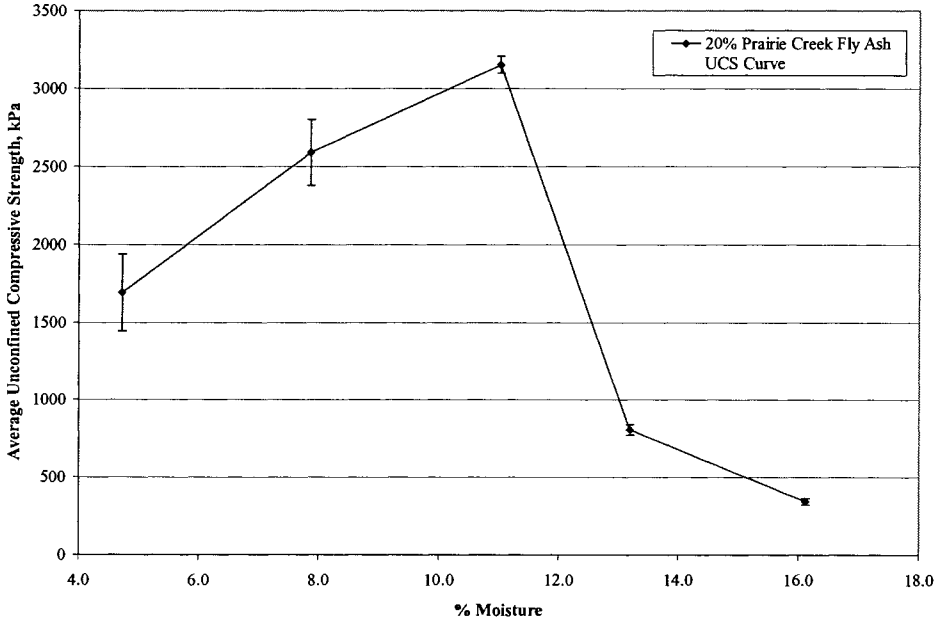

Figure 86. Moisture-Strength Curve for Limestone Screenings and 20% Prairie Creek Fly Ash

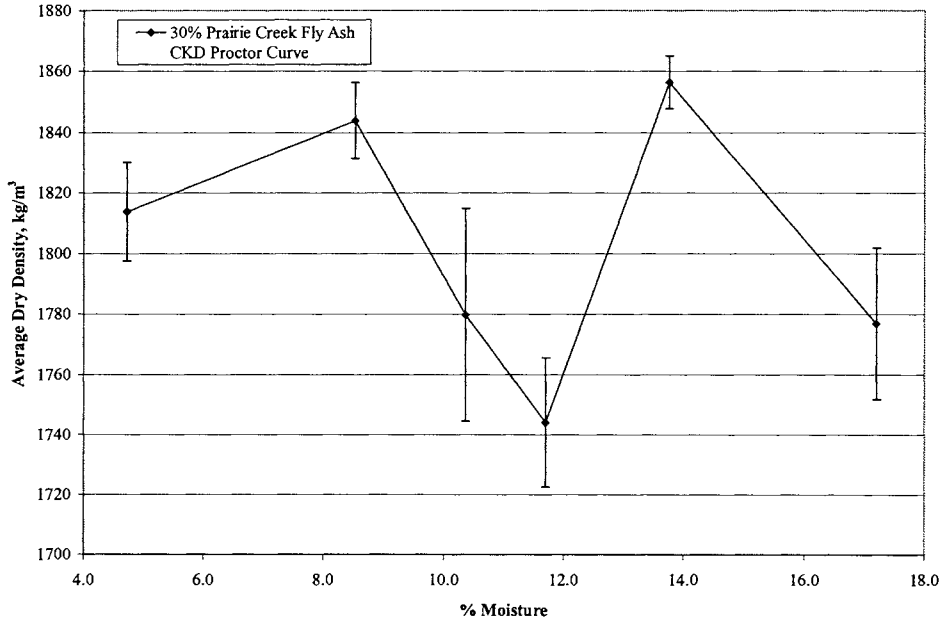

Figure 87. Limestone Screenings and 30% Prairie Creek Fly Ash Proctor Curve

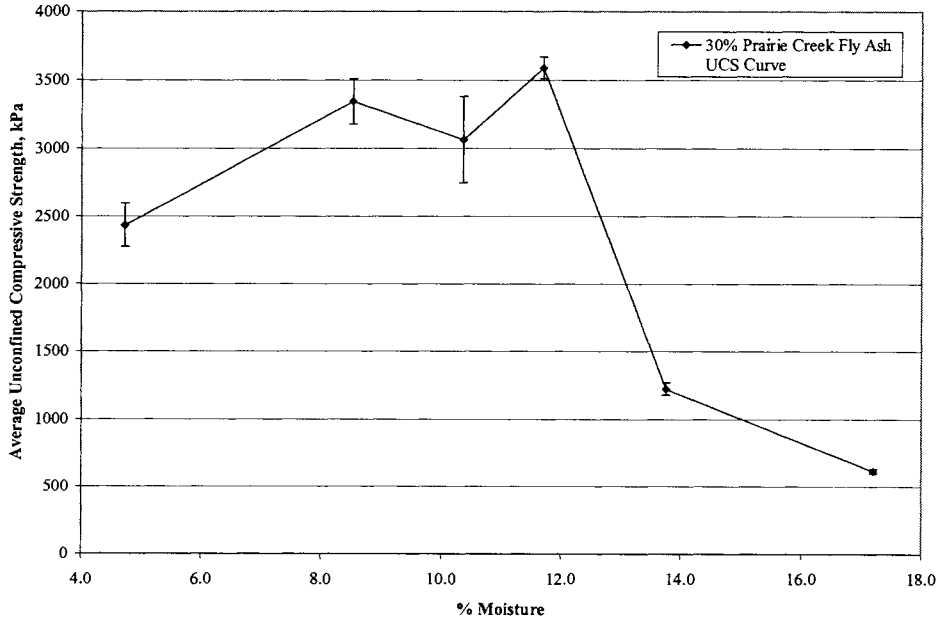

Figure 88. Moisture-Strength Curve for Limestone Screenings and 30% Prairie Creek Fly Ash

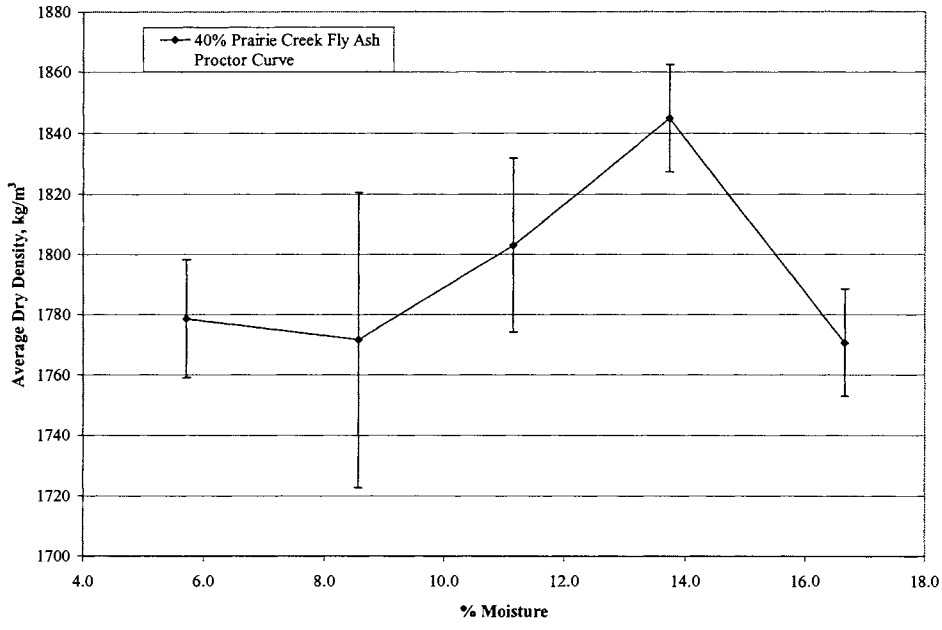

Figure 89. Limestone Screenings and 40% Prairie Creek Fly Ash Proctor Curve

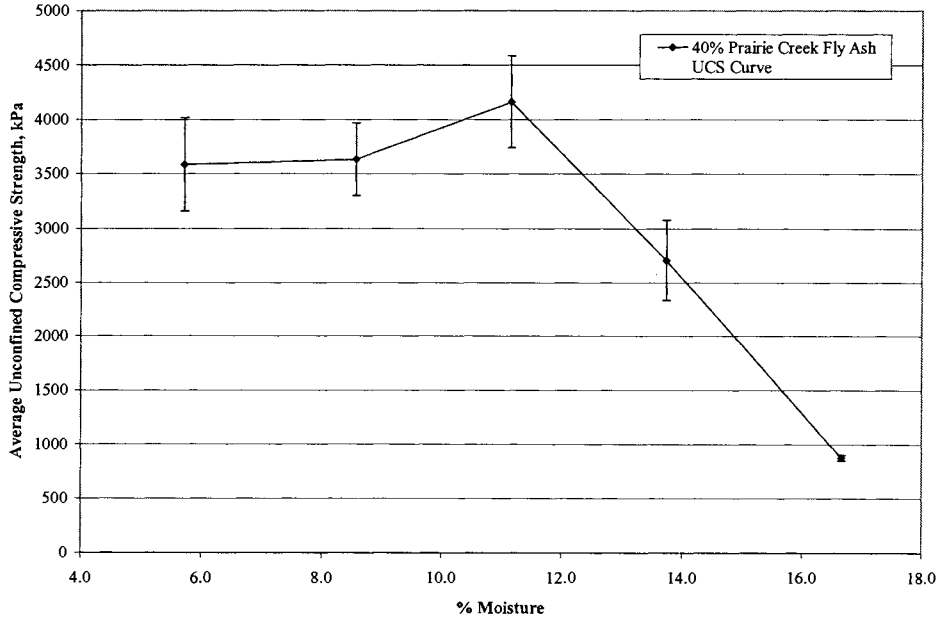

Figure 90. Moisture-Strength Curve for Limestone Screenings and 40% Prairie Creek Fly Ash

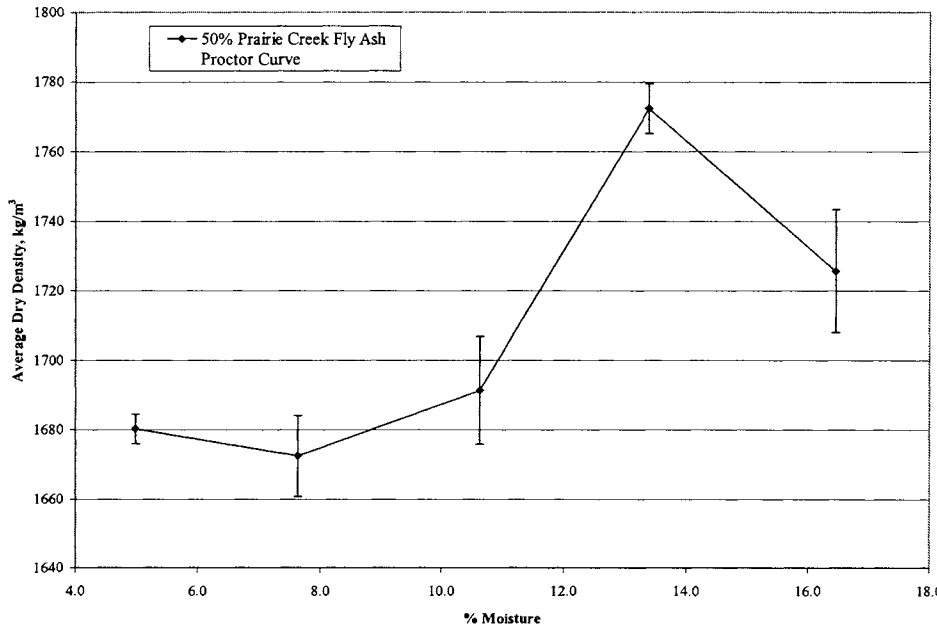

Figure 91. Limestone Screenings and 50% Prairie Creek Fly Ash Proctor Curve

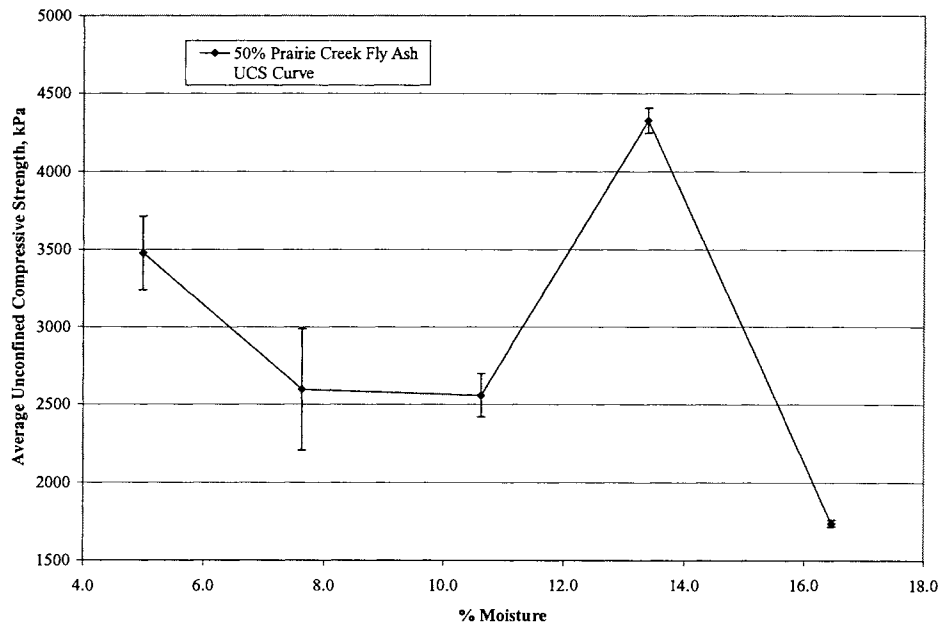

Figure 92. Moisture-Strength Curve for Limestone Screenings and 50% Prairie Creek Fly Ash

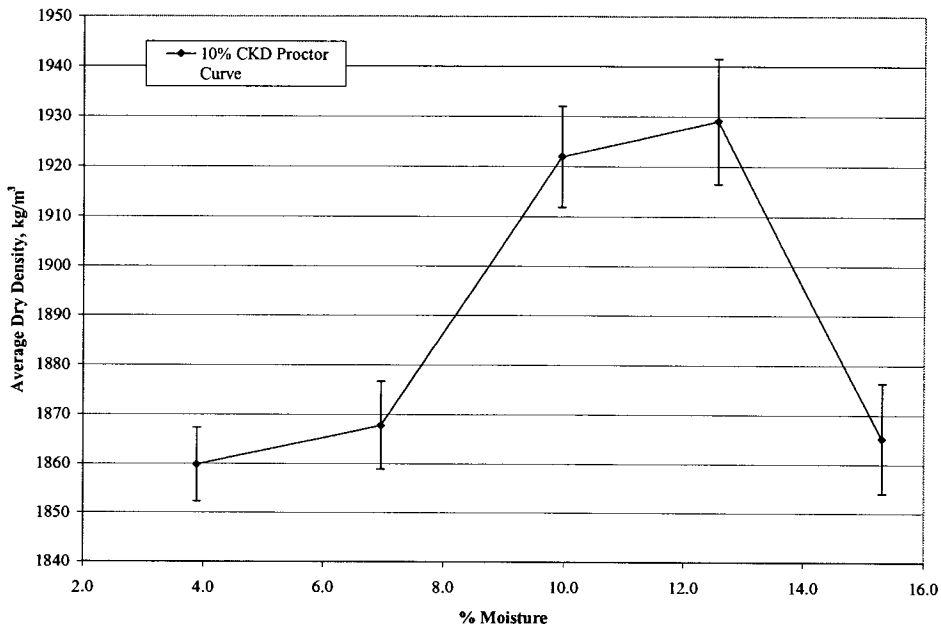

Figure 93. Limestone Screenings and 10% CKD Proctor Curve

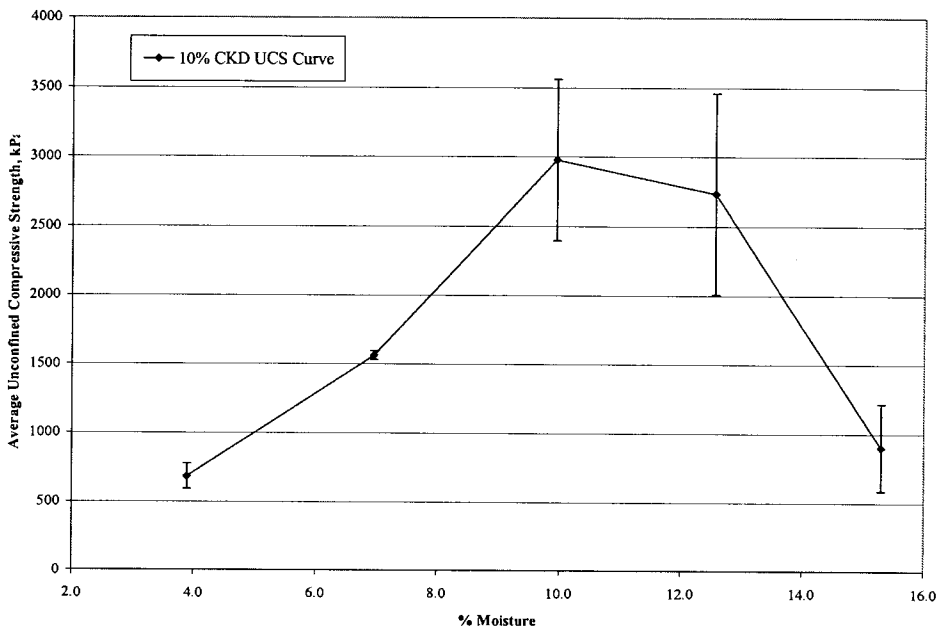

Figure 94. Moisture-Strength Curve for Limestone Screenings and 10% CKD

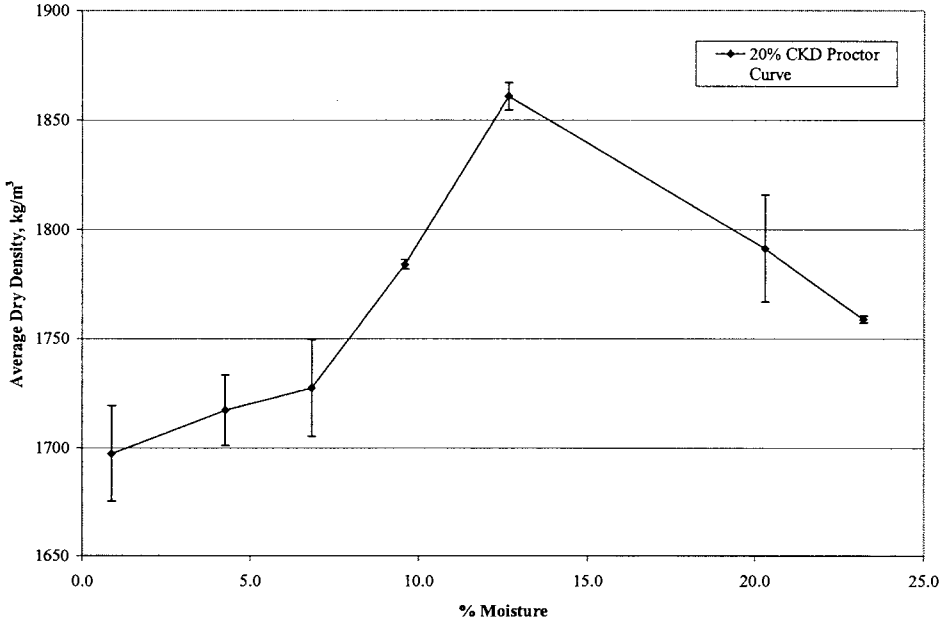

Figure 95. Limestone Screenings and 20% CKD Proctor Curve

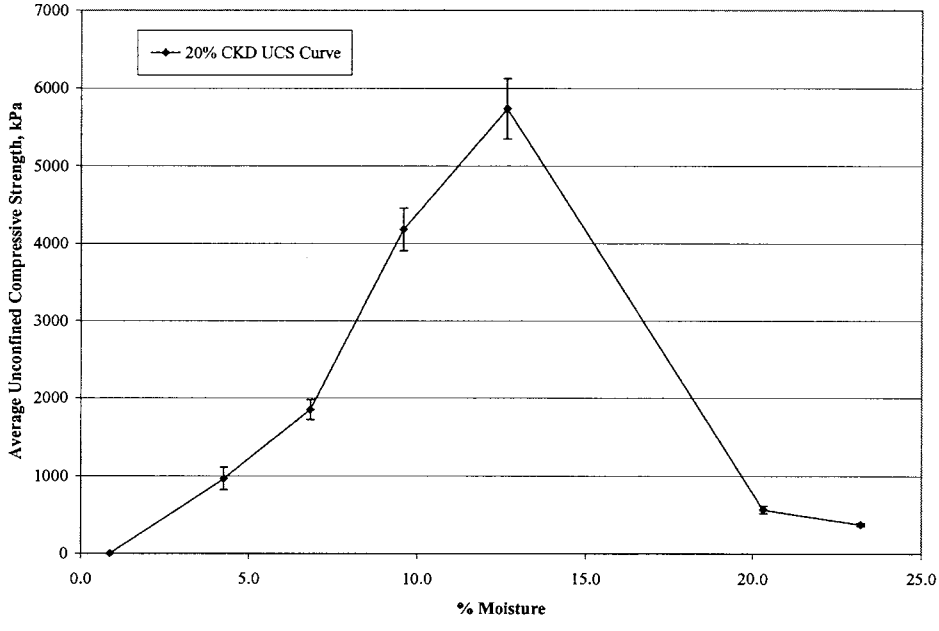

Figure 96. Moisture-Strength Curve for Limestone Screenings and 20% CKD

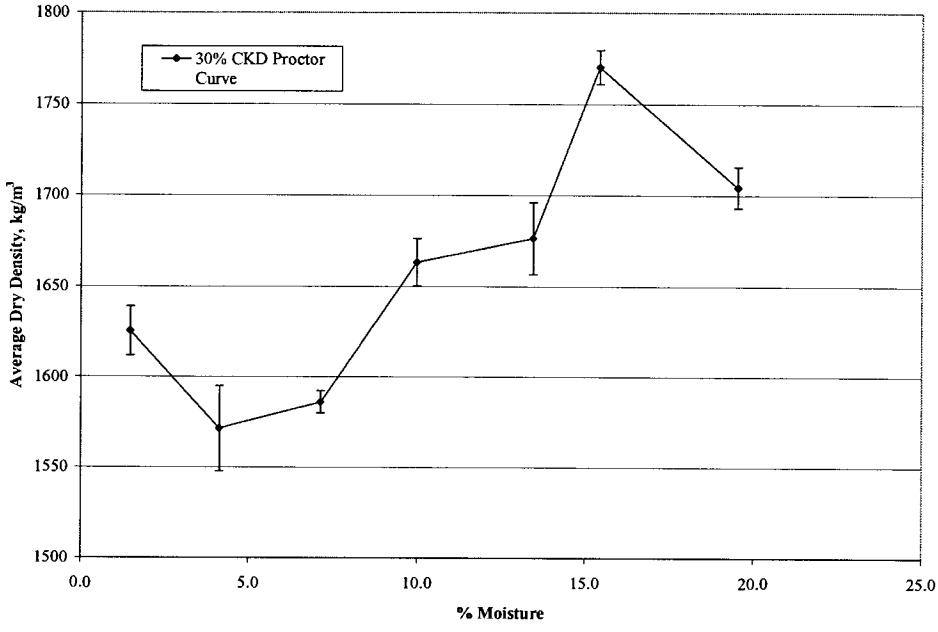

Figure 97. Limestone Screenings and 30% CKD Proctor Curve

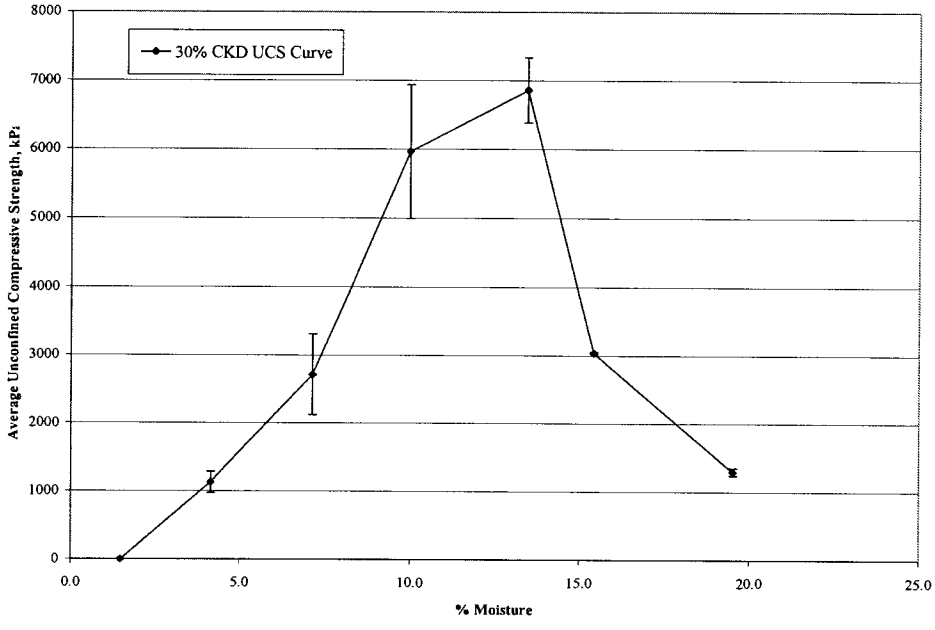

Figure 98. Moisture-Strength Curve for Limestone Screenings and 30% CKD

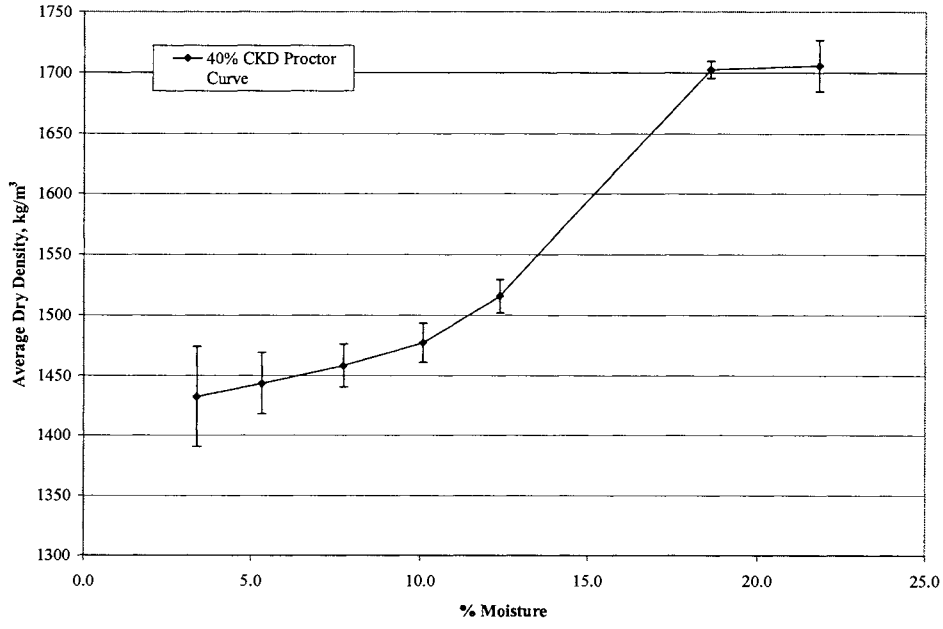

Figure 99. Limestone Screenings and 40% CKD Proctor Curve

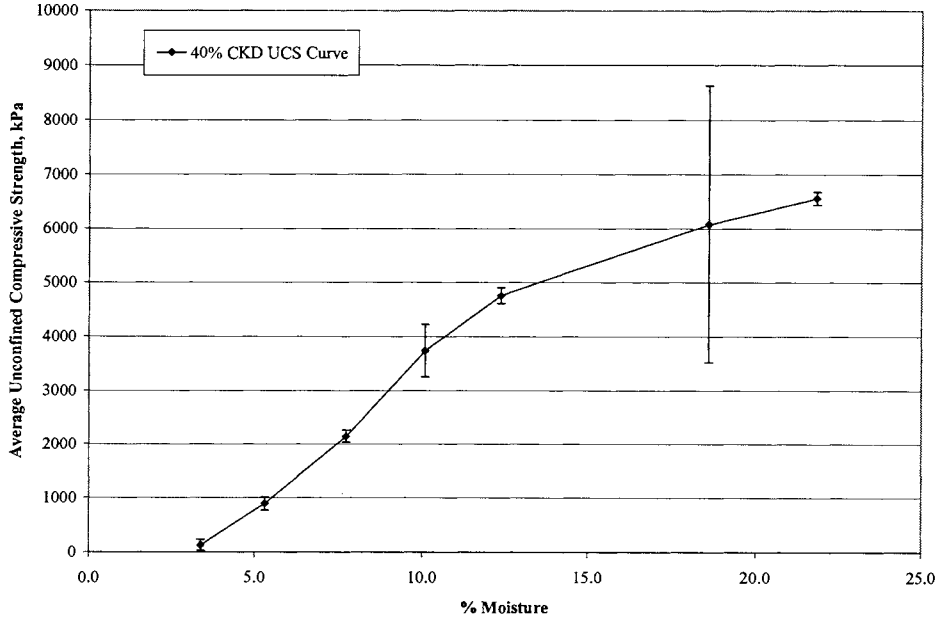

Figure 100. Moisture-Strength Curve for Limestone Screenings and 40% CKD

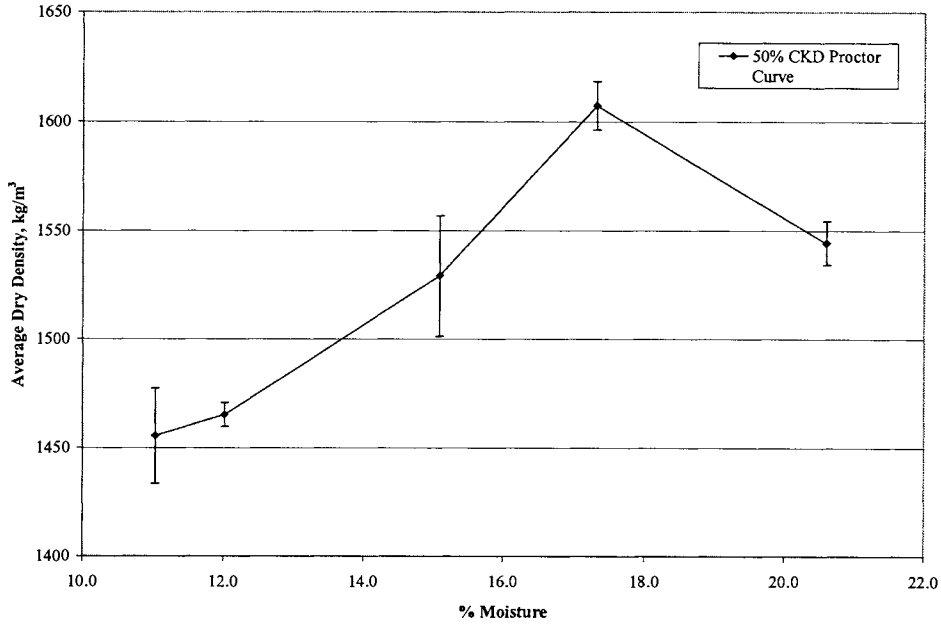

Figure 101. Limestone Screenings and 50% CKD Proctor Curve

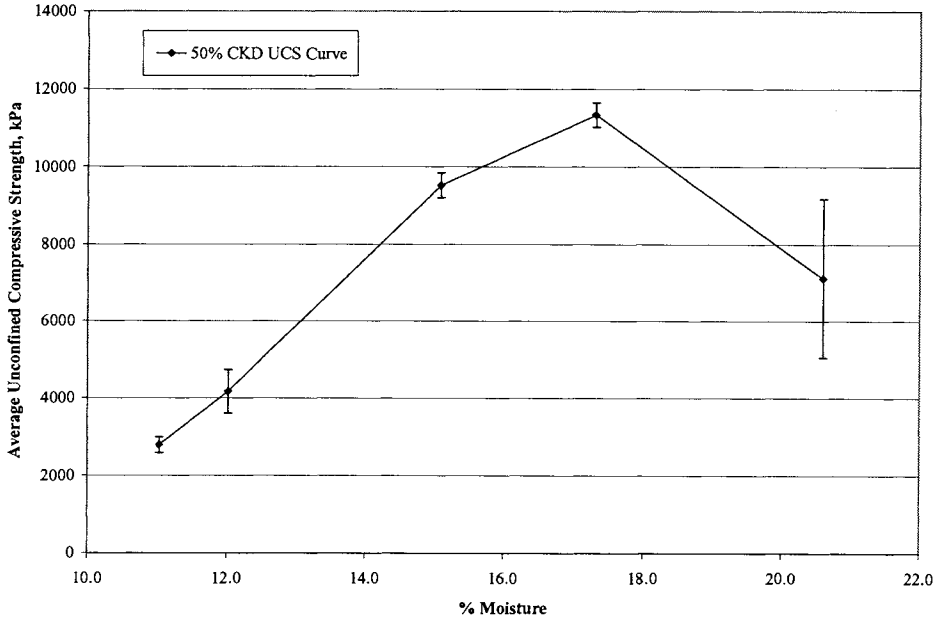

Figure 102. Moisture-Strength Curve for Limestone Screenings and 50% CKD

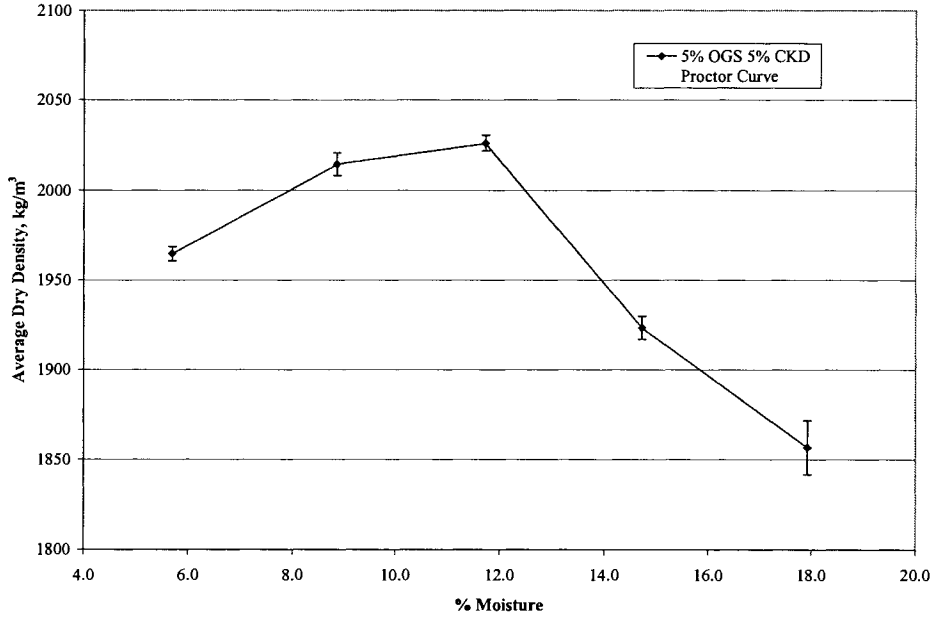

Figure 103. Limestone Screenings and 5% OGS Fly Ash and 5% CKD Proctor Curve

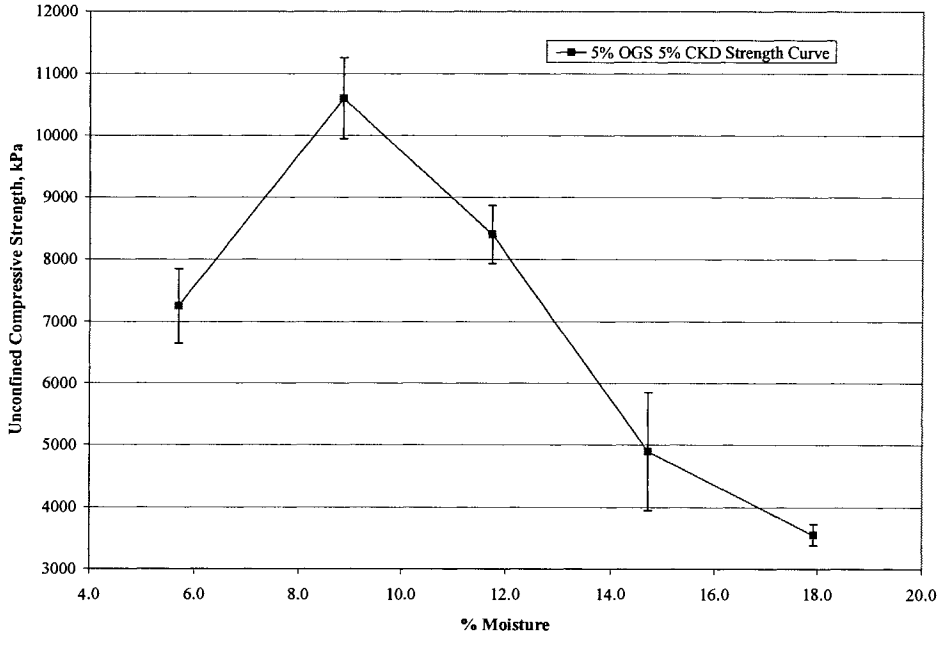

Figure 104. Moisture-Strength Curve for Limestone Screenings and 5% OGS Fly Ash and 5% CKD

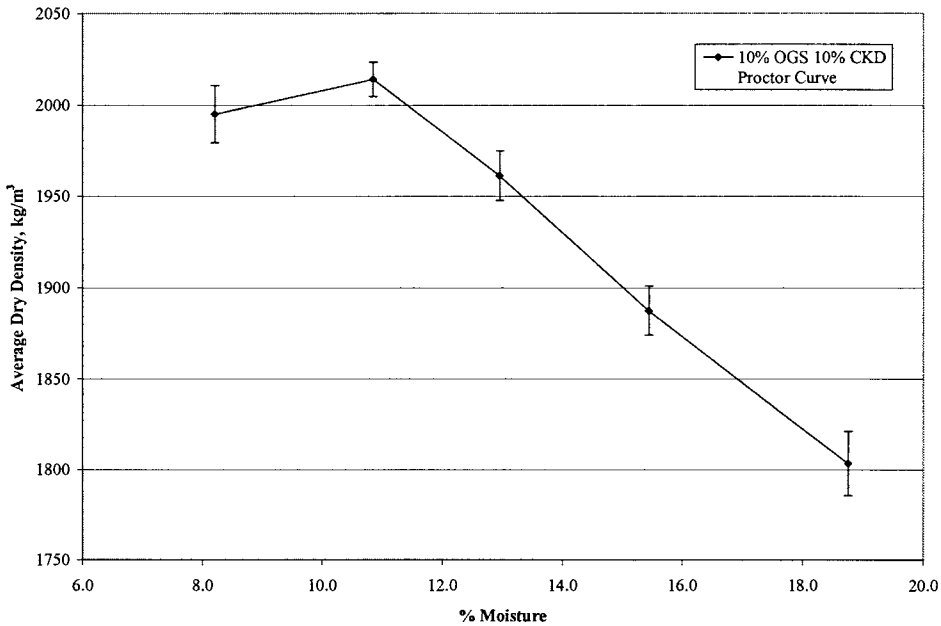

Figure 105. Limestone Screenings and 10% OGS Fly Ash and 10% CKD Proctor Curve

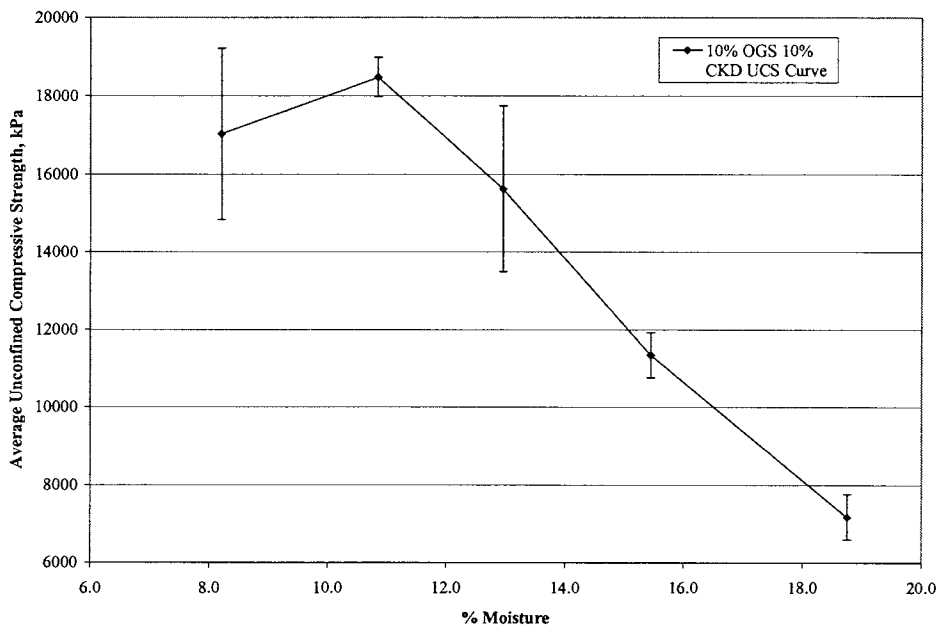

Figure 106. Moisture-Strength Curve for Limestone Screenings and 10% OGS Fly Ash and 10% CKD

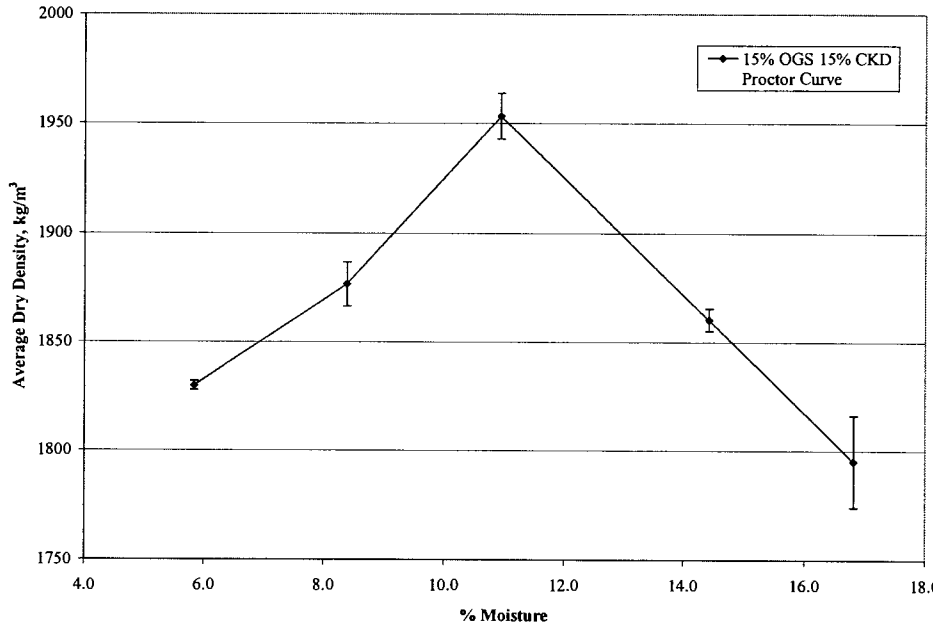

Figure 107. Limestone Screenings and 15% OGS Fly Ash and 15% CKD Proctor Curve

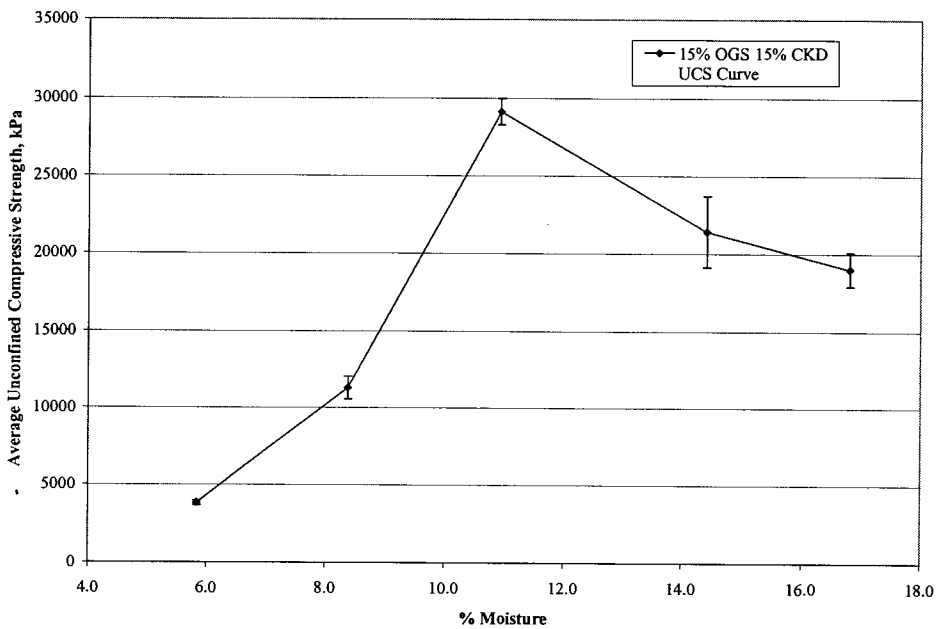

Figure 108. Moisture-Strength Curve for Limestone Screenings and 15% OGS Fly Ash and 15% CKD

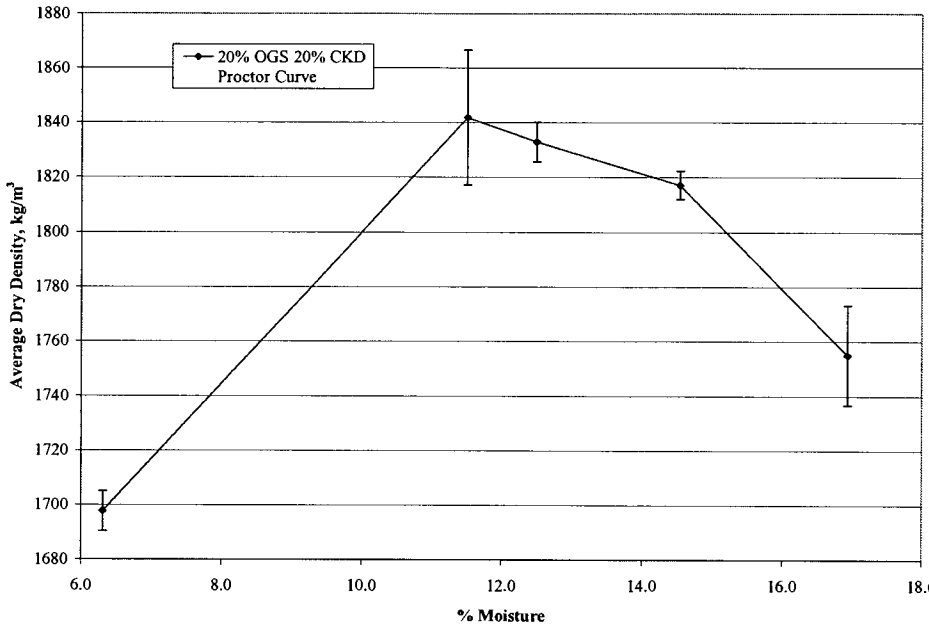

Figure 109. Limestone Screenings and 20% OGS Fly Ash and 20% CKD Proctor Curve

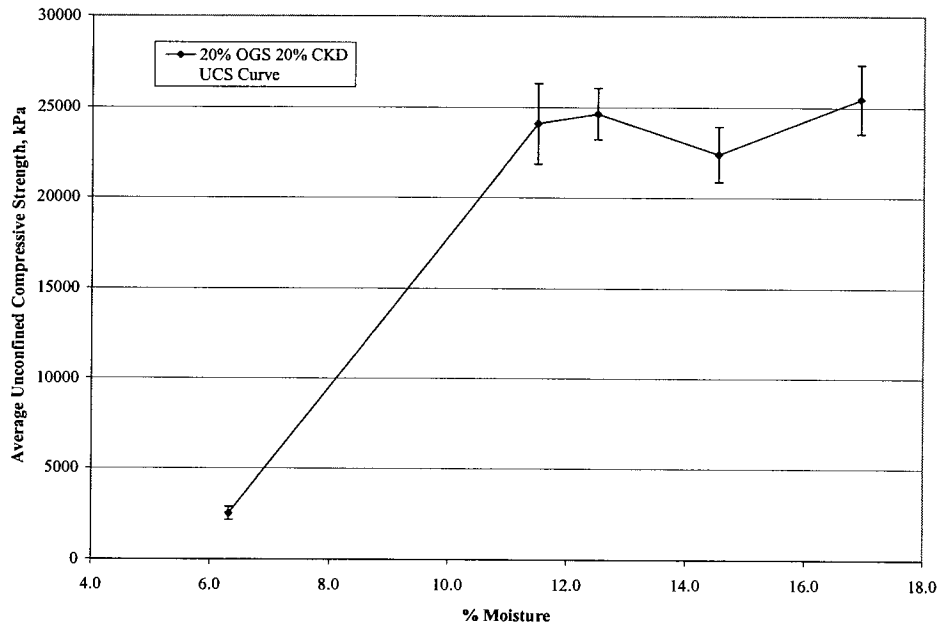

Figure 110. Moisture-Strength Curve for Limestone Screenings and 20% OGS Fly Ash and 20% CKD

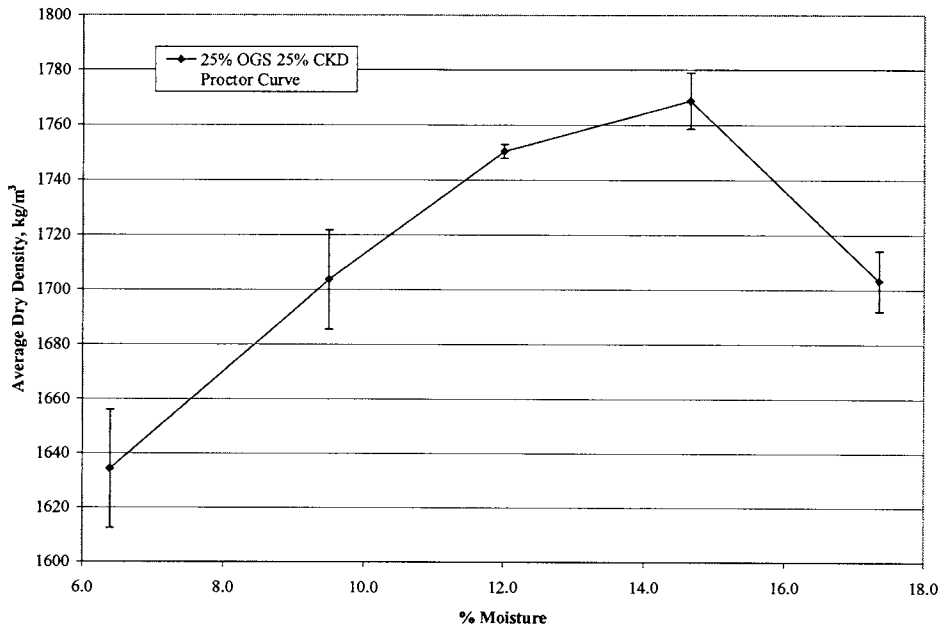

Figure 111. Limestone Screenings and 25% OGS Fly Ash and 25% CKD Proctor Curve

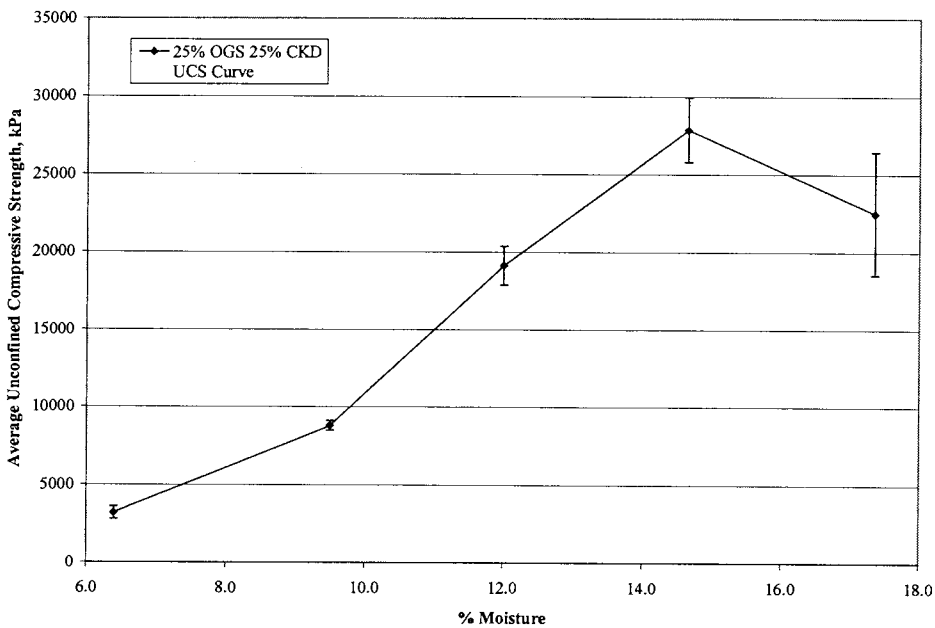

Figure 112. Moisture-Strength Curve for Limestone Screenings and 25% OGS Fly Ash and 25% CKD

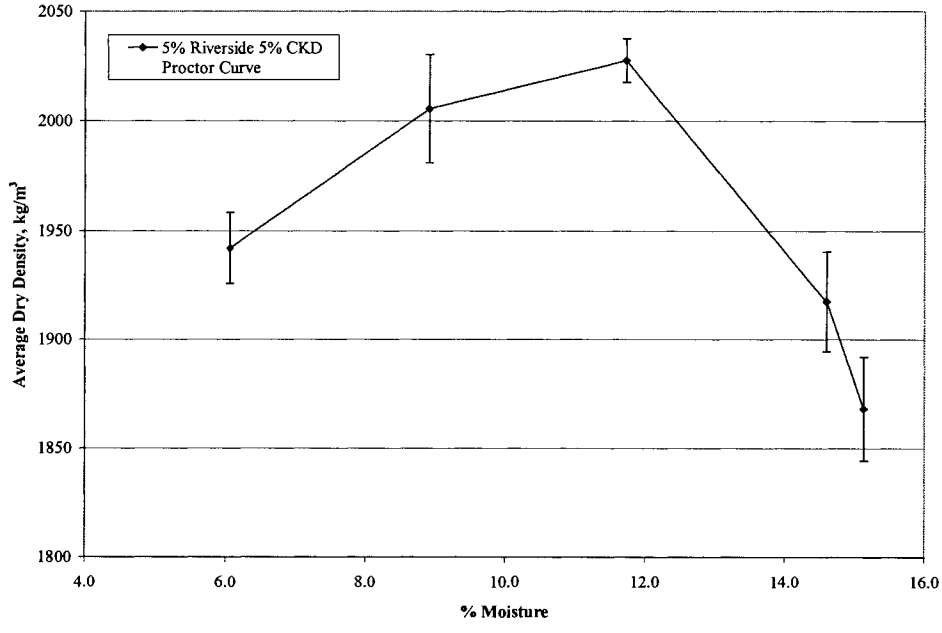

Figure 113. Limestone Screenings and 5% Riverside Fly Ash and 5% CKD Proctor Curve

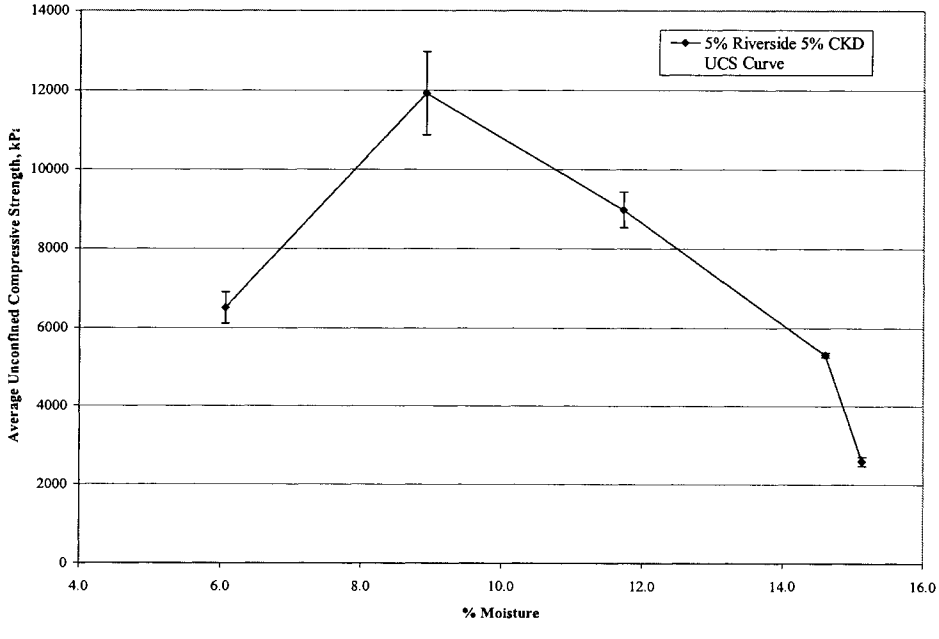

Figure 114. Moisture-Strength Curve for Limestone Screenings and 5% Riverside Fly Ash and 5% CKD

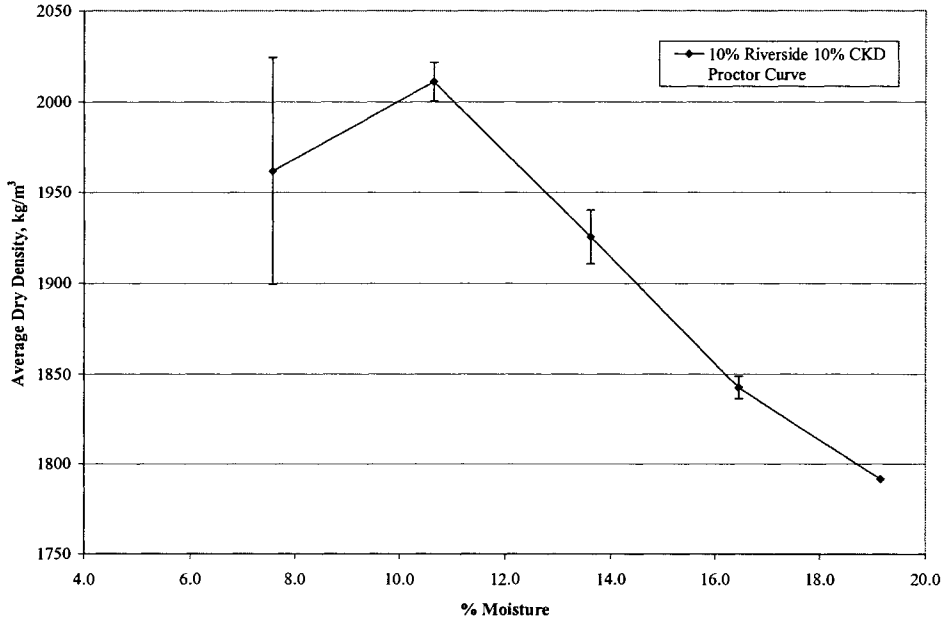

Figure 115. Limestone Screenings and 10% Riverside Fly Ash and 10% CKD Proctor Curve

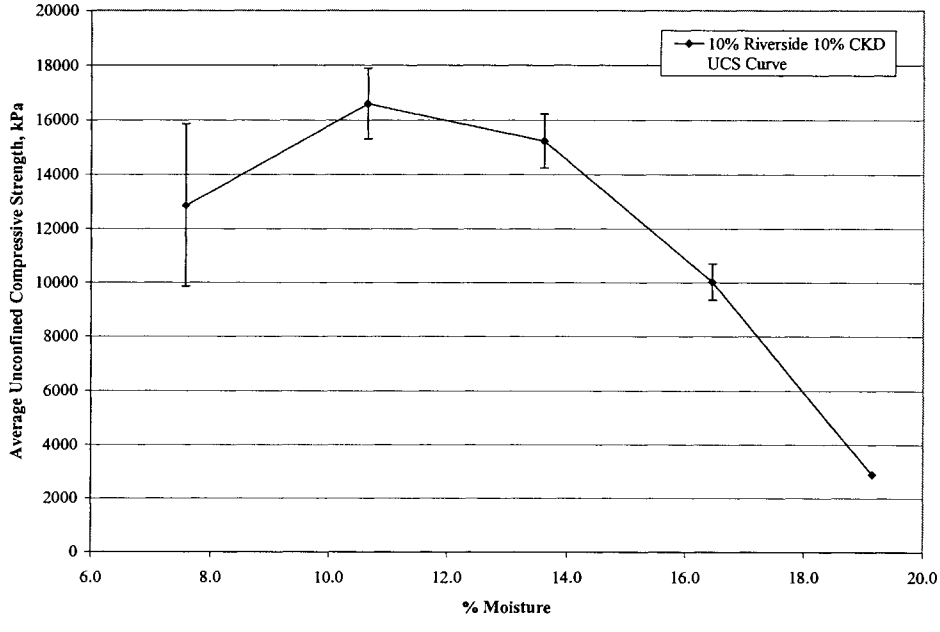

Figure 116. Moisture-Strength Curve for Limestone Screenings and 10% Riverside Fly Ash and 10% CKD

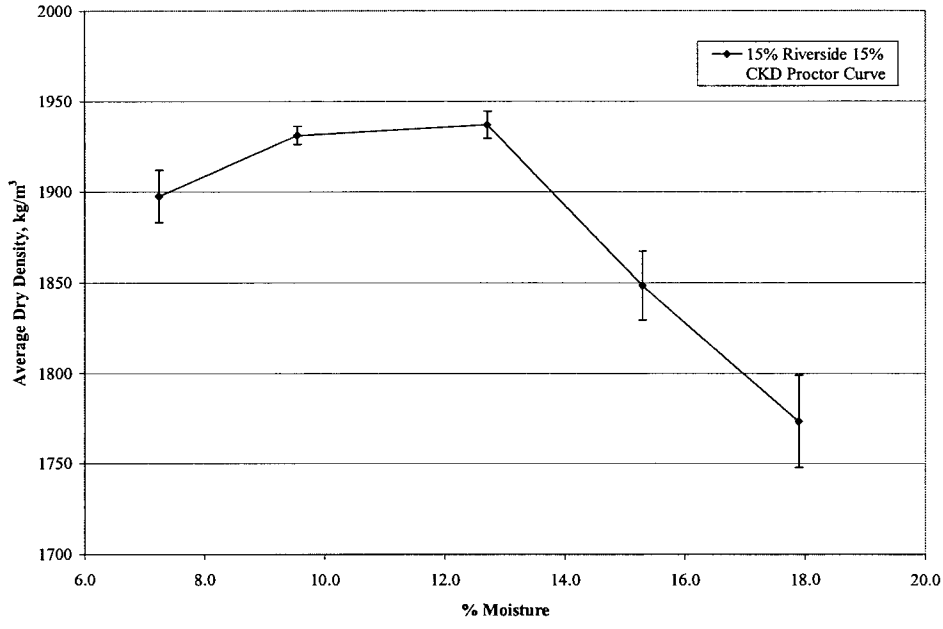

Figure 117. Limestone Screenings and 15% Riverside Fly Ash and 15% CKD Proctor Curve

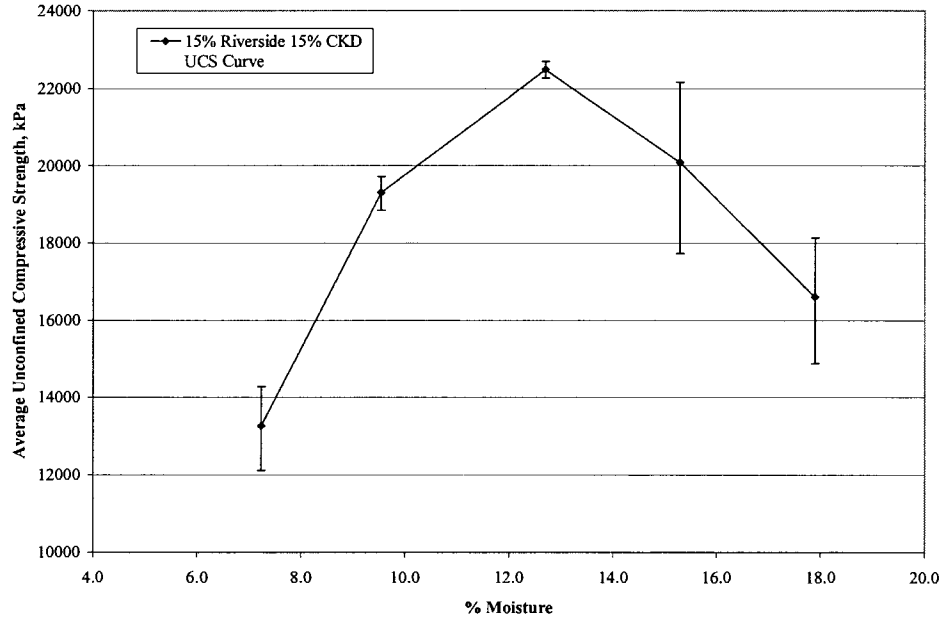

Figure 118. Moisture-Strength Curve for Limestone Screenings and 15% Riverside Fly Ash and 15% CKD

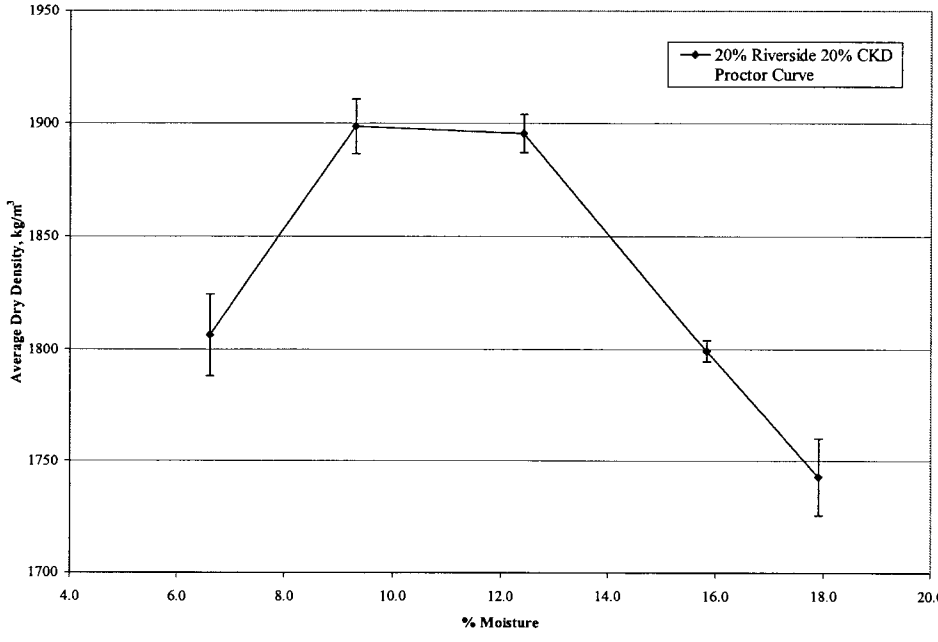

Figure 119. Limestone Screenings and 20% Riverside Fly Ash and 20% CKD Proctor Curve

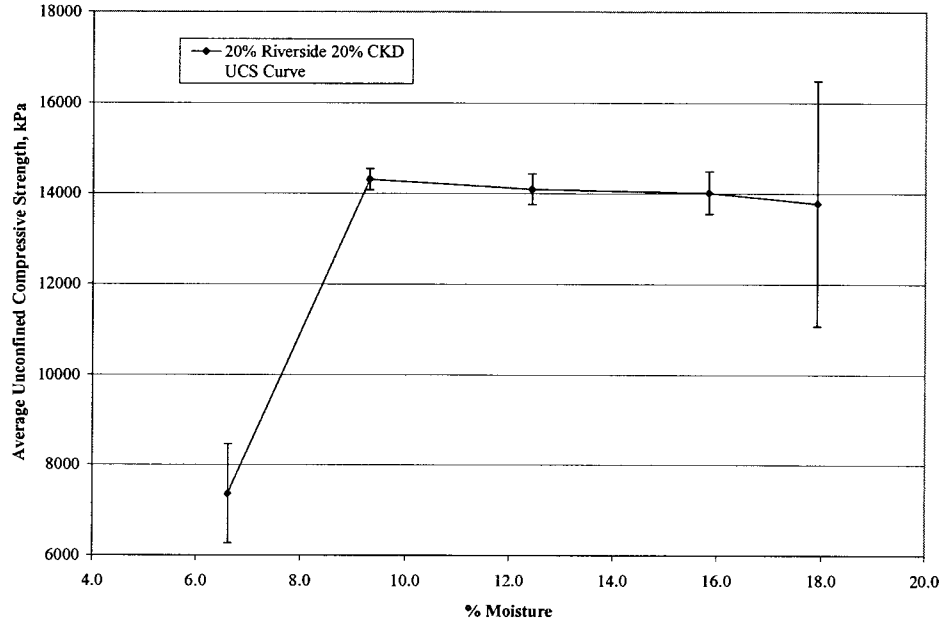

Figure 120. Moisture-Strength Curve for Limestone Screenings and 20% Riverside Fly Ash and 20% CKD

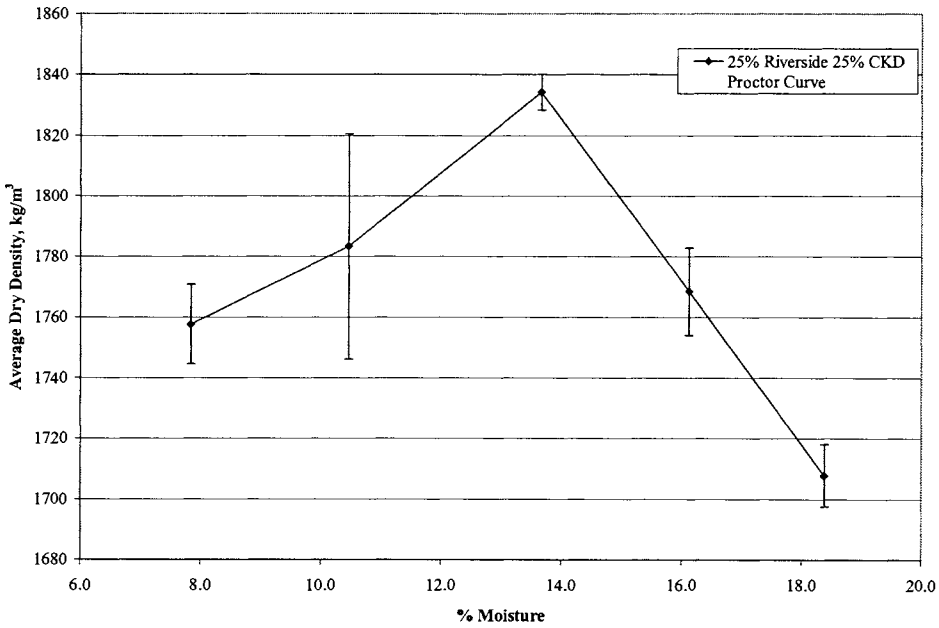

Figure 121. Limestone Screenings and 25% Riverside Fly Ash and 25% CKD Proctor Curve

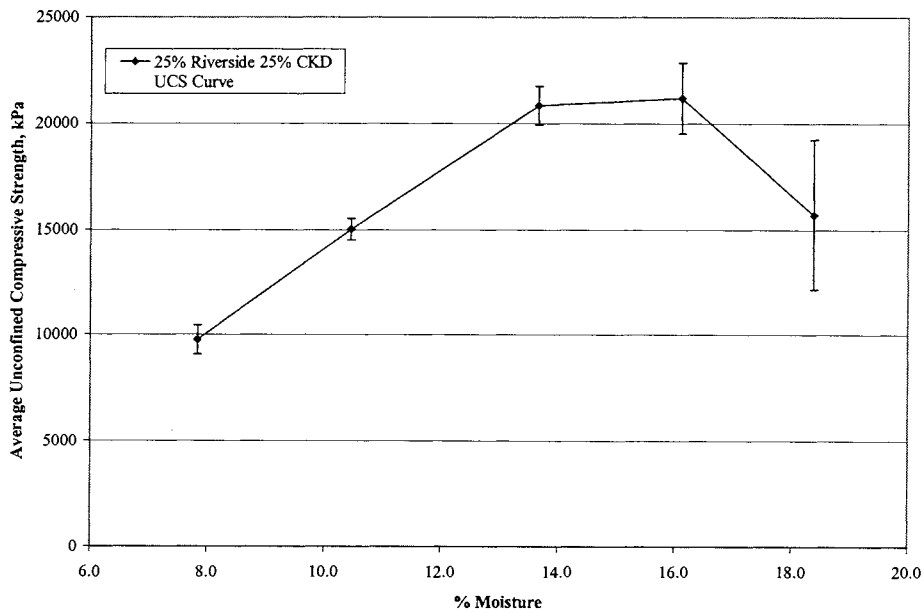

Figure 122. Moisture-Strength Curve for Limestone Screenings and 25% Riverside Fly Ash and 25% CKD

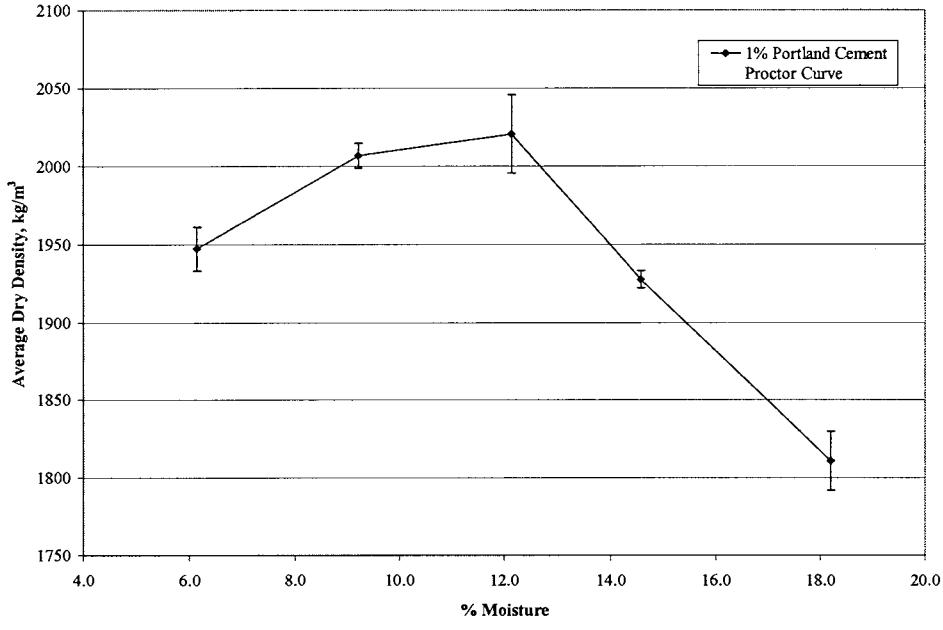

Figure 123. Limestone Screenings and 1% Portland Cement Proctor Curve

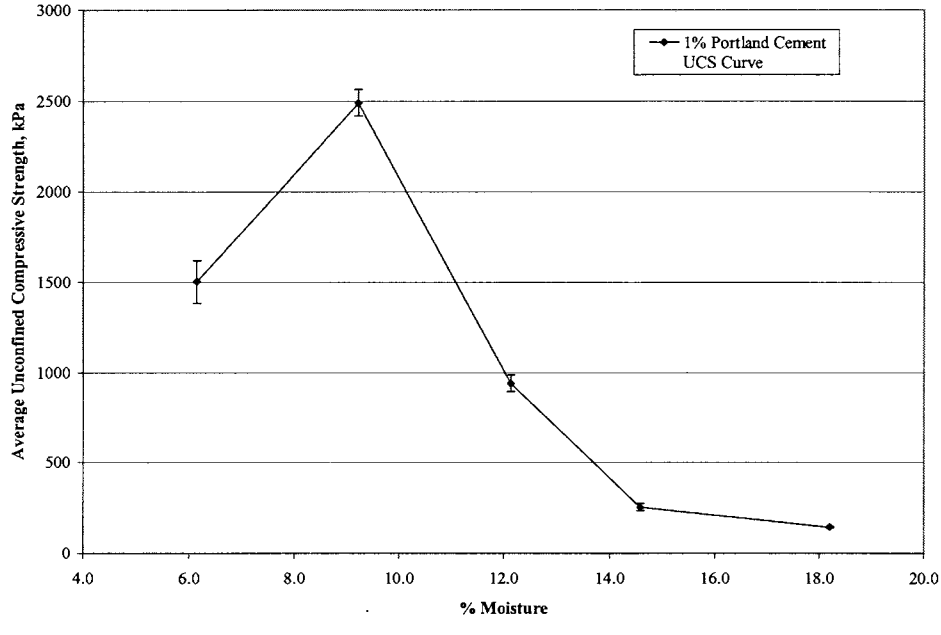

Figure 124. Moisture-Strength Curve for Limestone Screenings and 1% Portland Cement

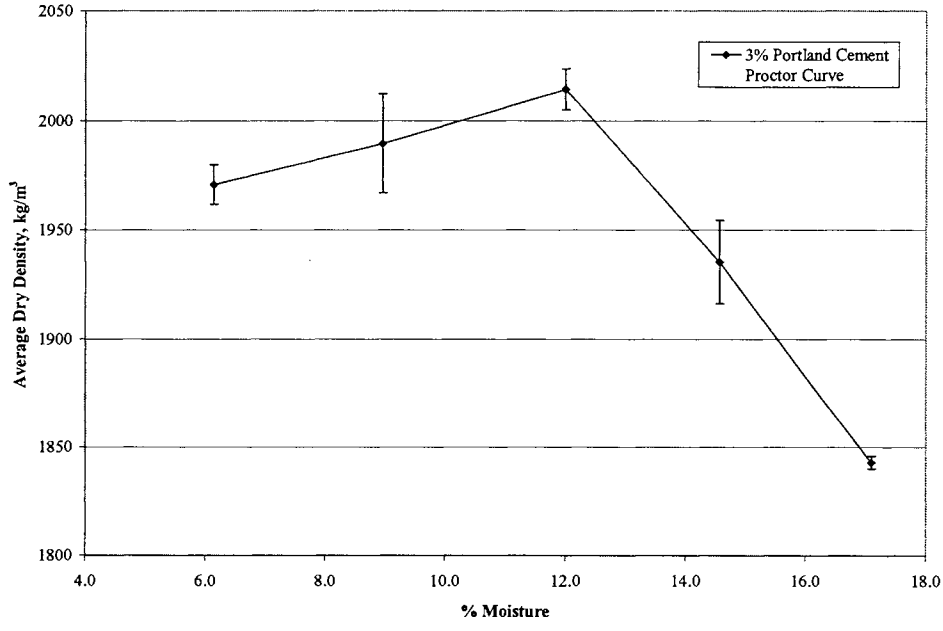

Figure 125. Limestone Screenings and 3% Portland Cement Proctor Curve

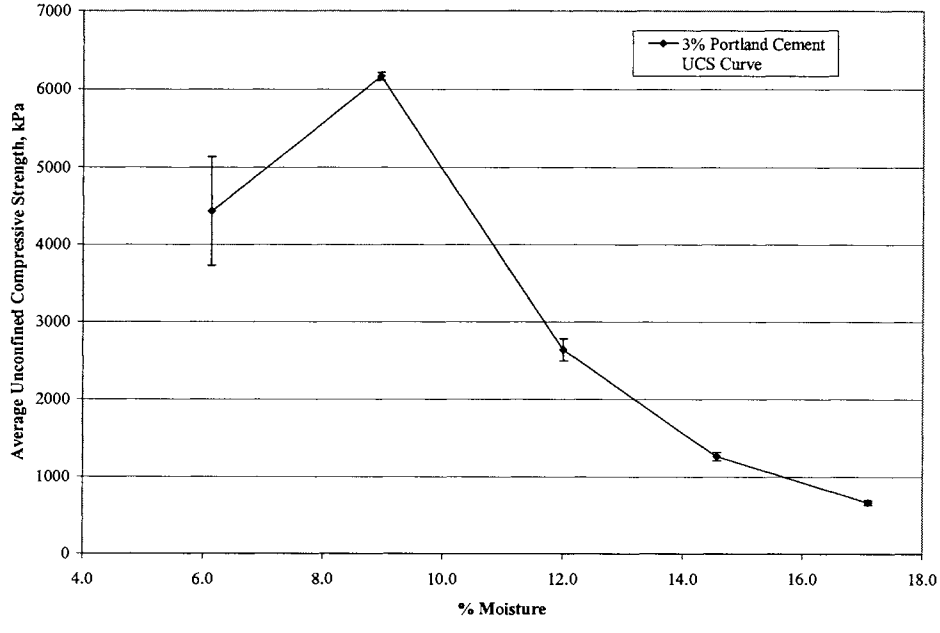

Figure 126. Moisture-Strength Curve for Limestone Screenings and 3% Portland Cement

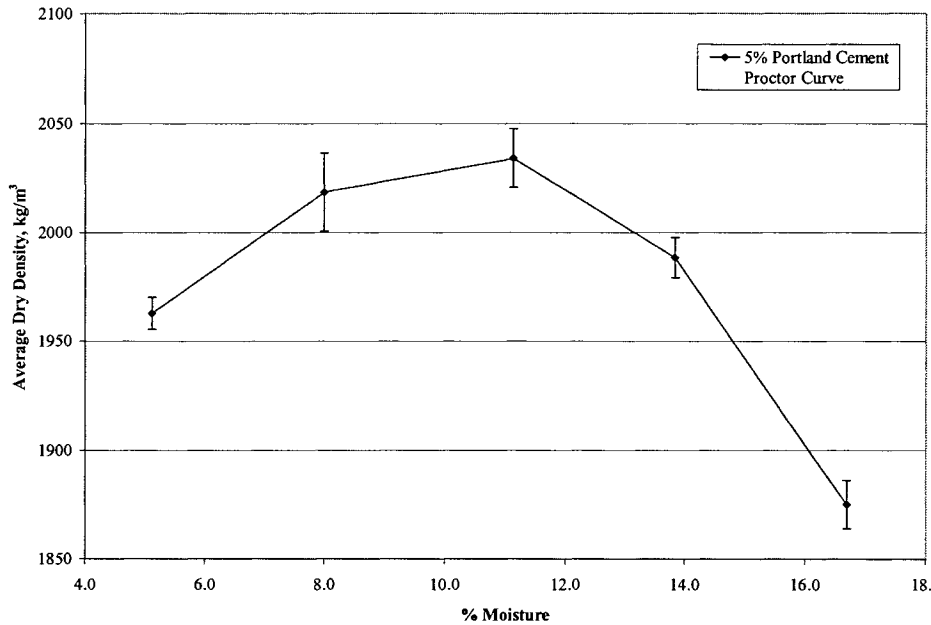

Figure 127. Limestone Screenings and 5% Portland Cement Proctor Curve

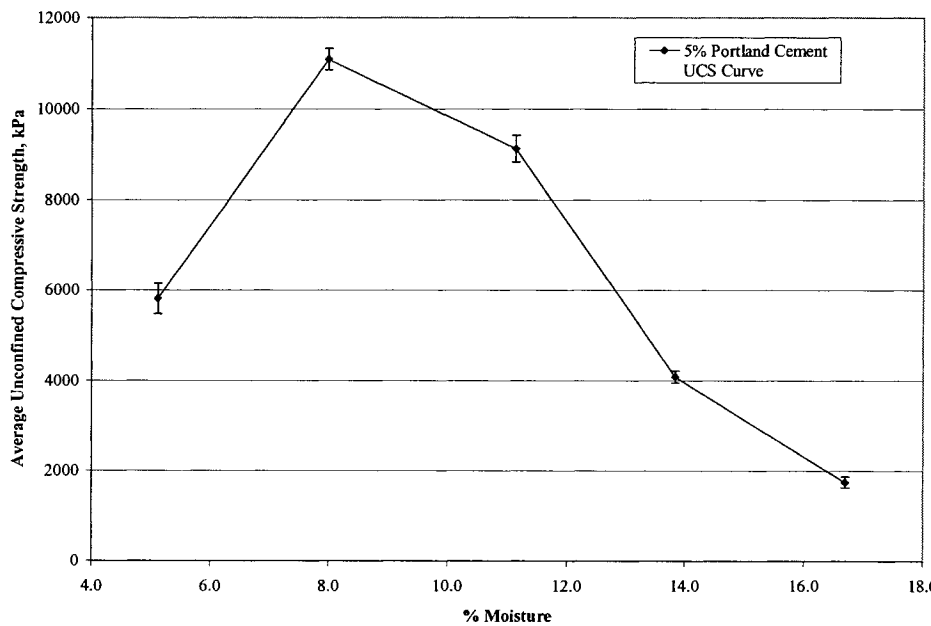

Figure 128. Moisture-Strength Curve for Limestone Screenings and 5% Portland Cement

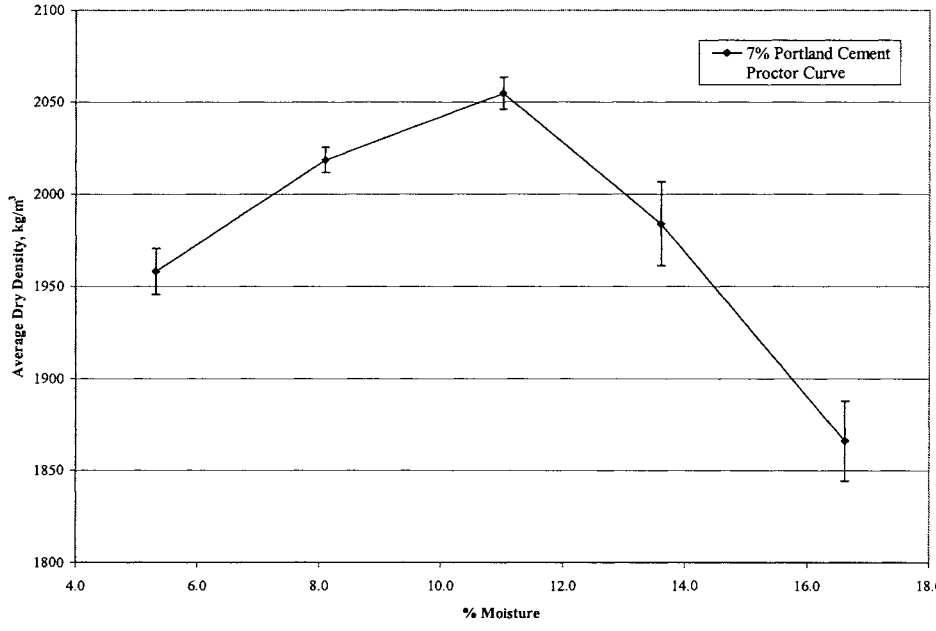

Figure 129. Limestone Screenings and 7% Portland Cement Proctor Curve

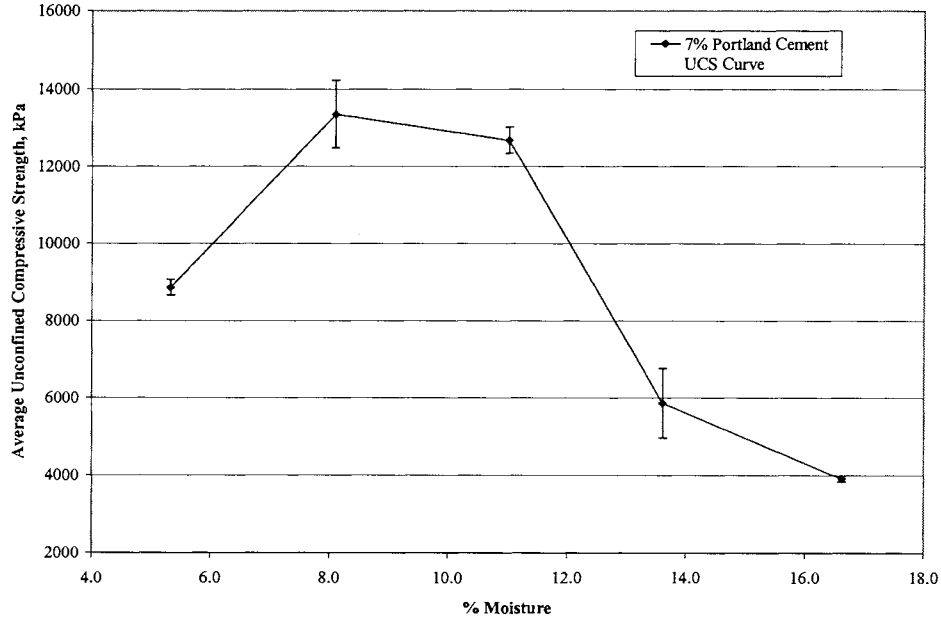

Figure 130. Moisture-Strength Curve for Limestone Screenings and 7% Portland Cement

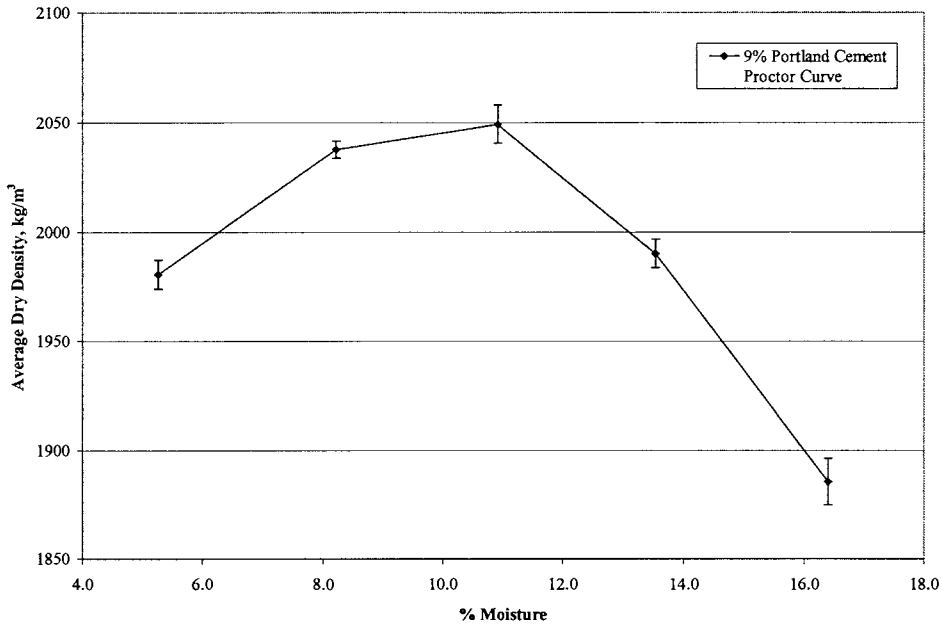

Figure 131. Limestone Screenings and 9% Portland Cement Proctor Curve

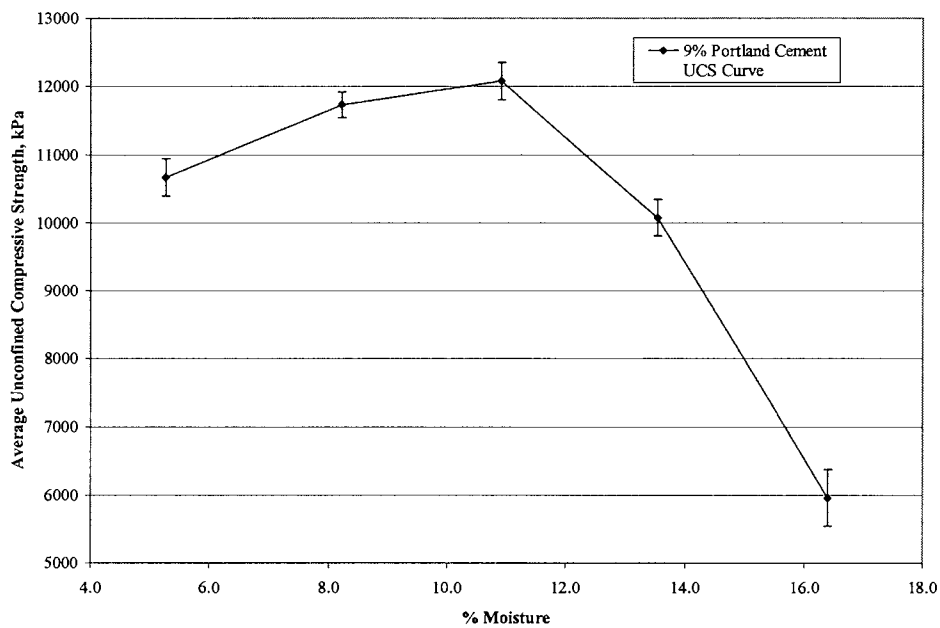

Figure 132. Moisture-Strength Curve for Limestone Screenings and 9% Portland Cement

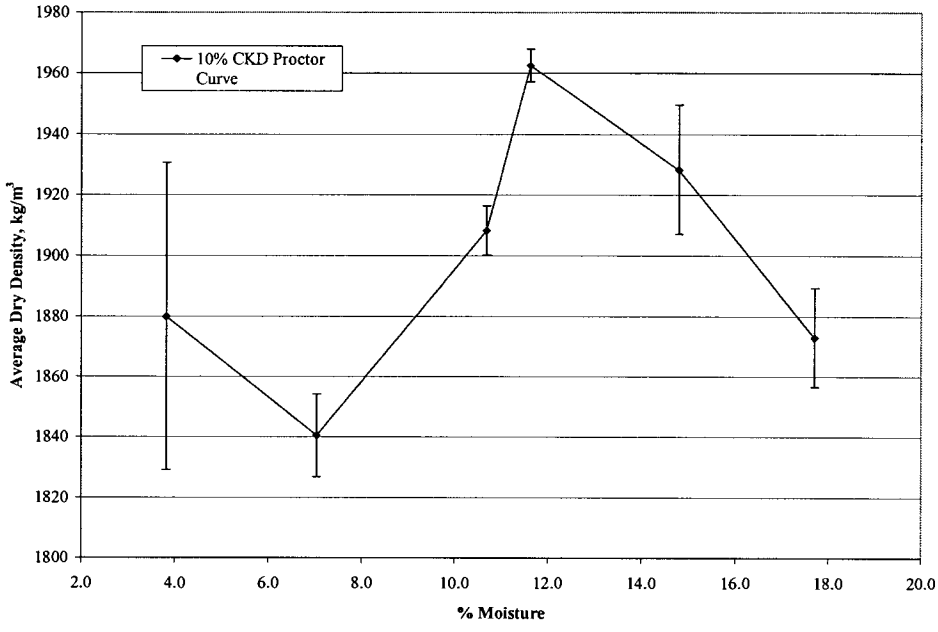

Figure 133. Manufactured Sand and 10% CKD Proctor Curve

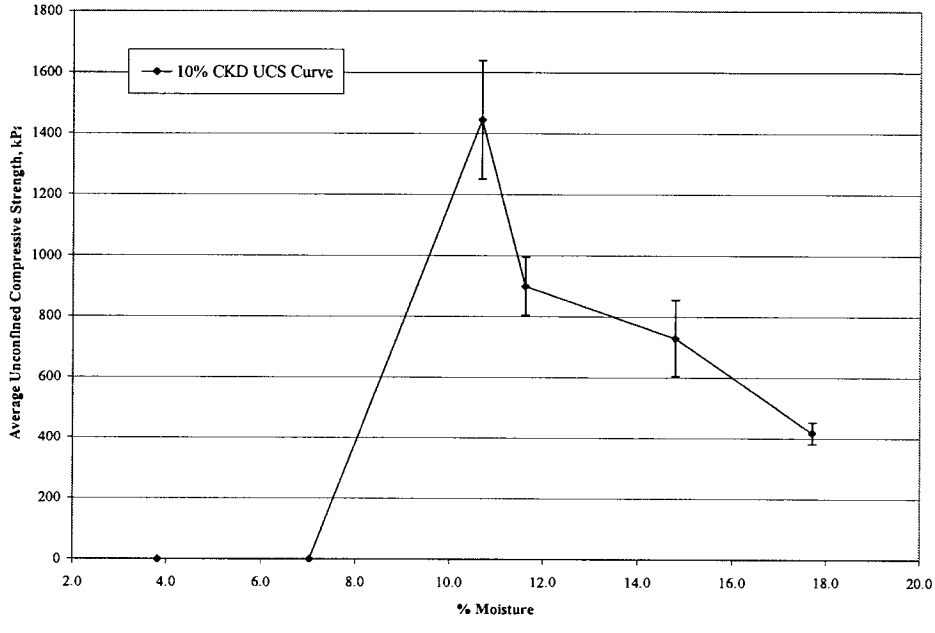

Figure 134. Moisture-Strength Curve for Manufactured Sand and 10% CKD

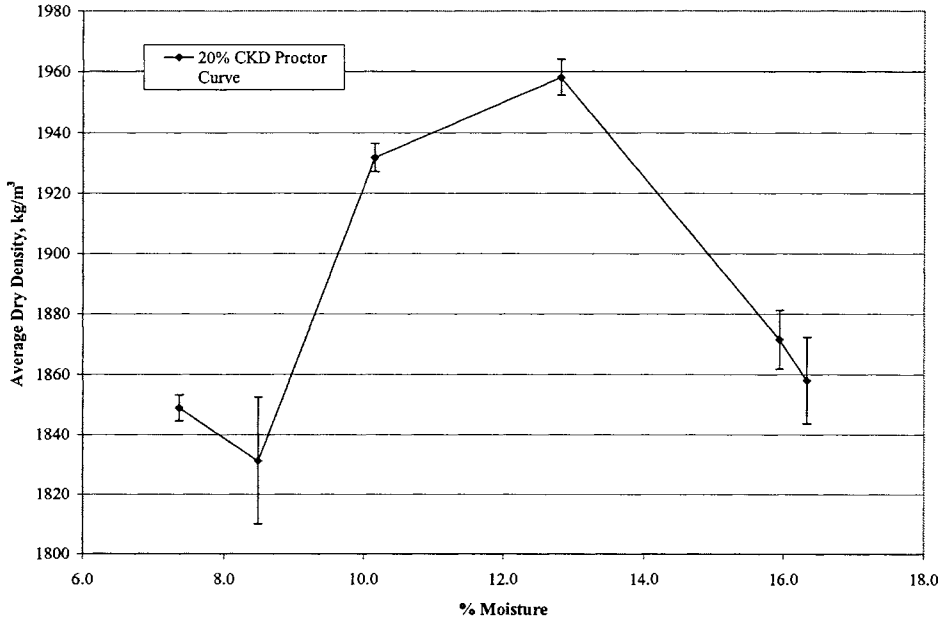

Figure 135. Manufactured Sand and 20% CKD Proctor Curve

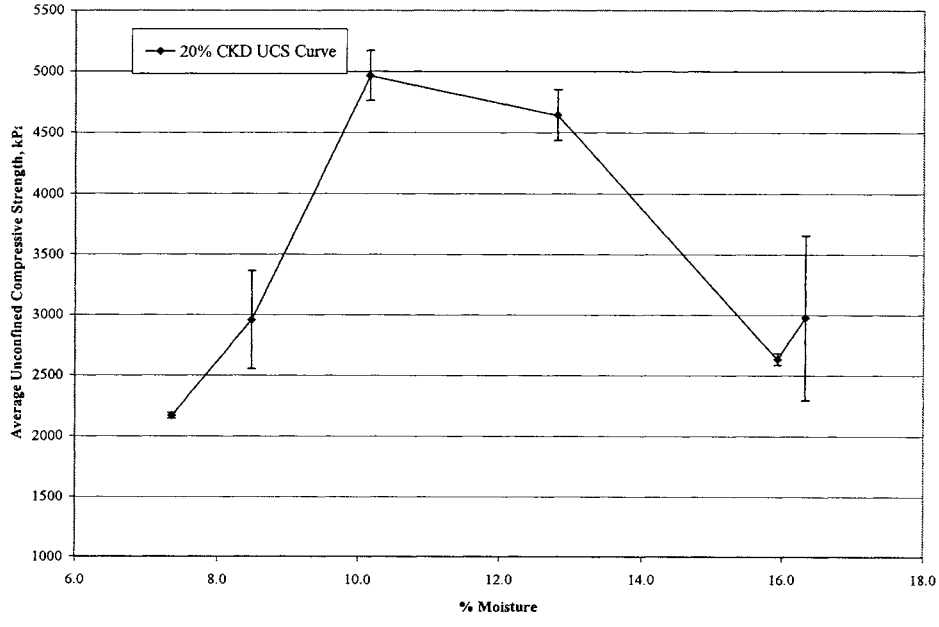

Figure 136. Moisture-Strength Curve for Manufactured Sand and 20% CKD

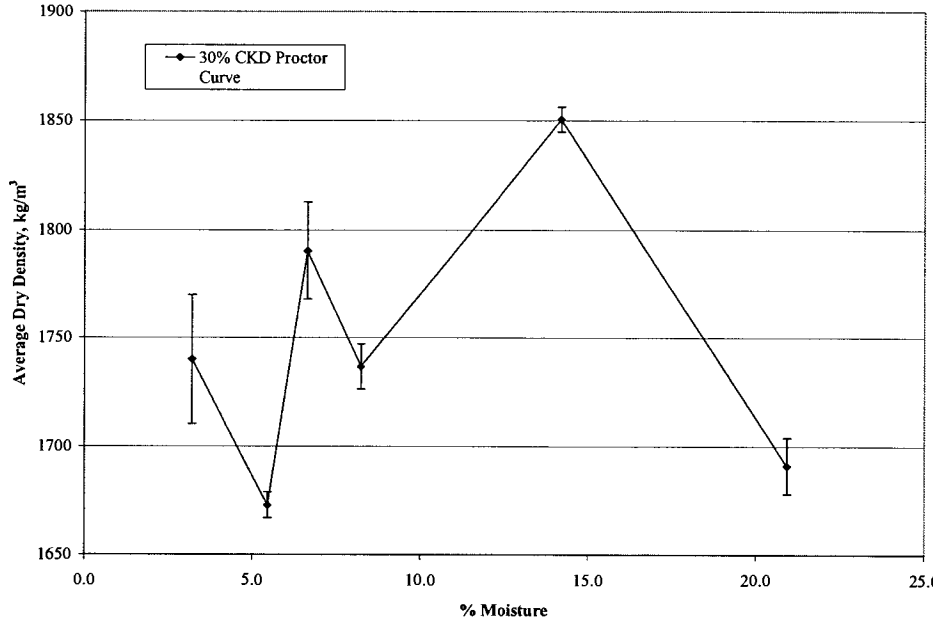

Figure 137. Manufactured Sand and 30% CKD Proctor Curve

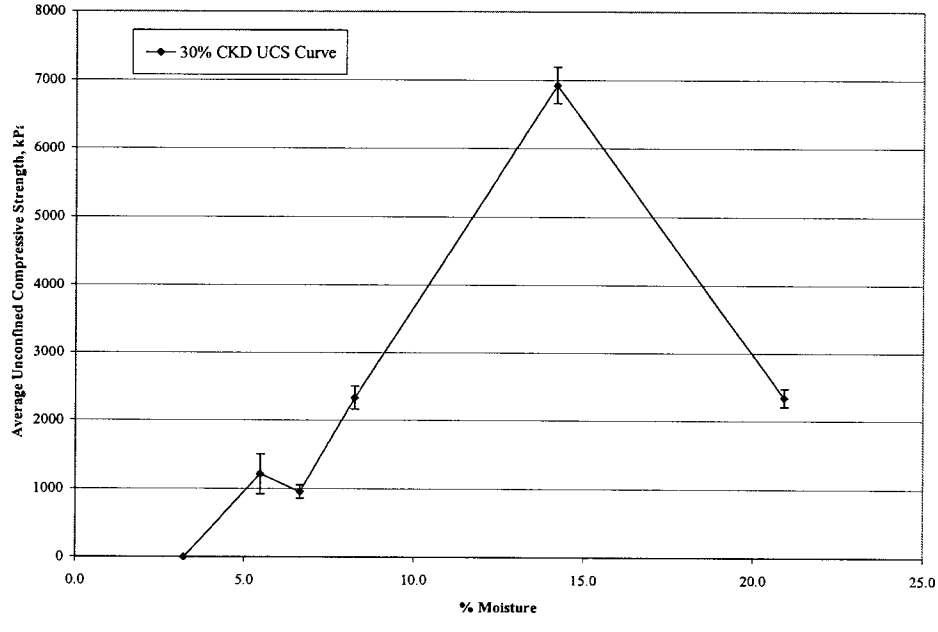

Figure 138. Moisture-Strength Curve for Manufactured Sand and 30% CKD

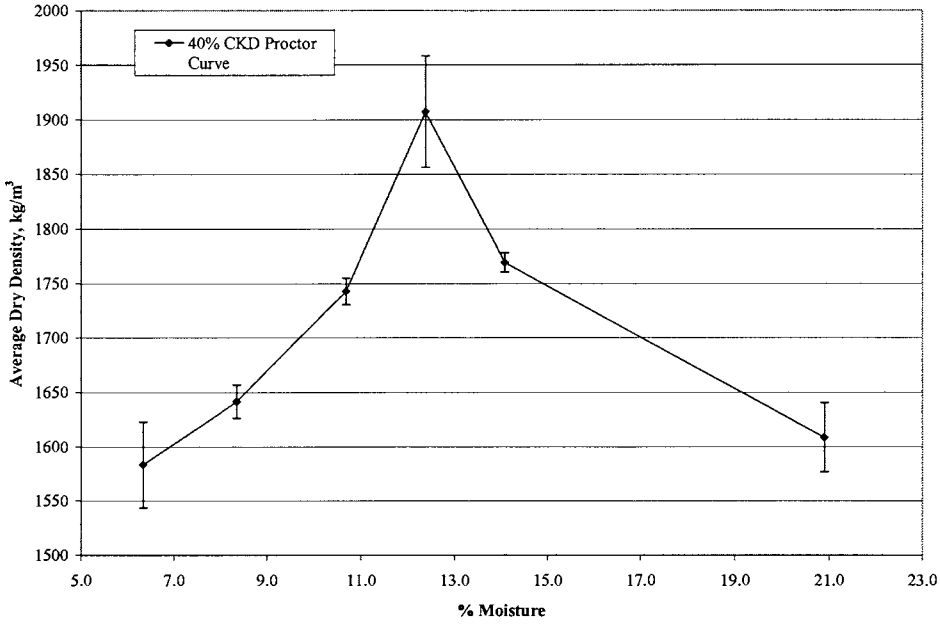

Figure 139. Manufactured Sand and 40% CKD Proctor Curve

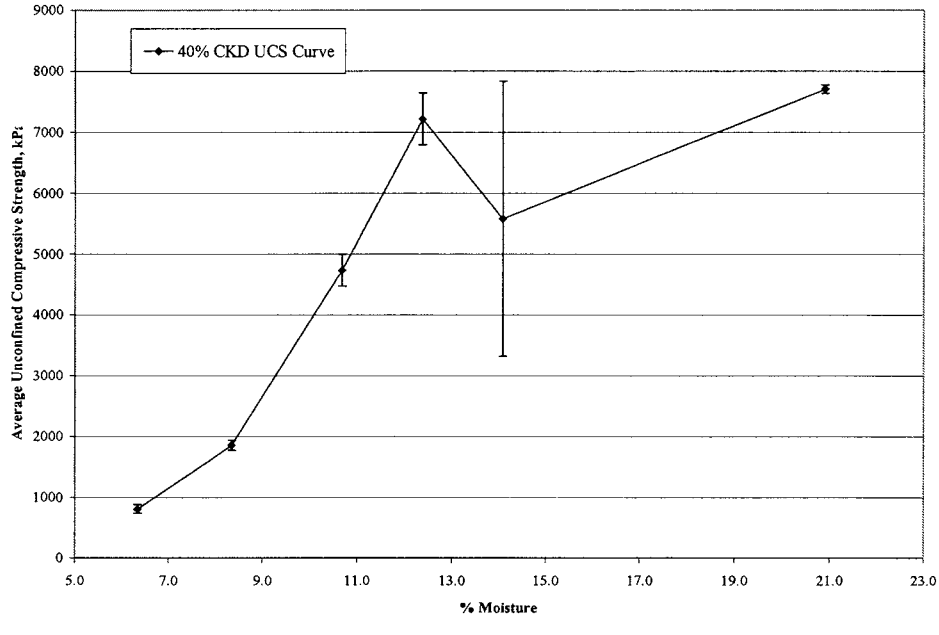

Figure 140. Moisture-Strength Curve for Manufactured Sand and 40% CKD

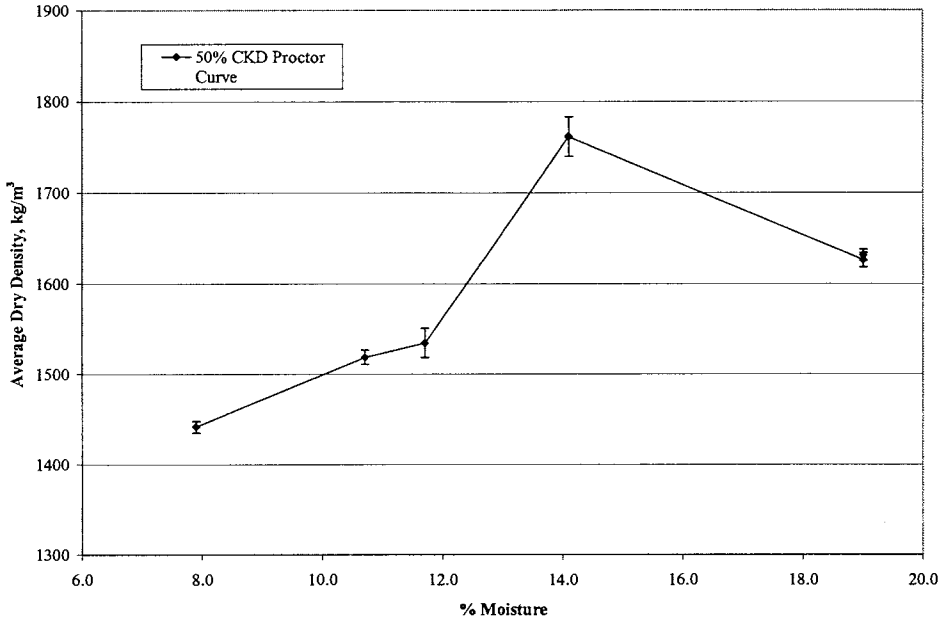

Figure 141. Manufactured Sand and 50% CKD Proctor Curve

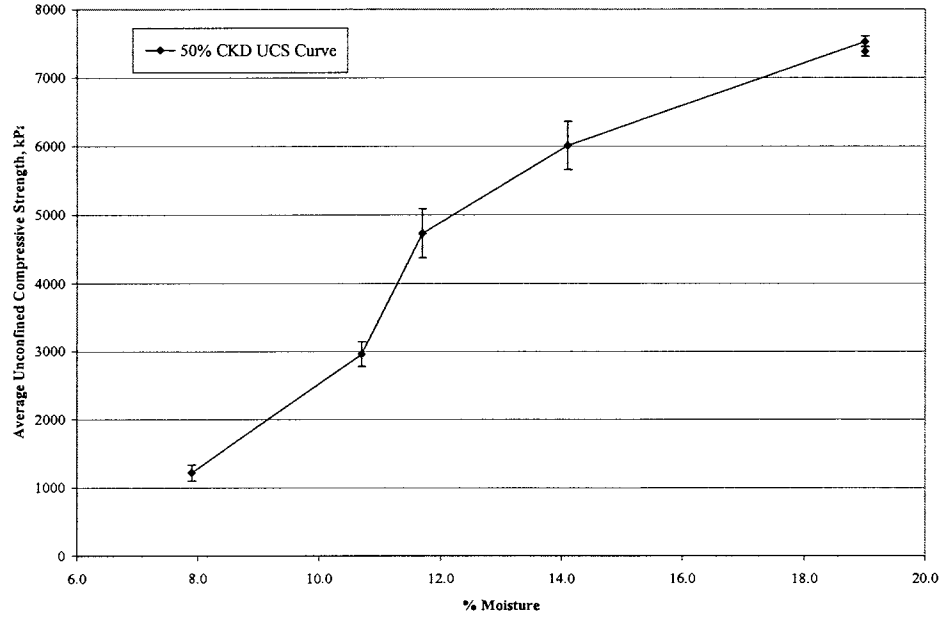

Figure 142. Moisture-Strength Curve for Manufactured Sand and 50% CKD

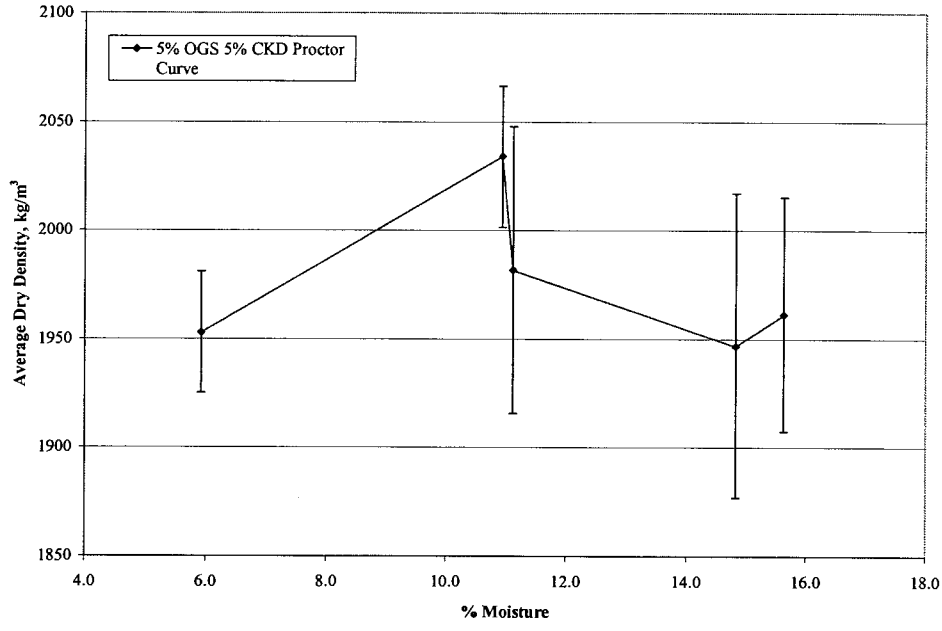

Figure 143. Manufactured Sand and 5% OGS Fly Ash and 5% CKD Proctor Curve

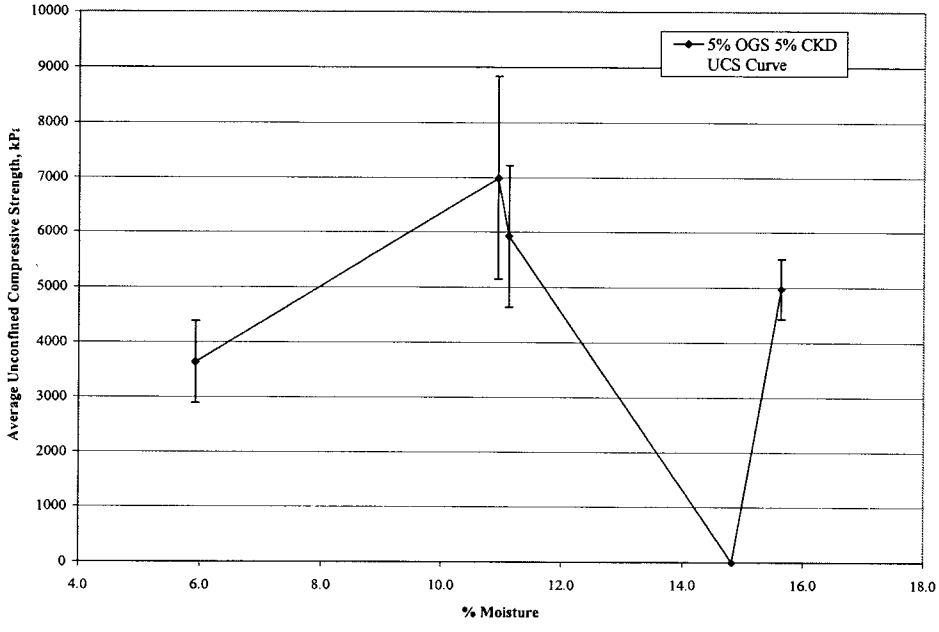

Figure 144. Moisture-Strength Curve for Manufactured Sand and 5% OGS Fly Ash and 5% CKD

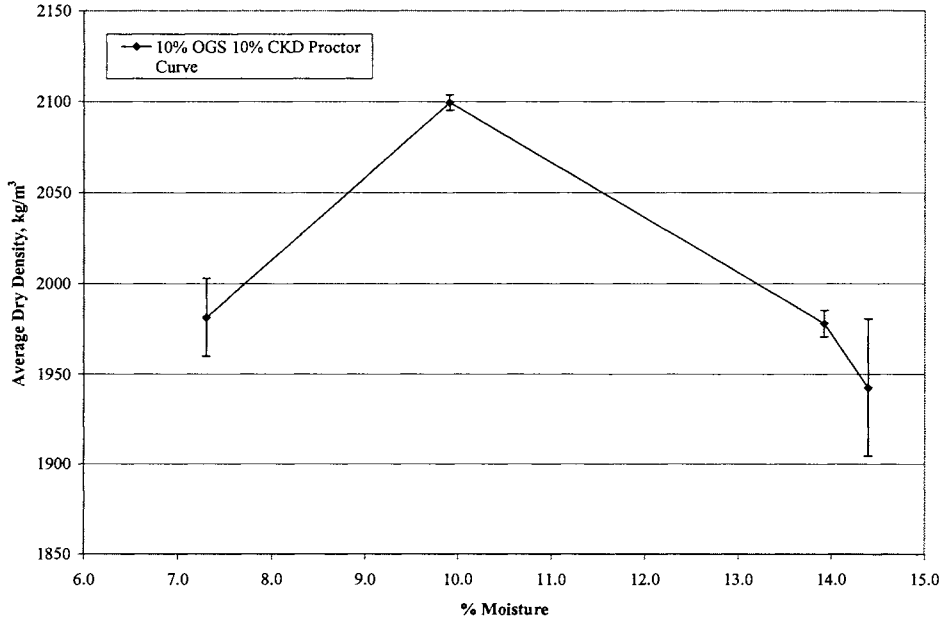

Figure 145. Manufactured Sand and 10% OGS Fly Ash and 10% CKD Proctor Curve

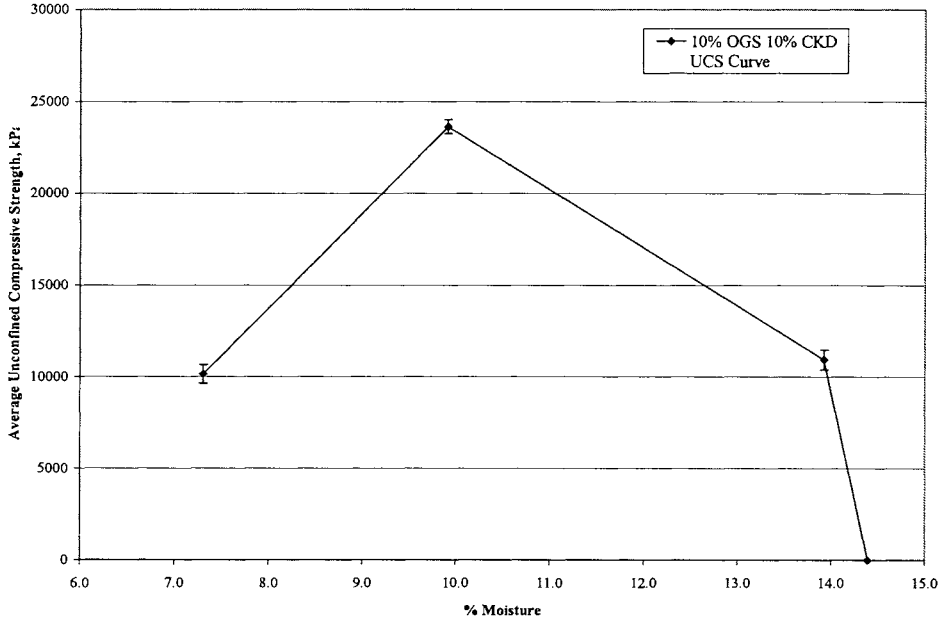

Figure 146. Moisture-Strength Curve for Manufactured Sand and 10% OGS Fly Ash and 10% CKD

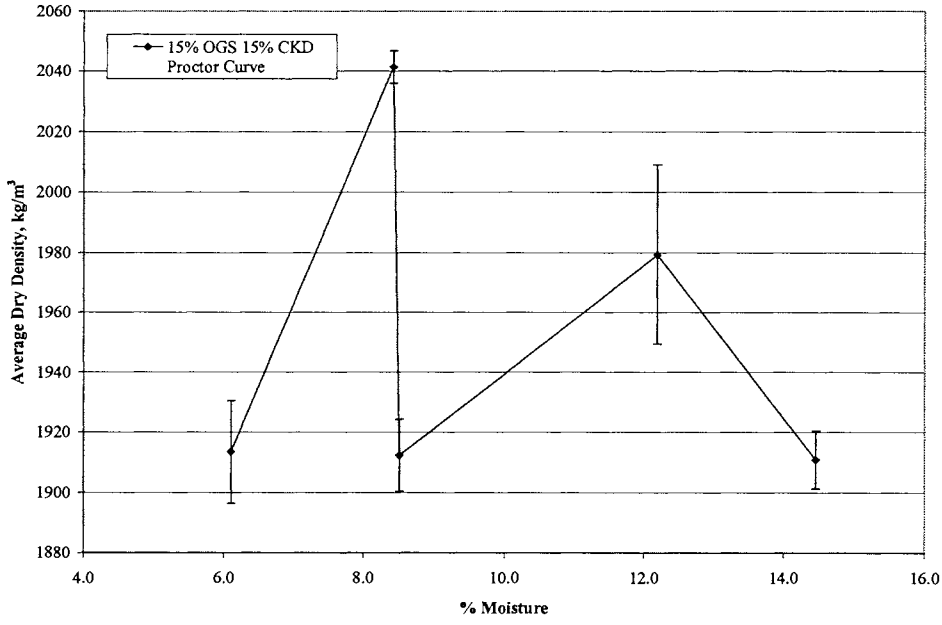

Figure 147. Manufactured Sand and 15% OGS Fly Ash and 15% CKD Proctor Curve

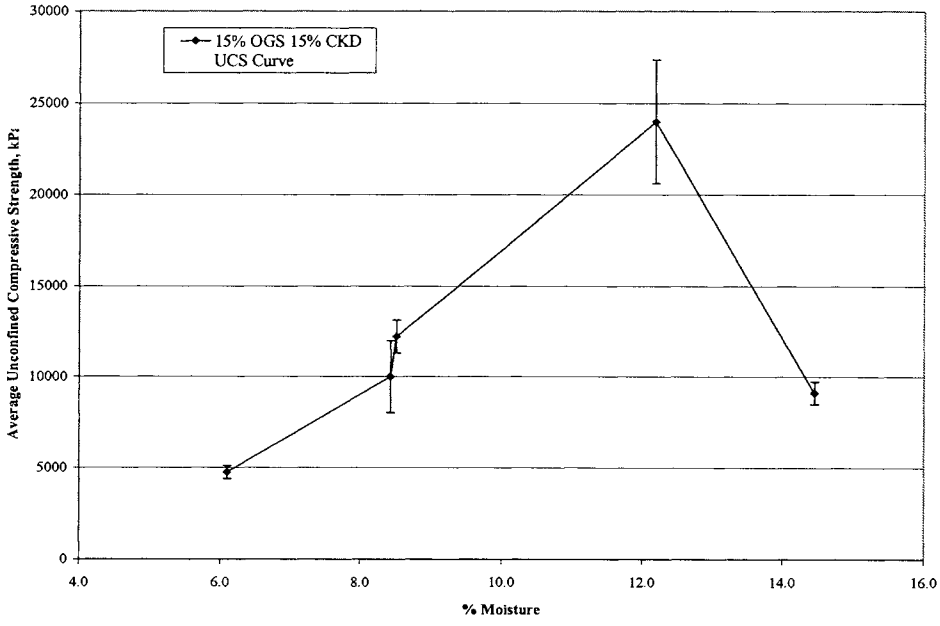

Figure 148. Moisture-Strength Curve for Manufactured Sand and 15% OGS Fly Ash and 15% CKD

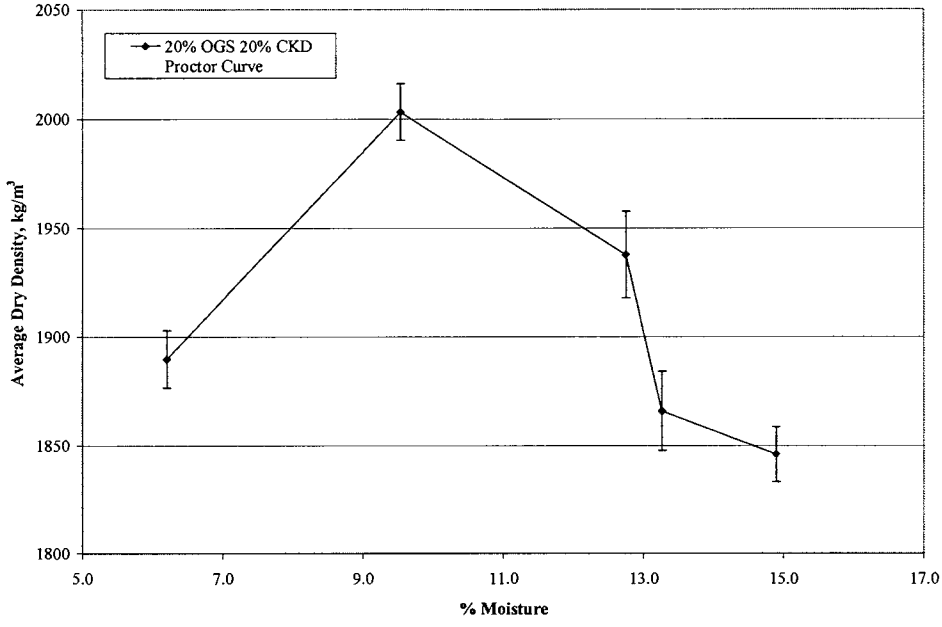

Figure 149. Manufactured Sand and 20% OGS Fly Ash and 20% CKD Proctor Curve

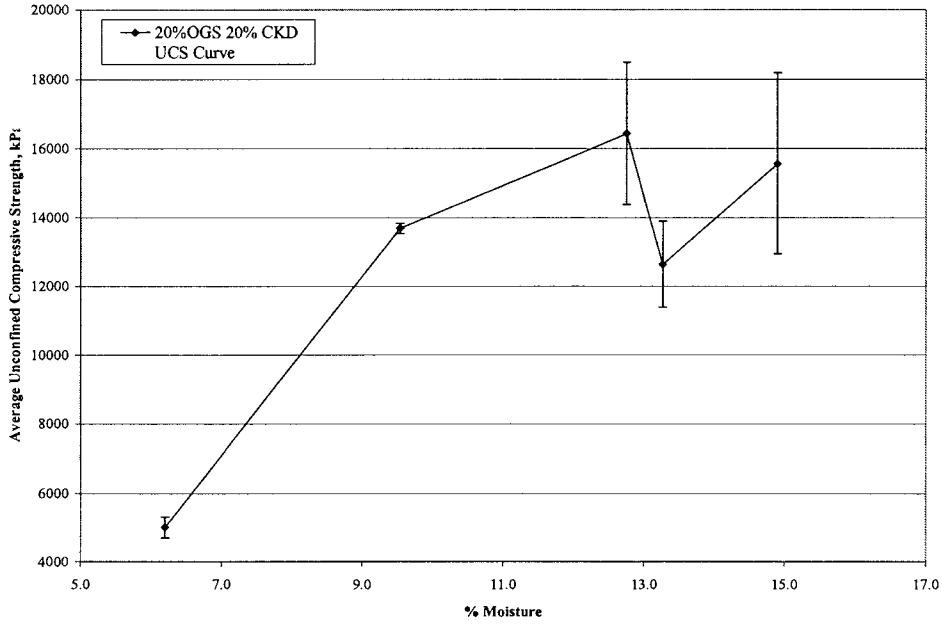

Figure 150. Moisture-Strength Curve for Manufactured Sand and 20% OGS Fly Ash and 20% CKD

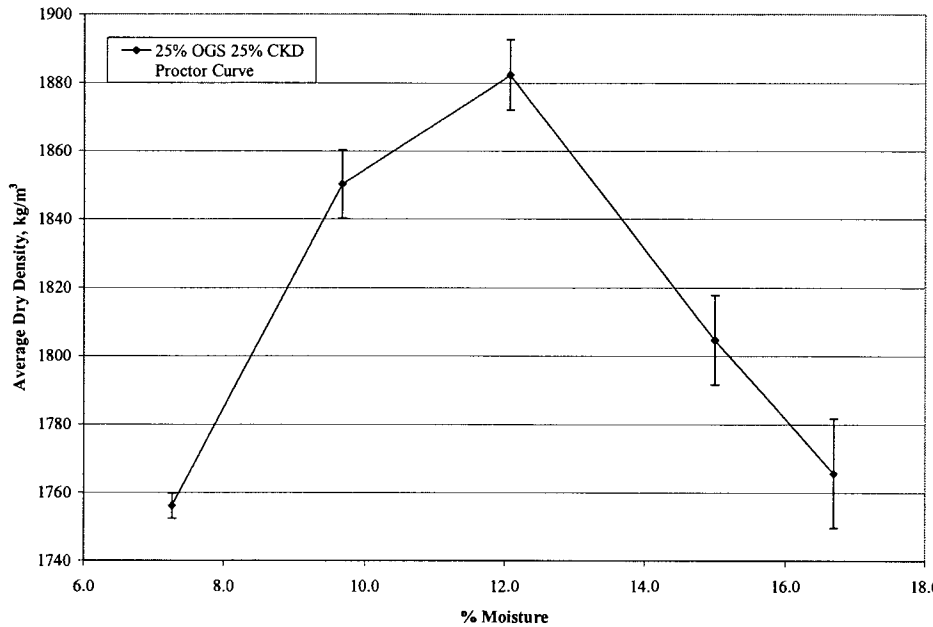

Figure 151. Manufactured Sand and 25% OGS Fly Ash and 25% CKD Proctor Curve

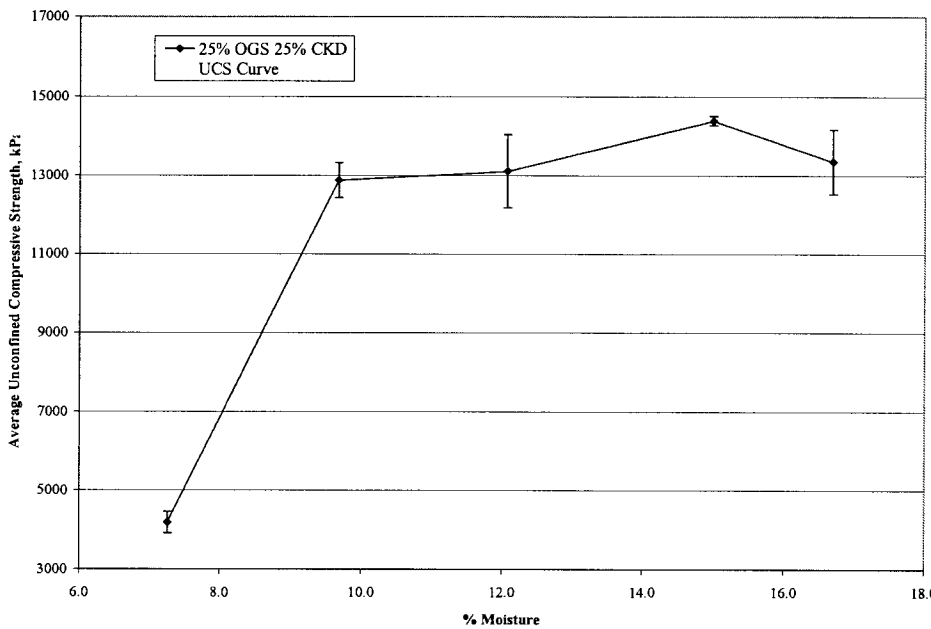

Figure 152. Moisture-Strength Curve for Manufactured Sand and 25% OGS Fly Ash and 25% CKD

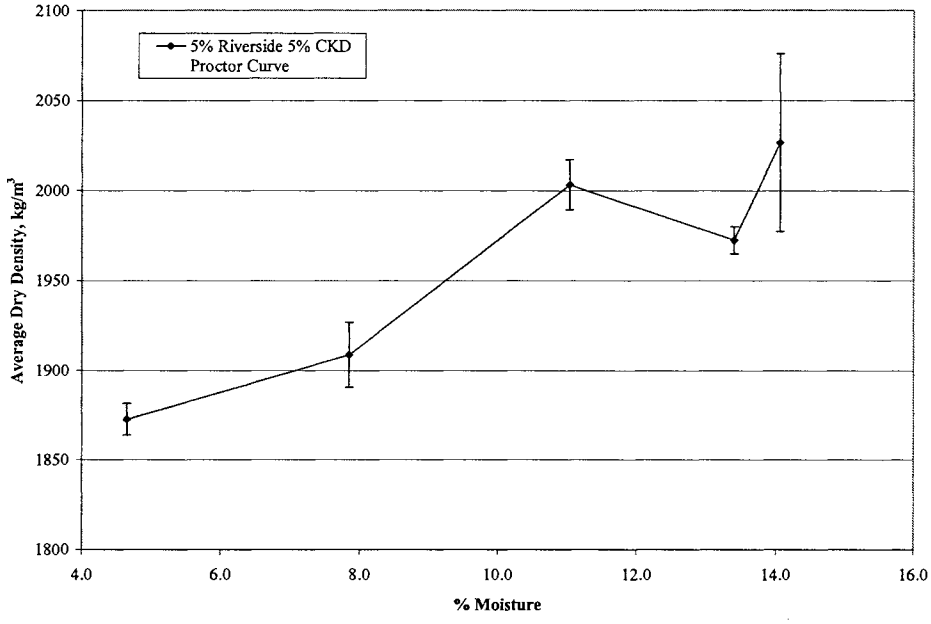

Figure 153. Manufactured Sand and 5% Riverside Fly Ash and 5% CKD Proctor Curve

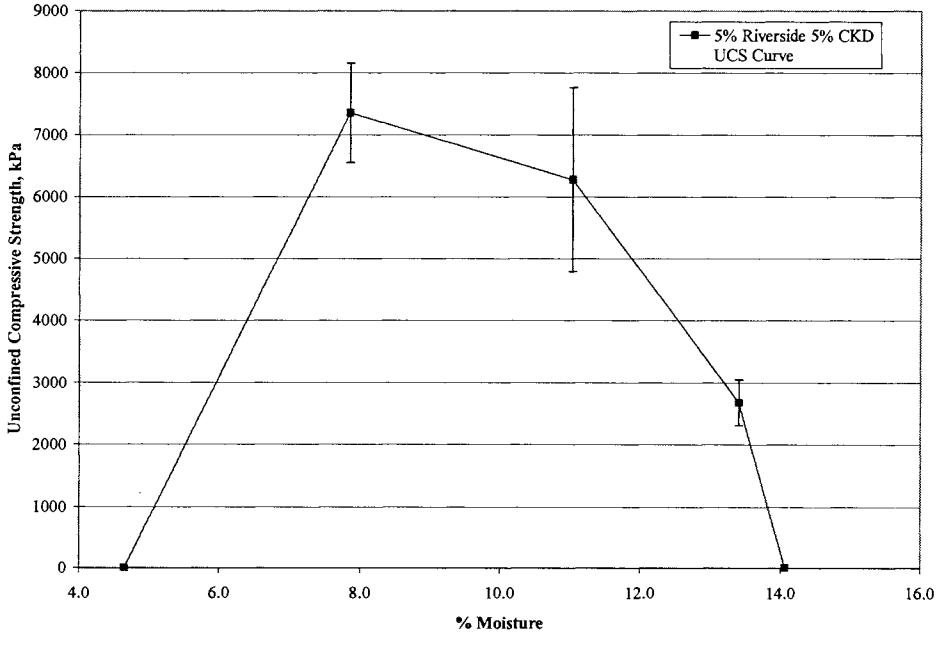

Figure 154. Moisture-Strength Curve for Manufactured Sand and 5% Riverside Fly Ash and 5% CKD

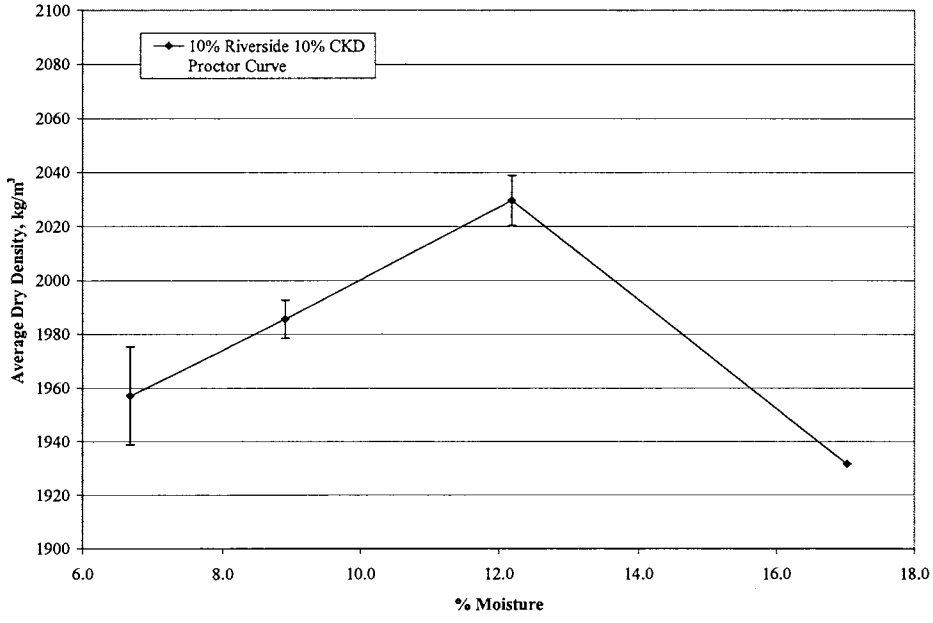

Figure 155. Manufactured Sand and 10% Riverside Fly Ash and 10% CKD Proctor Curve

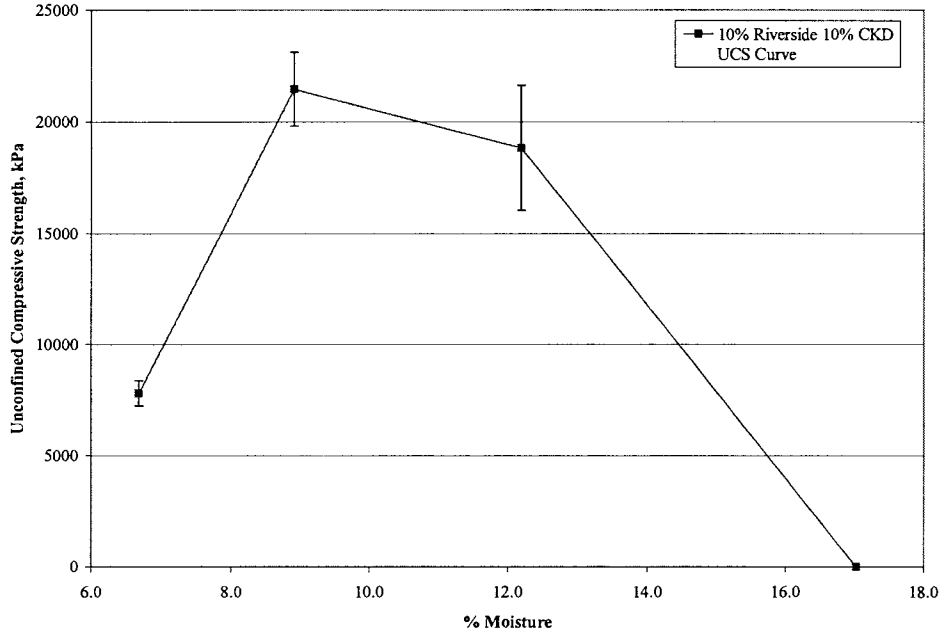

Figure 156. Moisture-Strength Curve for Manufactured Sand and 10% Riverside Fly Ash and 10% CKD

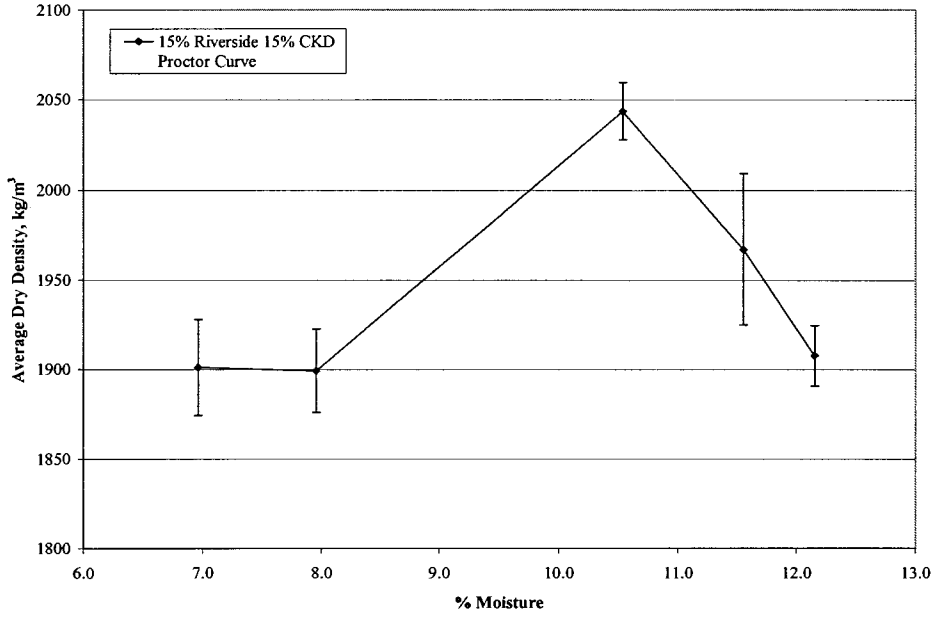

Figure 157. Manufactured Sand and 15% Riverside Fly Ash and 15% CKD Proctor Curve

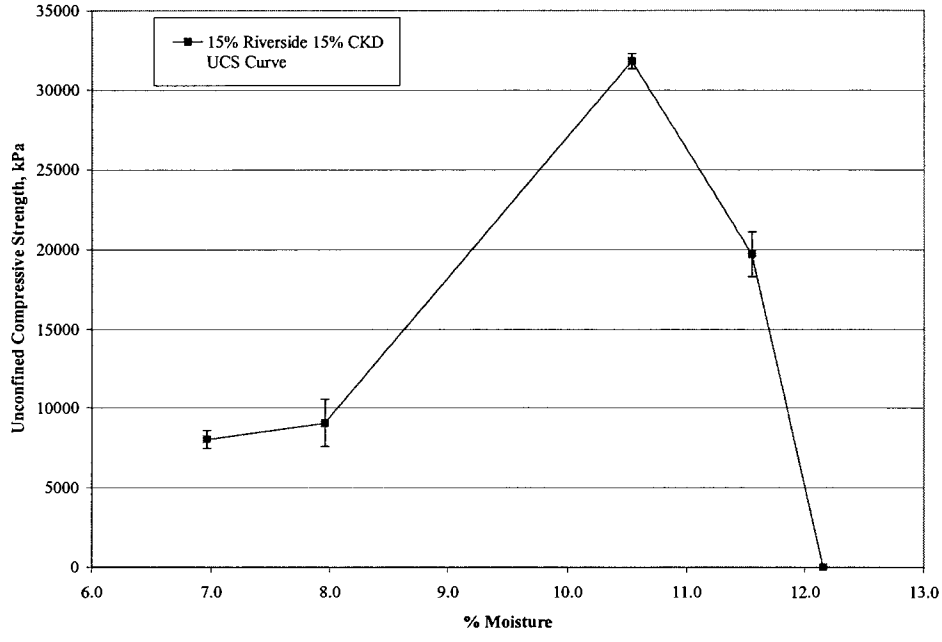

Figure 158. Moisture-Strength Curve for Manufactured Sand and 15% Riverside Fly Ash and 15% CKD

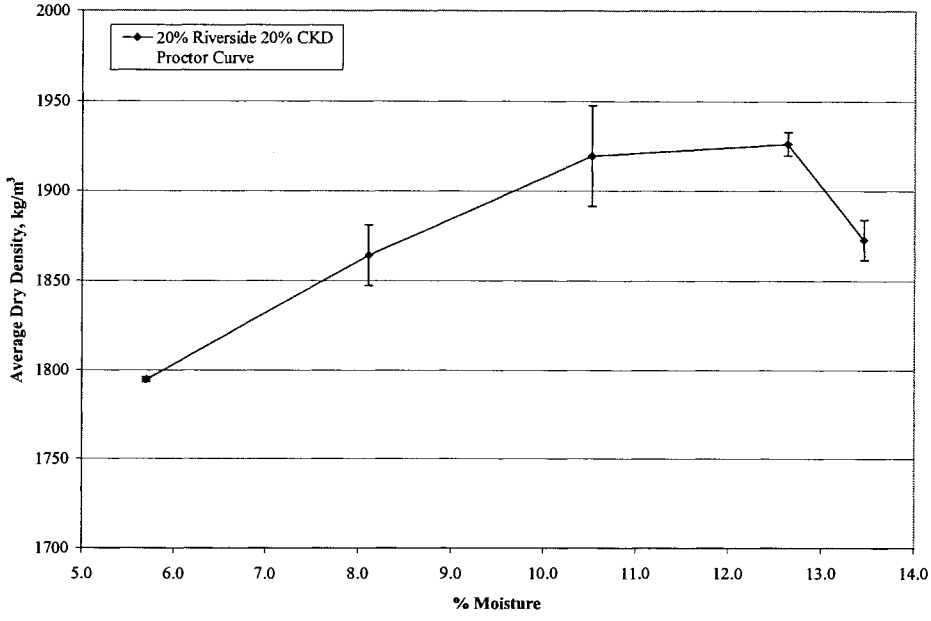

Figure 159. Manufactured Sand and 20% Riverside Fly Ash and 20% CKD Proctor Curve

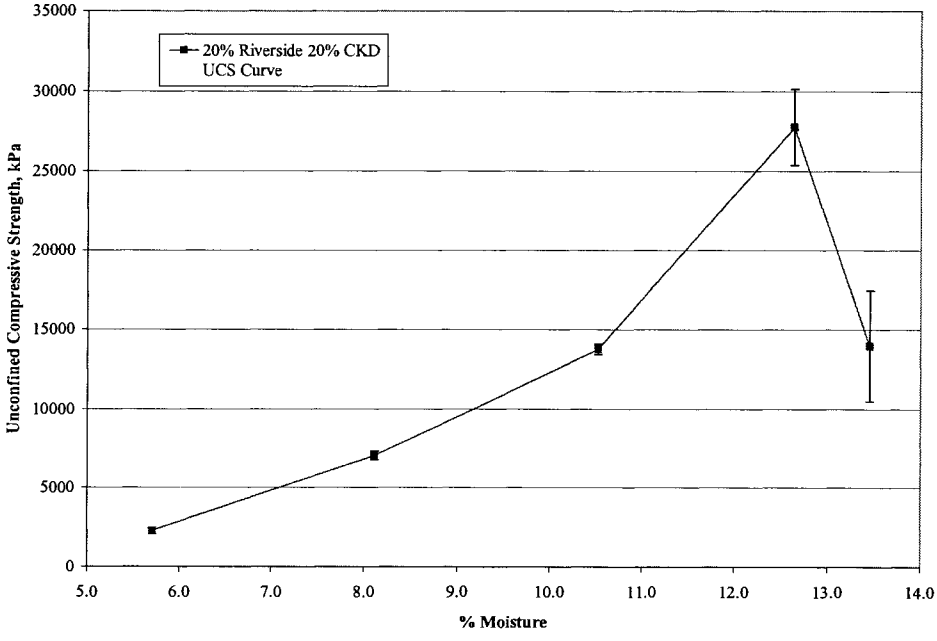

Figure 160. Moisture-Strength Curve for Manufactured Sand and 20% Riverside Fly Ash and 20% CKD

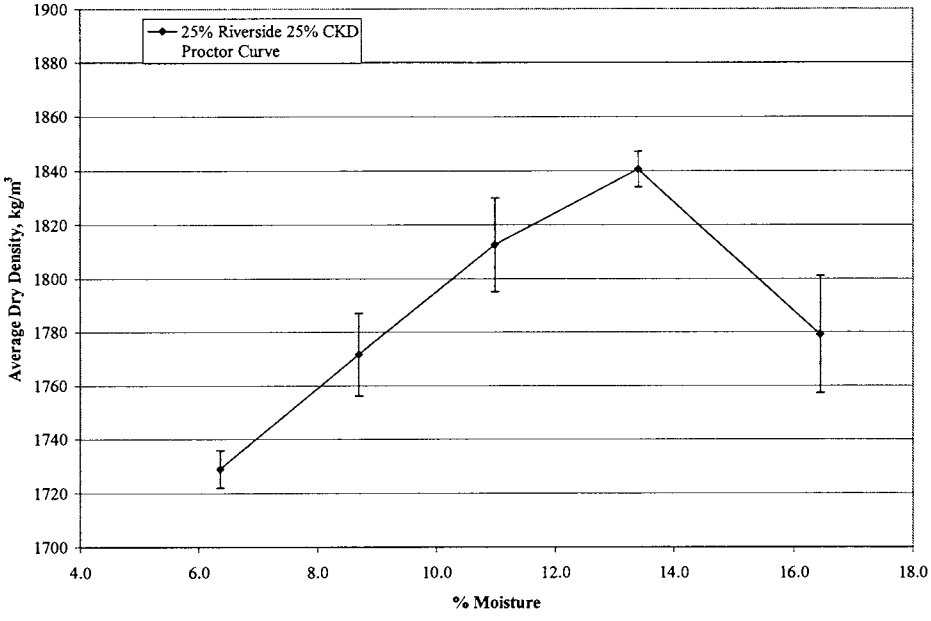

Figure 161. Manufactured Sand and 25% Riverside Fly Ash and 25% CKD Proctor Curve

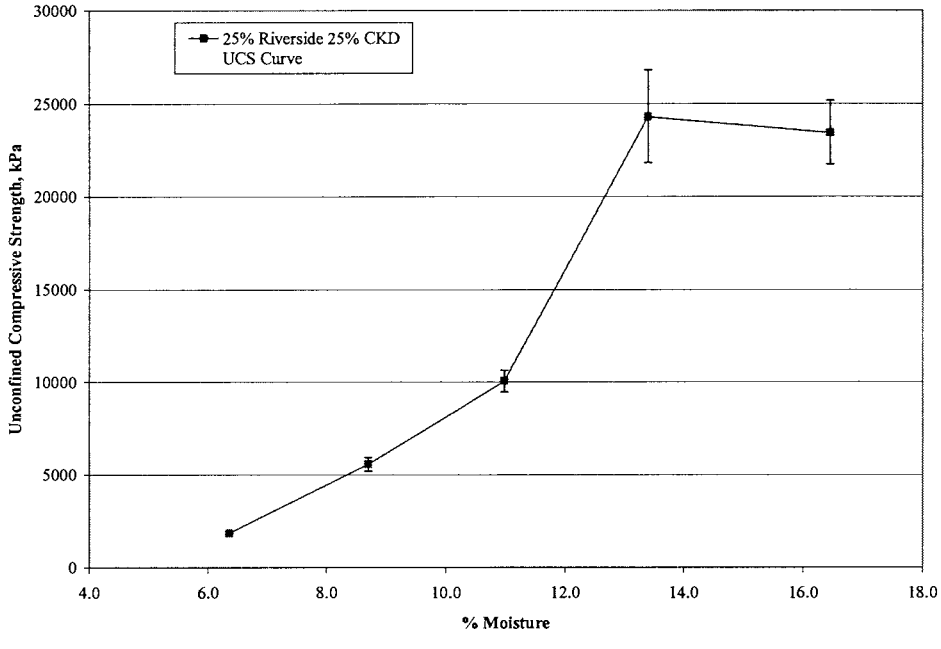

Figure 162. Moisture-Strength Curve for Manufactured Sand and 25% Riverside Fly Ash and 25% CKD

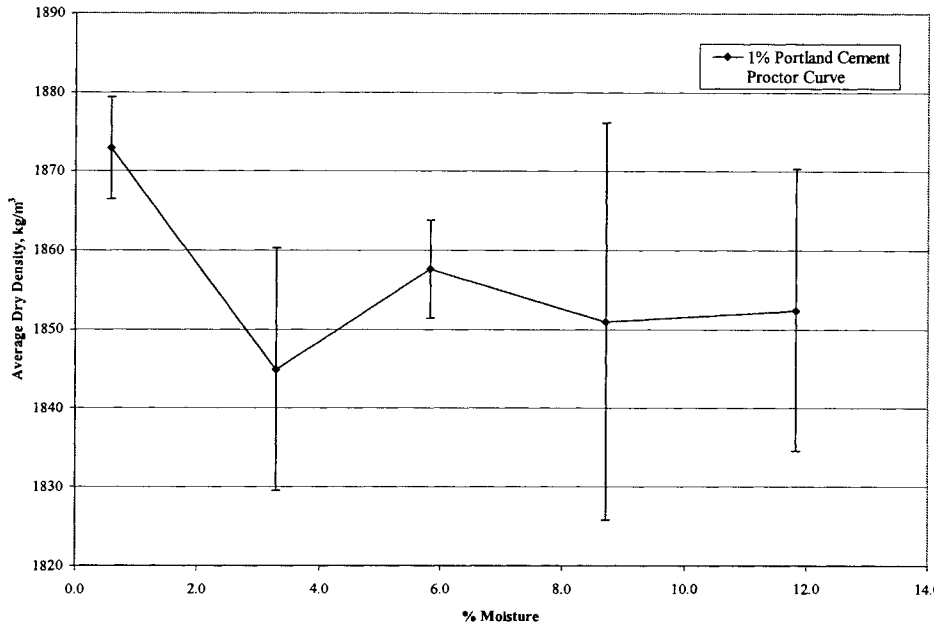

Figure 163. Manufactured Sand and 1% Portland Cement Proctor Curve

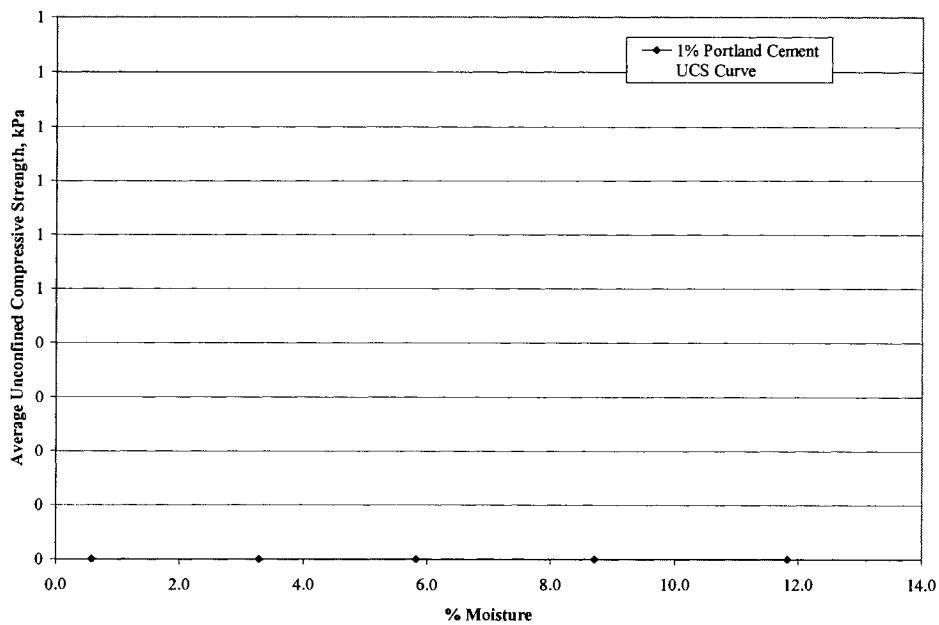

Figure 164. Moisture-Strength Curve for Manufactured Sand and 1% Portland Cement

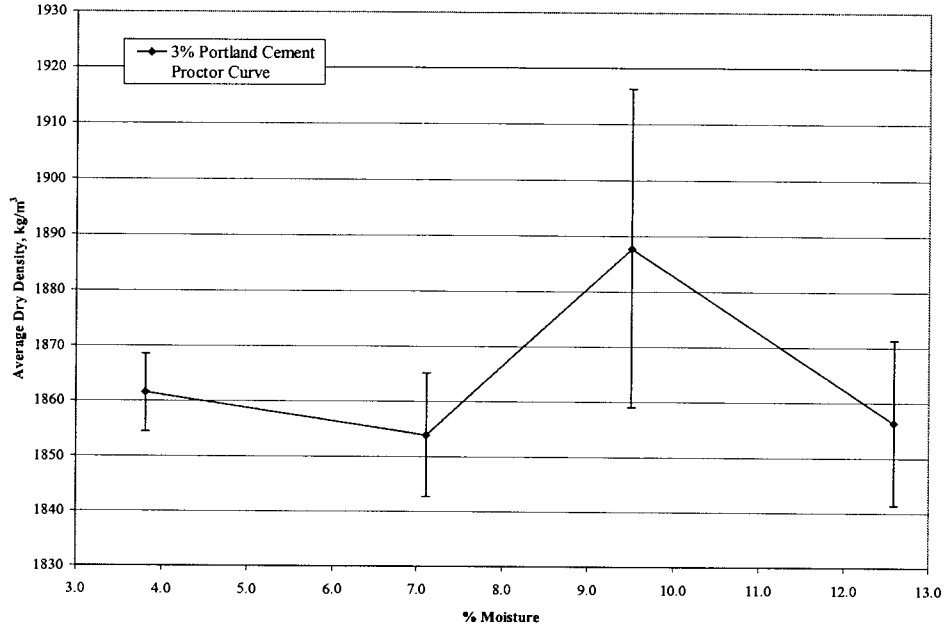

Figure 165. Manufactured Sand and 3% Portland Cement Proctor Curve

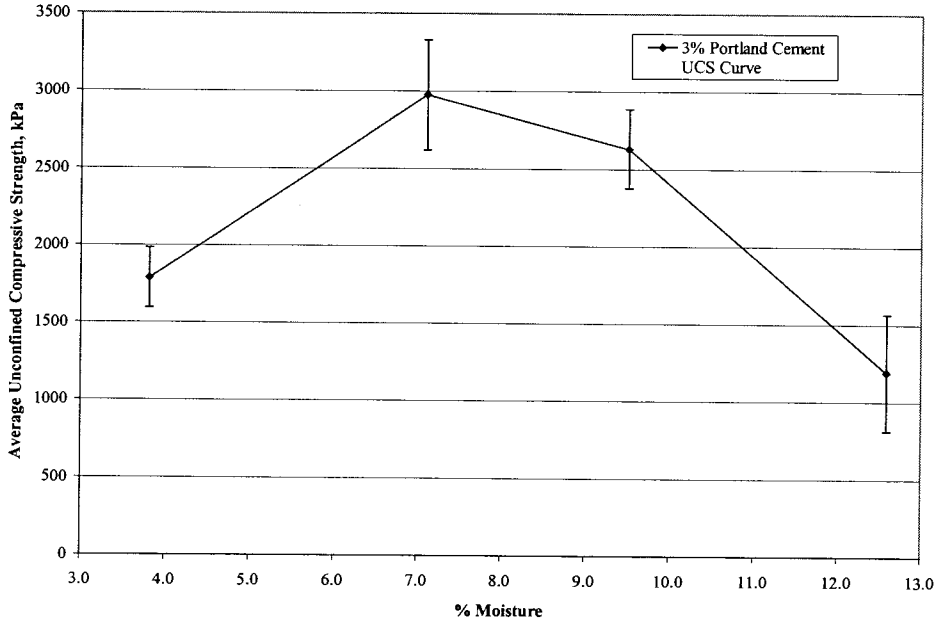

Figure 166. Moisture-Strength Curve for Manufactured Sand and 3% Portland Cement

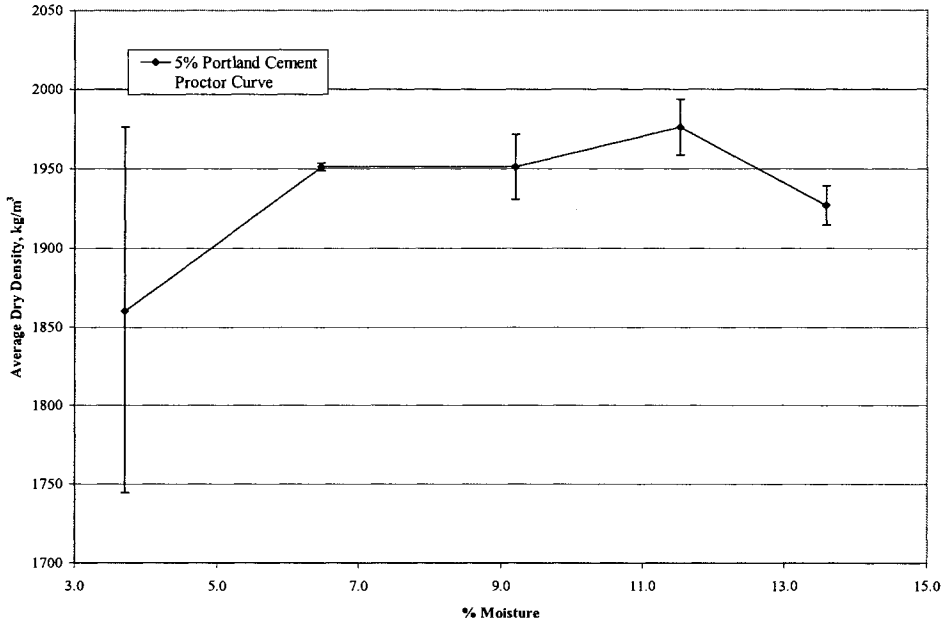

Figure 167. Manufactured Sand and 5% Portland Cement Proctor Curve

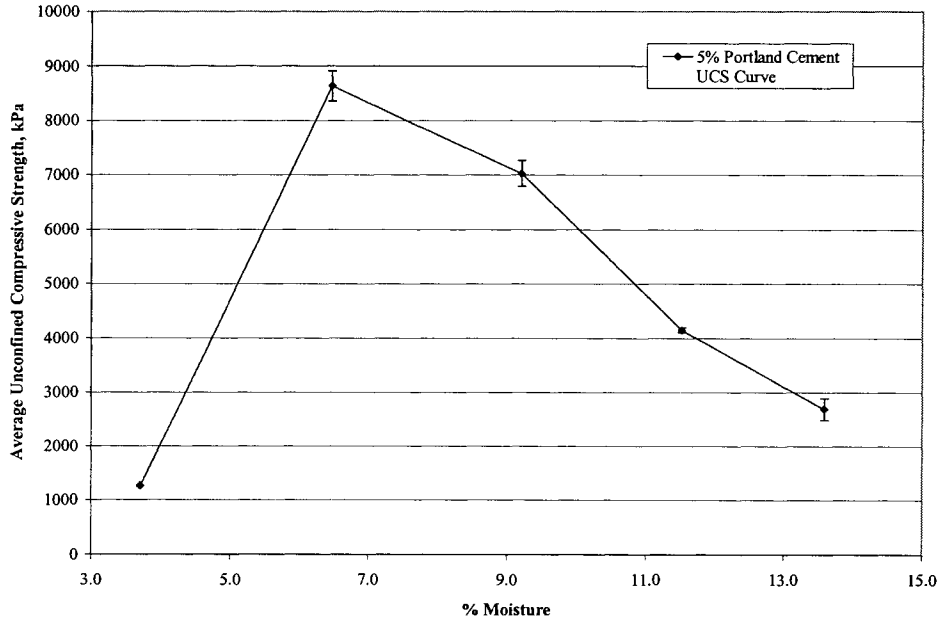

Figure 168. Moisture-Strength Curve for Manufactured Sand and 5% Portland Cement

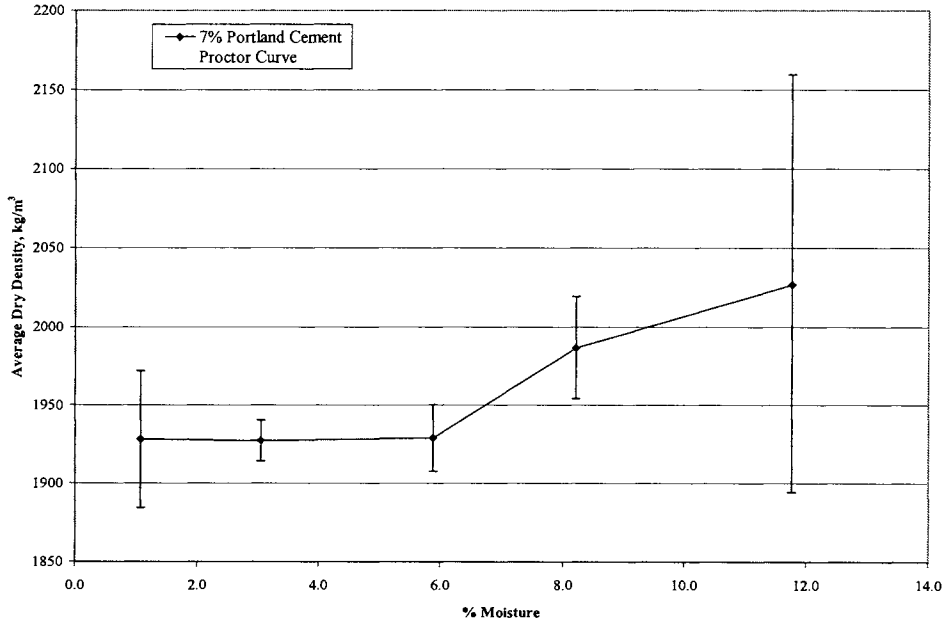

Figure 169. Manufactured Sand and 7% Portland Cement Proctor Curve

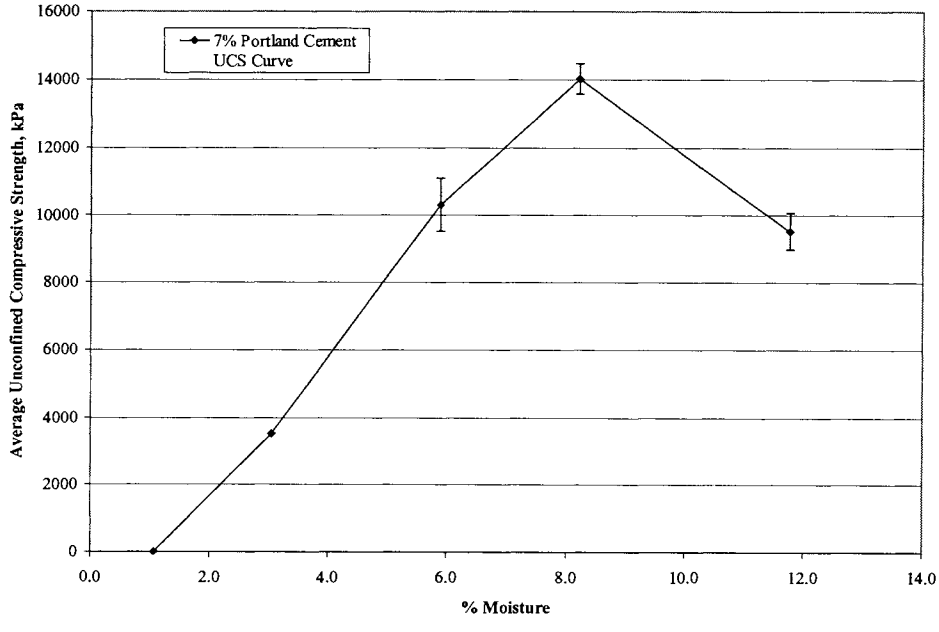

Figure 170. Moisture-Strength Curve for Manufactured Sand and 7% Portland Cement

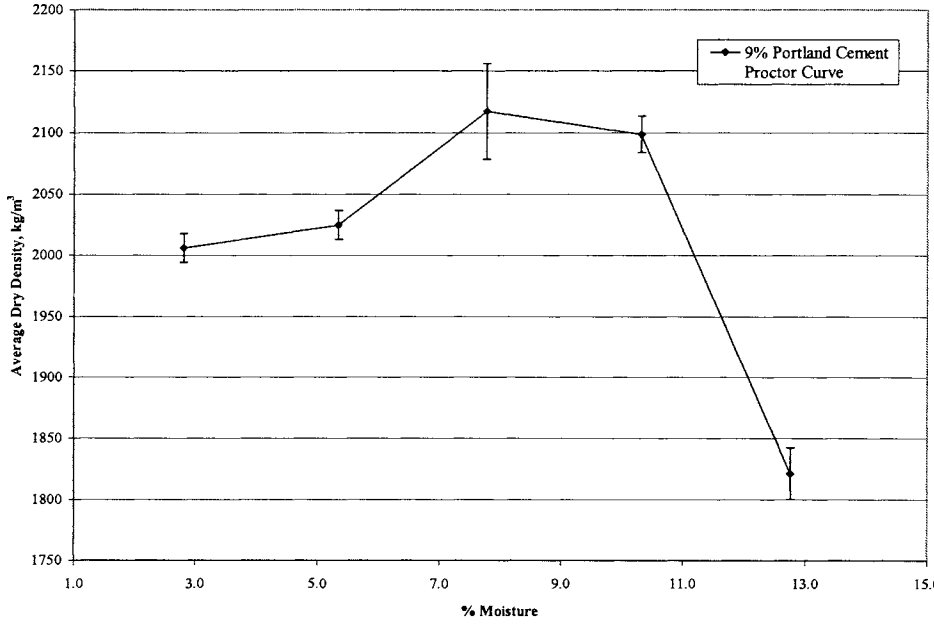

Figure 171. Manufactured Sand and 9% Portland Cement Proctor Curve

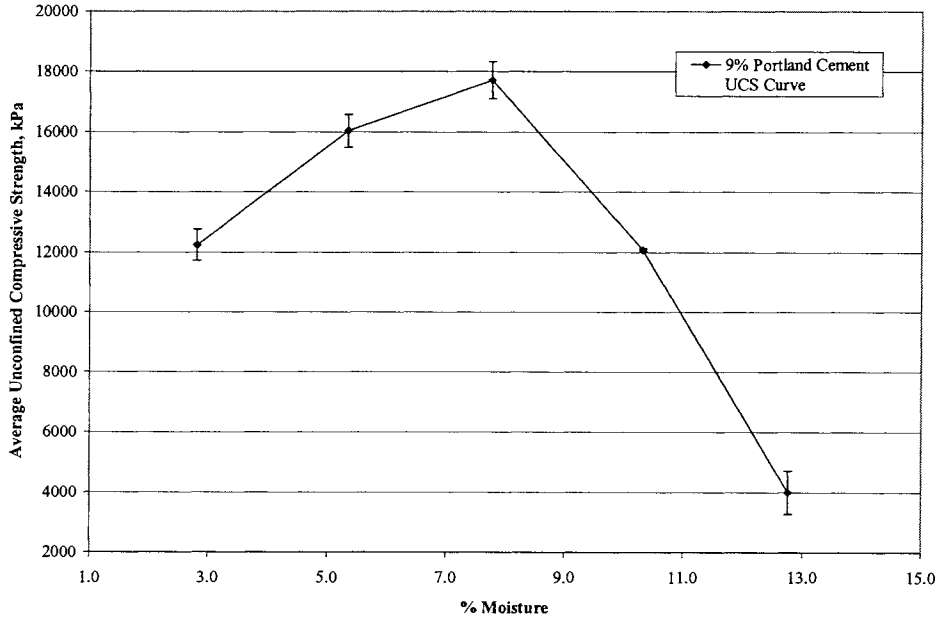

Figure 172. Moisture-Strength Curve for Manufactured Sand and 9% Portland Cement

Freeze-Thaw Durability Testing

This section details the results obtained from freeze-thaw durability testing on the maximum unconfined compression strength samples from each stabilizer evaluated for both the limestone screenings and manufactured sand.

Limestone Screenings

Figure 173 shows the percent volume change for limestone screenings samples during the freeze-thaw durability test. Table 13 shows these results in a tabular form. Note that the CKD samples expanded about 28%, and other samples containing CKD expanded significantly to over 15%. Note that the OGS-CKD and Prairie Creek Fly Ash samples lost volume near the end of the test. This was due to breakdown of the samples due to freeze-thaw action. This shows that CKD stabilized material is not a good construction material.

Table 14 shows the results for the percent mass loss for limestone screenings samples for the freeze-thaw durability test. Figure 174 shows the same results graphically. Note that the CKD samples were discontinued after cycle two and the Riverside-CKD samples were discontinued after cycle nine. Note that the Portland cement sample performed the best with about 5.5% mass loss, and all other samples failed the freeze-thaw durability test because their mass loss was greater than 14% (NAVFAC 1999).

For further details of limestone screenings samples, please see the pictures of each sample at the end of each cycle located in the Appendix.

Table 13. Percent Volume Change for Stabilized Limestone Screenings Freeze-Thaw Durability Test Samples

	Percent Volume Change				
Cycle	CKD	OGS-CKD	Riv-CKD	Portland Cement	Prairie Creek Fly Ash
0	18.9	6.4	7.4	0.9	0.8
1	21.1	7.7	9.3	1.1	0.6
2	27.2	8.0	9.0	0.2	0.7
3	-	12.3	10.3	0.7	0.3
4	-	14.2	16.2	0.2	0.5
5	-	16.1	16.5	-0.1	0.1
6	-	17.1	15.7	0.0	0.1
7	-	16.7	8.0	0.9	-0.5
8	-	18.9	8.2	-0.3	-0.4
9	-	10.1	7.5	0.0	-0.2
10	-	-0.4	-	0.0	-1.3
11	-	-2.6	-	-0.5	-2.3
12	-	-2.9	-	-0.6	-3.6

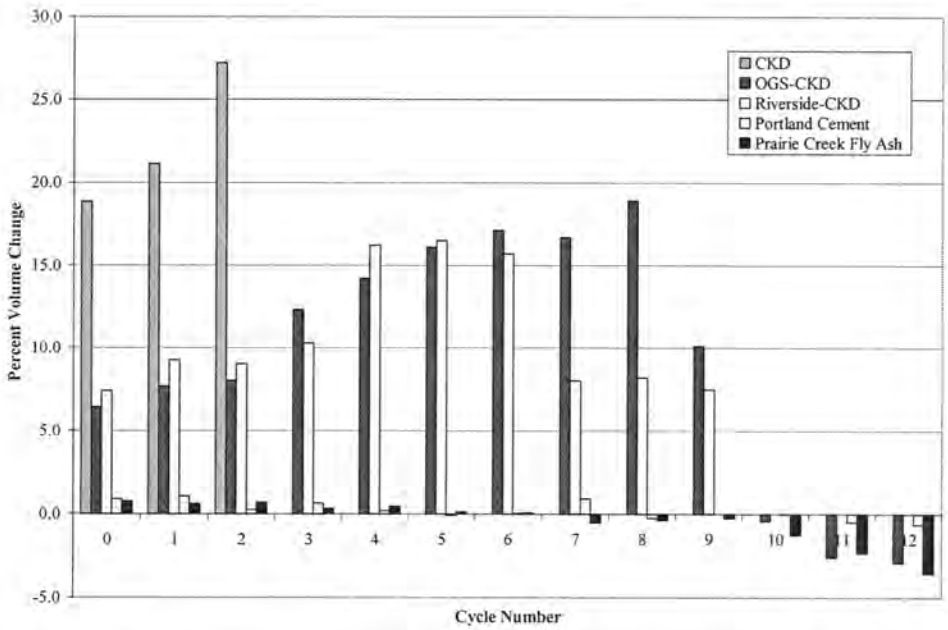

Figure 173. Percent Volume Change for Stabilized Limestone Screenings Freeze-Thaw Durability Test Samples

Table 14. Percent Mass Loss for Stabilized Limestone Screenings Freeze-Thaw Durability Test Samples

	Percent Mass Loss				
Cycle	CKD	OGS-CKD	Riv-CKD	Portland Cement	Prairie Creek Fly Ash
0	0.0	0.0	0.0	0.0	0.1
1	64.6	0.8	0.9	0.9	0.1
2	100.0	1.8	1.9	1.6	3.8
3	-	7.8	5.5	2.1	4.6
4	-	12.8	28.0	2.7	6.1
5	-	57.3	52.5	3.3	7.8
6	-	65.0	77.8	3.7	9.4
7	-	73.1	91.7	3.9	10.7
8	-	79.5	96.7	4.3	12.5
9	-	86.4	100.0	4.6	14.2
10	-	88.5	-	4.9	15.4
11	-	94.4	-	5.3	16.8
12	-	100.0	-	5.4	18.1

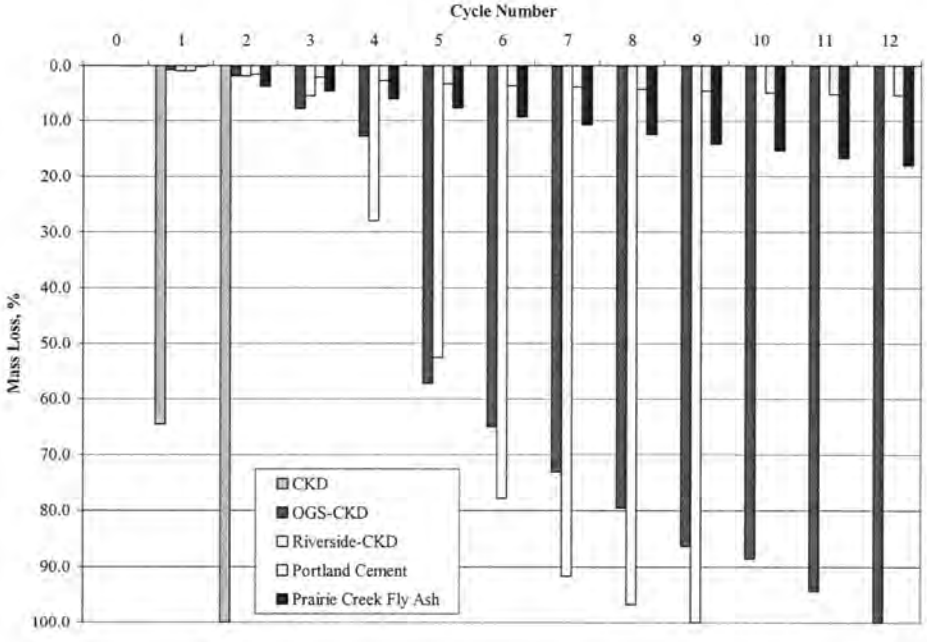

Figure 174. Percent Mass Loss for Limestone Screenings Freeze-Thaw Durability Test Samples

Manufactured Sand

Table 15 and Figure 175 show the tabular and graphical results for the volume change portion of the freeze-thaw durability test for manufactured sand mixtures, respectively. Note that the CKD and Riverside-CKD samples were discontinued after two and ten cycles, respectively. The results obtained for the CKD stabilized manufactured sand are consistent with the results obtained for the limestone screenings proving the CKD is not a good stabilizer. The OGS-CKD and Portland cement samples performed the best volumetrically with about 3% and less than 1% volume change, respectively.

Table 16 and Figure 176 show the tabular and graphical results for the percent mass loss portion of the freeze-thaw durability test for manufactured sand. According to the NAVFAC (1999) manual, both the OGS-CKD and Portland cement stabilized manufactured sand mixtures would be able to be used due to their respective mass losses being less than 14%.

For further detail on each sample's condition at the end of each cycle, please see the pictures located in the Appendix.

Table 15. Percent Volume Change for Stabilized Manufactured Sand Freeze-Thaw Durability Test Samples

	Percent Volume Change			
Cycle	CKD	OGS-CKD	Riv-CKD	Portland Cement
0	14.8	2.5	5.0	0.5
1	14.1	2.6	5.1	-0.1
2	26.5	3.1	6.3	0.5
3	-	1.7	5.8	0.2
4	-	1.3	7.4	0.8
5	-	2.0	7.9	0.2
6	-	0.8	10.0	0.5
7	-	1.8	11.9	0.7
8	-	1.6	14.9	0.6
9	-	1.1	11.2	0.3
10	-	0.4	7.3	0.5
11	-	0.4	-	0.0
12	-	0.7	-	0.6

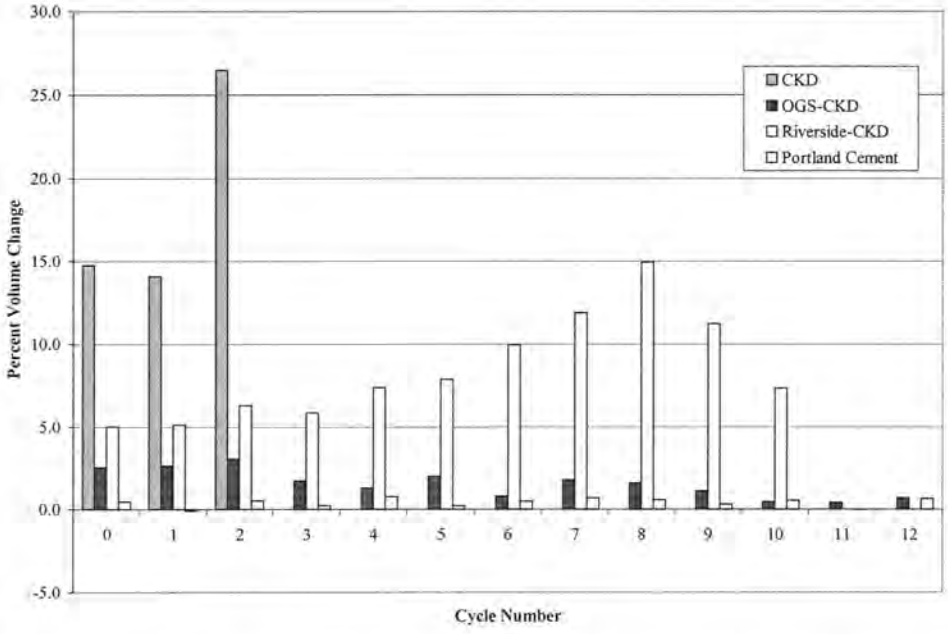

Figure 175. Percent Volume Change for Stabilized Manufactured Sand Freeze-Thaw Durability Test Samples

Table 16. Percent Mass Loss for Stabilized Manufactured Sand Freeze-Thaw Durability Test Samples

	Percent Mass Loss			
Cycle	CKD	OGS-CKD	Riv-CKD	Portland Cement
0	0.0	1.3	0.1	1.0
1	32.7	0.8	1.3	1.3
2	100.0	2.2	3.0	1.8
3	-	2.7	7.6	1.3
4	-	2.7	14.5	1.8
5	-	3.2	23.8	2.1
6	-	3.2	52.8	2.3
7	-	3.7	72.1	2.3
8	-	3.8	86.2	2.1
9	-	4.0	88.5	2.2
10	-	4.3	100.0	2.5
11	-	4.4	-	2.3
12	-	4.5	-	2.3

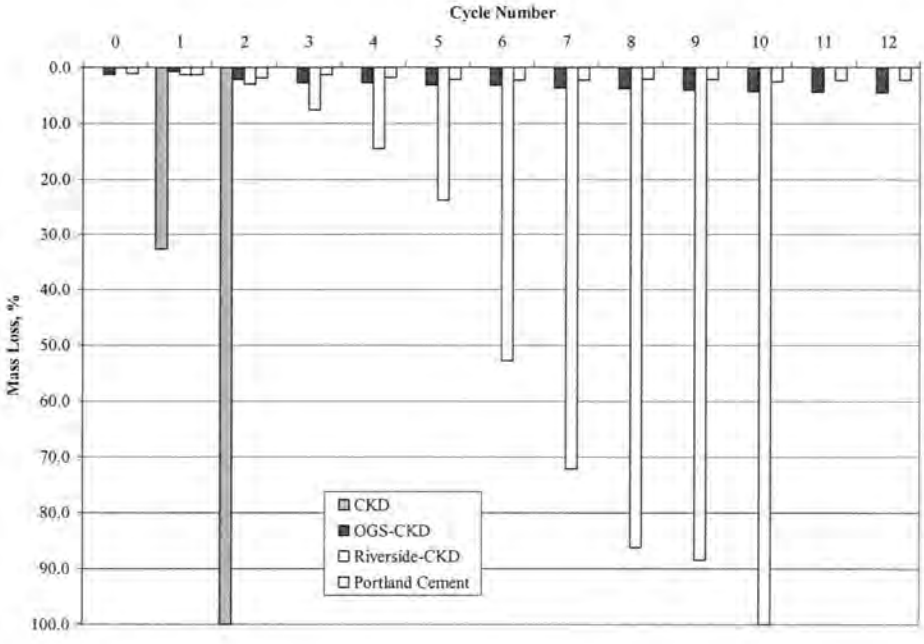

Figure 176. Percent Soil Cement Loss for Stabilized Manufactured Sand Freeze-Thaw Durability Test Samples

Wet-Dry Durability Testing

This section shows the results for wet-dry durability testing on the maximum unconfined compression strength samples from each stabilizer evaluated for both the limestone screenings and manufactured sand.

Limestone Screenings

Table 17 and Figure 177 show the tabular and graphical results for the volume change portion of the wet-dry durability test for stabilized limestone screenings mixtures. Note that the samples containing CKD had observed expansion much greater than those samples containing no CKD. The addition of class C fly ash to CKD cut the observed expansion about four times. These results show that the use of CKD as a stabilizer should be done only after extensive laboratory testing. Note that the Prairie Creek fly ash stabilized samples saw a reduction in volume due to sample breakdown.

Table 18 and Figure 178 show the tabular and graphical results for the percent mass loss for the wet-dry durability test for stabilized limestone screenings mixtures. Note that the OGS-CKD, Riverside-CKD, and Portland cement stabilized samples passed the wet-dry durability test according to NAVFAC (1999) with soil cement losses less than 14%.

For further detail of each stabilized sample, please see the pictures at the end of each cycle located in the Appendix.

Table 17. Percent Volume Change for Stabilized Limestone Screenings Wet-Dry Durability Test Samples

	Percent Volume Change				
Cycle	CKD	OGS-CKD	Riv-CKD	Portland Cement	Prairie Creek Fly Ash
0	19.2	7.8	9.1	0.0	0.5
1	28.4	8.3	7.7	-0.1	0.1
2	-	7.6	8.2	0.4	-0.1
3	-	8.0	8.6	0.8	0.1
4	-	7.4	7.9	0.3	-0.2
5	-	7.4	7.3	0.0	-0.5
6	-	7.8	7.6	0.0	-0.6
7	-	7.5	7.5	-0.1	-1.4
8	-	7.4	7.8	0.1	-1.7
9	-	7.5	7.4	-0.4	-1.9
10	-	7.3	7.4	0.0	-1.8
11	-	7.9	7.3	-0.2	-2.3
12	-	7.2	7.6	-0.4	-2.7

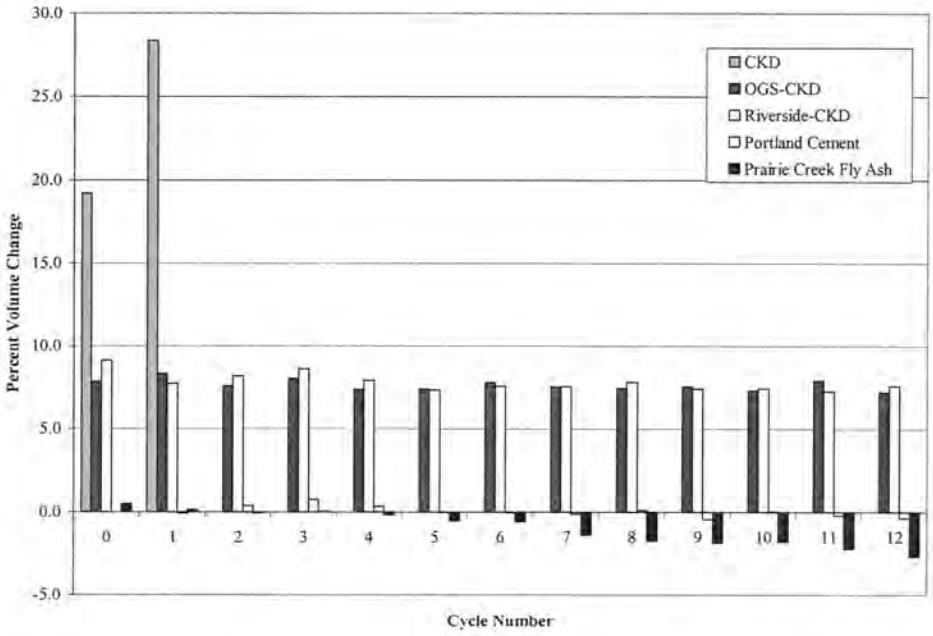

Figure 177. Percent Volume Change for Stabilized Limestone Screenings Wet-Dry Durability Test Samples

Table 18. Percent Mass Loss for Stabilized Limestone Screenings Wet-Dry Durability Test Samples

	Percent Mass Loss				
Cycle	CKD	OGS-CKD	Riv-CKD	Portland Cement	Prairie Creek Fly Ash
0	14.5	5.8	6.6	3.4	1.1
1	100.0	7.0	8.4	5.0	5.1
2	-	7.6	8.9	5.6	9.6
3	-	5.6	6.0	4.9	15.8
4	-	7.5	10.3	5.8	21.1
5	-	7.8	11.0	6.1	25.7
6	-	8.2	11.7	6.3	29.7
7	-	8.7	12.0	6.5	33.7
8	-	9.3	12.6	6.9	35.9
9	-	10.1	12.7	6.9	37.3
10	-	10.6	13.2	7.4	38.6
11	-	11.1	13.6	7.6	39.8
12	-	11.7	13.9	7.7	40.9

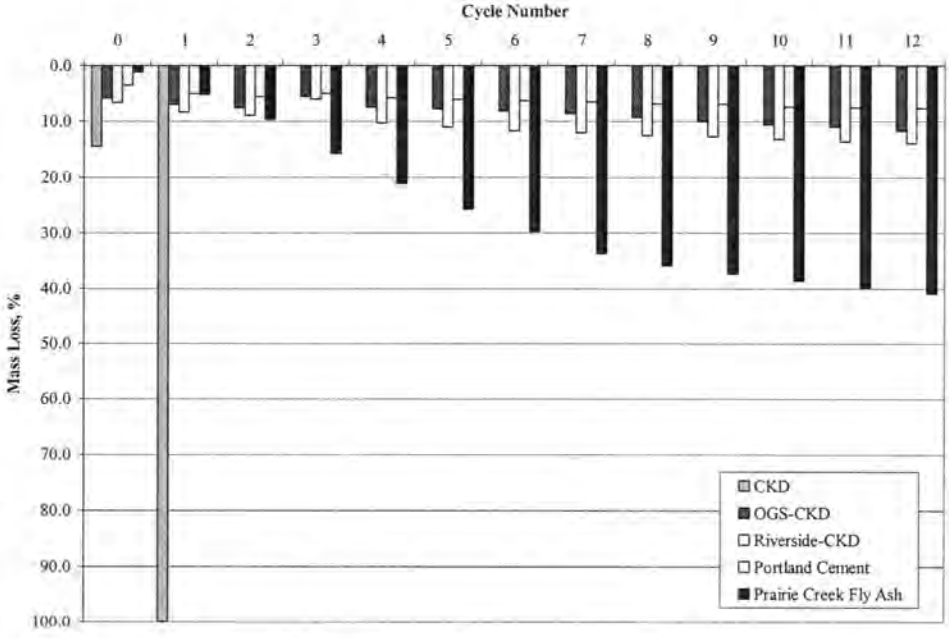

Figure 178. Percent Mass Loss for Stabilized Limestone Screenings Wet-Dry Durability Test Samples

Manufactured Sand

Table 19 and Figure 179 show the percent volume change for stabilized manufactured sand mixtures for wet-dry durability tests. Note that the CKD stabilized sample was discontinued after six cycles. Note that the Portland cement sample continued to perform the best with less than one percent volume change. Stabilized manufactured sand samples fared better in the wet-dry durability test than the stabilized limestone screenings. This is attributed to a more porous material allowing better movement of water throughout the sample.

Table 20 and Figure 180 show the percent soil cement loss for stabilized manufactured sand mixtures for wet-dry durability testing. Figure 180 shows that the Portland cement and OGS-CKD samples passed the durability test according to the NAVFAC (1999) manual.

For further detail of each stabilized sample, please see the pictures at the end of each cycle located in the Appendix.

Table 19. Percent Volume Change for Stabilized Manufactured Sand Wet-Dry Durability Test Samples

	Percent Volume Change			
Cycle	CKD	OGS-CKD	Riv-CKD	Portland Cement
0	11.9	1.8	7.3	0.2
1	17.5	3.1	6.0	-0.2
2	20.0	2.6	5.6	0.0
3	22.2	2.2	4.7	0.1
4	21.2	2.5	5.4	0.1
5	24.5	2.1	5.3	0.3
6	23.4	2.6	4.7	-0.1
7	-	2.3	4.9	0.1
8	-	2.3	5.0	0.1
9	-	1.4	4.5	0.2
10	-	2.7	5.0	-0.6
11	-	2.1	4.7	-0.7
12	-	2.1	4.4	-0.3

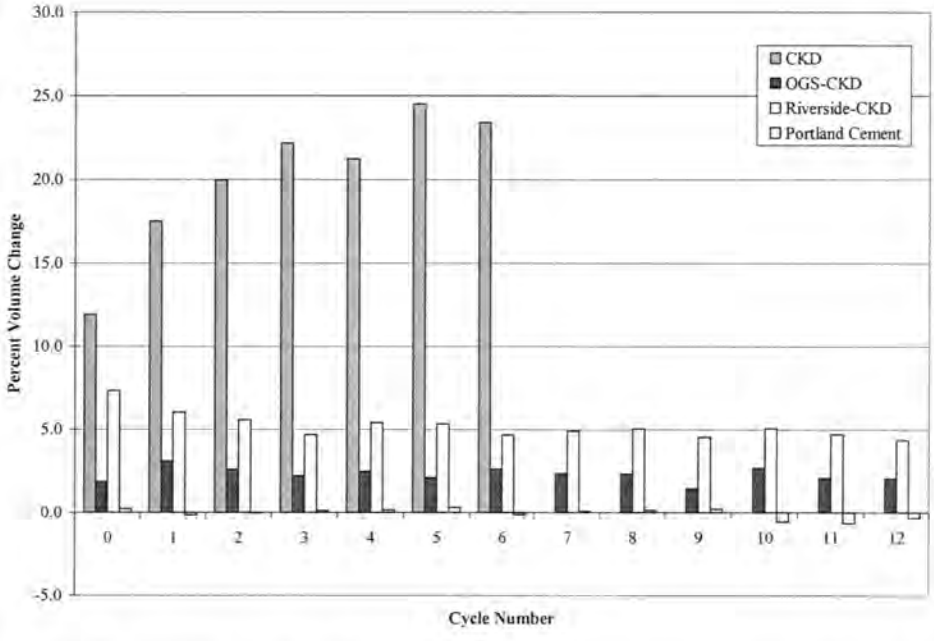

Figure 179. Percent Volume Change for Stabilized Manufactured Sand Wet-Dry Durability Samples

Table 20. Percent Mass Loss for Stabilized Manufactured Sand Wet-Dry Durability Samples

	Percent Mass Loss			
Cycle	CKD	OGS-CKD	Riv-CKD	Portland Cement
0	9.1	9.1	6.7	3.5
1	14.9	8.9	8.7	4.2
2	28.7	9.9	9.5	4.9
3	46.2	9.7	10.9	5.0
4	58.5	10.2	11.6	5.0
5	91.3	10.3	12.4	5.2
6	100.0	10.3	13.1	5.1
7	-	10.3	13.4	5.5
8	-	10.4	14.4	5.5
9	-	10.4	14.9	5.6
10	-	10.5	15.6	5.7
11	-	10.4	16.3	5.7
12	-	10.5	16.7	5.7

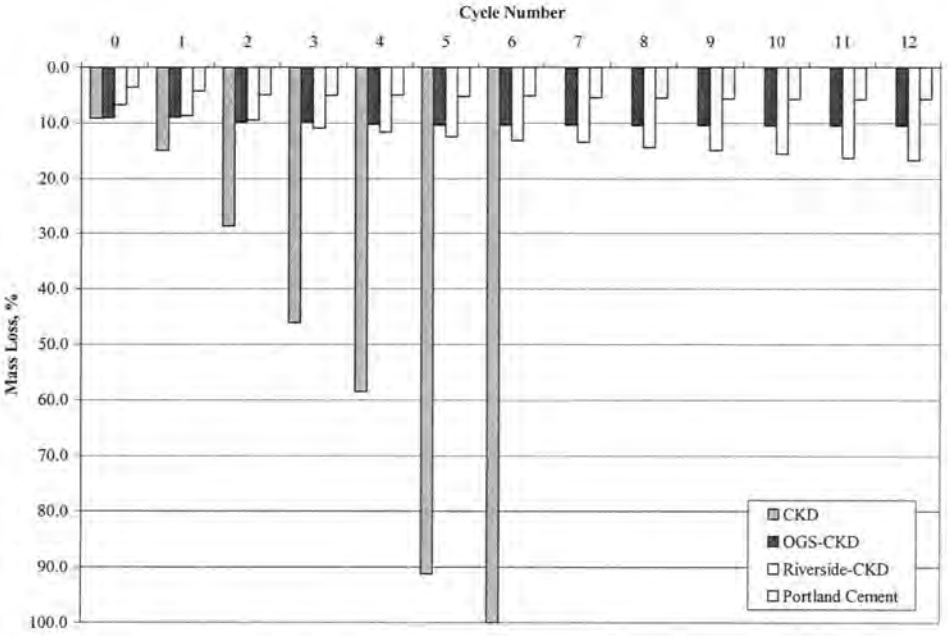

Figure 180. Percent Mass Loss for Stabilized Manufactured Sand Wet-Dry Durability Samples

Construction Operations

Using the detailed construction operation, an adequate structural layer utilizing stabilized limestone screenings was produced. Figure 76 shows the completed access road after construction. FWD results show an adequate structural layer by comparisons of deflection basins between the test and control sections.

One result of using CKD as a stabilizer is shown in Figure 181. The high heat of hydration of CKD makes a hot worksite. The high heat of hydration also caused piping of water vapor through the material, leading to material exhibiting a bubbling action shown in Figure 182.

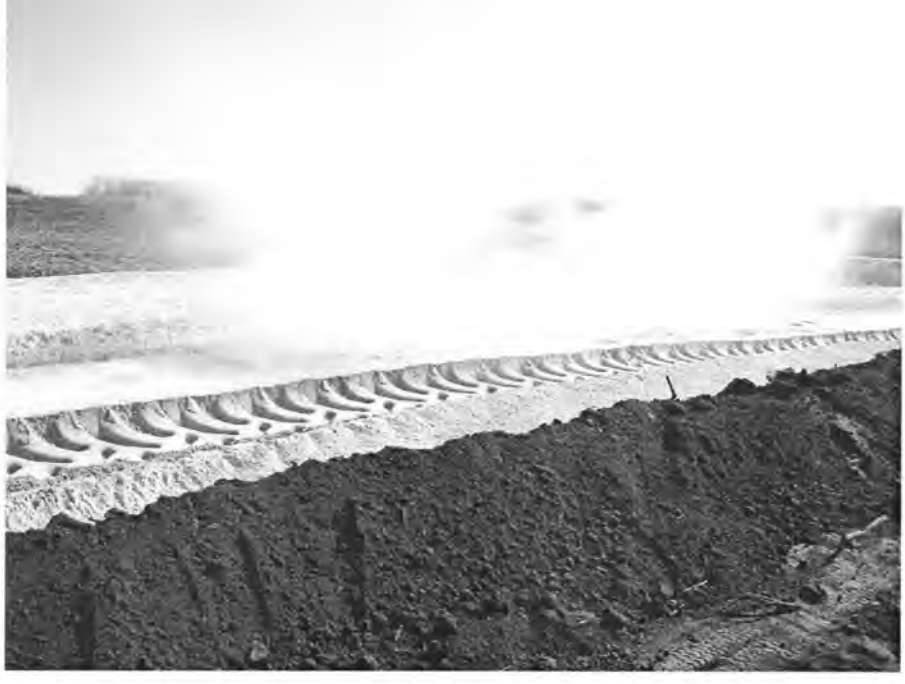

Figure 181. Steam Arising in Test Section One After Mixing Due to High Heat of Hydration

Figure 182. Water Vapor Causing Bubbling of Material before Compaction

Performance Monitoring

Results from performance monitoring are divided into five categories: (1) Falling Weight Deflectometer (FWD) testing shortly after construction, (2) Temperature data analysis through the use of I-Buttons installed during construction, (3) Clegg Impact Hammer testing, (4) Visual Observations, and (5) Dynamic Cone Penetrometer (DCP) testing.

Falling Weight Deflectometer

FWD results reveal equal deflection basins for the two test sections shortly after construction. FWD results show that the test sections are about two times as stiff as the control sections. Figure 183 shows the deflection basins for each section.

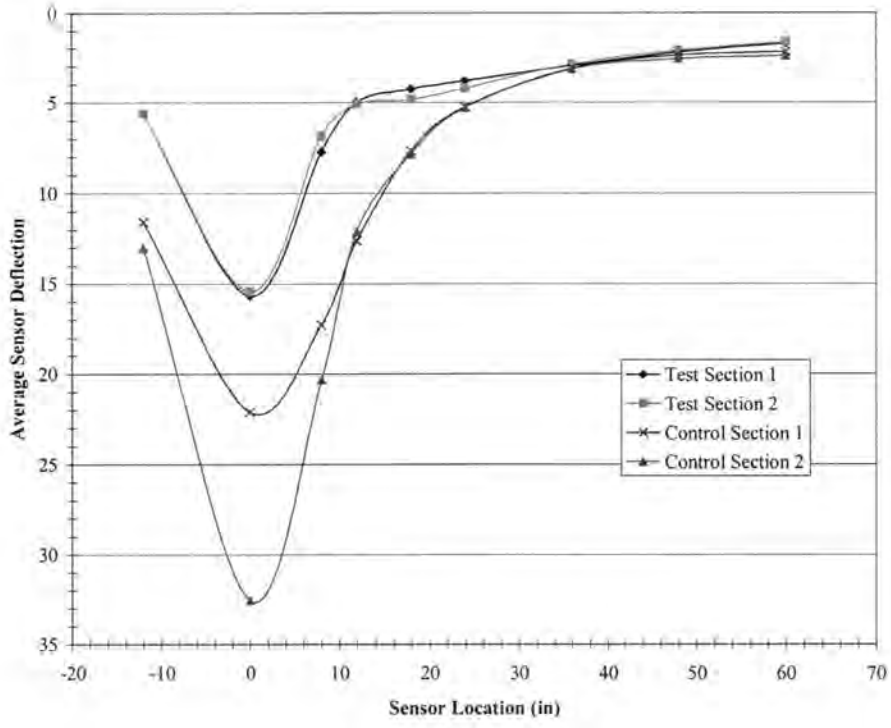

Figure 183. Average (4 Tests) FWD Deflection Basins for the Completed Access Road

Clegg Impact Hammer

Clegg Impact Hammer testing results show that the two test sections increased in stiffness after construction and then decreased slightly before increasing due to the winter freeze. Results also show that the CIV for test section two was about 2 times greater than that of test section one. Figure 184 shows the average Clegg Impact Value (CIV) for each test section

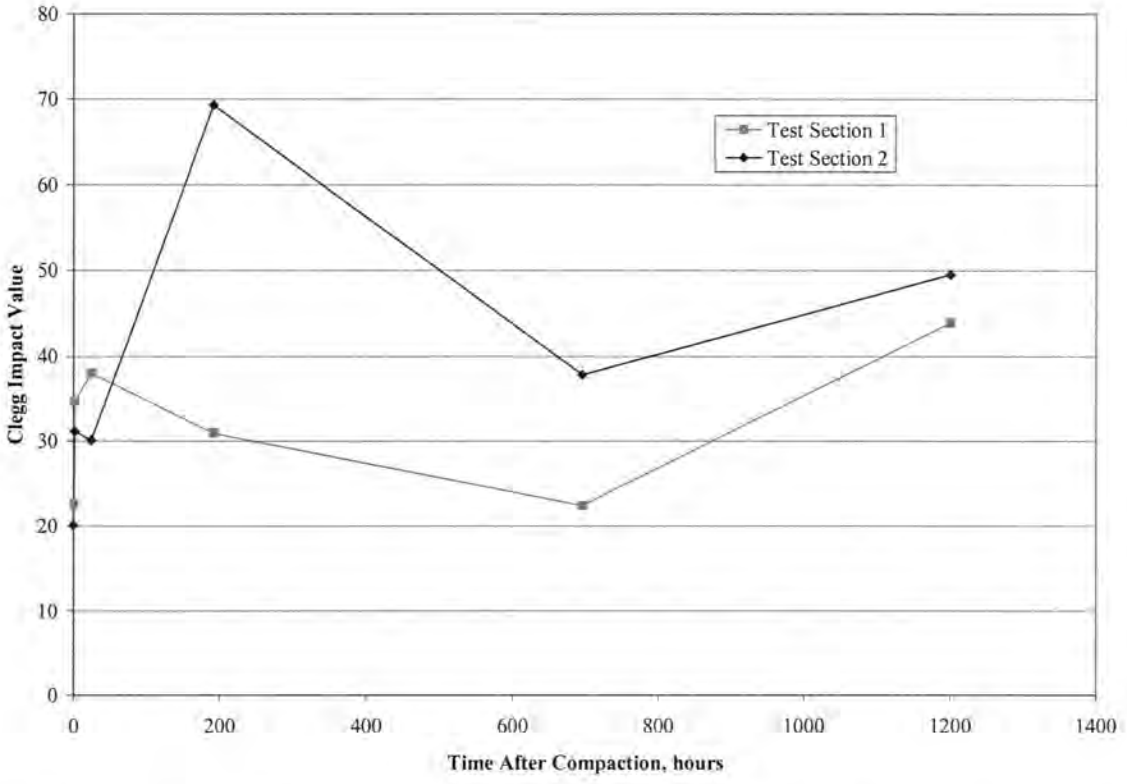

Figure 184. Average (3 Tests) Clegg Impact Value versus Time for Test Sections One and Two

I-Button Temperature Readings

Temperature readings results show that each test section has underwent two or three freeze-thaw cycles. The results also show that each test section has about the same temperature readings over time, and approximately the same heat of hydration of about 144°F. Figure 185 shows the relationship between time and the air and stabilized layer temperature for test sections one and two.

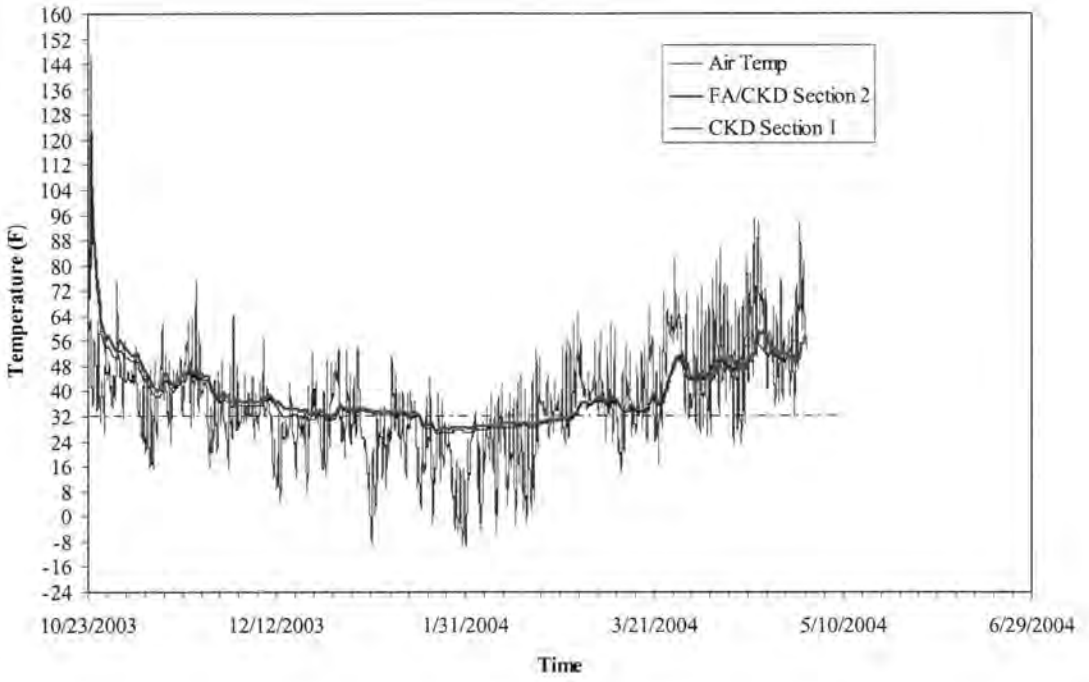

Figure 185. Temperature versus Time for Test Sections One and Two

Visual Observations

Visual observations to date show that the access road performed well in both test sections until the spring thaw when test section one appeared to fail under traffic loading. Test section two and both control sections appear to be performing well with some slight pothole development. Test section one was repaired through the use of 150 mm Macadam Stone.

February 13, 2004

All sections appear to be performing well on this date with an absence of rutting in all sections. Figure 186 shows test section one on February 13, 2004. Note the absence of

deformation. Figure 187 shows test section two on February 13, 2004. Also note the absence of rutting in this section. Figure 188 shows the control sections on February 13, 2004. The control sections appear to be performing well on this date.

Figure 186. Test Section One on February 13, 2004

Figure 187. Test Section Two on February 13, 2004

Figure 188. Control Sections One (Foreground) and Two (Background) on February 13, 2004

March 2, 2004

The following observations were noted on this site visit: test section one failed, high rut depths within the test section, macadam stone was used to provide access through the failed section, one of the temperature sensors within section one was not working properly, and I-Button temperature data showed thawing of stabilized sections.

On March 1, 2004 Iowa State University personnel were contacted by project owners and told that test section one had failed. Upon hearing the news, a site visit was conducted. Tests conducted during the site visit included: DCP, moisture sampling, and temperature data downloading. Visual observations showed wet or saturated stabilized layer and very high rutting depths. Figures 189 and 190 show the site conditions on March 2, 2004. Note the macadam stone placed in the failed section to provide access for construction traffic.

Moisture sampling on March 2, 2004 showed extremely wet conditions. Measured moisture contents for test section one were 21.7%, 25.7%, 54.4% and 55.9%. All of these moisture contents are well above the 19% optimum moisture content for strength.

Figure 189. Failed Test Section One March 2, 2004 with Macadam Stone and Rutting

Figure 190. Extensive Rutting in Test Section One on March 2, 2004

March 23, 2004

All sections appear to be performing well on the date of this site visit. Test section one, shown in Figure 191, has been stabilized and is no longer failing due to traffic. Note the absence of rutting in all sections. Figure 192 shows test section two. Figures 193 and 194 show control sections one and two, respectively. Note that there is some minor pothole development in control section two.

Figure 191. Test Section One on March 23, 2004

Figure 192. Test Section Two on March 23, 2004

Figure 193. Control Section One on March 23, 2004

Figure 194. Control Section Two on March 23, 2004

April 30, 2004

All sections appear to be performing well on this date. Note the absence of rutting in test sections one and two. Paving of the first 100 feet of the access road lead to the deposition of excess fill material onto test section one shown in Figure 195. Small potholes are continuing to form in control section two. Figures 195 to 197 show the site condition on April 30, 2004.

Figure 195. Test Section One on April 30, 2004

Figure 196. Test Section Two on April 30, 2004

Figure 197. Control Section One (Foreground) and Control Section Two (Background) on April 30, 2004

May 21, 2004

The site visit conducted May 21, 2004 revealed a completed asphalt entrance for the first 100 feet of the access road leading up to test section one shown in Figure 198. Figure 199 shows test section two and control section one. Temperature sensors one, two, three, and six were not working properly. Temperature sensor six was determined to be broken since the wires had been severed. The access road appears to be performing well under daily truck traffic loading at this time.

Figure 198. Test Section One on May 21, 2004

Figure 199. Test Section Two (Foreground) and Control Section One (Background) on May 21, 2004

DCP Testing Results

The DCP test was used to evaluate the failed section because it is a fast easy test. It was also chosen due to the many correlations to California Bearing Ratio (CBR). Figure 200 shows the DCP test being conducted. The DCP results were correlated to CBR and then plotted versus depth. Figures 201 to 205 show the CBR plots for test section one. Note the immediate drop in CBR in Figure 203. This shows the soft CKD stabilized layer. For comparison, a DCP test was conducted in test section two. Figure 206 shows the CBR plot for the DCP test conducted in test section two. Note the increase in CBR through the tested section. This shows that test section two is performing well as a structural layer.

Figure 200. DCP Testing on March 2, 2004

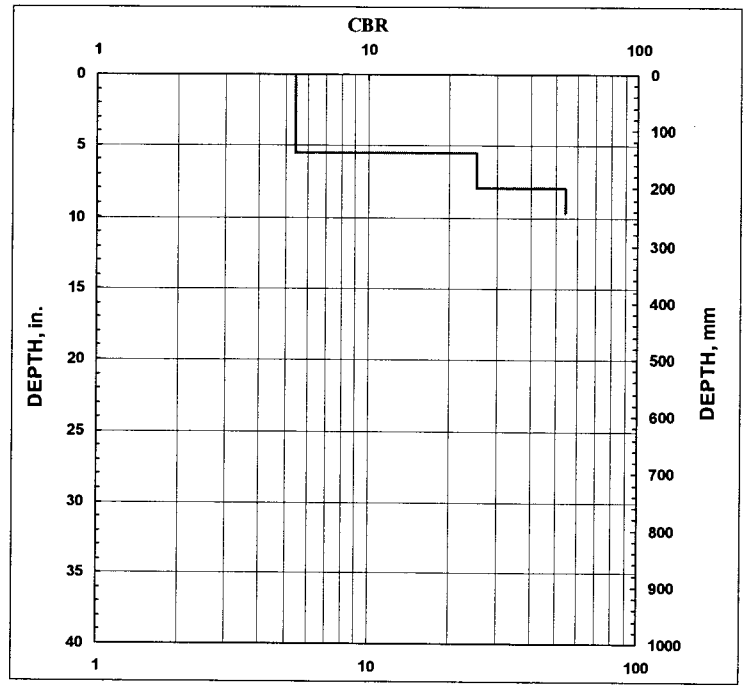

Figure 201. CBR Plot for Test Section One Location 1 on March 2, 2004

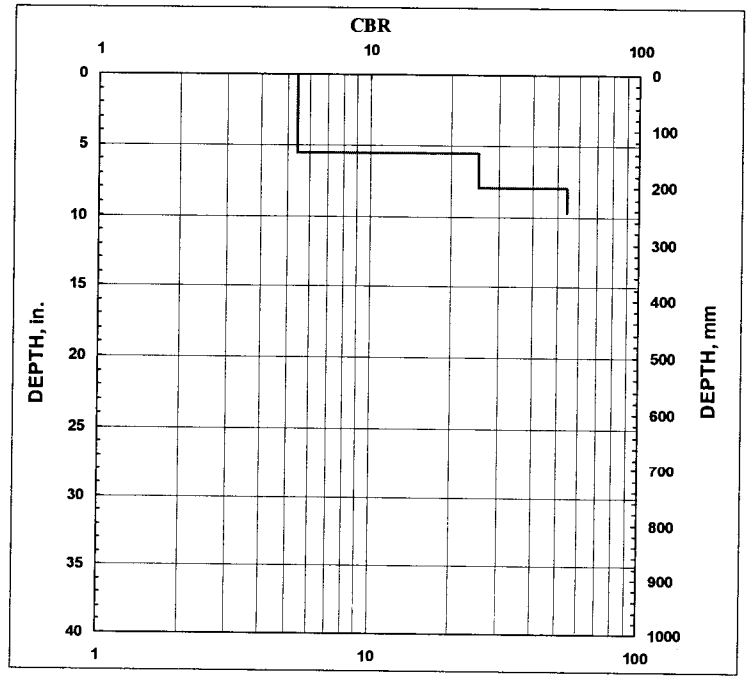

Figure 202. CBR Plot for Test Section One Location 2 on March 2, 2004

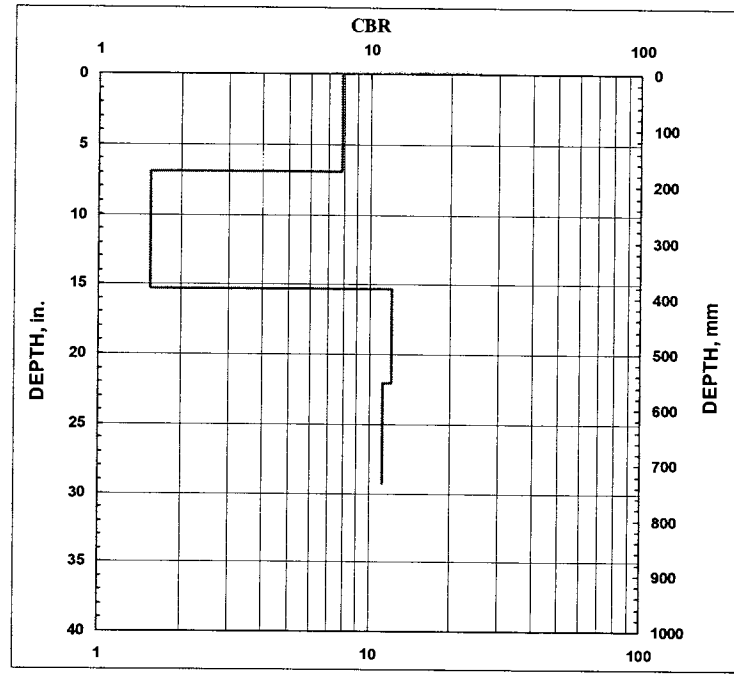

Figure 203. CBR Plot for Test Section One Location 3 on March 2, 2004

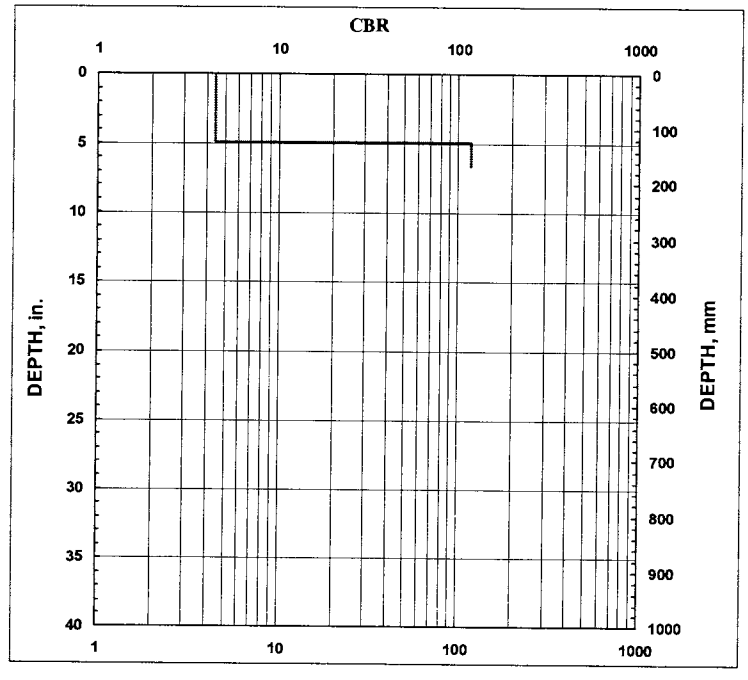

Figure 204. CBR Plot for Test Section One Location 4 on March 2, 2004

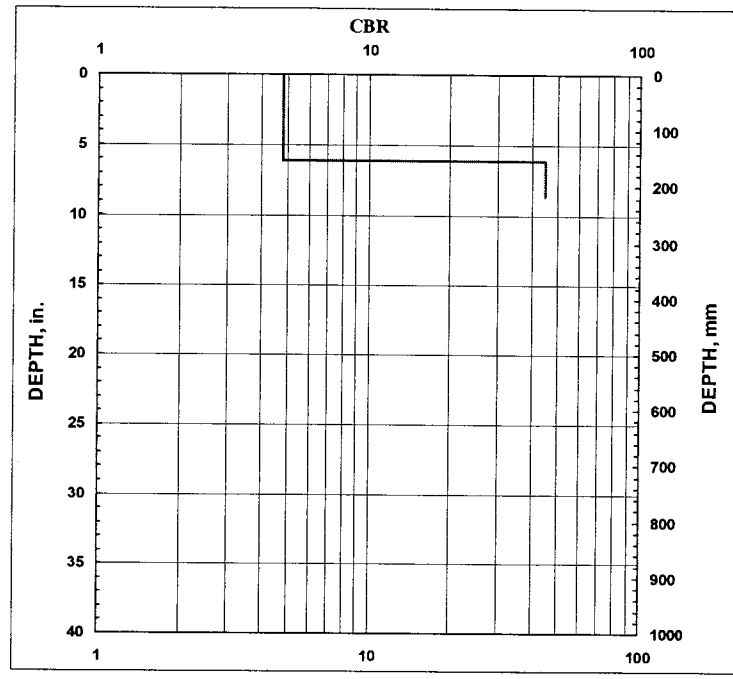

Figure 205. CBR Plot for Test Section One Location 5 on March 2, 2004

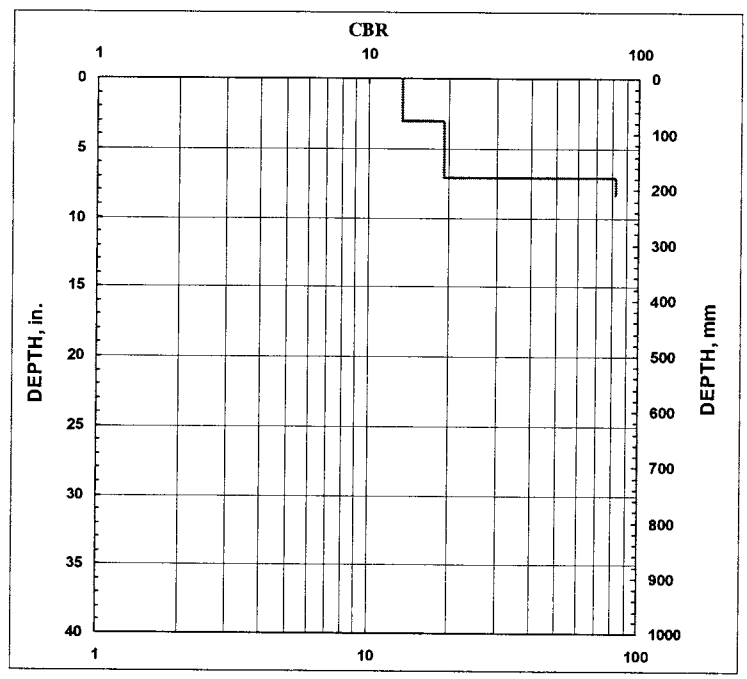

Figure 206. CBR Plot for Test Section Two on March 2, 2004

DISCUSSION

This discussion section discussed implications and applications detailed in the results section. The discussion section is broken into three categories: (1) Laboratory Results, (2) Construction Operations, and (3) Performance Monitoring.

Laboratory Results

The laboratory results discussed include: moisture-density relationship, moisture-strength relationship, freeze-thaw durability, and wet-dry durability.

Moisture-Density Characteristics

The moisture-density curves for each mixture are generally the same. The optimum moisture content increases slightly with increasing binder contents with the exception of the CKD mixtures which increase greatly. This is due to the high heat of hydration of CKD. The increasing optimum moisture content for maximum density is due to the grater amount of fines in the mixtures.

The optimum moisture contents for the limestone screenings range from about 9% to about 22%. The optimum moisture contents for the manufactured sand range from about 7% to about 19%.

The maximum dry densities for the limestone screenings mixtures are about the same. There is a slight decrease in maximum dry density for the OGS-CKD, Riverside-CKD, and Prairie Creek mixtures. The range of maximum dry densities for the limestone screenings mixtures is about 1600 kg/m^3 to about 2000 kg/m^3.

The manufactured sand maximum dry densities tend to remain constant as the binder content increases. CKD samples tend to have the highest maximum dry density of all mixtures followed by the Riverside and OGS-CKD mixtures. Ranges for the maximum dry density are 1600 kg/m^3 to about 2200 kg/m^3. Comparisons between the moisture density curves show no significant differences between stabilized limestone screenings and stabilized manufactured sand mixtures.

Using the data obtained from extensive moisture density testing, several mixtures could be proposed and constructed using the moisture-density curves detailed. This allows for a greater flexibility when in the construction stage due to availability of materials such as screenings, manufactured sand, and stabilizers.

Moisture-Strength Characteristics

The moisture-strength curves for limestone screenings mixtures show dramatic increases in optimum moisture content as the binder contents increase. The optimum moisture content based on strength ranges from about 9% to 19%. The most dramatic increase in optimum moisture content based on strength is shown in the CKD samples. This proves that CKD would be a great drying agent for saturated soil stabilization. The maximum strengths increase dramatically with the introduction of CKD. Strengths then increase once fly ash and CKD are blended to comprise a stabilizing agent. The OGS-CKD strengths are the highest with about 20,000 kPa unconfined compressive strength.

The optimum moisture contents based on strength for manufactured sand show the same general increasing trend found in the limestone screenings samples. The optimum moisture contents range from about 9.5% to about 21%. This wider range in moisture

content is due to the low optimum moisture content for Portland cement samples. In general, the CKD samples required more moisture to obtain maximum strength than did the Riverside-CKD, OGS-CKD, and Portland cement samples.

The manufactured sand maximum compressive strengths are comparable to the limestone screenings with exception to the Portland cement samples. The highest compressive strength for the manufactured sand was also a blended CKD-Riverside fly ash binder.

Further analysis of the data shows a striking decrease in strength occurs after optimum moisture content for strength has been passed. This characteristic is a very important detail to track when constructing the stabilized layer in the field. The optimum moisture content based on strength should not be passed by more than 1%. This may have been a minor contributing factor for the failure of test section one. Other more pressing factors are discussed in later sections.

Freeze-Thaw Durability

The freeze-thaw durability data shows that the CKD stabilized manufactured sand and limestone screenings performed poorly. Although the durability was increased when class C fly ash was added, the OGS mixture out performed the Riverside mixture due to the added sulfur content from the Riverside mixture. The Portland cement stabilized mixtures put performed all other mixtures throughout the course of this testing.

Stabilized manufactured sand out performed the stabilized limestone screenings in the freeze-thaw durability test. This is due to the sand having more open pore space allowing water to expand when freezing. Based solely on freeze-thaw durability test data, NAVFAC

(1999) recommends that OGS-CKD and Portland cement stabilized manufactured sand and Portland cement stabilized limestone screenings be incorporated as a construction material.

Wet-Dry Durability

Wet-dry durability test show that CKD stabilized samples performed poorly. This shows that CKD would not be a good stabilizer choice due to excessive volume change and mass loss. The OGS-CKD stabilized mixtures outperformed the Riverside-CKD stabilized mixtures. This is most likely due to the added sulfur content from the Riverside fly ash.

Based on wet-dry durability test data, NAVFAC (1999) recommends that the OGS-CKD, Riverside-CKD, and Portland cement stabilized limestone screenings, and OGS-CKD and Portland cement stabilized manufactured sand be incorporated as a construction material.

For the manufactured sand, the OGS-CKD and Portland cement stabilized samples passed both the freeze-thaw and wet-dry durability tests. The Portland cement stabilized limestone screenings samples passed both the freeze-thaw and wet-dry durability tests.

Construction Operations

Construction operations produced a suitable stabilized layer capable of supporting daily traffic for the sand plant. A suitable product was constructed; several improvements could be made to increase the effectiveness of the construction operation.

The first improvement would be to deposit the fly ash with something other than a bottom dump truck. Even though the wind was very active, and dust generation was kept to a minimum, using a bulldozer during the spreading process created a lot of dust. If a modified dump truck with an auger spreader were used, the deposition process would be much more uniform eliminating the need for spreading.

The second improvement that could be made would be to use other equipment other than pneumatic tanker trucks to move and deposit CKD. The pneumatic tanker truck deposition process was slow and inefficient. Valuable time, about two hours, was lost depositing the CKD. This delay time should be kept to a minimum so that the CKD and self-cementing fly ash undergoes minimum hydration. Hydrated fly ash and CKD are no longer chemically reactive; therefore nullifying their use as an active stabilizing agent.

The third improvement would be to have a better water supply available on site for construction mixing operations. Using a pulvamixer adding water through a spray bar in the drum seemed to work well with the exception of having only one water truck on site. Time was spent waiting on a full water truck to arrive to the site to continue mixing operations. Other improvements in this area would be to use a central batching plant with a pug mill. This type of operation would produce a much more uniform material for construction purposes due to added preciseness during the mixing process.

Use of CKD in field construction, posed some challenges due to the high heat of hydration. The high heat of hydration created a hot work environment even though this was constructed on a cool autumn day.

Performance Monitoring

Performance monitoring data has shown two very well constructed sections through the winter of 2003 to late February 2004. Performance data discussed in this section includes: FWD, CIV, temperature I-button, DCP, and visual observations.

Falling Weight Deflectometer

Use of the FWD to test the stiffness of each section was completed shortly after construction. The FWD deflection basins, Figure 183, show nearly identical stiffness distributions for each of the test sections. The deflection basin of control section one was about 2/3 of the deflection basin of control section two. This shows that the limestone screenings in both layers resist an impact load better than limestone screenings over manufactured sand. Note the deflection basins of the two test sections are about seven mils less than control section one and about seventeen mils less than control section two. This figure illustrates that the stabilization efforts were achieved.

Clegg Impact Hammer

Clegg Impact Hammer data shows initial gain in strength for the first 24 hours for both test sections one and two. Test section one then declines for about 28 days. After 28 days, temperatures started to drop below freezing. This is what leads to the increase in CIV for test section one. Test section two increases in CIV until about seven days after construction and then declines until about 28 days after construction when the temperatures started to go below the freezing point. The water in the stabilized section layers then started to freeze; thus leading to an increase in CIV for both test sections.

Temperature Data

Temperature data was taken in order to gain a better understanding of the heat of hydration, as well as the number of freeze-thaw cycles each section has underwent. Figure 185 shows that the temperature profiles for each section are nearly identical with two or three

freeze-thaw cycles for each section. It is believed that this freeze-thaw action, combined with wet-dry action due to rains, caused failure of test section one on March 2, 2004. The failure coincides very well with the increase in layer temperature increases above the freezing point.

The field data corresponds well with laboratory freeze-thaw and wet-dry durability data for the CKD samples. Using the data presented, it is recommended that CKD stabilization of limestone screenings proceed cautiously with durability testing and chemical analysis of the CKD and CKD stabilized material being the most important tests to be conducted prior to construction.

Dynamic Cone Penetrometer

DCP results show a lowering of the CBR value due to wet moisture conditions within the stabilized layer for test section one. The CBR plots show very low CBR values for test section one compared to those of test section two. The CBR plots show that the DCP is an effective tool for use in determining the depth of failure for test section one.

Visual Observations

Visual observation results show that test section two is performing well seven months, and three freeze-thaw cycles, after construction. Observations show that after macadam stone placement, test section one is able to handle traffic loading. Visual observations show that both control sections one and two are performing well with some pothole formation in control section two.

CONCLUSIONS

This section discusses the conclusions for this pilot project and is organized as follows: (1) Materials, (2) Construction operations, (3) Laboratory results, and (4) Performance monitoring results.

Materials

Materials testing confirmed that both fly ashes were class C, and that the CKD had a high amount of sulfur. Combinations of CKD and class C fly ash were found to significantly increase the unconfined compressive strength of the stabilized mixtures leading to a final product that is able to withstand daily quarry truck traffic.

The limestone screenings were typical of limestone aggregate production with a high fines content of about 26-30%. The manufactured sand was typical of crushed sand with low fines content around 10%.

Construction Operations

The documented construction operation showed that it is viable to stabilize limestone screenings in a cost effective and timely manner. Construction proceeded smoothly with the exception of CKD deposition and water availability. The documented construction procedure was very effective in producing a structural layer in road construction built of stabilized limestone screenings. The high heat of hydration of CKD produced a hot worksite.

Laboratory Results

The laboratory results warrant the following conclusions. The moisture-density curves are about the same for both the manufactured sand and limestone screenings. The moisture-strength curves show that an increase in moisture content beyond the optimum moisture content for strength leads to dramatically reduced unconfined compressive strengths. This proves that construction operations should use the optimum moisture content based on strength rather than the optimum moisture content based on density.

Freeze-thaw and wet-dry durability testing show that CKD stabilized limestone screenings and manufactured sand is not a viable construction alternative. Addition of class C fly ash with CKD significantly increased the durability of the mixtures, and Portland cement stabilized mixtures performed well in the durability tests. Manufactured sand samples fared better than the limestone screenings in the durability tests because there is more pore space allowing water to expand when freezing.

Performance Monitoring

The performance monitoring results warrant three conclusions. FWD results proved that stabilized limestone screenings can perform as a structural layer in road construction, and visual observations confirmed a well performing structural layer constructed of stabilized limestone screenings. The DCP results were effective in determining the depth of failure for test section one concluding that the DCP is and effective tool for determination of soft layer thicknesses. I-Button temperature data showed three freeze-thaw cycles showing that the corresponding failure of test section one follows laboratory results closely concluding that

test section one most likely failed due to a combination of expansive mineral formation, wet conditions, and freeze-thaw action.

RECOMMENDATIONS

Recommendations for future research are: further defining the mixture to binder content ratios near the optimum binder content for strength, investigating the influence of varying the CKD fly ash ratio from 1:1, and continuation of performance monitoring through visual observations and temperature data analysis. It is also recommended that FWD tests be conducted early spring after, or during, the thaw in order to investigate the change in stiffness due to freezing and thawing. Another area of future research is investigation of different binder or stabilizing agent such as bitumen.

The author also recommends that samples be taken of test section one for SEM analysis. This would provide more insight as to whether or not expansive mineral formation played a part in the failure of the test section.

CHAPTER 3. INVESTIGATION OF SUBGRADE NON-UNIFORMITY INFLUENCE ON PAVEMENT PERFORMANCE

ABSTRACT

Pavement rehabilitation costs millions of tax dollars a year. Pavement rehabilitation also costs millions of dollars a year in lost productivity impacting the general public and local businesses. Rehabilitation costs rise in the event of a complication such as subgrade reconstruction, modification of subgrade soils, and general construction difficulties.

To address the cost of pavement rehabilitation, the industry has adopted several methods of repair including diamond grinding and asphalt overlay. These remedies work unless the real problem lies within the subgrade and its non-uniform characteristics.

To provide insight into subgrade non-uniformity and its effects of pavement performance, civil engineering experts need to look at the whole pavement system to determine if a more effective, economical solution exists. The purpose and goal of this study was to investigate the influence of non-uniform subgrade on pavement responses that affect pavement performance. This project set forth three objectives:

1. Generate field data from 10 to 12 local subgrade or pavement reconstruction projects in Iowa;
2. Using field data, develop finite element models to measure pavement performance in terms of pavement responses of stress and deflection;

3. Conduct statistical analysis of the results to determine if there exists a correlation between pavement performance and subgrade non-uniformity.

GeoGauge, nuclear density gauge, Clegg Impact Hammer, and Dynamic Cone Penetrometer (DCP) tests were used to evaluate the subgrade conditions found at each project. ISLAB 2000 finite element software was used to determine critical pavement responses including stress and deflection.

Overview of Results and Conclusions

Field data shows that hydrated fly ash (HFA), self-cementing fly ash stabilized subgrade, and granular subbases exhibit less variability than natural subgrade soils. ISLAB 2000 data shows that pavement stresses decrease when the pavement is modeled using a uniform subgrade. Statistical analysis showed that the modulus of subgrade reaction did not fit either the beta or normal distribution.

Conclusions of this study illustrate that pavement performance is affected by non-uniform subgrade. Pavement life can be increased through the use of stabilized subgrade, HFA or granular subbase. Uniform subgrade produces less variability in pavement modeling results allowing for an increased confidence in pavement design.

INTRODUCTION

Pavement rehabilitation cost millions of dollars per year in the United States. The costs increase in the event of complications such as rebuilding subgrade, modification of soils, and construction difficulties. Even though a subgrade is designed to last 100 years,

sometimes pavement rehabilitation is occurring once every 40 to 60 years due to inadequate subgrade. If pavement performance can be increased by extending the lifecycle of the subgrade, money can be saved. Simple things can be completed, such as addition of fly ash for subgrade stabilization; however, the up front cost of this solution inhibits this construction philosophy.

The question raised is this: is the up front cost worthy of investing in stabilization techniques or correct subgrade construction techniques that increase pavement performance? The first step in persuading organizations to consider investing in the up front cost is to prove without a doubt the long term effects on the pavement performance.

This project sets out to investigate the influence of non-uniform subgrade on pavement stresses and deflections that directly impact pavement performance. The three objectives needed to accomplish this goal are as follows:

1. Generate field data from 10 to 12 local subgrade or pavement reconstruction projects in Iowa;
2. Using field data, develop finite element models to measure pavement performance in terms of pavement responses of stress and deflection;
3. Conduct statistical analysis of the results to determine if there exists a correlation between pavement performance and subgrade non-uniformity.

Conclusions of the research confirmed that there is a link between pavement performance and subgrade non-uniformity. Finite element analysis proves that a uniform subgrade reduces critical pavement responses such as stress and deflection leading to increased pavement life. Statistical analysis showed that field results for hydrated fly ash (HFA), granular subbase, and self-cementing fly ash treated subgrade tend to be more

uniform when comparing the coefficient of variation. Analysis of the finite element data show shows that distributions tested for the modulus of subgrade reaction did not fit the data. Analysis also shows that uniform modeling conditions produce stresses that have less variability. Reliability was also increased with the modeling of a uniform subgrade.

This chapter is organized in the following manner:

- Literature Review
- Methods
- Materials
- Results
- Discussion
- Conclusions
- Recommendations

LITERATURE REVIEW

To provide context for this study, this literature review section details subgrade modeling theories, sources of pavement stress, pavement failure mechanisms, and finite element models. This review also briefly describes past research documenting the effects of spatial variation.

Overview

Since the first concrete pavement was placed in Bellefontaine, Ohio in 1893, rigid pavement design and analysis has become ever more important in today's society (Huang 2004). In 2001 there was approximately 59,000 miles of rigid pavement in the United States

(Huang 2004). With pavement rehabilitation costs ever rising, research needs to be completed in the area of subgrade non-uniformity and its effect on pavement performance.

Subgrade Models

In geotechnical engineering, the solution of a slab-on-grade soil-structure interaction problem has been simplified. Concrete pavements and foundations are generally treated as an elastic plate, and the soil supporting the pavement or foundation is assumed to be linear elastic, isotropic, and homogeneous. In reality, the stress-strain behavior of the soil is nonlinear, irreversible, anisotropic, and inhomogeneous.

The above mentioned complexities of soils have led to the development of idealized models in order to provide a representation of soil behavior under certain loading and boundary conditions. There are two widely accepted subgrade models, the dense liquid and elastic solid (Huang 2004; Khazanovich 1994; Ioannides 1984; Darter et al. 1995). Authors are quick to note that although the dense liquid and elastic solid models are widely used to simplify the slab-on-grade soil-structure interaction, in reality soil behavior actually falls somewhere in between the two models.

The first section of subgrade models will discuss the dense liquid model's advantages and disadvantages. The second section of subgrade models will discuss the elastic solid model's advantages and disadvantages.

Dense Liquid Model

The dense liquid model states that the supporting soil acts like a bed of closely spaced, independent, linear springs (Khazanovich 1994; Ioannides 1984; Darter et al. 1995). Westergaard simplified the solution by stating that the reactive pressure between the slab and

the subgrade at any given point is directly proportional to the deflection at that point and is independent of the deflections at other points (Huang 2004; Ioannides 1984; Darter et al. 1995; Khazanovich 1994). Huang, (2004), notes that this type of foundation is also called a Winkler foundation or a Winkler spring.

Westergaard is given credit for the studies of stresses and deflections of pavements using the dense liquid foundation. Westergaard developed equations for temperature curling, and three loading cases for large slabs; corner loading, edge loading, and interior loading (Huang 2004). Westergaard also assumed full contact between the slab and subgrade (Huang 2004).

An advantage of the dense liquid model is that it allows consideration of load transfer at Portland cement concrete (PCC) slab joints (Khazanovich 1994). This is especially useful because it allows development of a couple major distress types including: faulting, pumping, and corner breaking (Khazanovich 1994).

Khazanovich (1994) notes a disadvantage of the dense liquid model is that it assumes no shear interaction between adjacent spring elements resulting in a foundation parameter, k, which is sensitive to the radius of the plate used in determining it (Darter et al. 1995). The foundation parameter, k, is determined by dividing the change stress by the change in deflection (Bowles 1996). Bowles (1996) noted that the plate load test required to obtain k is an expensive time consuming test requiring large loads to produce small deflections.

Huang (2004) notes several k value approximations for soils as follows: Low support k values range from 75-120 pci, Medium support k values range from 130-170 pci, High support k values range from 180-220 pci, and Very high support k values range from 250-400 pci. Soils characteristic of low support are fine grained soils with high silt and clay

contents (Huang 2004). Huang, (2004), notes that soils providing medium support are sand and gravel mixtures with moderate clay or silt contents, and soils exhibiting high support are sand and gravel mixtures free of plastic fines. Cement treated subbases exhibit very high support (Huang 2004).

Elastic Solid Model

The elastic solid model is considered as a linearly elastic, isotropic, homogeneous solid of semi-infinite extent (Ioannides 1984). Darter et al. (1995) stated that under the elastic solid model, the load applied to the surface of the foundation is assumed to produce a continuous and infinite deflection basin.

Ioannides (1984) and Khazanovich (1994) note that one benefit of the elastic solid foundation is that it is a more realistic representation of actual subgrade behavior because it takes into account the effect of shear interaction between adjacent support elements. This leads to deflections influenced by stresses adjacent to the point at which the deflection is being measured.

Disadvantages of the elastic solid foundation model are: mathematical complexity and inability to model the discontinuity of a deflection profile that occurs are joints (Ioannides 1984; Khazanovich 1994). Ioannides, (1984), notes that elastic problems are governed by integral or differential equations.

Pavement Distress

PCC pavement distresses come from two sources: design and construction deficiency (Huang 2004). Distresses are further broken down into functional, structural, load associated, and non-load associated distresses. Types of distress in PCC pavements include:

blowups, corner breaks, durability cracking, joint faulting, joint deterioration, longitudinal cracks, popouts, pumping and water bleeding, spalling, transverse cracks, edge punchout, and localized distress (Huang 2004; Strategic Highway Research Program (SHRP) 1990).

Several of these distresses are beyond the designers control such as blowups, durability cracking, and popouts because they are mainly non-load associated distresses (Huang 2004; SHRP 1990). These distresses are effectively controlled to proper inspection and construction practices. The rest of this section will focus on load associated distresses, specifically faulting and joint deterioration.

SHRP (1990) and Huang (2004) describe faulting as a difference in elevation across a transverse or longitudinal joint. Faulting is caused by either a buildup of loose material under the trailing slab or depression of the leading slab (Huang 2004). The buildup or erosion of materials is caused by pumping and water bleeding. Pumping is the ejection of water and solids from a crack under heavy loads (SHRP 1990; Bhatti et al. 1996). This action is detrimental to the pavement performance due to it causing subgrade non-uniformity. Bhatti et al. (1996) noted that in order to prevent pumping and the associated loss of support, a drainable base needed to be installed.

Pavement stresses are usually at the maximum in the center edge of a fully supported slab (Huang 2004). When pumping causes erosion and loss of support at a joint, the maximum stress now occurs at the joint in a corner loading case (Huang 2004). Loss of support can significantly increase pavement stresses; therefore increasing pavement distresses and ultimately leading to premature failure of the pavement section.

Past Research

This section details past research projects investigating spatial variation or subgrade uniformity.

Ohio SHRP Test Road, U.S. Rt. 23, Delaware, Ohio

This project constructed in August of 1996 for the study of four objectives: (1) study of structural factors for flexible pavements, (2) study of structural factors for rigid pavements, (3) study of environmental effects in the absence of heavy traffic, and (4) asphalt program field verification studies. For the purpose of this paper, objectives one through three will be discussed.

For this study, the project length was 3 miles and the northbound were constructed of PCC, and the southbound lanes were constructed of asphalt concrete (AC). The ramps to the southbound section were constructed of PCC and AC to investigate environmental effects. Site topography was flat and fine grained soils, A-4, A-6, and A-7-6, were discovered with a depth to groundwater about 4.3 feet below the surface. Several base types and combinations were used for this project including: dense-graded aggregate base, asphalt-treated base, permeable asphalt-treated base, permeable cement-treated base, and a lean concrete base.

Subgrade soils were compacted by sheepsfoot roller to 100% maximum dry density compacted 12 inches below pavement subgrade surface. Field tests included: nuclear density gauge, and FWD on the subgrade, base and pavement after the completion of each layer. The FWD data was used to back-calculate elastic modulus values.

Conclusions from this study show great variability in subgrade stiffness calculated form the FWD data even though all subgrade soil layers satisfied compaction requirements.

Excessive rutting was observed in one asphalt section and it was determined that insufficient subgrade stiffness led to premature pavement distress. This reinforced the conclusion that relative compaction alone is not enough to assure pavement performance, and the subgrade soils stiffness must be measured and controlled (Sargand et al. 2000).

Spatial Variation of Soil Stiffness

Soil parameters vary from point to point, even normally homogeneous layers. Grabe (1993) noted that there is a need to describe the spatial variation in order to predict geotechnical performance and deal with risk and reliability. It was shown that differential stiffness values lead to differential settlements. These differential settlements then cause dynamic forces inducing further settlement.

Conclusions from this study are: measurements show that there is no pattern of measured soil stiffness, natural variation of the subgrade is transmitted to the pavement due to repeated loadings of passing vehicles, and soil transmits its variance gradually to the surface of the pavement (Grabe 1993).

Support under PCC Pavements

This study was undertaken to further understand loss of support under PCC pavements, and design subgrade k-value. It was noted that stresses and deflections that affect the performance of a PCC slab depend on several support factors. These factors include:

- Subgrade soil stiffness;
- Base type, stiffness and thickness;
- Frictional resistance between the slab and base;

- Freeze-thaw action in the base and subgrade;
- Seasonal moisture levels in the subgrade and untreated base;
- Load transfer at joints;
- Erosion of base or subgrade material from traffic loading, poor drainage, or pavement movement; and
- Temperature and moisture gradient within the slab.

Research notes that design k-values should be top of embankment because top of base k-values are unreasonably high and not recommended for design. It also recommends that the design k-value be a seasonally adjusted k-value and account for some loss of support due to erosion.

Results of the study conclude that an increased k-value will always reduce tensile stress in the slab due to loading if there is no temperature gradient, and k-values increase for shorter spacing; therefore, increasing the number of applications to terminal serviceability (Darter et al. 1995).

METHODS

The methods section overviews the testing and statistical methods used throughout this study. Methods include: (1) Generate field data, (2) Generate finite element models to measure pavement performance, and (3) Conduct statistical analysis.

Objective One: Generate Field Data

Field data was generated to provide technical data for generation of subgrade finite element models to measure pavement performance. Field data was generated using a grid system and conducting several in-situ tests at each grid point.

Task 1: Research and Select Projects

Research and selection of projects began in late July 2002. Research of existing pavement removal projects was conducted using Iowa Department of Transportation (IDOT) personnel input.

For this study, twelve different project locations were considered and tested. Soils tested included representative Iowa soils as well as different construction materials such as hydrated fly ash (HFA) and granular subbases including special backfill and modified subbase.

Project 1

Project 1 was located along Highway 63 in Eddyville, Iowa. This project utilized HFA from the nearby Ottumwa Generating Station as a construction material. The HFA was chosen to replace select subgrade soils on the project due to limited availability of select soils. The project length, about one mile, was constructed and tested in August 2002. Figure 207 shows the location of Project 1. Note the circle area indicates project area and the arrow directs which way is north.

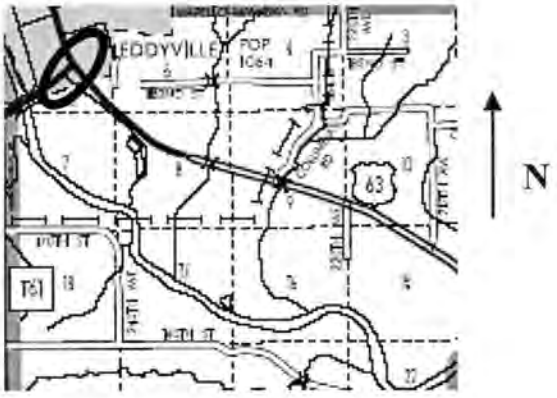

Figure 207. Project 1 Location

Project 2

Project 2 was located along state Highway 330 northeast of Bondurant about five miles. This project investigated an abandoned section of Highway 330 after pavement removal. Pavement removal showed a slab on subgrade soil. Subgrade soils were tested and documented upon pavement removal in September 2002. Figure 208 shows the location of Project 2.

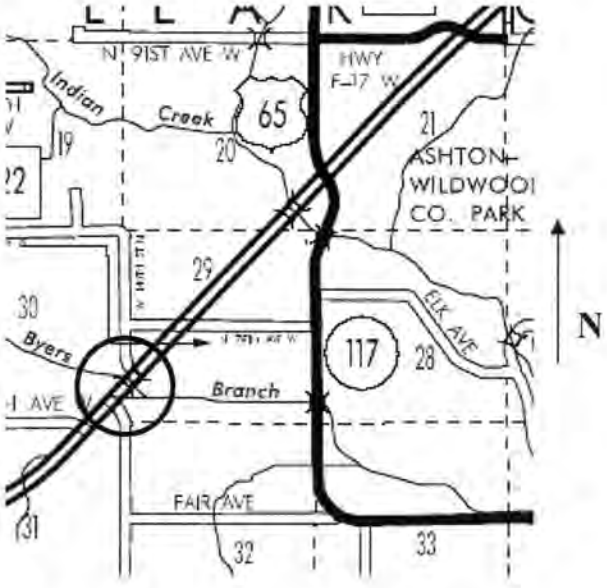

Figure 208. Project 2 Location

Project 3

Project 3 was located in Ames, Iowa on a deteriorated section of Knapp Street. The project reconstruction was about a half mile in length. Subgrade soils were documented, tested, and modeled. Knapp Street is located 2 blocks south of Lincoln Way just west of the Iowa State University Campus. Project 3 was tested in May 2003. Figure 209 shows the project location of Knapp Street.

Project 4

Project 4 was also Knapp Street located in Ames, Iowa. Documentation and testing of the granular subbase was completed in June 2003. Figure 209 shows the project location.

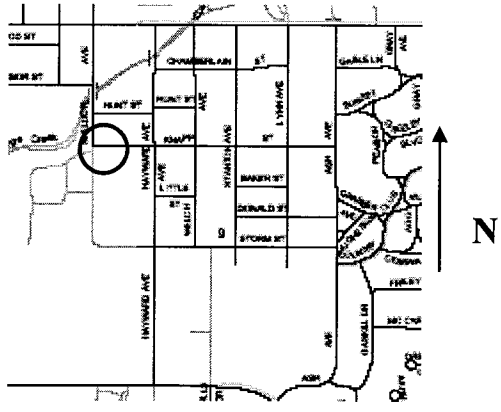

Figure 209. Project Location for Projects 3 and 4

Project 5

Project 5 was located in West Des Moines, Iowa along the Interstate 235 corridor at 35th Street. For this project, the subgrade underneath the existing westbound I-235 entrance ramp was tested upon pavement removal. Testing for Project 5 was completed in May 2003.

Project 6

Project 6 was also located in West Des Moines on the newly constructed westbound I-235 entrance ramp at 35th Street. Material tested was modified subbase, and testing was completed in June 2003. Figure 210 denotes the project location of Projects 5 and 6.

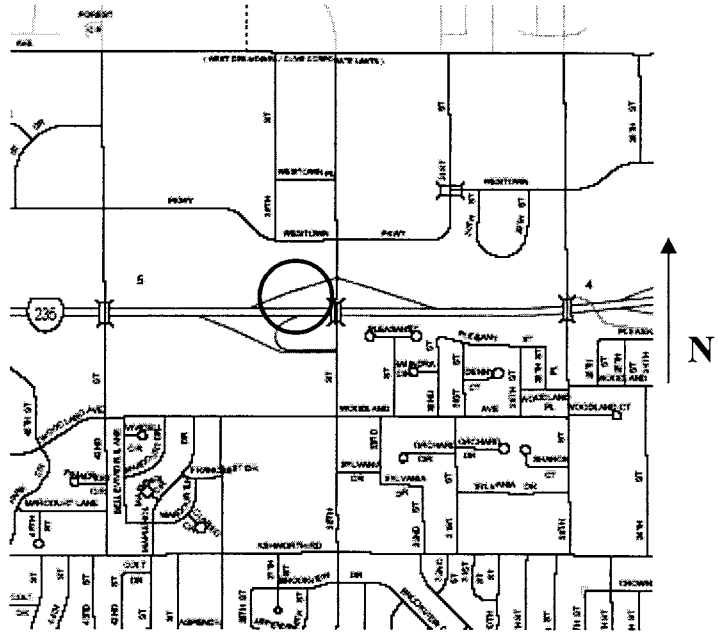

Figure 210. Project Location for Projects 5 and 6

Project 7

Project 7 was located on state Highway 34 about five miles east of Fairfield, Iowa. Testing for this project was completed on subgrade embankment soils constructed during the 2002 construction season. Testing for Project 7 was completed in July 2003. Figure 211 shows the location for Project 7.

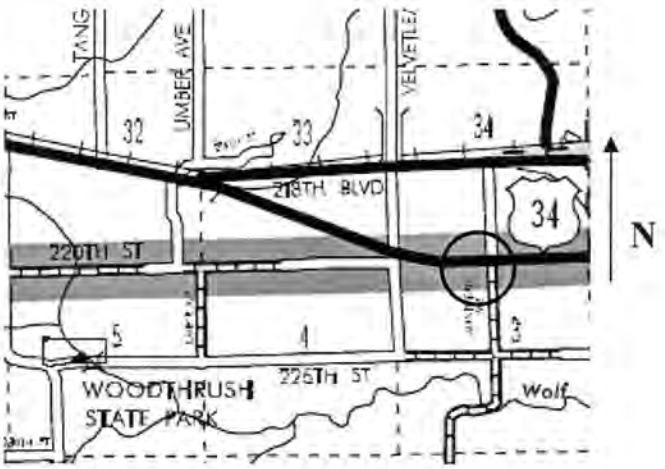

Figure 211. Project 7 Location

Project 8

Project 8 was located on U.S. Highway 218 in Henry County about 3 miles north of the Henry County and Lee County line. Testing was completed in July 2003 on a newly constructed embankment built earlier in the construction season of 2003. Figure 212 shows the location for Project 8.

Project 9

Project 9 included testing subgrade soils on northbound Interstate 35 about two miles north of U.S. Highway 20. Testing was conducted after existing pavement removal in June of 2003. Figure 213 shows the project location.

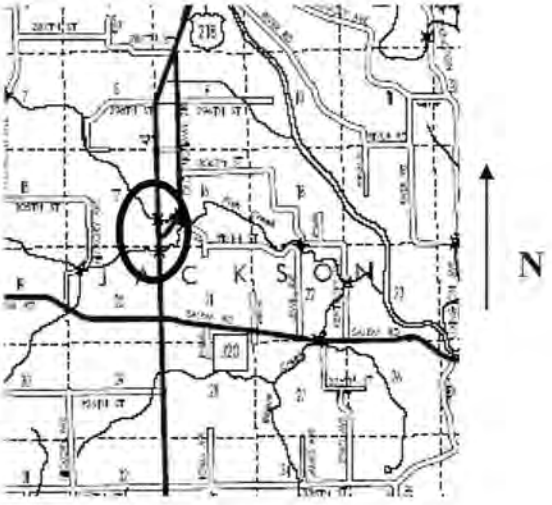

Figure 212. Location of Project 8

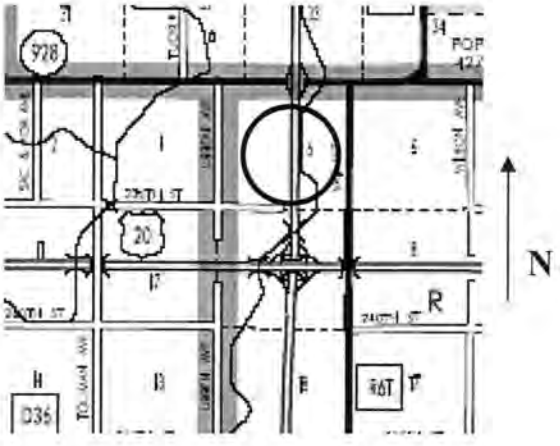

Figure 213. Location of Project 9

Project 10

Project 10 stemmed from current research in Ames, Iowa located at Jack Trice Stadium about 1 mile north of U.S. Highway 30 on Elwood Drive. Testing took place in September 2002 on a mixture of RAP and subgrade soil. For further information on this material or project, please refer to Chapter One.

Project 11

Project 11 continued testing at Jack Trice Stadium after self-cementing fly ash stabilization was completed. Testing was completed in September 2002 before the asphalt surface layer was placed. Figure 214 shows the project location for Projects 10 and 11.

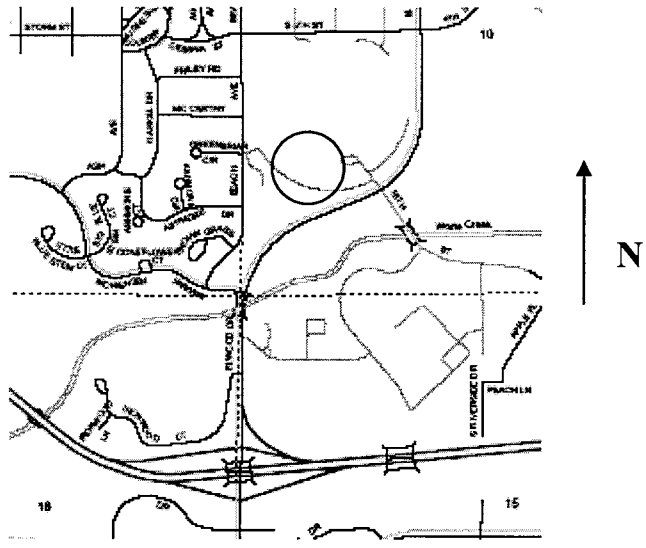

Figure 214. Project Location for Projects 10 and 11

Project 12

Project 12 is located at the intersection of University and Guthrie Avenue in Des Moines, Iowa along the I-235 reconstruction corridor. Testing was completed on special backfill in August 2003. The project location is shown in Figure 215.

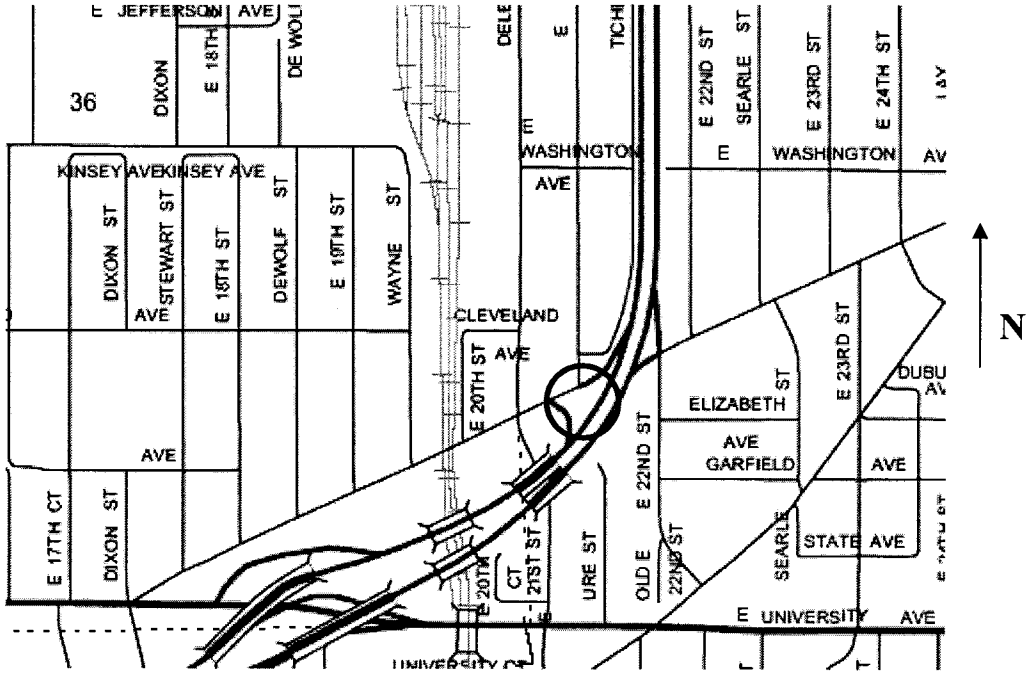

Figure 215. Project Location for Project 12

Task 2: Grid Pavement and Document Pavement Quality

A grid was set out on the pavement surface prior to pavement removal to provide test locations and to document pavement distress locations. Table 21 shows a summary of all grid spacing for field tests. Note that the X direction is perpendicular to the driving lane and the Y direction is parallel to the driving lane.

Table 21. Grid Spacing for Each Project

Project Number	Project Name	Number of Tests	Grid Spacing (ft) X	Y
1	Eddyville Bypass	33	10	8
2	Highway 330	33	10	8
3	Knapp Street Subgrade	51	6	6
4	Knapp Street Subbase	24	6	6
5	35th Street Subgrade	130	4	4
6	35th Street Subbase	24	10	10
7	Highway 34	85	6	6
8	Highway 218	85	6	6
9	Interstate 35	85	6	6
10	Jack Trice Lot S1 Before Ash	18	10	8
11	Jack Trice Lot S1 After Ash	18	10	8
12	University-Guthrie Avenue	30	6	6

Task 3: Perform DCP Tests

The DCP test was conducted in order to determine the average stiffness of the soil site in terms of penetration resistance in mm/blow. DCP tests were conducted to a depth of about 450 mm. Figure 216 shows a DCP test being conducted.

Figure 216. DCP Testing on Westbound Entrance Ramp of I-235 at 35th Street in West Des Moines

Task 4: Perform Clegg Impact Hammer Test

The Clegg Impact Hammer was used in order to obtain another stiffness value for the soil being tested. The Clegg Hammer test was chosen because it is a fast easy test to conduct. The Clegg Impact Hammer is shown in Figure 217.

Task 5: Perform GeoGauge Test

The Humboldt GeoGauge test was used to determine the modulus and stiffness of the soil at each location. The GeoGauge is shown in Figure 218.

Figure 217. Clegg Impact Hammer

Figure 218. GeoGauge

Task 6: Perform Nuclear Density Gauge Test

Nuclear density gauge readings were taken at each test point to establish an average dry density and moisture content of the subgrade or subbase. Tests were conducted to a depth of 300 mm. Figure 219 shows the nuclear density gauge used for testing.

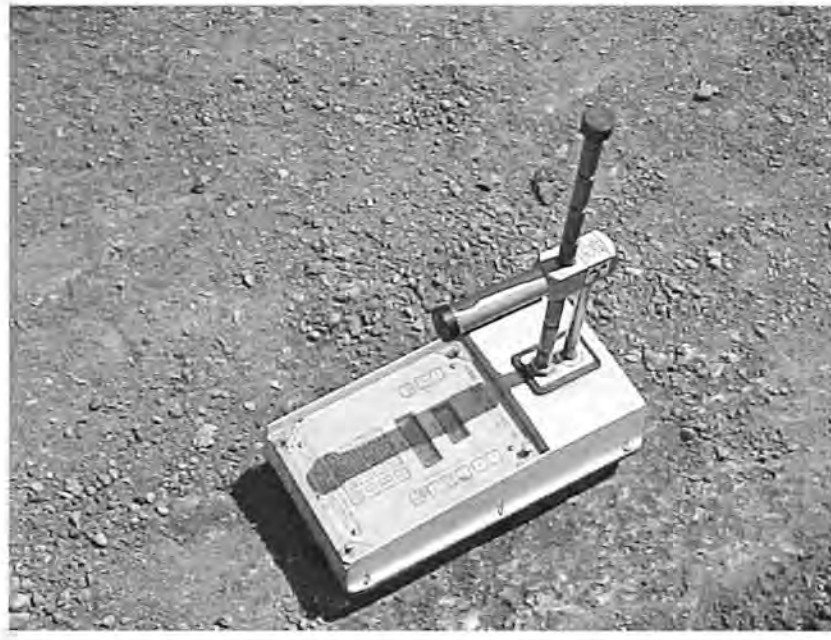

Figure 219. Nuclear Density Gauge

Task 7: Analyze Subgrade Material

To analyze the subgrade material, several test methods were employed.

- ASTM D 422-63 [Standard Test Method for Particle-Size Analysis of Soils]
- ASTM D 2487-90 [Standard Test Method for Classification of Soil for Engineering Purposes]
- ASTM D 4318-84 [Standard Test for Liquid Limit, Plastic Limit, and Plasticity Index of Soils]

Upon completion of subgrade testing, the material test was sampled using two, five gallon plastic containers with lids. The samples were transported back to the laboratory where the soil clods were reduced. The material was then prepared for particle size analysis according to ASTM D 422. After particle size analysis was completed, the index properties were determined using ASTM D 4318. Finally the soil was classified using ASTM D 2487.

Objective Two: Generate Finite Element Models to Measure Pavement Performance

Background

Pavement modeling was completed using ISLAB 2000, a finite element analysis tool designed specifically for rigid pavements. ISLAB 2000 is a powerful analysis tool that allows up to four layers plus the subgrade in an analysis. Outputs for the ISLAB 2000 software are deflection and maximum stress in units of inches and psi respectively.

For the purpose of this study, one layer was modeled. The pavement layer's responses were modeled using estimated subgrade modulus of reaction values and a Winkler Spring foundation. Figure 220 depicts the Winkler foundation.

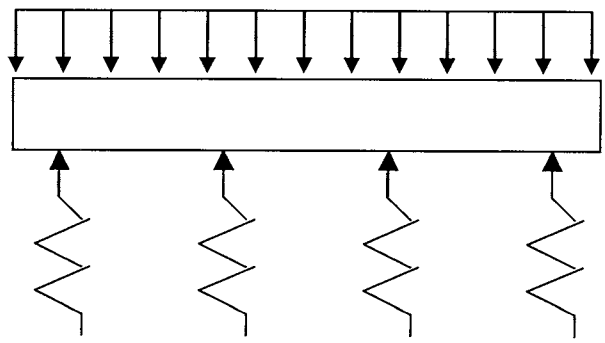

Figure 220. Winkler Spring Foundation

Task 1: Estimate Modulus of Subgrade Reaction

The modulus of subgrade reaction was estimated from GeoGauge modulus values. The modulus values were first converted to English units and then the reduced Vesic equation, Equation 1, was applied to estimate the modulus of subgrade reaction (Bowles 1996).

$$K_s = \frac{E_s}{B(1-\mu^2)}$$

Equation 1. Reduced Vesic Equation

Where the plate diameter, B, is assumed equal to 30 inches; Poisson's Ratio, μ, assumed to be .35; and modulus values, E_s, are obtained from the GeoGauge measurements.

Upon estimating the modulus of subgrade reaction, the estimations were checked through various charts and graphs in order to assure a reasonable approximation.

Task 2: Determine Remaining Input Variables

Table 22 shows the variables included in pavement modeling and their dimensions. Note that the only variables that did not remain constant throughout pavement modeling were the number of wheels, tire pressure, load, wheel spacing, and contact area.

Values estimated for load and vehicle purposes were derived from the American Association of State Highway Officials (AASHO) Road Test vehicles. With ever increasing axle configurations and weights, deviation from the AASHO road test need to be considered.

For the purpose of this study, derivation from the AASHO axle configurations was completed using a standard 18-wheeler tandem axle and a large farm grain cart configuration.

Vehicle values for these two configurations can be found in Table 23. These configurations were modeled using data from Project 2 due to statistical analysis showing that Project 2 had the most variability.

Table 22. Input Variables for ISLAB 2000

Variable	Unit	Value
PCC Pavement Thickness	in	10.5
Load Transfer Efficiency	Percent	90
Poisson's Ratio (PCC)		0.15
PCC Modulus	psi	4,000,000
PCC Unit Weight	lb/in^3	0.087
Number of Wheels		2
Tire Pressure	psi	80
Tire Contact Area	in^2	112.6
Wheel Spacing	in	96
Axle Load	pounds	18,000

Table 23. Alternate Axle Design Values

Model	Variable	Unit	Value
Grain Cart	Number of Wheels		2
	Tire Pressure	psi	20
	Tire Contact Area	in^2	700.1
	Wheel Spacing	in	165
	Axle Load	pounds	28,000
18-Wheeler	Number of Wheels		4
	Tire Pressure	psi	110
	Tire Contact Area	in^2	38.7
	Wheel Spacing	in	102
	Tire to Tire Spacing	in	3
	Axle Load	pounds	34,000

Task 4: Determine Load Placement

Load placement for PCC slabs creates a wide range of pavement responses depending upon location, subgrade characteristics and pavement type. For the purpose of this study, the load was placed at the corner and center of each slab 18 inches from the pavement edge.

Task 5: Determine Pavement Responses

ISLAB 2000 pavement responses were calculated and recorded for statistical analysis. For this study, the maximum principle stress and maximum deflection for the bottom of the slab was investigated.

Task 6: Repeat Tasks 2 to 4 for Each Project Using the Average Modulus of Subgrade Reaction

Upon initial analysis of each project, ISLAB 2000 was used to determine the pavement responses associated with a perfectly uniform subgrade. Modeling a uniform subgrade was completed in order to analyze the difference in results obtained modeling a non-uniform subgrade compared to those modeling a uniform subgrade.

The average modulus of subgrade reaction value for each project was used in the modeling process and the ensuing pavement responses were determined and recorded for statistical analysis.

Task 7: Determine Pavement Life

Pavement life was determined by applying the ERES/COE equation to the ISLAB 2000 results. The ERES/COE equation, Equation 2, was developed from Army Corp of Engineers data by Darter in 1988.

$$\log N = 2.13\ SR^{-1.2}$$

Equation 2. ERES/COE Fatigue Model

Where N is the number of repetitions to failure and SR is the stress ratio equal to the total tensile stress in the slab divided by the concrete modulus of rupture. Generally if the SR is kept below ½ the number of repetitions to failure become infinite.

The number of repetitions to failure was then divided by an estimated number of repetitions per year resulting in a pavement lifespan.

Objective Three: Perform Statistical Analysis on Field Data and ISLAB 2000 Results

Statistical analysis was completed on the field data and ISLAB 2000 results to determine if there was a meaningful relationship between subgrade variability and pavement performance.

Task 1: Determine Average and Standard Deviation for Field Data

The average, standard deviation, and coefficient of variation were determined for each field test completed. The results were tabulated, then compared and contrasted.

Task 2: Perform SAS Analysis of ISLAB 2000 Results

Statistical analysis of the ISLAB 2000 results was completed using SAS statistical analysis software. The results of the SAS analysis are mean, median, mode, standard deviation, coefficient of variation, and a test to determine if the data is normally distributed.

Task 3: Perform a Beta Test of ISLAB 2000 Results

Statistical analysis was conducted upon the data to determine if the data fit a beta distribution. The statistical analysis software used to perform this test was JMP 5.0.

Task 4: Determine Reliability

The reliability of the ISLAB 2000 results was determined using the process outlined by Duncan (2000). First the most likely value for the factor of safety was determined using the maximum principle stress divided by the average for each project. The coefficient of variation of the standard deviations was determined, and then the probability of failure was determined.

MATERIALS

This section presents an analysis of the subgrade materials used during this study. Field testing consisted of nuclear density gauge, GeoGauge, DCP, Clegg Impact Hammer, and grain size distribution analysis of the soil.

Nuclear Density Gauge

The resulting average dry density and moisture content for each project are displayed in Table 24. Also shown are the corresponding standard deviations and coefficient of variations. Note the low standard deviations for Projects 1 and 11 proving that fly ash treatment reduces subgrade variability in terms of density and moisture content.

GeoGauge

Table 25 shows the average modulus and stiffness values for each project obtained from GeoGauge™ testing. The GeoGauge results show general remarkable increased stiffness for Projects 1 and 11, as well as the subbase tested for Project 12.

Dynamic Cone Penetrometer

The average mean DCP index values for each project are shown in Table 26. All tests were conducted to a depth of about 450 mm. The DCP data exhibits the expected trend of a decreased DCP index for the stiffer materials found on Projects 1, 11, and 12. Note the decrease in DCP index between Projects 3 and 4. This shows that the addition of granular subbase increases the stiffness and will add support to the overlying PCC pavement.

Table 24. Nuclear Density Gauge Data for Each Project

		Nuclear Density Gauge						
Project Number	Project Name	Number of Tests	Average Moisture Content %	Standard Deviation	Coefficient of Variation	Average Dry Density kg/m^3	Standard Deviation	Coefficient of Variation
1	Eddyville Bypass	33	9.5	0.67	7.0	1704	26.99	1.6
2	Highway 330	33	11.5	1.21	10.5	1919	29.16	1.5
3	Knapp Street Subgrade	51	15.3	3.35	21.8	1725	163.16	9.5
4	Knapp Street Subbase	24	10.4	0.86	8.3	1669	68.31	4.1
5	35th Street Subgrade	130	12.9	1.75	13.6	1868	46.89	2.5
6	35th Street Subbase	24	8.5	1.35	15.8	1815	120.37	6.6
7	Highway 34	85	7.1	0.96	13.4	2028	54.72	2.7
8	Highway 218	85	7.6	1.07	14.1	1990	56.34	2.8
9	Interstate 35	85	8.7	1.77	20.4	2012	83.14	4.1
10	Jack Trice Lot S1 Before Ash	18	8.1	1.06	13.0	1960	56.18	2.9
11	Jack Trice Lot S1 After Ash	18	8.8	0.89	10.1	1804	49.50	2.7
12	University-Guthrie Avenue	30	6.7	3.14	46.9	1640	81.23	5.0

Table 25. GeoGauge Data for Each Project

			GeoGauge					
Project Number	Project Name	Number of Tests	Average Stiffness MN/m	Standard Deviation	Coefficient of Variation	Average Modulus MPa	Standard Deviation	Coefficient of Variation
1	Eddyville Bypass	33	14.82	2.93	19.7	128.53	25.44	19.8
2	Highway 330	33	2.36	1.23	52.0	20.49	10.67	52.1
3	Knapp Street Subgrade	51	1.60	1.14	71.4	13.87	9.87	71.2
4	Knapp Street Subbase	24	9.54	1.55	16.2	82.77	13.44	16.2
5	35th Street Subgrade	130	4.72	0.95	20.1	40.91	8.08	19.8
6	35th Street Subbase	24	5.88	1.78	30.3	50.98	15.43	30.3
7	Highway 34	85	5.81	1.21	20.8	50.39	10.47	20.8
8	Highway 218	85	7.22	2.07	28.7	63.00	17.82	28.3
9	Interstate 35	85	4.68	1.11	23.8	40.95	9.35	22.8
10	Jack Trice Lot S1 Before Ash	18	9.65	1.58	16.4	83.73	13.73	16.4
11	Jack Trice Lot S1 After Ash	18	16.30	3.50	21.5	140.41	29.52	21.0
12	University-Guthrie Avenue	30	15.72	3.40	21.7	136.36	29.53	21.7

Table 26. DCP Data for Each Project

			DCP		
Project Number	Project Name	Number of Tests	Average Mean DCP Index, mm/blow	Standard Deviation	Coefficient of Variation
1	Eddyville Bypass	33	10.79	1.82	16.9
2	Highway 330	33	26.93	5.03	18.7
3	Knapp Street Subgrade	51	56.55	17.35	30.7
4	Knapp Street Subbase	24	20.77	4.15	20.0
5	35th Street Subgrade	130	34.22	7.17	20.9
6	35th Street Subbase	24	20.07	9.43	47.0
7	Highway 34	85	25.23	6.35	25.2
8	Highway 218	5	18.86	8.29	43.9
9	Interstate 35	85	37.29	9.99	26.8
10	Jack Trice Lot S1 Before Ash	18	20.81	2.98	14.3
11	Jack Trice Lot S1 After Ash	18	15.93	1.25	7.8
12	University-Guthrie Avenue	30	13.64	6.10	44.7

Clegg Impact Hammer

The average Clegg Impact Value (CIV) for each project can be found in Table 27. The Clegg Impact Hammer data show the same trends as the DCP and GeoGauge data. This is to be expected as the CIV is also a measure of the soil stiffness

Table 27. Clegg Impact Value Data for Each Project

		Clegg Impact Hammer			
Project Number	Project Name	Number of Tests	Average CIV	Standard Deviation	Coefficient of Variation
1	Eddyville Bypass	33	27.4	4.68	17.1
2	Highway 330	33	6.4	1.62	25.3
3	Knapp Street Subgrade	51	5.5	3.36	60.9
4	Knapp Street Subbase	24	23.5	3.12	13.3
5	35th Street Subgrade	130	6.2	2.01	32.4
6	35th Street Subbase	24	20.7	5.68	27.5
7	Highway 34	85	10.4	1.67	16.1
8	Highway 218	85	27.2	7.03	25.8
9	Interstate 35	85	9.3	3.82	41.2
10	Jack Trice Lot S1 Before Ash	18	21.6	4.04	18.7
11	Jack Trice Lot S1 After Ash	18	25.2	4.48	17.8
12	University-Guthrie Avenue	30	29.3	11.70	40.0

Grain Size Analysis

A grain size analysis was conducted on each of the project soils in order to classify it according to the Unified Soil Classification System (USCS). The soil classification symbol and group name for each project can be found in Table 28.

Table 28. Unified Soil Classification System Soil Classifications for Each Project

		Unified Soil Classification System	
Project Number	Project Name	Symbol	Group Name
1	Eddyville Bypass	GP-GM	Poorly Graded Gravel with Silt and Sand
2	Highway 330	SM	Silty Sand
3	Knapp Street Subgrade	SC	Clayey Sand
4	Knapp Street Subbase	GW-GM	Well Graded Gravel with Silt and Sand
5	35th Street Subgrade	CL	Lean Clay with Sand
6	35th Street Subbase	GP-GM	Poorly Graded Gravel with Silt and Sand
7	Highway 34	SM	Silty Sand
8	Highway 218	CL	Sandy Lean Clay
9	Interstate 35	CL-ML	Sandy Silty Clay
10	Jack Trice Lot S1 Before Ash	SC	Clayey Sand
11	Jack Trice Lot S1 After Ash	SM	Silty Sand with Gravel
12	University-Guthrie Avenue	GP-GM	Poorly Graded Gravel with Silt and Sand

RESULTS

This results section is divided into two components: (1) Pavement modeling and (2) Statistical analysis. Each section details specific outcomes pertaining to that section.

Pavement Modeling

This section details results obtained from the pavement modeling process outlined in the Methods section. ISLAB 2000 results show decreased pavement stress and deflection with increased subgrade stiffness due to the addition of self-cementing fly ash, HFA, or granular subbase. ISLAB 2000 modeling of uniform subgrade results in a slight decrease in average pavement stress, deflection, and standard deviation for most projects.

ISLAB 2000 Results

This section discusses results pertaining to the ISLAB 2000 pavement modeling. The ISLAB 2000 finite element modeling results show a few notable trends including: an overall general decrease in maximum principal stress and pavement deflection as the modulus of subgrade reaction increases. Past research shows this is to be expected.

Comparisons between the non-uniform and uniform modeling results show a reduction in average maximum principal stress. These results show that the uniform pavement will ultimately perform better since the pavement life is determined by the stress ratio. The stress ratio is lowered when the resulting pavement tensile stress is reduced compared to the modulus of rupture. This then increases the number of repetitions to failure for the section leading to a longer service life.

Once each project had been modeled, the results were extracted and compared. Figures 221 and 222 are sample outputs for the ISLAB 2000 program. Note that Figure 221 shows the magnitude and distribution of the maximum principal stress at the bottom of the pavement layer, and Figure 222 shows the maximum deflection of the bottom the pavement layer. Both figures were obtained from analysis conducted on Project 12.

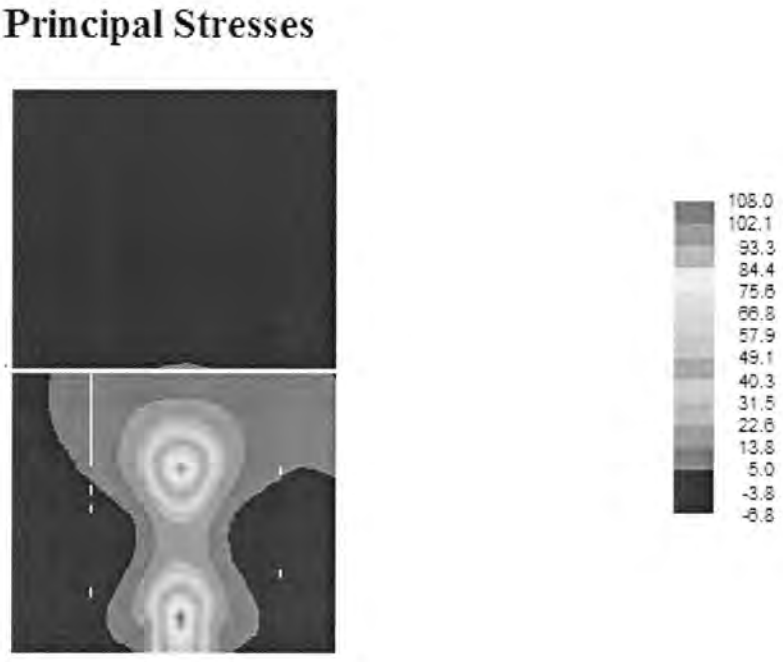

Figure 221. Non-Uniform Subgrade Maximum Principal Stress Distribution for Project 12

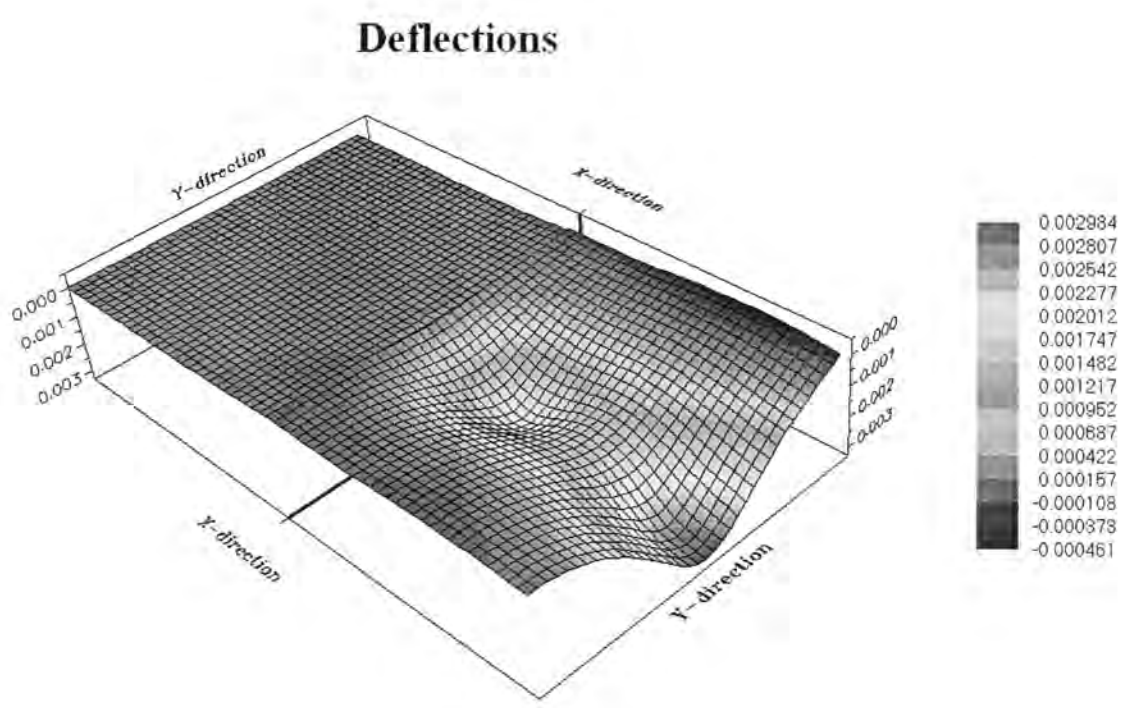

Figure 222. Non-Uniform Subgrade Maximum Deflections for Project 12

Table 29 summarizes the project name and number, number of ISLAB 2000 results, average maximum principal stress, average maximum deflections, and their respective standard deviations for the non-uniform analyses. Table 30 summarizes the project name and number, number of ISLAB 2000 results, average maximum principle stress, average maximum deflections, and their respective standard deviations for the uniform analysis. For further information on the individual stresses and deflections for a particular project, please see the Appendix for the individual output files.

Table 29. Average Maximum Principal Stresses and Deflections for All Projects Using Non-Uniform Subgrade

			Non-Uniform					
Project Number	Project Name	Number of ISLAB 2000 Test Points	Average Maximum Principal Stress kPa	Standard Deviation	Coefficient of Variation	Average Maximum Deflection mm	Standard Deviation	Coefficient of Variation
1	Eddyville Bypass	40	722.33	45.96	6.36	0.111	0.064	57.10
2	Highway 330	40	855.55	156.19	18.26	0.549	0.320	58.28
3	Knapp Street Subgrade	16	820.93	128.52	15.66	0.396	0.171	43.11
4	Knapp Street Subbase	8	739.09	46.19	6.25	0.124	0.050	40.03
5	35th Street Subgrade	18	849.37	34.98	4.12	0.265	0.103	38.79
6	35th Street Subbase	12	848.56	71.33	8.41	0.163	0.068	42.00
7	Highway 34	32	725.90	129.44	17.83	0.252	0.107	42.64
8	Highway 218	32	715.60	125.31	17.51	0.225	0.098	43.77
9	Interstate 35	32	728.50	144.15	19.79	0.296	0.123	41.52
10	Jack Trice Lot S1 Before Ash	18	763.93	63.65	8.33	0.158	0.076	47.75
11	Jack Trice Lot S1 After Ash	8	729.64	41.83	5.73	0.103	0.045	44.16
12	University-Guthrie Avenue	6	777.32	32.20	4.14	0.148	0.068	45.58
13	Highway 330 with Grain Cart	40	1222.01	218.48	17.88	0.861	0.440	51.09
14	Highway 330 with 18-Wheeler	38	913.28	168.24	18.42	0.768	0.461	60.00

Table 30. Average Maximum Principal Stresss and Deflections for All Projects Using Uniform Subgrade

		Uniform						
Project Number	Project Name	Number of ISLAB 2000 Test Points	Average Maximum Principal Stress kPa	Standard Deviation	Coefficient of Variation	Average Maximum Deflection mm	Standard Deviation	Coefficient of Variation
1	Eddyville Bypass	40	712.19	55.78	7.83	0.110	0.040	36.44
2	Highway 330	40	847.88	141.84	16.73	0.464	0.180	38.83
3	Knapp Street Subgrade	16	818.66	107.14	13.09	0.361	0.156	43.12
4	Knapp Street Subbase	8	726.77	54.14	7.45	0.120	0.050	42.07
5	35th Street Subgrade	18	828.76	29.26	3.53	0.255	0.094	37.05
6	35th Street Subbase	12	832.68	72.98	8.76	0.156	0.066	42.13
7	Highway 34	32	705.51	130.93	18.56	0.231	0.094	40.51
8	Highway 218	32	693.16	117.02	16.88	0.195	0.078	40.27
9	Interstate 35	32	717.68	145.26	20.24	0.270	0.110	40.76
10	Jack Trice Lot S1 Before Ash	18	749.62	72.97	9.73	0.155	0.060	38.73
11	Jack Trice Lot S1 After Ash	8	712.86	54.66	7.67	0.103	0.039	38.06
12	University-Guthrie Avenue	6	779.24	12.34	1.58	0.130	0.045	34.44
13	Highway 330 with Grain Cart	40	1206.96	194.56	16.12	0.765	0.248	32.36
14	Highway 330 with 18-Wheeler	38	878.48	91.85	10.46	0.623	0.211	33.80

Pavement Life Results

Table 31 shows the number of repetitions to failure for each project for both the non-uniform and uniform subgrade modeling conditions. Note that simulation of a uniform

subgrade produced a larger number of repetitions to failure for each project tested. This proves that uniformity of subgrade has an influence on pavement life.

Table 31. Number of Repetitions to Failure For All Projects Using Non-Uniform and Uniform ISLAB 2000 Results

		Non-Uniform			Uniform		
Project Number	Project	Average Maximum Principal Stress (kPa)	Standard Deviation	Number of Repetitions to Failure	Average Maximum Principal Stress (kPa)	Standard Deviation	Number of Repetitions to Failure
1	Eddyville Bypass	722	46.0	3.80E+15	712	55.8	7.03E+15
2	Highway 330	856	156.2	5.20E+12	848	141.8	7.15E+12
3	Knapp Street Subgrade	821	128.5	2.30E+13	819	107.1	2.55E+13
4	Knapp Street Subbase	739	46.2	1.44E+15	727	54.1	2.92E+15
5	35th Street Subgrade	849	35.0	6.72E+12	829	29.3	1.63E+13
6	35th Street Subbase	849	71.3	6.95E+12	833	73.0	1.37E+13
7	Highway 34	726	129.4	3.08E+15	706	130.9	1.06E+16
8	Highway 218	716	125.3	5.70E+15	693	117.0	2.35E+16
9	Interstate 35	729	144.2	2.64E+15	718	145.3	5.03E+15
10	Jack Trice Lot S1 Before Ash	764	63.6	3.70E+14	750	73.0	7.98E+14
11	Jack Trice Lot S1 After Ash	730	41.8	2.47E+15	713	54.7	6.74E+15
12	University-Guthrie Avenue	777	32.2	1.85E+14	779	12.3	1.68E+14
13	*Highway 330	1222	218.5	1.95E+08	1207	194.6	2.60E+08
14	**Highway 330	913	168.2	5.73E+11	878	91.9	2.08E+12

* Modeled with a Large Grain Wagon

** Modeled with a 18-Wheeler

M_R (kPa) = 3792.25

Statistical Analysis

This section details results obtained from statistical analysis of the generated field data and ISLAB 2000 pavement modeling data. Statistical analysis generally shows that HFA, self-cementing fly ash treated subgrade, and granular subbases perform better with a smaller standard deviation and coefficient of variation.

Field Data Statistical Analysis

The field statistical analysis section is further broken down into the results for the nuclear density gauge, GeoGauge, Clegg Impact Hammer, and DCP. Each section discusses the results for each project and compares the projects.

Nuclear Density Gauge

Nuclear density gauge statistical analysis results, Table 24, show several things. First, the results show very wet subgrade soil conditions for Project 3. Wet subgrade soil conditions were also encountered at Project 2 and Project 5. These three projects all had one thing in common. The projects were all located under an existing PCC pavement placed on natural subgrade. With the absence of a drainage layer to expedite water removal, the soils became saturated.

The remaining projects show fairly uniform moisture contents ranging from about 6.5% to 10.5%. Note that increasing the number of test points does not necessarily decrease the standard deviation of the test results as one would expect. Also note that one of the highest standard deviations is occurring for Project 12 a granular subbase, which in theory is

a very uniform material. Note that the standard deviation for Projects 1 and 11 are very low. This is an indication of uniformity

GeoGauge

The GeoGauge data, Table 25, shows several results worth noting. First, there is a significant increase in stiffness from about 1.60 MN/m to about 16.30MN/m for natural subgrade soils to either fly ash treated or granular base course materials. The same trend can be found in the modulus values. This result is to be expected as the granular base material is a stronger stiffer material.

Note the high stiffness and modulus values for Projects 1, 11, and 12. This proves that addition of self-cementing fly ash, HFA, or granular subbase increases the underlying support for pavements. Also note the low stiffness values for the saturated subgrade soils on Project 3.

One observation that is noteworthy is that the number of test points influences the standard deviation. The general trend is that the standard deviation is reduced with the increase in the number of data points. This is not true for all field data.

DCP

DCP results, Table 26, show a decrease in the mean DCP index as the material gains stiffness. The range of average mean DCP indices is about 56 mm/blow for subgrade soils on Project 3 to about 10 mm/blow for the HFA material located on Project 1. These results follow logically with the stiffness data presented in the GeoGauge section.

Note that the greatest standard deviation of mean DCP index occurred on Project 3 where the soils were saturated and showed the largest average mean DCP index. Note the

low mean DCP index values for the HFA and granular subbases. One exception to these low DCP index values for subgrade occurs on Project 8 where the subgrade soil had been used as a haul road for earthwork for an extensive period of time. Note that the DCP index correlates well with the GeoGauge and Clegg Impact Hammer data.

Clegg Impact Hammer

CIV data, Table 27, shows the same trend as the GeoGauge and DCP data. As the CIV increases, the stiffness also increases and the mean DCP index reduces. The range of CIV values is from about 5.5 to about 29.3 for Project 3 to Project 12.

Notable observations include high CIV on projects testing subbase, HFA, or self-cementing fly ash treated soils. Exceptions to these observations include Projects 8 and 10. The section tested on Project 8 was used as a haul road for several months by the contractor doing the earthwork that summer, and Project 10 was tested in late summer thus producing a subgrade that is stiffer due to lack of moisture.

Note that the low standard deviations occurred on unlikely projects. One would think that Project 1 would have a lower standard deviation due to the uniformity of the HFA used. The high subgrade modulus and corresponding modulus of subgrade reaction leads to reductions in pavement stresses. The reduced pavement stresses lead to longer pavement life.

ISLAB 2000 Statistical Analysis

ISLAB 2000 SAS Analysis

The statistical analysis for the ISLAB 2000 data is shown in Tables 29 and 30. Note that only the average, standard deviation, and coefficient of variation are displayed. Further information such as an analysis of variance and test for normality can be found in the Appendix with the SAS output file.

The results of the SAS output files show that the modulus of subgrade reaction values for both the uniform and non-uniform models are not normally distributed. This is to be expected for the modulus of subgrade reaction values because there is a lower bound value of zero. SAS analysis shows that the some stress and deflection data is normally distributed.

ISLAB 2000 Beta Distribution Analysis

The Beta distribution analysis of the modulus of subgrade reaction showed that the data does not converge in a beta distribution. The Beta distribution outputs can be found in the Appendix.

Repeated attempts to determine the distribution of the data led to normalization of the modulus of subgrade reaction data. The data was divided by the largest modulus of subgrade reaction throughout all of the testing, and then an attempt was made to fit the data to a Beta distribution. Results concluded that the data does not fit a Beta distribution.

Pavement Reliability

Table 32 shows the reliability results for maximum principle stress for both the non-uniform and uniform subgrade modeling cases. Note that for all but four projects, the

reliability increased by making the subgrade uniform. Note that the probability of failure to meet the results obtained is 100 minus the reliability. This shows that the factor of safety used in design can be reduced slightly because if increased confidence in the pavement responses.

Table 32. Reliability of ISLAB 2000 Results for Non-Uniform and Uniform Subgrade Modeling Conditions

Project Number	Project Name	Reliability %	
		Non-Uniform	Uniform
1	Eddyville Bypass	95.3	93.7
2	Highway 330	98.9	99.5
3	Knapp Street Subgrade	93.3	96.8
4	Knapp Street Subbase	90.9	90.8
5	35th Street Subgrade	92.0	99.0
6	35th Street Subbase	95.6	96.7
7	Highway 34	94.9	95.6
8	Highway 218	97.9	99.0
9	Interstate 35	91.8	92.3
10	Jack Trice Lot S1 Before Ash	90.9	90.6
11	Jack Trice Lot S1 After Ash	95.5	93.9
12	University-Guthrie Avenue	83.6	99.3
13	Highway 330 with Grain Cart	99.0	99.7
14	Highway 330 with 18-Wheeler	98.3	100.0

DISCUSSION

This section discusses implications and applications detailed in the results section. This discussion section is divided up into two parts: (1) Pavement modeling and (2) Statistical analysis.

ISLAB 2000 Pavement Modeling

ISLAB 2000 pavement modeling comparisons show a decrease in maximum principle stress and pavement deflection as the modulus of subgrade reaction increases. Past research shows that this is to be expected. Decreasing the pavement stress under load increases the pavement life. This proves that the cost of self-cementing fly ash stabilization, granular subbase, or HFA base may be worth the initial cost. Decreasing the stresses in the PCC slab also allows a reduction in pavement thickness if the PCC pavement stresses were initially within the allowable design stresses.

One important point to remember when approaching the data presented here is that geomaterials such as soil and rock behave very differently when saturated for extended periods of time. This leads the author to say that very different results are possible if each project were tested during the spring thaw or in the middle of winter. Soil stiffness and the modulus of subgrade reaction are key parameters studied that are influenced greatly by seasonal changes in climate. The softening of subgrade during the spring thaw would lead to very different results for this study due to the increased pavement stresses.

Comparisons between the uniform and non-uniform subgrade show that subgrade non-uniformity has an effect upon pavement performance. The increased pavement life

shows that uniformly constructed subgrades will increase the number of repetitions to failure ultimately leading to lower cost roadways by way of reduced pavement maintenance.

Note that for this study, all loads were placed 18 inches from the edge of the pavement. The pavement stresses would increase if the load were placed at the edge of the slab. This would decrease the pavement life significantly due to the much greater pavement stresses.

Another limitation of the finite element analysis was the subgrade itself. Literature and research shows that if voids are modeled underneath the PCC pavement, the maximum stress occurs during the corner loading rather than the mid-span loading. The voids can occur due to erosion, pumping, or localized settlement underneath the pavement. This study did not study the effect of voids underneath the PCC pavement. The corner loadings with voids could lead to higher pavement stresses thereby reducing the pavement life.

The results for pavement life show an increased pavement life for uniform subgrades over the non-uniform subgrades. Both sets of data are very high numbers. These numbers are high because of the loading conditions modeled. Not every vehicle travels 18 inches in from the pavement edge. Estimates have placed up to 5% of vehicles at the edge of the pavement. This would increase the pavement stresses considerably and significantly reduce the pavement life.

Statistical Analysis

Field Data Statistical Analysis

The coefficient of variation (CV) values show that variability is significantly reduced with the addition of a granular subbase and self-cementing fly ash stabilized subgrade. The

HFA base used in Project 1 also shows low variability. The low variability exhibited by these materials will increase confidence in the pavement design.

Decreasing variability allows the pavement designer to reduce the factor of safety for the pavement design allowing for some cost saving measures to be undertaken such as reduction in granular subbase thickness, base thickness in asphalt design, or PCC pavement thickness.

The pavement designer could opt to keep a pocket factor of safety in the design by basing the pavement design upon a more variable subgrade thus increasing the pavement life and reducing the cost to taxpayers.

ISLAB 2000 Statistical Analysis

Attempts to fit the ISLAB 2000 results to a distribution failed showing that the data is not beta or normally distributed. If the data were normally distributed, the pavement design could be made more efficient by using a percentage of the distributed stress in the pavement design. This would allow for a better pavement design allowing the designer to determine what stress level is feasible for design.

Basing the design on stresses allows for a better designed pavement. The AASHTO 2002 Design Guide will have a mechanistic-empirical design philosophy based more on pavement stresses combined with traditional empirical design. Current design practices use equivalent single axle loads (ESAL's) for design. The main drawback is that determining the amount of ESAL's can be very hard. Using stress to calculate the number of repetitions to failure may allow for better design providing the years of service life were calculated using appropriate growth factors.

The variability reduction shown when pavement was modeled using a uniform subgrade shows that non-uniformity does play a role in pavement performance. A uniform subgrade shows longer pavement life through less variability in pavement stresses.

The increase in reliability through the use of a uniform subgrade will allows pavement designers to reduce the factor of safety in their design. Using this approach, cost savings will be incurred through the use of thinner pavement sections. If the factor of safety is not reduced in the design, the pavement life will increase due to the increased capacity afforded by the thicker pavement section and reduced pavement stresses attributed to the uniform subgrade.

CONCLUSIONS

This section discusses conclusions for this study and is organized into the following sections: (1) Materials, (2) Pavement modeling, and (3) Statistical analysis.

Materials

Testing of subgrades concluded that using a granular subbase, HFA base, or self-cementing fly ash treated subgrade decreases the variability of field test results. Results from the DCP, Clegg Impact Hammer, and GeoGauge proved similar suggesting a correlation between the three instruments.

Pavement Modeling

Pavement modeling proved that there is a link between subgrade non-uniformity and pavement performance. Uniform subgrade modeling conditions produced lower average

deflections and maximum principle stresses. The lower stress values then predicted longer pavement life.

Statistical Analysis

Statistical analysis results warrant two conclusions. The field results for HFA, granular subbases and self-cementing fly ash treated subgrade tend to be more uniform according to the coefficient of variation.

Statistical analysis of the ISLAB 2000 pavement modeling results show that the data obtained is not beta or normally distributed. Analysis proves that uniform modeling conditions produce average stresses that have less variability when comparing the coefficient of variation for over half of the projects. All but two projects saw a reduction in variability when comparing the coefficient of variation for average deflections.

Pavement response reliability increased with the addition of uniform subgrade proving that subgrade non-uniformity influences pavement performance.

RECOMMENDATIONS

The author recommends several things for future research. First, it is recommended that the current research be continued for more projects within Iowa to provide for a larger data set. One very beneficial project would include Western Iowa loess because that soil in nature is very uniform.

Other recommendations include: varying slab length and thickness in the finite element modeling. This would allow for variability in mid-span calculated stresses. Addition of curling effects into the analysis would create higher pavement stresses.

Modeling of voids at the joints to simulate loss of support due to pumping and erosion would study the effects of increased corner stresses.

Another recommendation is to study the effects of material saturation. Material saturation would produce lower stiffness and modulus values that would drive the modulus of subgrade reaction down leading to higher pavement stresses and reduced pavement life.

GENERAL CONCLUSIONS

General conclusions for this research show that self-cementing fly ash stabilization of RAP-soil mixtures is economically feasible and structurally capable of supporting construction traffic. The increase stiffness from the addition of self-cementing fly ash increases capacity improving the long term pavement performance. Addition of self-cementing fly ash increases the consolidated shear strength about five times.

Construction operations and field results proved that stabilization of limestone screenings is viable, cost effective, and produces an adequate structural layer for road construction. The moisture density curves for manufactured sand and limestone screenings are about the same, and the moisture-strength curves show a dramatic decrease in strength beyond the optimum moisture content for strength. Durability testing concluded that CKD stabilized manufactured sand and limestone screenings are not viable construction alternatives, and the addition of class C fly ash with CKD significantly increased the durability of the mixtures.

Testing and statistical analysis of subgrade materials concluded that granular subbase, self-cementing fly ash treated subgrade, and HFA decrease the variability of field results. Finite element modeling proved that a link exists between subgrade non-uniformity and pavement performance. Uniform modeling conditions produced lower average deflections and stresses increasing pavement life. Statistical analysis concluded that modeling uniform subgrade conditions produce average stresses that have less variability than those for non-uniform modeling conditions. Pavement response reliability increased with the addition of uniform subgrade proving that subgrade non-uniformity influences pavement performance.

GENERAL RECOMMENDATIONS

The author recommends a subgrade-soil-fly ash stabilization project be conducted in Western Iowa loess soils to determine of the process would be suitable for stabilization of the problematic loess soils.

The author recommends continuation of research in stabilization of limestone screenings by varying the fly ash-CKD ratio from 1:1 and studying the effects. Current field monitoring practices are also recommended to continue for at least one more winter-spring season.

The author recommends continuation of current research in the subgrade modeling area with several minor changes including: studying the effects of modeling different seasonal subgrade conditions, studying the effects of load placement variation, and changing thicknesses of the modeled pavement layer. The author also recommends that other projects within Iowa be studied to provide a larger database of results. It is also recommended that curling and temperature stresses be introduced into the analysis as this would produce much higher stresses in the pavement layer.

APPENDIX

This appendix contains informational data for each of the three chapters and is organized onto one DVD-ROM. Each chapter contains its own folder labeled 1, 2, and 3 for Chapters 1, 2, and 3 respectively.

System requirements for the DVD: IBM PC or 100% compatibles; Windows ME or higher; hard disk (1GB minimum); Microsoft Office 2000 or higher.

The DVD contains spreadsheet data, formatted in EXCEL 2000 or higher, pertaining to field and laboratory tests; pictures (JPEG format) of laboratory tests, field tests, and field conditions; ISLAB 2000 software (EXCEL 2000 required), and the input and output files (WordPad or Notebook) for the ISLAB 2000 program. Statistical analysis (SAS) output files are also stored and are formatted in Microsoft Word 2000 or better. Beta distribution analysis output files are stored and formatted using JMP 5.1.

REFERENCES CITED

American Coal Ash Association. (1991). *Flexible Pavement Manual.* American Coal Ash Association, Washington, D.C.

American Coal Ash Association. "Who we are." http://www.acaa-usa.org/who.htm. Accessed August 29, 2003.

Asphalt Paving Association of Oregon. "Who is APAO?" http://www.apao.org/faq.shtml. Accessed December 29, 2003.

ASTM C593. (2001). "Standard specification for fly ash and other pozzolans for use with lime." *Annual Book of ASTM Standards, Vol. 04.01*, ASTM, Philadelphia, PA.

ASTM C618. (2001). "Standard specification for coal fly ash and raw or Calcined natural pozzolan for use as a mineral admixture in concrete." *Annual Book of ASTM Standards, Vol. 04.02*, ASTM, Philadelphia, PA.

ASTM D422. (2001). "Standard test method for particle-size analysis of soils." *Annual Book of ASTM Standards, Vol. 04.08*, ASTM, Philadelphia, PA.

ASTM D559. (2001). "Standard test methods for wetting and drying compacted soil-cement mixtures." *Annual Book of ASTM Standards, Vol. 04.08*, ASTM, Philadelphia, PA.

ASTM D560. (2001). "Standard test methods for freezing and thawing compacted soil-cement mixtures." *Annual Book of ASTM Standards, Vol. 04.08*, ASTM, Philadelphia, PA.

ASTM D698. (2001). "Standard test methods for laboratory compaction characteristics of soil using standard effort (12,400 ft-lbf/ft^3 (600 kN-m/m^3))." *Annual Book of ASTM Standards, Vol. 04.08*, ASTM, Philadelphia, PA.

ASTM D2487. (2001). "Standard Classification of soils for engineering purposes (unified soil classification system)." *Annual Book of ASTM Standards, Vol. 04.08*, ASTM, Philadelphia, PA.

ASTM D4318. (2001). "Standard test methods for liquid limit, plastic limit, and plasticity index of soils." *Annual Book of ASTM Standards, Vol. 04.08*, ASTM, Philadelphia, PA.

ASTM D4767. (2001). "Standard test method for consolidated undrained triaxial compression test for cohesive soils." *Annual Book of ASTM Standards, Vol. 04.08*, ASTM, Philadelphia, PA.

Baghdadi, Z., Fatani, M., and Sabban, N. (1995). "Soil modification by cement kiln dust." *Journal of Materials in Civil Engineering* 7(4), New York, NY 218-222.

Barnes, A. (1997). "Pavement thickness design using reclaimed hydrated Iowa Class C fly ash as a base material." MSci thesis, Iowa State University, Ames, IA.

Bhatti, M., Barlow, J., Stoner, J. (1996). "Modeling damage to rigid pavements caused by subgrade pumping." *Journal of Transportation Engineering* 122(1), New York.

Bowles, J. (1996). *Foundation analysis and design*. McGraw-Hill, New York.

Boynton, R. (1980). *Chemistry and technology of lime and limestone*. John Willey & Sons, Inc., New York.

Broadbent, J. (1988). "Limestone fines improve Arizona low volume road." *Roads & Bridges,* 26(9), Des Plaines, IL.

CMI Corporation. (1994). *A Practical Guide to Soil Stabilization and Road Reclamation Techniques*, Oklahoma City.

Çokça, E. (2001). "Use of Class C fly ashes for the stabilization of an expansive soil." *Journal of Geotechnical and Geoenvironmental Engineering*, 127(7), ASCE, New York.

Collins, R., and Emery, J. (1983). "Kiln dust – fly ash systems for highway bases and subbases." *Final Report: FHWA/RD-82/167*, Federal Highway Administration, Springfield, VA.

Cooley, L., Huner, M., and Brown, E. (2002). "Use of screenings to produce hma mixtures." *NCAT Report No. 2002-10*, National Center for Asphalt Technology, Auburn University, AL.

Crovetti, J. (1998). "Construction and performance of fly ash-stabilized cold in-place recycled asphalt pavement in Wisconsin." *Transportation Research Record 1730*, Transportation Research Board, Washington, D.C.

Darter, M., Hall, K., and Kuo, C. (1995). "Support under Portland cement concrete pavements." *National Cooperative Highway Research Program Report 372*, Transportation Research Board, Washington, D.C.

Duncan, J. (2000). "Factors of safety and reliability in geotechnical engineering." *Journal of Geotechnical and Geoenvironmental Engineering*, 126 (4), ASCE, New York.

Ferguson, G. (1993). "Use of self-cementing fly ashes as a soil stabilization agent." *ASCE Geotechnical Special Publication No. 36*, ASCE, New York.

GAI Consultants Inc. (1992). "Fly ash design manual for road and site applications, Vol. 1: Dry or Conditioned Placement." *EPRI TR-100472, Vol. 1, Final Report*, EPRI, Palo Alto, CA. Glogowski, P., Kelly, J., McLaren, R., Burns, D: Authors.

Gantenbein, B. (2002). "Pilot program: Fly ash stabilization used as alternative to subgrade stabilization in Waukesha County." *Western Builder, March 7, 2002*, Reed Construction Data Circulation, Norcross, GA.

Grabe, J. (1993). "Spatial variation of soil stiffness: Spectral density approach." *Soil Dynamics and Earthquake Engineering* (13), Great Britain.

Huang, Y. (2004). *Pavement analysis and design*. Pearson Prentice Hall, New Jersey.

Ioannides, A. (1984). "Analysis of slabs-on-grade for a variety of loading and support conditions." PhD. Dissertation, University of Illinois, Urbana, IL.

Joint Departments of the Army and Air Force. (1994). "Soil stabilization for pavements." *Technical Manual No. 5-822-14 and Air Force Manual No. 32-1019*, Headquarters Departments of the Army and the Air Force, Washington, D.C.

Khazanovich, L. (1994). "Structural analysis of multi-layered concrete pavement systems." PhD. Dissertation, University of Illinois, Urbana, IL.

Khoury, N., and Zaman, M. (2002). "Effect of wet-dry cycles on resilient modulus of class c coal fly ash-stabilized aggregate base." *Transportation Research Record 1787*, Transportation Research Board, Washington D.C.

Klassen, S., and Jones, K. (1985). "Low cost fly ash-sand stabilized roadway." *Construction Report Project HR-259*, Iowa Highway Research Board, Iowa Department of Transportation, Ames, IA.

Legere, G., and Tremblay, H. (2003). "Laboratory and field evaluation of cement kiln dust and lime for stabilizing clayey silt on low-volume unpaved roads." *Transportation Research Record 1819*, Transportation Research Board, Washington D.C.

Miller, G., and Zamon, M. (2000). "Field and laboratory evaluation of cement kiln dust as a soil stabilizer." *Transportation Research Record 1714*, Transportation Research Board, Washington D.C.

Misra, A. (1998). "Stabilization characteristics of clays using class c fly ash." *Transportation Research Record 1611*, Transportation Research Board, Washington D.C.

Misra, A. (2000). "Utilization of western coal fly ash in construction of highways in the Midwest." *MATC UMC 96-2 Final Report*, Mid-America Transportation Center, University of Nebraska-Lincoln, Lincoln, NE.

Nady, R. (1997). "Prepared discussion." *Association of Asphalt Paving Technologists* (66), Washington D.C.

Nalbantoglu, Z., and Gucbilmez, E. (2002). "Utilization of an industrial waste in calcareous expansive clay stabilization." *Geotechnical Testing Journal*, (25), Washington D.C. 78-84.

Nelson, J., Tymkowicz, S., and Callahan, M. (1994). "An investigation of emulsion stabilized limestone screenings." *Final Report: Iowa Highway Research Board Project HR-389*, Iowa Highway Research Board, Ames, IA.

Oates, J. (1998). *Lime and limestone – Chemistry and technology, production and uses.* Wiley-VCH Weinheim; New York.

Parsons, R. (2002). "Subgrade improvement through fly ash stabilization." *Miscellaneous Report*, Kansas University Transportation Center, University of Kansas, Lawrence, KS.

Rupnow, T. (2002). "Subgrade stabilization using recycled asphalt pavement and fly ash mixtures." *Transportation Scholars Conference Compendium of Student Papers*, Midwest Transportation Consortium, Iowa State University, Ames, IA.

Sargand, S., Masada, T., Wasniak, D. (2000). "Constructing and controlling compaction of earth fills." *ASTM STP 1384*, American Society for Testing and Materials, West Conshohocken, PA.

Searle, A. (1935). *Limestone & its products – Their nature, production, and uses*. Ernest Benn Limited, London.

Şenol, A., Bin-Shahafique, Md., Edıl, T., and Benson, C. (2002). "Use of class c fly ash for stabilization of soft subgrade." *Procedures, Fifth International Congress on Advances in Civil Engineering*, Istanbul, Turkey.

SHRP. (1990). Distress identification manual for the long-term pavement performance studies. Strategic Highway Research Program, National Research Council, Washington, D.C.

Taha, R. (2003). "Evaluation of cement kiln dust-stabilized reclaimed asphalt pavement aggregate systems in road bases." *Transportation Research Record 1819*, Transportation Research Board, Washington D.C.

Taha, R., Al-Harthy, A., Al-Shamsi, K., Al-Zubeidi, M. (2002). "Cement stabilization of reclaimed asphalt pavement aggregate for road bases and subbases." *Journal of Materials in Civil Engineering*, (14), New York, NY, 239-245.

Taha, R., Ali, G., Basama, A., Al-Turk, O. (1999). "Evaluation of reclaimed asphalt pavement aggregate in road bases and subbases." *Transportation Research Record 1652*, Transportation Research Board, Washington D.C.

Terrel, R., Epps, J., Barenberg, E., Mitchell, J., Thompson, and Thompson, M. (1979). "Soil stabilization in pavement structures: A user's manual." *FHWA-IP-80-2, Vol. 1*, Department of Transportation, Federal Highway Administration, Washington, D.C.

Terrel, R., Epps, J., Barenberg, E., Mitchell, J., Thompson, and Thompson, M. (1979). "Soil stabilization in pavement structures: A user's manual." *FHWA-IP-80-2, Vol. 2*, Department of Transportation, Federal Highway Administration, Washington, D.C.

Thomas, Z. (2002). "Engineering properties of soil-fly ash sub grade mixtures." *Transportation Scholars Conference Compendium of Student Papers*, Midwest Transportation Consortium, Iowa State University, Ames, IA.

Thomas, Z. (2003). "Engineering properties and construction guidelines for soil stabilized with self-cementing fly ash." MSci thesis, Iowa State University, Ames, IA.

US Navy. (1999). "Materials testing." *Naval Facilities Engineering Command Publication NAVFAC MO 330*, Fort Leonard Wood, MO.

Vandenbossche, J., and Johnson, A. (1994). "Soil stabilization of low volume roads." *Research Implementation Series, Number 19*, Minnesota Local Road Research Board, St. Paul, MN.

White, D. (2002). "Sutherland generating station and Ottumwa-Midland landfill access roads – Field performance." *ISU-ERI-Ames Report 01060*, Engineering Research Institute, Iowa State University, Ames, IA.

White, D., and Bergeson, K. (2000). "US highway 151 ash stabilization research project." *Progress Report ERI Project 400-60-85-00-3009*, Engineering Research Institute, Iowa State University, Ames, IA

Winkerton, H., and Pamukcu, S. (1991). "Soil stabilization and grouting." *Foundation Engineering Handbook, 2nd Edition*, New York, NY.

Wu, Z. (1999). "Structural performance of cold recycled asphalt pavements." *Transportation Scholars Conference Compendium of Student Papers*, Midwest Transportation Consortium, Iowa State University, Ames, IA.

Zia, N., and Fox, P.J. (2000). "Engineering properties of loess-fly ash mixtures for road bases." *Transportation Research Record 1717*, Transportation Research Board, Washington D.C.

ACKNOWLEDGEMENTS

The author would like to thank the Iowa Department of Transportation, Federal Highway Administration, Center for Transportation Research and Education, Martin Marietta Aggregates, and the Iowa Fly Ash Affiliates for sponsoring this research. The author would also like to express his gratitude to the many construction companies that worked with and around him during the course of this study including: Rileys Construction Company, C.J. Moyna and Sons, Manatts, and Construct Inc. The author would also like to thank his major professor Dr. David White for his expertise, experience, and guidance throughout the course of this study. Thanks also go to other committee members Dr. Halil Ceylan for advice and guidance on pavement modeling and Dr. Thomas Rudolphi for serving on this committee.

The author would also like to express his gratitude to Zach Thomas, Joels Malama, Isaac Drew, Cliff Schafer, Pavana Vennapusa, Blake Vosburg, Clinton Halverson, and Matthew Cushman, for their help in both the field and laboratory. Without their help, the author would still be testing certain projects. The author would also like to thank Don Davidson for his guidance and willingness to lend a helping hand with laboratory equipment use.

The author would like to thank Ms. Karen Picone for her understanding, help, and guidance while revising this manuscript. Without her help and guidance on technical writing skills, this manuscript would not be what it is today.

The author would like to thanks his family for all of their love and support through the college years and into graduate studies. Their kindness and understanding are much appreciated. Last, the author would like to thank his fiancée Jennifer for her love,

encouragement, and support over the last two years. Many thanks go to her for reading over this manuscript, helping out with late nights at the laboratory, and having an overall understanding of the amount of time required making this project happen.